The Elastic Properties and High Strain Compressive Behaviour of Micro- and Nano-sized Irregular Honeycombs and Open-cell Foams

By

HONGCHAO ZHANG

A Thesis Submitted in Fulfillment of the Requirements for the Degree of Doctor of Philosophy (PhD)

Cardiff School of Engineering

Cardiff University

September 2014

DECLARATION

This work has not previously been accepted in substance for any degree and is not concurrently submitted in candidature for any degree.

Signed…… (candidate) Date ……

STATEMENT 1

This thesis is being submitted in partial fulfillment of the requirements for the degree of ……(insert MCh, MD, MPhil, PhD etc, as appropriate)

Signed……(candidate) Date ……

STATEMENT 2

This thesis is the result of my own independent work/investigation, except where otherwise stated. Other sources are acknowledged by explicit references.

Signed……(candidate) Date ……

STATEMENT 3

I hereby give consent for my thesis, if accepted, to be available for photocopying and for inter-library loan, and for the title and summary to be made available to outside organisations.

Signed……(candidate) Date ……

I would like to dedicate this thesis to my loving family

Abstract

Cellular solids widely exist in nature. Many researchers have analyzed the mechanical properties of macro-sized cellular solids. Following the rapid development of nano science and manufacturing technology, micro- and nano-sized cellular solids (i.e. honeycombs and open-cell foams) are now widely used in many areas. The purpose of this study is to investigate the elastic properties and the high strain compressive behaviour of micro- and nano-sized periodic random irregular honeycombs and open-cell foams.

In general, at the micro-meter scale, the strain gradient effect plays an important role in deformation. Meanwhile, at the nano-meter scale, the surface elasticity and the initial stress or strain are the dominant deformation mechanisms. According to the equivalence of the bending, transverse shear, torsion, and axial stretching or compression rigidities, these effects can be incorporated into the simulations by using the obtained equivalent Young's modulus, Poisson's ratio, and cross-sectional size.

The results of this study indicate that the elastic properties and high strain compressive behaviour of micro- and nano-sized irregular honeycombs and open-cell foams are size-dependent and tunable. The smaller cross-sectional size of the cell walls/struts, the larger the dimensionless Young's modulus, bulk modulus, shear modulus, the tangent modulus and the dimensionless compressive stress, and the smaller the Poisson's ratio. Both the dimensionless Young's modulus and compressive stress of nano-sized irregular honeycombs can be controlled to vary over a range of around 100% by adjusting the amplitude of the initial strain in the cell wall direction between -0.06 and 0.06. For nano-sized irregular open-cell foams, both the dimensionless Young's modulus and compressive stress can be controlled to vary over a range of about 50% by adjusting the amplitude of the initial strain between -0.1 and 0.1. The cell regularity also significantly influences the elastic properties and the high strain compressive behaviour of micro- and nano-sized irregular honeycombs and open-cell foams.

Acknowledgements

First and foremost, I would like to gratefully thank my supervisors Dr. Hanxing Zhu and Prof. David Kennedy for their patience and continuous guidance throughout my entire PhD study. They encouraged and inspired me to do my best on my PhD study.

I would like to thank Prof. Junfeng You and Dr. Sivakumar Kulasegaram. Without Prof. Junfeng You's kind support enabled me to grasp the ANSYS software. Dr. Sivakumar Kulasegaram also gave me useful advice for my research work.

I would like to thank Dr. Jonathan Evans, who carefully proofread my thesis and gave me useful advice on the improvement of my English.

I also would like to thank all of the staff at the research office of Engineering School. Due to their kind help and efficient work, I have been able to concentrate on my research work.

Without the support of my loving family, I would not have been able to complete my PhD study. I would like to deeply thank my Mum and Dad, who never lost patience and confidence in me, they always encouraged and supported me during my PhD study. Meanwhile, I would like to thank my loving girlfriend, Miss Kailin Zou. She has given me encouragement, understanding, and emotional support during my PhD study, especially during the last few months.

Finally, I would like to thank all my friends, who made my life more wonderful in the UK.

Table of Contents

List of Figures

List of Tables

Symbols

A	The area of the cell strut cross-section
A_0	The area of the unit square
A_{xz} , A_{yz}	The areas of the top, right edge/surface of honeycomb or open-cell foam
A^*	The Zener's anisotropy factor
b , b_0	The actual/initial width of the cell walls
D_b	The bending rigidity of the cell walls or struts
D_C	The axial stretching or compression rigidity of the cell walls or struts
D_S	The transverse shear rigidity of the cell walls
D_t	The torsion rigidity of the cell struts
d , d_0	The actual and initial circular cross-sectional diameter of the cell struts
d_n	The distance between two neighboring nuclei in a perfectly regular hexagonal honeycomb or body centered cubic (BCC) foam
E	The Young's modulus of honeycomb or foam
E_1 , E_2	The in-plane Young's moduli of honeycomb or the Young's moduli of open-cell foam in the x and y directions
$\overline{E_1}$	The non-dimensional in-plane Young's modulus of honeycomb
E_{100}	The Young's modulus of regular open-cell Kelvin foam in the 100 lattice direction

E_3	The out-of-plane Young's modulus of honeycomb
$\overline{E_3}$	The non-dimensional out-of-plane Young's modulus of honeycomb
E_e	The equivalent Young's modulus of the beam element material
E_S	The Young's modulus of the solid material
F_x, F_y	The forces in the *x* and *y* directions
G	The shear modulus of honeycomb or foam
G_{12}	The in-plane effective shear modulus of foam
G_{31}	The out-of-plane shear modulus of honeycomb
$\overline{G_{31}}$	The non-dimensional out-of-plane shear modulus of honeycomb
G_e	The equivalent shear modulus of the beam element material
G_S	The shear modulus of the solid material
h, h_e, h_0	The actual, equivalent and initial thickness of the cell walls
I	The second moment of the cross-sectional area of the cell walls or struts
i, j	Nodes on the left, top or front edge/surface of the periodic random irregular Voronoi honeycomb or open-cell foam
i', j'	The corresponding nodes on the right, bottom or back edge/surface of the periodic random irregular Voronoi honeycomb or open-cell foam
J	The polar second moment of the cell strut cross-sectional area
K	The in-plane bulk modulus of honeycomb

$\overline{K}$	The non-dimensional in-plane bulk modulus of honeycomb
k	The number of the cell walls/struts
L , L_x , L_y , L_z , $L^{'}$, $L_x^{'}$, $L_y^{'}$, $L_z^{'}$	The initial and actual side lengths of the unit random periodic honeycomb or open-cell foam
l , l_k , l_0 , l_{0k}	The actual and initial lengths of the cell walls/struts
l_m , l_n	The material length parameters at the micro- and nano-meter scales
M	The total number of the cell walls/struts
N	The total number of complete cells in the unit square area or cube
R_e	The equivalent circular cross-sectional radius of the cell struts
R_0	The initial circular cross-sectional radius of the cell struts
S	The surface elasticity modulus
$S_{11}, S_{12}, S_{13}, S_{22}, S_{23}, S_{33}, S_{44}, S_{55}, S_{66}$	The components of the compliance matrix
$u_i^{left}, u_j^{left}, u_i^{top}, u_j^{top}, u_i^{front}, u_j^{front}$	The *x*-displacements of nodes on the left, top or front edge/surface of the periodic random irregular Voronoi honeycomb or open-cell foam
$u_{i'}^{right}, u_{j'}^{right}, u_{i'}^{bottom}, u_{j'}^{bottom}, u_{i'}^{back}, u_{j'}^{back}$	The *x*- displacements of the corresponding nodes on the right, bottom or back edge/surface of the periodic random irregular Voronoi honeycomb or open-cell foam
Δu_x , Δu_y	The elongations in the *x* and *y* directions
$V^{'}$, V_0	The actual and initial volumes of a unit cube
ν	The Poisson's ratio of honeycomb or foam

v_{12} , v_{21}	The in-plane Poisson's ratio of honeycomb or open-cell foam
v_{31}	The out-of-plane Poisson's ratio of honeycomb
v_e	The equivalent Poisson's ratio of the beam element material
v_i^{left} , v_j^{left} , v_i^{top} , v_j^{top} , v_i^{front} , v_j^{front}	The *y*-displacements of the nodes on the left, top or front edge/surface of the periodic random irregular Voronoi honeycomb or open-cell foam
$v_{i'}^{right}$, $v_{j'}^{right}$, $v_{i'}^{bottom}$, $v_{j'}^{bottom}$, $v_{i'}^{back}$, $v_{j'}^{back}$	The *y*-displacements of the corresponding nodes on the right, bottom or back edge/surface of the periodic random irregular Voronoi honeycomb or open-cell foam
v_S	The Poisson's ratio of the solid material
w_i^{left} , w_j^{left} , w_i^{top} , w_j^{top} , w_i^{front} , w_j^{front}	The *z*-displacements of the nodes on the left, top or front surface of the periodic random irregular open-cell foam
$w_{i'}^{right}$, $w_{j'}^{right}$, $w_{i'}^{bottom}$, $w_{j'}^{bottom}$, $w_{i'}^{back}$, $w_{j'}^{back}$	The *z*-displacemments of the corresponding nodes on the right, bottom or back surface of the periodic random irregular open-cell foam
x , y , z	The original nodal coordinates of the cell walls/struts
x' , y' , z'	The corresponding nodal coordinates of the cell walls/struts
α	The degree of cell regularity
δ	The minimum distance between any two neighboring nuclei in a random irregular honeycomb or foam
ε_0^h	The initial strain in the thickness direction of the cell walls
ε_0^L	The initial strain in the length direction of the cell walls/struts
ε_0^r	The initial strain in the radial direction of the cell struts
ε_0^W	The initial strain in the width direction of the cell walls

ε_x, ε_y	The effective strains in the *x* and *y* directions
θ_i^{left}, θ_i^{top}, θ_i^{front}	The rotations of the nodes on the left, top or front edge/surface of the periodic random irregular Voronoi honeycomb or open-cell foam
$\theta_{i'}^{right}$, $\theta_{i'}^{bottom}$, $\theta_{i'}^{back}$	The rotations of the corresponding nodes on the right, bottom or back edge/surface of the periodic random irregular Voronoi honeycomb or open-cell foam
ρ	The relative density of honeycomb or open-cell foam
ρ^*	The density of a foam
ρ_S	The density of the solid materials
ρ_0	The initial relative density of honeycomb or open-cell foam
σ	The compressive stress
$\overline{\sigma}$	The non-dimensional compressive stress
σ_0^L	The initial stress in the length direction of the cell walls/struts
σ_0^r	The initial stress in the radial direction of the cell struts
σ_0^W	The initial stress in the width direction of the cell walls
σ_x, σ_y	The effective stresses in the *x* and *y* directions
τ_0	The initial surface stress

Abbreviations

BCC	Body centered cubic
FCC	Face centered cubic
RVE	Representative volume element

Chapter 1 Introduction

1.1 Background and motivation

Cellular solids widely exist in nature, examples include wood and bones. At the macro-meter scale, regular and irregular cellular solids materials and structures exist and can be manufactured (Gibson and Ashby, 1997). Since they are light in weight and have excellent strength, stiffness, low thermal conductivity, and high energy absorption capacity, they are utilized in many areas, such as thermal insulation, spacecraft, ship, and vehicle structures, as shown in Figures 1.1 and 1.2.

Figure 1.1. Examples of applications of advanced cellular materials (Wadley, 2014).

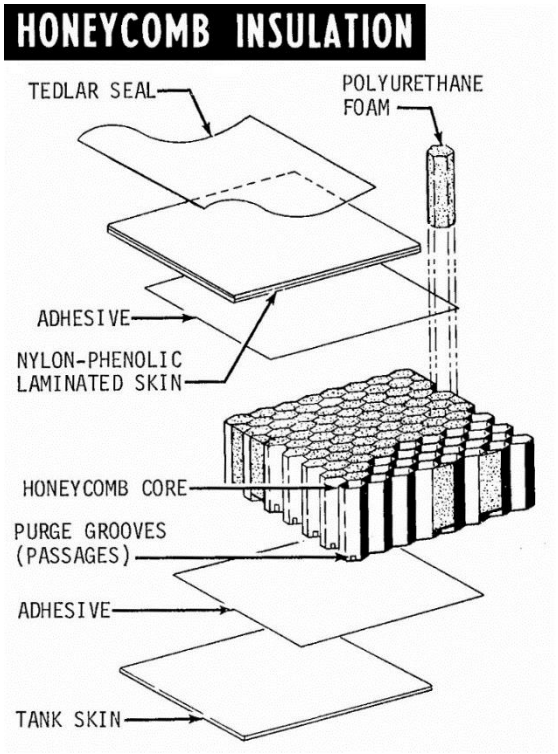

(a)

(b)

Figure 1.2. (a) Honeycomb insulation panel for the insulation of the booster rockets (Jetzer, 2010). (b) Aluminium foam metal for energy absorption (ERG).

The elastic properties of macro-sized regular and irregular honeycombs and open-cell foams have been very extensively investigated by many researchers (Chen et al., 1999, Chen, 2011, Christensen, 2000, Gibson and Ashby, 1997, Gong and Kyriakides, 2005,

Gong et al., 2005a, James Ren and Silberschmidt, 2008, Konstantinidis et al., 2009, Mills, 2007b, Van der Burg et al., 1997, Zhu et al., 2000, Zhu et al., 2001a, Zhu et al., 1997a, Zhu and Mills, 2000, Zhu et al., 1997b, Zhu et al., 2006, Zhu and Windle, 2002, Sotomayor and Tippur, 2014a, Sotomayor and Tippur, 2014b).

With the rapid development of nano science and manufacturing technology, at the micro- and nano-meter scales, regular and irregular cellular materials and structures can be fabricated by electrochemical and chemical etching methods[1] (Bilousov et al., 2013, Kramer et al., 2004, Nishihara et al., 2005). For example, Karmer et al. (2004) produced the irregular nanoporous gold structure by etching silver-gold alloy in perchloric acid (as shown in Figure 1.3). Nishihara et al. (2005) made the regular silica gel micro-honeycomb by ice templating (as shown in Figure 1.4).

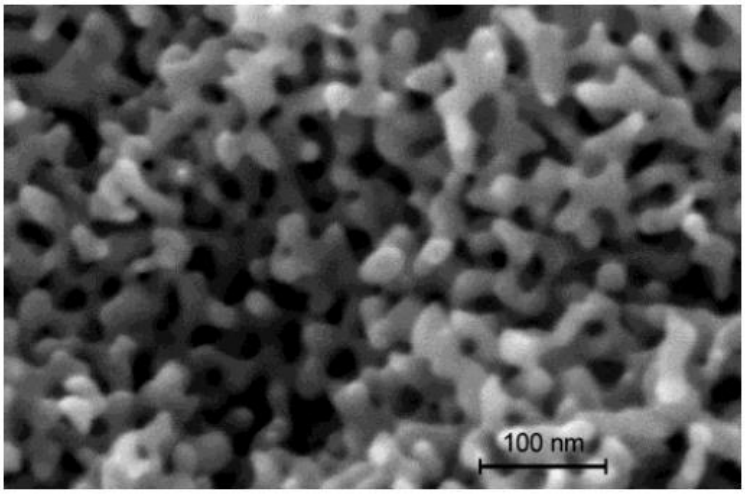

Figure 1.3. Scanning electron micrograph of the nanoporous gold structure (Kramer et al., 2004).

[1] Micro- and nano-sized cellular materials and structures both can be fabricated by these methods.

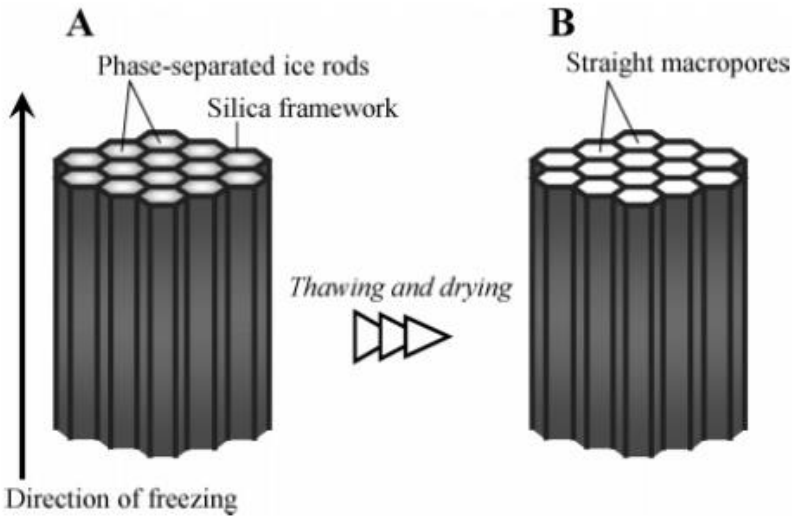

Figure 1.4. Model which illustrates the formation of regular micro-honeycomb by ice templating. (A) The microstructure formed by the phase separation during unidirectional freezing of silica hydrogels. An array of straight ice rods with polygonal cross sections is formed. Silica framework is formed at the interspace of the ice rods. (B) After removal of the ice rods by thawing and drying, macropores are formed as a replica of the ice rods (Nishihara et al., 2005).

Synthetic micro- and nano-sized regular and irregular cellular materials have an increasing number of applications in many different areas. They are widely used in Microelectromechanical Systems (MEMS) and Nanoelectromechanical Systems (NEMS), such as the actuator materials of nano-sensors (Kramer et al., 2004, Wagner et al., 2013, Weissmüller et al., 2003, Zhao et al., 2013). The regular micro- and nano-sized cellular materials are used as active layer in gas sensors which are based on various operating principles, such as capacitive, resistive, gravimetric and optical sensing (as shown in Figure 1.5). Zhao et al. (2013) produced irregular nanoporous polyelectrolyte membranes on the surface of an optical fiber for testing high pH-sensing performance (as shown in Figure 1.6). Synthetic micro- and nano-sized

regular and irregular cellular materials also have potential biological and medical applications which involve sorting, isolating and releasing biological molecules (Adiga et al., 2009) (as shown in Figure 1.7).

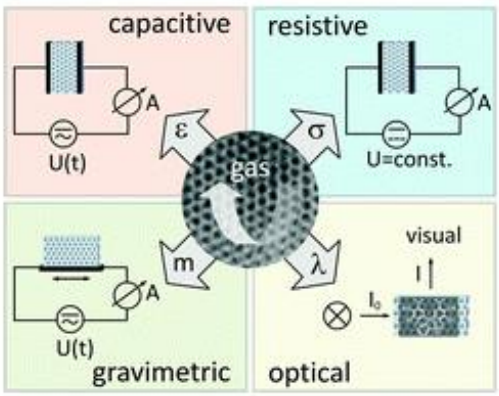

Figure 1.5. Active layer which is made by regular micro- and nano-sized cellular materials in gas sensors based on various operating principles, such as capacitive, resistive, gravimetric and optical sensing (Wagner et al., 2013).

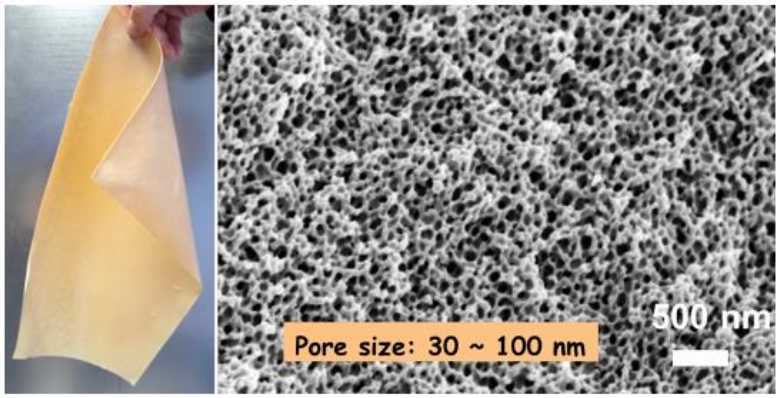

Figure 1.6. Irregular nanoporous polyelectrolyte Membrane (Zhao et al., 2013).

The mechanical properties are critical in enabling the different types of functions of micro- and nano-sized materials and structures. According to the previous description, micro- and nano-sized regular and irregular cellular materials and structures have

numerous potential applications. Therefore, to ensure the functions and to enhance the potential applications of micro- and nano-sized regular and irregular cellular materials, a better understanding of the mechanical properties of those materials is highly demanded. The elastic properties of micro- and nano-sized regular honeycombs and open-cell foams have previously been studied (Zhu, 2010b, Zhu and Wang, 2013).

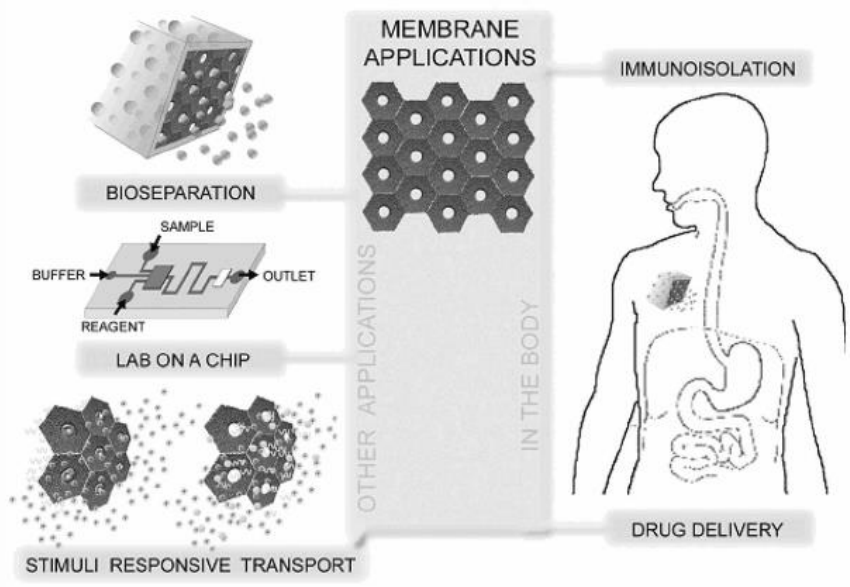

Figure 1.7. Biological applications of nanoporous materials (Adiga et al., 2009).

It has been generally recognized that the strain gradient effect plays an important role in the deformation at the micro-meter scale (Toupin, 1962, Fleck and Hutchinson, 1993, Aifantis, 1999, Gao et al., 1999, Yang et al., 2002, Lam et al., 2003, Tsagrakis et al., 2003, Zhu, 2010b, Zhu and Wang, 2013), and that the surface elasticity and the initial stress or strain are the dominant deformation mechanisms at the nano-meter scale (Miller and Shenoy, 2000, Zhu and Karihaloo, 2008, Zhu and Wang, 2013, Zhu, 2010b, Kramer et al., 2004, Biener et al., 2009, Zhu et al., 2012a). According to the

previous research works, it can be found that nobody has simulated the mechanical properties of micro- and nano-sized random irregular honeycombs and open-cell foams. This research project aims to fill this gap, and to investigate the elastic properties and the high strain compressive behaviour of micro- and nano-sized random irregular honeycombs and open-cell foams.

1） The strain gradient Effect

The phenomenon of the strain gradient effect has been observed at the micro-meter scale by many researchers (Fleck et al., 1994, Lam et al., 2003, Nix and Gao, 1998, Stölken and Evans, 1998). For examples, Fleck et al. (1994) found that when the copper wire diameter was decreased from 170 to 12μm, the torsional resistance in the copper wire were increasing, however, there was no effect of the copper wire diameter in the uniaxial tensile testing. Stölken and Evans (1998) observed that decreasing the nickel foil thickness from 50 to 12.5μm leaded to the increase of the bending resistance of the nickel foil. The indentation test (Atkinson, 1995, Ma and Clarke, 1995, McElhaney et al., 1998, Nix, 1989) (as shown in Figure 1.8) also proved the existence of the strain gradient effect, the hardness of single and polycrystalline metallic materials was doubled when the indentation depth was decreased from 10 to 1μm.

Most of micro- and nano-structures are designed and applied in the elastic regime of the deformation, however the observed strain gradient effect is usually in plastic regime. According to Sun et al. (2007), they compared the molecular statics simulation of Cu and Si nanoplates bending to the strain gradient elasticity solution,

and found that the strain gradient effect also existed in the elastic regime of the deformation. In general, the deformation energy density can describe the elastic behavior of the materials. In the conventional elastic theory, the deformation energy is contributed by the strain. However, according to the hypothesis of the strain gradient elasticity (Lam et al., 2003), not only the strain but also the strain gradient will make a contribution to the deformation density.

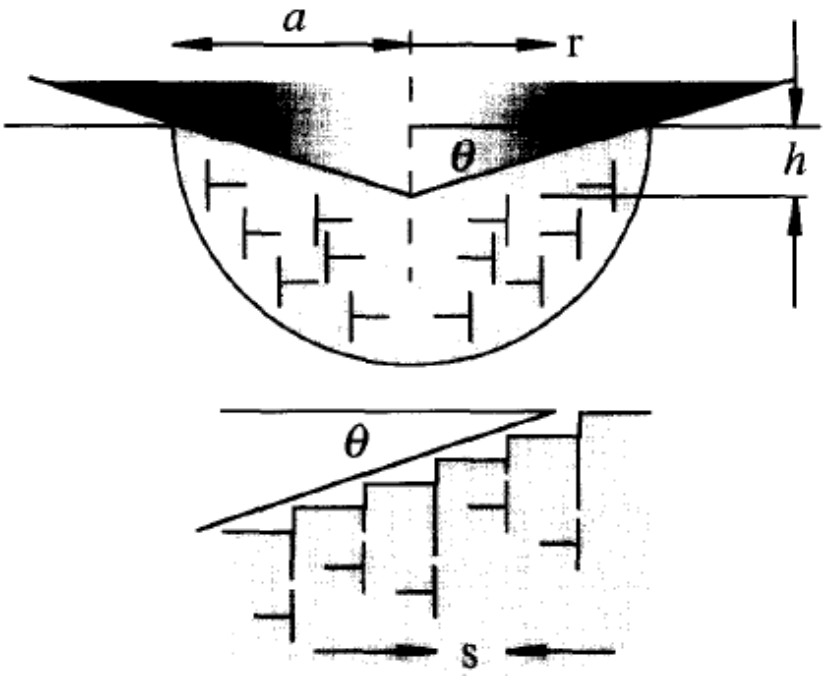

Figure 1.8. The schematic of the indentation testing by a rigid conical indentation (Nix and Gao, 1998).

Actually, the strain gradient effect is related to the curvature of the material, and indicates the hardness of the material. A material characteristic length parameter can characterize the size dependence of the hardness and the strain gradient effect (Gao et

al., 1999, Haque and Saif, 2003, Nix and Gao, 1998, Sun et al., 2007, Zhu and Karihaloo, 2008). The length parameter is related to the shear modulus, yield strength and Burgers vector of the material (Gao et al., 1999, Haque and Saif, 2003). This length parameter scale is estimated to be at the micro-meter scale (Fleck et al., 1994, Hutchinson, 2000, Stölken and Evans, 1998), and this implies that the strain gradient effect exists at the micro-meter scale and its contribution is size dependent. The strain gradient effect can explain the size dependent hardening effect of the material in elastic deformation.

Because the strain gradient effect is related to the deformation curvature of the material, so there is no strain gradient for the elastic behavior when uniaxial stretching or compressing the material (Lam et al., 2003). For bending test, the strain gradient effect would exist. For example, Sun et al. (2007) found the bending theory based on the strain gradient elasticity. According to the obtained bending rigidity (Sun et al., 2007), it can be found that if the thickness of the plate is closed to the material characteristic length parameter, the dimensionless bending rigidity in the strain gradient elasticity would become twice of that of the conventional bending rigidity. It implies that at the micro-meter scale, the bending capacity would increase and the material would become harder. Lam et al. (2003) and Zhu and Karihaloo (2008) also got the similar results about the relationship between the hardness and the size of the material. So it can be found that the strain gradient effect can greatly affect the elastic properties of micro-sized structures.

2） The surface elasticity

According to Rubio-Bollinger et al. (2001), their experiment results have shown that the tensile strength of a freely suspended chain of single gold atoms is about twice that of a bulk metallic material, and they also found that the detailed local atomic arrangement at the chain bases can greatly affect the total effective stiffness of the nanostructure. These experimental results imply the existence of surface effects at the nano-meter scale.

Why does this phenomenon exist? For a spherical particle, the surface area is proportional to the square of the diameter, and the volume is proportional to the cubic of the diameter. Thus the surface area to volume ratio is inversely proportional to the diameter. With the decrease of the particle diameter, especially at the nano-meter scale, the surface area to volume ratio will increase significantly, and the percentage of the atoms on the surface of the spherical particle will also increase significantly. The experiment results (Rubio-Bollinger et al., 2001) about the influence of the atomic arrangement on the mechanical properties of nanostructure demonstrates that the surface effect exists at the nano-meter scale, and also indicates the relationship between the diameter, the surface and the bulk of the material.

The elastic modulus on the surface and the bulk can be defined as surface elastic modulus and bulk elastic modulus (Miller and Shenoy, 2000). In fact, the surface elasticity effect is about the effect of the surface elastic modulus, and it is relevant to the surface stress. The nature of the chemical bonding of the surface atoms is very

different from the bonding of the interior atoms. If the surface atoms are unconstrained, the interatomic distance of the surface atoms is in equilibrium which is different from that of the interior atoms. According to this, it can be considered that there is a stress on the surface of the solid. The surface stress is the reversible work per unit area against surface deformation at constant number of surface atoms, and this surface deformation is caused by the elastic stretch of the pre-existing surface. The surface stress of a solid could be positive (if tensile stress) or negative (if compressive stress) (Cammarata, 1994, Miller and Shenoy, 2000, Müller and Saúl, 2004, Zhu and Karihaloo, 2008). The total surface stress consists of two parts, the first one is the initial surface stress before the deformation, and the second one is the deformed surface stress which is proportional to the surface modulus. In general, the surface stress is non-zero even if the stress in the bulk is very small, and the surface stress will change if there is a deformation and its direction is parallel to the surface. Miller and Shenoy (2000) used the surface elastic modulus, bulk elastic modulus and a length (defining the size of the structure) to represent effective stiffness properties. The surface elastic modulus to the bulk elastic modulus ratio was defined as the material intrinsic length which sets the scale about the effect of the surface. The material intrinsic length to the length (defining the size of the structure) ratio can define the surface elastic effect at effective stiffness properties.

Miller and Shenoy (2000) did a simple analysis about the effect of surface elasticity, When a plate is axially stretched, the strain energy is stored in the surface and bulk of

the plate. When the thickness of the plate is decreased, the stored energy in the surface will can be compared with that in the bulk. Furthermore, the axial force which across the cross-section of the plate is contributed by surface stresses and bulk stresses. Decreasing the thickness of the plate will lead to the increase of the contribution from the surface stress. So the effect of surface can be affected by the dimension of the material. Zhu et al. (2009) also demonstrated the surface elasticity effect on the bending stiffness of nanofilms.

3） The initial stress/strain

Actually, the initial stress is a residual stress on the surface and the bulk before the deformation. For macrostructure, the surface area to volume ratio is very small, then the initial surface stress is thus ignored, and the bulk stress is also ignored before applying the deformation on the structure. However, for nanostructure, because of the large ratio of the surface area to volume, the initial surface stress will pay more contribution to the elastic stiffness of the structure. Then the initial residual stress could significantly affect the effective stiffness properties of the structure at the nano-meter scale.

As the above description about the total surface stress, it can be found that the initial surface stress always exists on the surface before applying the deformation on the structure. The existence of the initial surface stress controls the equilibrium at the interatomic distance of the surface atoms. According to the analysis about pure

bending of a nanoplate and nanobeam (Zhu et al., 2009), it can be found that the initial surface stress is proportional to the initial residual stress and strain in the bulk, and it is also inversely proportional to the thickness of the structure. So the effect of the initial residual stress and strain can link with the initial surface stress effect. From the analytical results about the bending stiffness of the nanoplate and nanobeam (Zhu et al., 2009), the initial surface stress or residual strain and the surface elasticity have the relative effect on the bending stiffness. It implies that the initial stress can affect the elastic properties of nanostructures.

The initial surface stress or initial strain can be controlled by an applied voltage (Kramer et al., 2004, Weissmüller et al., 2003). According to Weissmüller et al. (2003), the surface stress of nanostructures is dependent on surface charge density. For nanostructures, the surface area to volume ratio would be larger, the space-charge regions at the surface will have an impact on the overall performance of the nanostructure. A voltage can be applied by an electrolyte which impregnates the nanostructure. The surface electronic charge density can be controlled by this voltage (as shown in Figure 1.9). Then the initial surface stress would be changed and the dimension of structure can shrink or extend. According to the previous research (Kramer et al., 2004, Weissmüller et al., 2003), it can be found that the deformation of many types of materials can be induced by an applied voltage, such as ceramics, polymers, carbon nanostructures and metals.

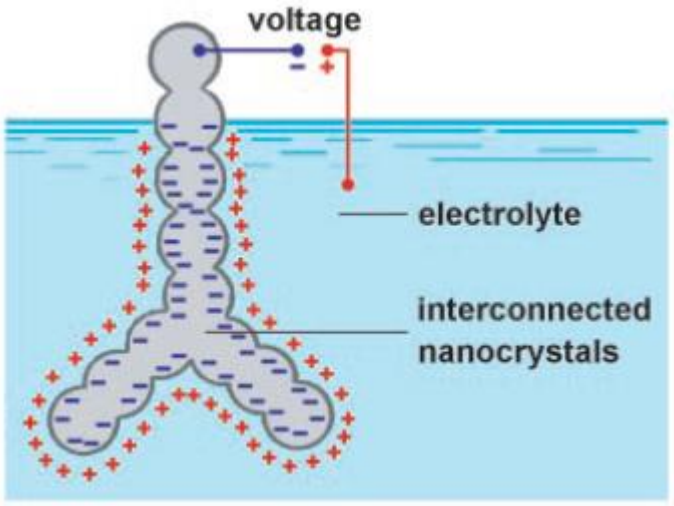

Figure 1.9. The schematic of an interconnected array of charged nanoparticles immersed in an electrolyte (Weissmüller et al., 2003).

1.2 Objectives and contributions of the thesis

Honeycombs and foams are the main forms of cellular solid structures (more details are shown in Chapter 2). The general purpose of this thesis is to shed some light on the linear elastic properties and the high strain compressive behaviour of micro- and nano-sized periodic random irregular honeycombs and open-cell foams. The main objectives and contributions of this PhD research work consist of four different topics and the results will be presented in four different chapters (Chapters 3, 4, 5 and 6). The four topics are:

1. The elastic properties of micro- and nano-sized periodic random irregular honeycombs, including: the five independent elastic constants and the results; the main factors that can affect the elastic properties; the methodology to incorporate

these effects into the simulations; and, the tunable ranges of the elastic properties.

2. The high strain compression behaviour of micro- and nano-sized periodic random irregular honeycombs, including: the main factors that can affect the high strain compressive responses; the effects of these factors on compressive responses; and, the tunable ranges of the high strain compressive responses.
3. The elastic properties of micro- and nano-sized periodic random irregular open-cell foams, including: the three independent elastic constants and the results; the main factors that can affect the elastic properties; the methodology to incorporate these effects into the simulations; and, the tunable ranges of those properties.
4. The high strain compression behaviour of micro- and nano-sized periodic random irregular open-cell foams, including: the main factors that can affect the high strain compressive behaviour; the effects of those factors on the compressive mechanical responses; and, the tunable ranges of the compressive mechanical responses.

1.3 Layout of the thesis

To achieve the main objectives, this thesis consists of seven chapters, as follows.

Chapter 1 presents the relevant background and motivation of this research project, the objectives and contributions are also clearly described.

Chapter 2 provides a brief review of the structure of cellular solids. It describes the mechanics models of honeycombs and foams and also shows the linear and geometrically nonlinear elastic properties of macro-sized regular and irregular

honeycombs and open-cell foams. The last part of Chapter 2 presents the rigidities of micro- and nano-sized uniform plate and beam with a circular cross-section, as well as the elastic properties of micro- and nano-sized regular honeycombs and open-cell foams.

In Chapter 3, the elastic properties of micro- and nano-sized periodic random irregular honeycombs are obtained by numerical simulation analysis using ANSYS. The effects of some main factors such as the cell strut/wall thickness, initial stress or strain, cell regularity and relative density are investigated. According to the main deformation mechanisms, such as bending, transverse shear and axial stretching or compression, the equivalent rigidities are used in this chapter. The size-dependent and initial stress or strain effects are incorporated into the simulations by using the equivalent material properties and the cell wall thickness.

Chapter 4 shows the effects of the cell wall thickness, initial stress/strain and cell regularity on the high strain compressive behaviour of micro- and nano-sized periodic random irregular honeycombs by numerical simulation analysis.

Chapter 5 investigates the effects of the cell strut thickness, initial stress/strain and cell regularity on the elastic properties of micro- and nano-sized periodic random irregular open-cell foams by numerical simulation analysis. To incorporate these effects into simulations, this chapter presents how to obtain the equivalent material properties and the cell strut thickness from the bending, torsion and axial stretching/compression rigidities.

In Chapter 6, the high strain compressive behaviour of micro- and nano-sized periodic random irregular open-cell foams are analyzed by numerical simulation analysis, together with the main factors effects investigated (i.e. the size-dependent, initial stress or strain and cell regularity).

Chapter 7 concludes the objectives of this thesis and briefly summaries the processes of achieving these targets. In addition, it presents the research limitations and makes several recommendations for future research.

Chapter 2 Literature review

2.1 Introduction

Cellular solids are common in nature, examples include wood, coral, and bones. Due to the particular structure of cellular solids, these types of material exhibit very special mechanical, thermal, electrical, and acoustic properties (Gibson and Ashby, 1997). Consequently, they are widely used in many fields, such as manufacturing engineering, chemical engineering, electrical engineering and so on. The advances in manufacturing techniques have allowed us to vividly mimic nature materials and to produce micro- and nano-structured cellular solids. Consequently, this PhD research focuses on the mechanical properties of micro- and nano-sized cellular materials.

2.2 The structure of cellular solids

Gibson and Ashby (1997) have done very extensive research work on the mechanical properties of cellular materials. However, since they did not consider the size effect, their results show that the mechanical properties of cellular materials depend mainly on cell shape and relative density.

2.2.1 Typical structures of cellular solids

The structure of cellular solids looks like a network with an interconnection of solid

struts or plates on the edges and faces of cells. There are three typical structures of cellular solids, which are: two-dimensional honeycombs, three-dimensional open-cell foams, and three-dimensional closed-cell foams (Gibson and Ashby, 1997). Figures 2.1 (a), (b), and (c) show these three typical structures.

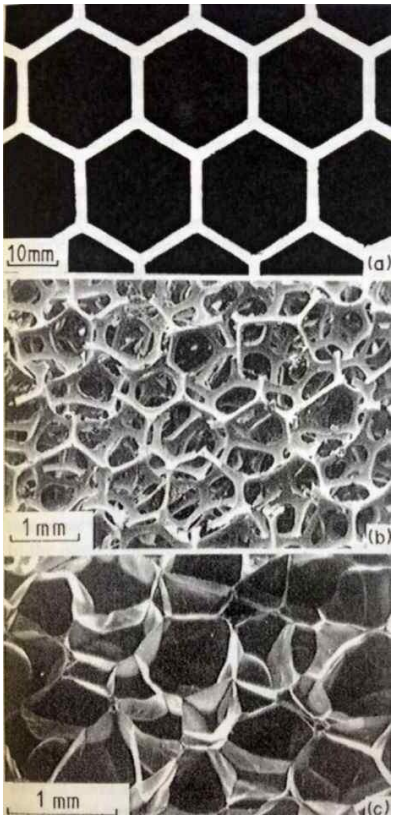

Figure 2.1. Three typical structures of cellular solids: (a) a two-dimensional honeycomb; (b) a three-dimensional foam with open cells; and, (c) a three-dimensional foam with closed cells (Gibson and Ashby, 1997).

A honeycomb is a two-dimensional array of polygons in a plane area. In contrast, a three-dimensional foam consists of polyhedrons in a 3D space. According to the component parts (solid edges and faces of cells), three-dimensional foams are classified as open-cell foams and closed-cell foams: if a structure only contains solid edges of cells, then it is a three-dimensional open-cell foam; and, if solid edges and

faces of cells are both contained in a foam, then it is called a three-dimensional closed-cell foam. Actually in the real world, a foam can contain both open- and closed-cell foam, when the cell face of closed-cell foam are blown away, it becomes an open-cell foam.

2.2.2 Cell shape

Gibson and Ashby (1997) have summarized the types of regular cell shapes. In two dimensional honeycombs, the unit cells have several types of shapes, including triangle, square, and hexagon and so on. For a given type of cell shape, each of the unit cells is connected by their edges and they can completely fill the plane. In three dimensional foams, there are also several types of shapes, such as tetrahedron, triangular prism, rectangular prism, hexagonal prism, octahedron, tetrakaidecahedron, and so on. The identical cells are connected by the cell faces and edges, and they can completely fill the 3D space. Foams with different cell shapes exhibit different mechanical properties.

2.2.3 Relative density

Relative density (ρ_0) is the most important characteristic of cellular solids. It is defined as the density of a foam (ρ^*) divided by the density of the solid materials (ρ_S), and is given as

$$\rho_0 = \frac{\rho^*}{\rho_S} \tag{2.1}$$

The relative density of most cellular solids is generally smaller than 0.3, sometimes smaller than 0.003 (Gibson and Ashby, 1997). Cellular solids can be divided into low-density and high-density. For low-density honeycombs and foams, their relative densities are less than 0.2 (Gibson and Ashby, 1997) and 0.1 (Mills, 2007b), respectively. The relative density of cellular solids depends directly on their cell structure.[2] It greatly influences the mechanical properties of two-dimensional honeycombs and three-dimensional open-cell and closed-cell foams.

2.3 Mechanical models of 2D honeycombs and 3D foams

2.3.1 Models of 2D honeycombs

Honeycombs can be classified as regular and irregular according to their cell shape (Gibson and Ashby, 1997). Regular honeycombs could have different regular cell shapes, such as triangle, square, and hexagon. It is easy to manufacture regular honeycombs. There are natural honeycombs, such as a bee's honeycomb. In nature, honeycomb materials are more likely to have irregular cells. Two-dimensional random irregular Voronoi tessellations[3] are often used as geometrical models of irregular honeycombs. In a 2D Voronoi tessellation, the space is divided into convex polygons

[2] The variation of the relative density has the relation with cell edges and faces thickness (Gibson and Ashby, 1997).

[3] The original model of 2D Voronoi tessellations was made by Voronoi.

or cells (Gibson and Ashby, 1997, Zhu et al., 2001b). Voronoi tessellations can be constructed according to following assumptions (Boots, 1982, Zhu et al., 2001b). Figure 2.2 (c) shows the schematic about the cell growth.

1) All the nuclei of the cells occur simultaneously;
2) During the cell growth process, the locations of all the nuclei remain unchanged;
3) For each cell, the growth rate remains the same rate in all directions;
4) The linear growth rate is the same for all the cells; and,
5) Growth ceases whenever and wherever a cell comes into contact with a neighbouring cell.

Based on the above assumptions, Chen et al. (1999) and Zhu et al. (2001a, 2001b) have generated periodic Voronoi honeycombs. Figure 2.2 shows an example of random periodic Voronoi honeycomb, which is constructed by the software developed by Zhu et al. (2001a, 2001b, 2006). The cell edges of periodic Voronoi honeycombs are assumed as uniform. The periodic Voronoi model is selected from the middle small square of a large square which is consisted by nine same sized small squares. In each of the small square, the Voronoi model is the same, so this Voronoi model can be seen as periodic and the representative volume element of the honeycomb. Then the characteristic properties of this periodic Voronoi model can represent that of the whole irregular honeycomb. $L \times L$ is the size of the unit random irregular honeycomb model. In this model, the degree of cell regularity (α), the number of complete cells (N), and the relative density (ρ_0) are the three typical parameters to define the structural model of a random periodic Voronoi honeycomb.

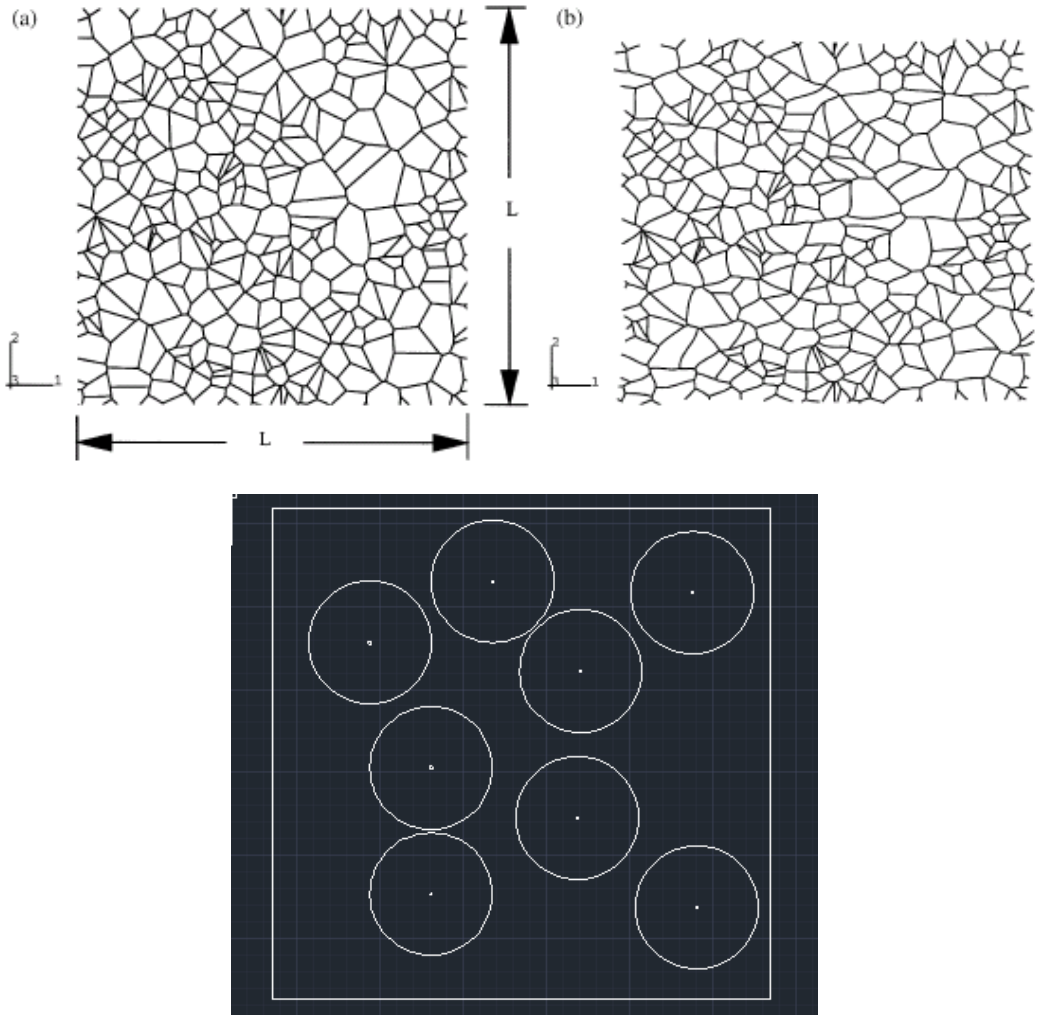

(c)

Figure 2.2. (a) An undeformed random Voronoi honeycomb (N =300, α =0.0). (b) The deformed structure with periodic boundary conditions (Zhu et al., 2001a); (c) the schematic about the cell growth for eight nuclei.

The degree of cell regularity, α, is defined as (Zhu et al., 2001a, Zhu et al., 2001b, Zhu et al., 2006, Zhu et al., 2013)

$$\alpha = \frac{\delta}{d_n} \tag{2.2}$$

where δ is the minimum distance between any two neighbouring nuclei in a random irregular honeycomb, and d_n is the distance between two neighbouring nuclei in a

perfectly regular hexagonal honeycomb with the same number of complete cells, and is given as (Zhu et al., 2001a, Zhu et al., 2001b, Zhu et al., 2006, Zhu et al., 2013)

$$d_n = \sqrt{\frac{2A_0}{N\sqrt{3}}} \tag{2.3}$$

where A_0 is the area of the unit square (i.e. $L \times L$), and N is the total number of complete cells in the unit square area. From Equation (2.2), the ratio of δ to d_n is the degree of the cell regularity. Figure 2.3 shows the structural models of random periodic Voronoi honeycombs with different degrees of cell regularity.

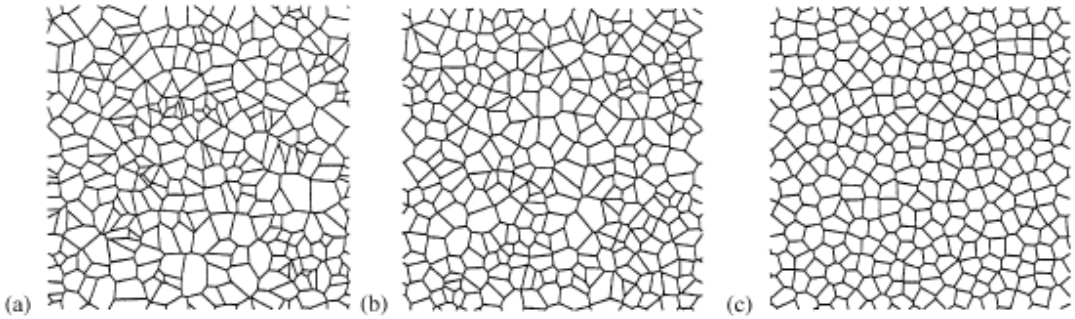

Figure 2.3. Voronoi samples with 300 cells and varying degrees of regularity: (a) α = 0.1, (b) α = 0.4 and (c) α = 0.7 (Zhu et al., 2001a).

The third parameter is the relative density of random periodic Voronoi honeycombs, which is given by (Chen et al., 1999, Zhu et al., 2000, Zhu et al., 2001a, Zhu et al., 2013)

$$\rho_0 = (h_0 \sum_{k=1}^{M} l_{0k}) / L^2 \tag{2.4}$$

where l_{0k} are the cell wall lengths, L is the side length of the unit random periodic honeycomb (as shown in Figure 2.2), h_0 is the thickness of the cell wall, and M is the total number of the cell walls.

Zhu et al. (2001a) have shown that the in-plane mechanical properties of random irregular Voronoi honeycombs are isotropic under linear elastic regime. Silva et al. (1995) also got approximately the same results for non-periodic Voronoi honeycombs. However, Bouakba et al. (2012) described a mathematical formulation for a novel Voronoi-type cellular structure with anisotropic mechanical characteristics. In this case, Bouakba applied slide boundary conditions, which make the structure stiffer.

2.3.2 Models of 3D open-cell and closed-cell foams

The perfectly regular foam with tetrakaidecahedron cells (i.e. the Kelvin foam) (Zhu et al., 1997a, Mills, 2007b) is often used as the structural or mechanics model for three dimensional foams. In addition, the Gibson and Ashby model is also often used as a regular foam because of its simple structure (Gibson and Ashby, 1997). Three dimensional foams can include open-cell and closed-cell foams (Gibson and Ashby, 1997).

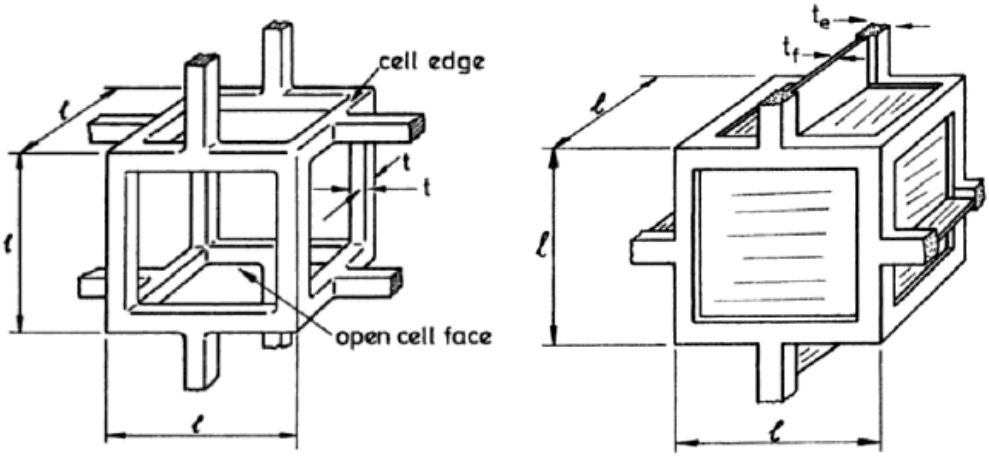

(a) (b)

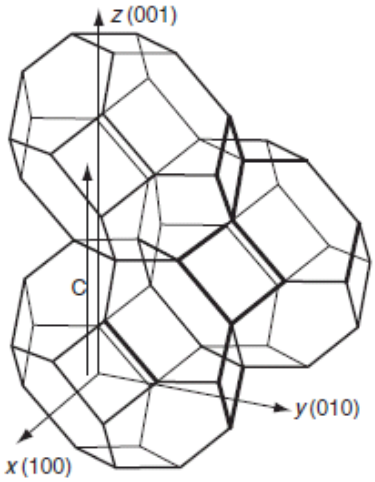

(c)

Figure 2.4. (a) Gibson and Ashby model for open-cell foams (Gibson and Ashby, 1997), (b) Gibson and Ashby model for closed-cell foams (Gibson and Ashby, 1997), and (c) Kelvin model (Mills, 2007b).

There are two strategies to generate the structural or mechanics models for irregular foams (Mills, 2007b). The first one is to generate a random foam structure and check if the cell statistics are similar to foams. The second strategy is to measure the vertex positions of a section of real foam, and then use these data to construct a computer model. For the first strategy, the usual way to do it is using Voronoi tessellations. Mills (2007b) concluded the assumptions of modelling 3D Poisson Voronoi tessellations model, which are similar to those for 2D Voronoi honeycombs models, as follows:

1) All bubble nuclei occur at random positions simultaneously;
2) The growth rate of the bubbles is constant and independent of direction until they come to contact with neighbouring bubbles; and,
3) During this process, the centroid of each bubble does not move.

Based on these assumptions, Zhu et al. (2000), and Zhu and Windle (2002) have

constructed periodic random irregular Voronoi foams. Similarly to the construction of 2D Voronoi tessellations, once the first nucleation point has been created, the distances between each subsequent random point and the existing nuclei should be larger than a minimum distance (δ). The cell edges of periodic Voronoi foams are assumed as uniform. The periodic Voronoi model is selected from the middle small cube of a large cube which is consisted by 27 same sized small cube. In each of the small cube, the Voronoi model is the same, so this Voronoi model can be seen as periodic and the representative volume element of the open-cell foam. Then the characteristic properties of this periodic Voronoi model can represent that of the whole irregular open-cell foam. The degree of cell regularity α is defined as (Zhu et al., 2000, Zhu and Windle, 2002)

$$\alpha = \frac{\delta}{d_n} \tag{2.5}$$

where δ is the minimum distance between any two neighbouring nuclei in a random irregular foam, and d_n is the distance between two neighbouring nuclei in a perfectly regular body centered cubic (BCC) foam with the same number of tetrakaidecahedral cells, and is given as (Zhu et al., 2000, Zhu and Windle, 2002)

$$d_n = \frac{\sqrt{6}}{2}\left(\frac{V_0}{\sqrt{2}N}\right)^{\frac{1}{3}} \tag{2.6}$$

where V_0 is the volume of a unit cube, and *N* is the total number of complete cells in the unit cube. From Equation (2.5), for a regular lattice with identical tetrakaidecahedral cells, δ is equal to d_n and the degree of the cell regularity is 1.

All of the cell struts are assumed to have the same uniform cross-section. Thus, the relative density of a random irregular periodic Voronoi open-cell foam is given by (Zhu et al., 2000, Zhu and Windle, 2002)

$$\rho_0 = (A\sum_{k=1}^{M} l_{0k}) / V_0 \tag{2.7}$$

where l_{0k} are the cell strut lengths, A is the area of the cell strut cross-section, and M is the total number of the cell struts.

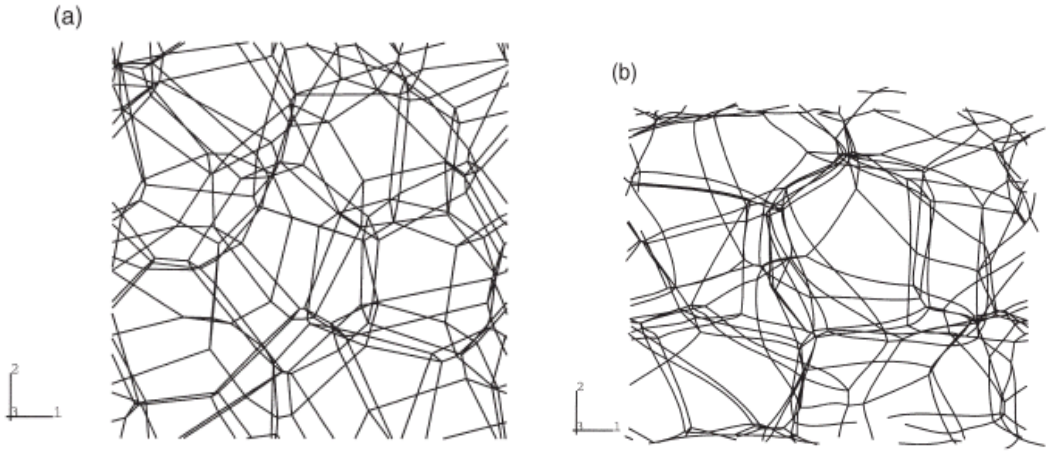

Figure 2.5. (a) An undeformed random Voronoi foam with 27 complete cells. (b) The deformed structure with periodic boundary conditions (Zhu et al., 2000).

Figure 2.5 shows an example of an undeformed and the deformed periodic random Voronoi open-cell foams (Zhu et al., 2000). Shulmeister et al. (1998) modelled the mechanical properties of open-cell foams by random Voronoi models and finite element analysis. However, their models are not periodic and thus they were not able to use periodic boundary conditions in their simulations. Roberts and Garboczi (2002) also generated a 3D Voronoi model of open-cell foams with a relative density of 0.05. Their structure is based on the regular BCC lattices of cells (i.e. the BCC or Kelvin

foam). The nuclei positions were created from the centres of the BCC cells by introducing a random offset. With the increasing amplitude of the random offset, the proportion of random cells in the cube was increased from 0% to 58% (Mills, 2007b). Given that all of the struts on boundary faces are perpendicular to the boundary in the model of Van der Burg et al. (1997), their structural model is consequently stiffer than the regular Kelvin foam (Zhu et al., 1997a). Boundary conditions have a large influence on the structure's mechanical response (Chen et al., 1999, Zhu et al., 2001a, Zhu and Windle, 2002). Van der Burg et al. (1997) randomized foams based on BCC (body centered cubic) and FCC (face centered cubic) lattices. According to their prediction, the Young's modulus rises by 46% with the increase of randomness (Van der Burg et al., 1997, Mills, 2007b). Gan et al. (2005) generated irregular open-cell foams by offsetting the position of the vertex of the regular Kelvin foam, and thus found that the Young's modulus obtained from such irregular foams is very close to that of a regular Kelvin foam. Kraynik et al. (2003) generated a random monodisperse foam, which started from Voronoi partitions of randomly packed spheres. The geometry of the random monodisperse foam is closer to that of real foams than the initial Voronoi models (Kraynik et al., 2003, Mills, 2007b). However, it also differs from polymer foams. Zhu et al. (1999) found that the total edge length of irregular open-cell foams increases with the degree of cell irregularity and that the Young's modulus of a highly irregular open-cell foam is nearly 50% higher than that of a regular Kelvin foam. The compressive stress-strain response of highly irregular open-

cell foams is more non-linear than the Kelvin model (Zhu and Windle, 2002, Mills, 2007b). However, the lateral strain results, which were predicted by FEA modelling, are better than the Kelvin model (Mills, 2007b).

Reberts and Garboczi (2001) created a closed-cell Voronoi foam model. The edges of this model had circular cross sections. The lowest relative density of the models was 0.104 and the predicted Young's modulus was 10% higher than the Kelvin model.

2.4 Elastic properties of 2D honeycombs and 3D foams

There are several ways to obtain the mechanical properties of cellular materials. Gibson and Ashby (1997) obtained the properties of honeycombs or foams as functions of the relative density by dimensional analysis, and then used experimental data to fit these functions and hence to determine the constants or coefficients in the functions (Gibson and Ashby, 1982, Gibson et al., 1982 , Gibson and Ashby, 1997). The second way is to use the finite element method or structural mechanics to analyse the repeating unit cells of regular honeycombs or foams (Warren and Kraynik, 1987, Warren et al., 1989, Masters and Evans, 1996, Zhu et al., 1997a, Zhu et al., 1997b, Mills and Zhu, 1999, Zhu and Mills, 1999, Zhu and Mills, 2000, Zhu and Melrose, 2003, Zhu, 2010b, Zhu et al., 2012b). The elastic properties or the stress and strain relations of honeycombs or foams can be obtained as functions of the honeycomb or foam relative density and the Young's modulus of the material from which the foam is produced. Reconstructing the exact structure of a real honeycomb or foam is another

way to do this. The mechanical properties of such real structural models can be obtained using finite element method analysis (Drenckhan and Langevin, 2010, Bouakba et al., 2012, Silva et al., 1995, Silva and Gibson, 1997, Zhu et al., 2000, Zhu et al., 2001a, Zhu et al., 2006, Zhu and Windle, 2002, Zhu et al., 2014b, Zhu et al., 2013, Jebur et al., 2011). The following sections will briefly review the mechanical properties of 2D honeycombs and 3D foams with cells from macro-meter scale, down to micro- and nano-meter scales.

2.4.1 The elastic properties of macro-sized 2D honeycombs and 3D foams

According to the above descriptions, the cell structure, cell shape, relative density, and material properties all have an influence on the mechanical properties of two-dimensional honeycombs and three-dimensional foams. The mechanical properties of these materials may be different in different directions.

2.4.1.1 The elastic properties of macro-sized 2D honeycombs

Many researchers have studied the elastic properties of honeycombs. Gibson et al. (1982), and Gibson and Ashby (1997) derived the in-plane (If the cross section plane of the honeycomb is the *xy* plane, then the xy plane is in-plane, the other planes can be seen as out-of-plane.) elastic constants for regular honeycombs with cell walls of

uniform thickness by considering cell wall bending as the sole deformation mechanism. Warren and Kraynik (1987) also studied the in-plane elastic constants, they took cell wall bending and stretching as the main deformation mechanisms. Master and Evan (1996) made a theoretical analysis on the in-plane elastic constants of honeycombs. Silva et al. (1995) and Zhu (2010b) found the closed form in-plane elastic constants of regular honeycombs with the consideration of cell wall bending, stretching or compression, and transverse shear. Sun and Pugno (2013) analyzed in-plane stiffness of hierarchical honeycombs and considered cell wall bending, stretching or compression, and also shear deformation. Generally speaking, the in-plane deformation of honeycombs involves cell wall bending, transverse shear and axial stretching or compression, and the dominant deformation mechanism is the plane-strain bending of the cell walls and not plane-stress bending.

The out-of-plane mechanical properties of hexagonal honeycombs have also been studied by many people (Deqiang et al., 2010, Doyoyo and Mohr, 2003, Khan et al., 2012, Lin et al., 2013, Meraghni et al., 1999, Pan et al., 2006, Xu et al., 2012, Zhu and Chen, 2011). Zhu and Chen (2011) obtained all five of the independent elastic constants of hexagonal honeycombs with cell walls of either uniform or non-uniform thickness. Because almost all of the cellular solids have orthotropic symmetry, including the honeycombs and open-cell foams, it means that there are three perpendicular mirror planes in the structure. Then the independent compliances of the stiffness matrix are reduced to nine ($S_{11}, S_{12}, S_{13}, S_{22}, S_{23}, S_{33}, S_{44}, S_{55}, S_{66}$) (Gibson

and Ashby, 1997). For the regular hexagonal honeycomb, because it has a plane of isotropy, so it can be found that the relations between the compliances matrix ($S_{11} = S_{22}$, $S_{44} = S_{55}$, $S_{13} = S_{23}$), then the independent elastic constants are reduced from nine to five (Gibson and Ashby, 1997, Kim and Christensen, 2000). They are E_1, v_{12}, E_3, v_{31}, G_{31}. E_1 is the in-plane Young's modulus, v_{12} is the in-plane Poisson's ratio, E_3 is the out-of-plane Young's modulus, v_{31} is the out-of-plane Poisson's ratio, and G_{31} is the out-of-plane shear modulus. Zhu and Chen (2011) considered the in-plane deformation of honeycombs contains a combination of cell wall bending (which is plane-strain deformation), transverse shear and axial stretching/compression, and assumed a unit of the connected three half cell walls as a representative volume element to analyse the characteristic properties of regular hexagonal honeycomb. This is mainly because a regular hexagonal honeycomb can be constructed by thousands of the connected three half cell walls (likes a periodic unit cell), so this part can be seen as a representative volume element of regular hexagonal honeycomb, and the elastic properties of this part can be considered as that of regular hexagonal honeycomb. Zhu and Chen (2011) applied a global in-plane compressive stress to the representative volume element of regular hexagonal honeycomb in the *x* direction, obtained the displacements and strains in the *x* and *y* direction, and then derived the in-plane Young's modulus and Poisson's ratio. Zhu and Chen (2011) assumed that the size of the honeycomb core is much larger than the cell length, and applied a shear loads on the area of the representative volume element, then according to their obtained the

shear stress and strain, the in-plane shear modulus of the honeycomb can be found. Generally, the out-of-plane Young's modulus of a honeycomb is proportional to the Young's modulus of the solid material, and the out-of-plane Poisson's ratio of a honeycomb is the same as the Poisson's ratio of the solid material (Gibson and Ashby, 1997, Kim and Christensen, 2000). For regular hexagonal honeycombs with uniform cell walls, it is easily to obtain the relationship between the relative density (ρ) and the thickness (h), the length of cell walls (l) (i.e. the equation is $\rho = \frac{2h}{\sqrt{3}l}$ (Zhu and Chen, 2011)). Using the classical structural mechanics, the five independent elastic properties of honeycombs can be obtained as functions of the bending stiffness D_b, the transverse shear stiffness D_S, and the axial stretching or compression stiffness D_C. They can be easily converted to be functions of the honeycomb relative density. For the detailed derivation of the five independent elastic constants, readers can refer to Zhu and Chen (2011) and Zhu (2010b). The five independent elastic constants of regular hexagonal honeycomb are obtained as (Zhu and Chen, 2011)

$$\overline{E_1} = \frac{1\text{-}\nu_S^2}{1.5E_S\rho^3}\frac{16\sqrt{3}D_bD_SD_C}{D_SD_Cl^3b+12D_bD_Clb+36D_SD_blb} = \frac{1}{1+(\frac{4.05}{1-\nu_S^2}+\frac{1.8\nu_S}{1-\nu_S^2})\rho^2} \tag{2.8}$$

$$\nu_{12} = \frac{D_SD_Cl^2+12D_bD_C-12D_bD_S}{D_SD_Cl^2+12D_bD_C+36D_bD_S} = \frac{1+\frac{(1.05+1.8\nu_S)\rho^2}{(1-\nu_S^2)}}{1+\frac{(4.05+1.8\nu_S)\rho^2}{(1-\nu_S^2)}} \tag{2.9}$$

$$\overline{E_3} = \frac{E_3}{E_S\rho} = 1 \tag{2.10}$$

$$\overline{G_{31}} = \frac{G_{31}}{G_S \rho} = \frac{1}{2} \tag{2.11}$$

$$\nu_{31} = \nu_S \tag{2.12}$$

where $\overline{E_1}$, $\overline{E_3}$ and $\overline{G_{31}}$ are the non-dimensional in-plane Young's modulus, out-of-plane Young's modulus and out-of-plane shear modulus, respectively. E_S, G_S and ν_S are the Young's modulus, shear modulus and Poisson's ratio of the solid material, ρ is the relative density of the regular hexagonal honeycomb. D_b, D_S and D_C are the bending, transverse shear and axial stretching/compression rigidities of macro-sized cell walls or cell struts, respectively. *l* is the cell wall length, *b* is the cell wall width. The reason for obtaining the non-dimensional values is to diminish the effects of Young's modulus of the solid material and the relative density. The non-dimensional results are thus more useful and easily to be compared with other results. The obtained $\overline{E_1}$ and ν_{12} are the same as those of Zhu (2010b) and slightly different from those of Silva et al. (1995) because they treated all the in-plane deformation as the plane-stress deformation. When the relative density is very small, the obtained $\overline{E_1}$ is close to that of Gibson and Ashby (1997). The obtained $\overline{E_3}$, $\overline{G_{31}}$ and ν_{31} are the same as the previous results (Gibson and Ashby, 1997, Kim and Christensen, 2000). For macro-sized honeycombs, all of elastic constants are independent of the cell size (i.e. the effects of the strain gradient, surface elasticity and initial strain are absent).

2.4.1.1.1 Isotropic properties of regular and random Voronoi honeycombs

The in-plane elastic properties of regular honeycombs are isotropic (Gibson and Ashby, 1997, Masters and Evans, 1996). Masters and Evans (1996) also found that re-entrant cell honeycombs are highly anisotropic, even considering square symmetric the off-axis properties. For irregular Voronoi honeycombs, Zhu et al. (2001a) obtained numerical results (as shown in Table 2.1) to demonstrate the isotropic elastic properties. It can be seen from Table 2.1 that the results of the non-dimensional Young's modulus in the *x* direction and *y* directions are almost the same, and they meet the relationship between the shear modulus, Young's modulus and Poisson's ratio for an isotropic material ($G = \frac{E}{2(1+\nu)}$).

Model No.	$\bar{E}_1^*$	$\bar{E}_2^*$	ν_{12}^*	ν_{21}^*	$\bar{G}^*$
1	1.70486	1.70476	0.9996	0.9995	0.398969
2	1.91737	1.91733	0.9995	0.9995	0.469870
3	1.82772	1.82783	0.9995	0.9996	0.488761
4	2.09751	2.09744	0.9995	0.9994	0.509333
5	1.74359	1.74360	0.9995	0.9996	0.439977
6	1.88401	1.88423	0.9995	0.9996	0.528507
7	1.97268	1.97271	0.9995	0.9995	0.500681
8	1.77014	1.77016	0.9995	0.9995	0.446948
9	1.99425	1.99433	0.9995	0.9995	0.520716
10	1.84976	1.84977	0.9995	0.9995	0.467092
11	1.77813	1.77796	0.9996	0.9995	0.396446
12	1.73963	1.73974	0.9995	0.9996	0.465712
13	1.83070	1.83062	0.9996	0.9995	0.434138
14	1.88923	1.88925	0.9995	0.9995	0.478929
15	1.56059	1.56056	0.9996	0.9996	0.381688
16	1.97552	1.97551	0.9995	0.9995	0.492171
17	2.08766	2.08760	0.9995	0.9995	0.508948
18	1.92964	1.92949	0.9995	0.9995	0.443840
19	1.81511	1.81511	0.9995	0.9995	0.453753
20	1.58177	1.58184	0.9996	0.9996	0.416200
Mean	1.847492	1.847492	0.999525	0.999525	0.4621339
Std. dev.	0.140839	0.140832	4.33085E-5	5.36210E-5	4.15508E-02

Table 2.1. The non-dimensional Young's modulus, shear modulus and Poisson's ratio

of 20 isotropic, periodic Voronoi honeycombs with relative density 0.01 and regularity parameter α =0.0, as determined by FEA (Zhu et al., 2001a).

2.4.1.1.2 Boundary conditions

According to Chen et al. (1999), three types of boundary conditions are often used in computer simulations. The first one is the mixed boundary condition, as shown in Figure 2.6 (a). The second one is the prescribed displacement boundary condition, as given in Figure 2.6 (b). Finally, the third one is the periodic boundary condition, as shown in Figure 2.6 (c). The mixed boundary conditions fix the normal displacement on each edge of the mesh, and ignore the tangential force and the bending moment at each node of the boundary. On the previous research works, many researchers have used mixed boundary conditions (Silva and Gibson, 1997, Silva et al., 1995, Triantafyllidis and Schraad, 1998). However, due to neglect of the bending moment,

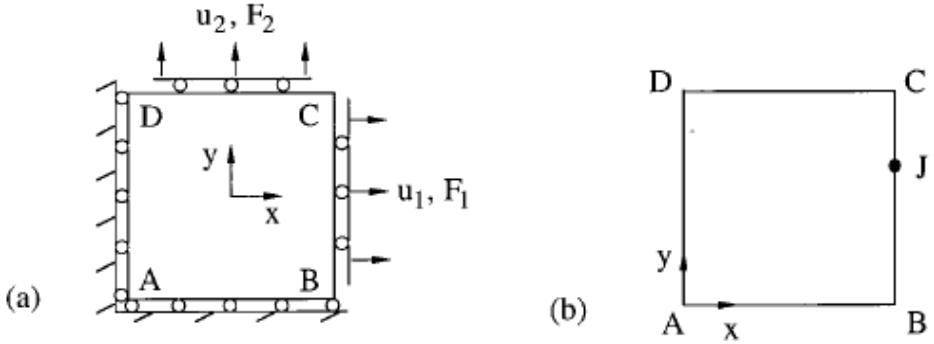

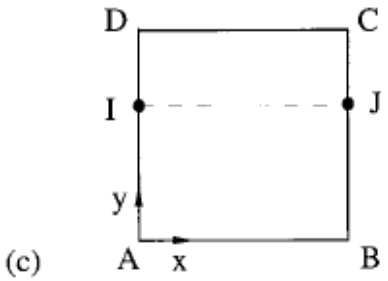

Figure 2.6. Three different types of boundary condition: (a) mixed boundary conditions, (b) prescribed displacement boundary conditions, and (c) periodic boundary conditions (Chen et al., 1999).

the struts at the boundaries have free rotations and this leads to underestimating the effective Young's modulus. Furthermore, the mixed boundary conditions also underestimate the yield strength (Chen et al., 1999). The representative of prescribed displacement boundary conditions is sticking grip. This type of boundary condition imposes very strong restrictions and it is suitable for solving problems of plastic deformation. Periodic boundary conditions are more suitable for most mechanics analyses. When modelling the in-plane compression of a periodic Voronoi honeycomb in the *y* direction, the periodic boundary conditions (Zhu et al., 2001a, Zhu et al., 2006) assume that the expansion between the corresponding nodes on the opposite edges of the periodic model is the same in the *x* and *y* directions, and the corresponding nodes on the opposite edges of the model have the same displacements in other directions and have the same rotation. Zhu et al. (2001a) compared the mixed boundary conditions and the periodic boundary conditions using regular honeycomb models, and demonstrated that the periodic boundary conditions are more suitable than the mixed boundary conditions to be used in solving problems about the elastic properties of honeycombs. Zhu et al. (2006) and Alsayednoor et al. (2013) used the periodic

boundary conditions to analyze the large strain compressive response of 2D periodic honeycombs.

2.4.1.1.3 Linear elastic properties (under small deformation)

Gibson and Ashby (1997) obtained the in-plane linear-elastic properties of regular honeycombs. Their results show that a larger honeycomb relative density will lead to a stiffer and stronger honeycomb. Silva et al. (1995) used non-periodic Voronoi models to simulate the mechanical behaviour of honeycombs. Zhu et al. (2001a) used periodic Voronoi models and periodic boundary conditions to predict the elastic properties of honeycombs. Zhu et al (2001a) also found that highly irregular honeycombs have Young's modulus and shear modulus about 25% larger than those of the perfect regular honeycombs. Increasing the cell regularity leads to a decrease of the effective Young's modulus and the shear modulus, and an increase of the bulk modulus (as shown in Figure 2.7).

Relative density also affects the elastic properties of random Voronoi honeycombs. Generally, the larger the relative density, the smaller the non-dimensional in-plane Young's modulus and the in-plane Poisson's ratio.

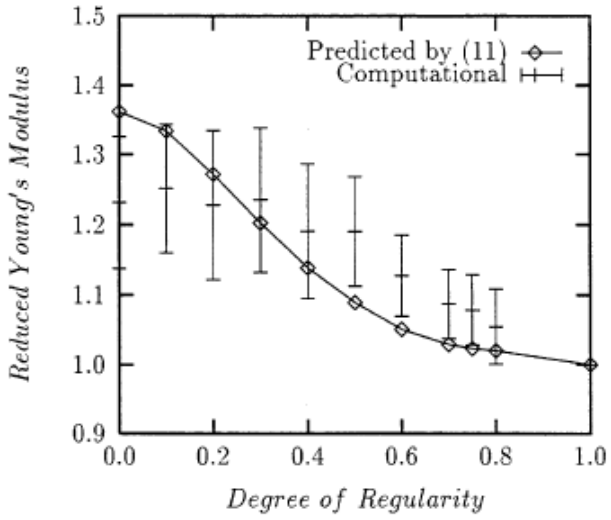
Predicted by (11)
Computational
Reduced Young's Modulus
Degree of Regularity
1.5
1.4
1.3
1.2
1.1
1.0
0.9
0.0
0.2
0.4
0.6
0.8
1.0

(a)

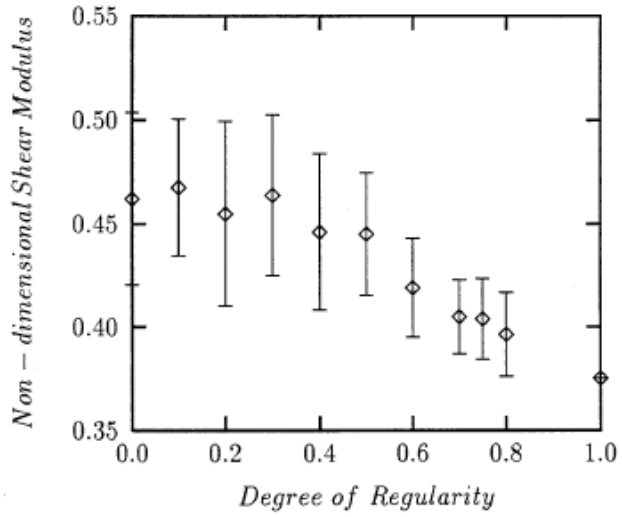
Non − dimensional Shear Modulus
Degree of Regularity
0.55
0.50
0.45
0.40
0.35
0.0
0.2
0.4
0.6
0.8
1.0

(b)

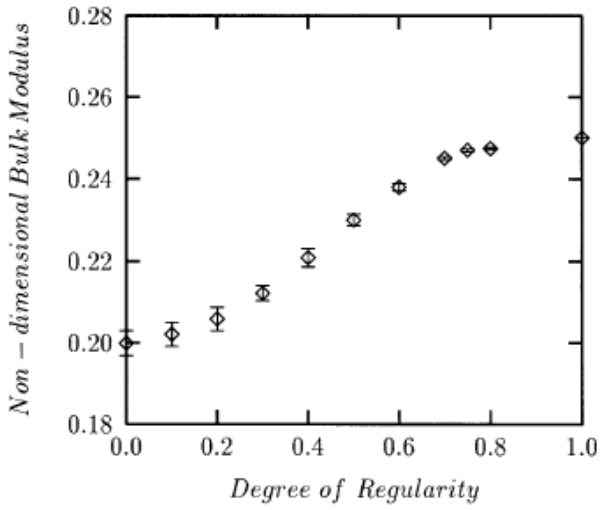

(c)

Figure 2.7. Effects of cell regularity (a) on the reduced Young's modulus, (b) on the non-dimensional shear modulus, and (c) on the non-dimensional bulk modulus of random Voronoi honeycombs having a constant relative density 0.01 (Zhu et al., 2001a).

2.4.1.1.4 Non-linear elastic properties (under large deformation)

The in-plane compression of regular honeycomb structure has been studied by many researchers (Gibson and Ashby, 1982, Masters and Evans, 1996, Papka and Kyriakides, 1994, Warren and Kraynik, 1987, Zhu and Mills, 2000). Gibson et al. (1982), and Gibson and Ashby (1997) conducted a theoretical analysis and obtained the in-plane compressive and tensile stress and strain responses for regular honeycombs, as shown in Figure 2.8. In compression, the stress is initially proportional to the compressive strain in the linear-elastic regime, and then remains at nearly a constant plateau because of cell wall buckling, and goes into a final regime with a sudden steeply rising stress because of cell wall contact. The in-plane tensile deformation of honeycombs is

very different from the compressive deformation. The cell walls are initially bent, and they are then stretched and the tangent modulus increases with the tensile deformation.

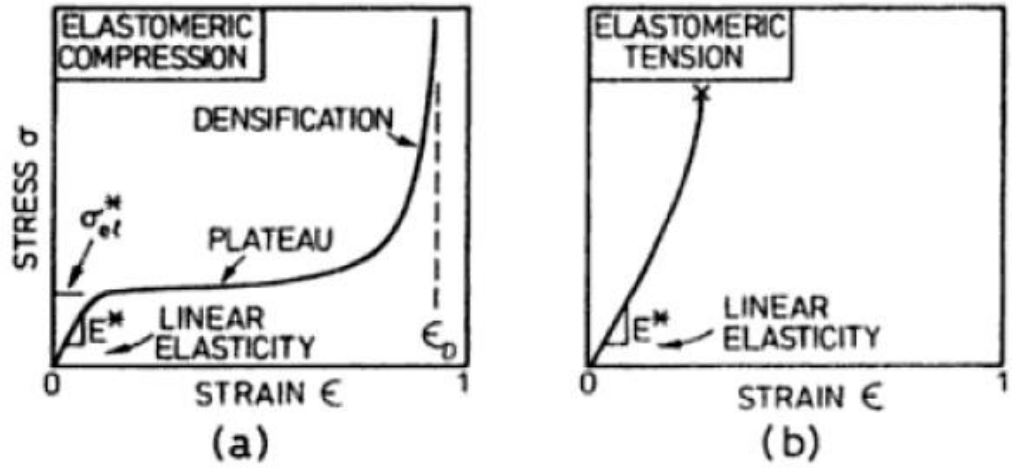

Figure 2.8. (a) Compressive stress-strain curves for elastomeric honeycomb, and (b) tensile stress-strain curves for elastomeric honeycomb (Gibson and Ashby, 1997).

Zhu et al. (2006) found that, when compared with a more regular honeycomb, a highly irregular honeycomb has a larger tangential modulus at low compressive strain, and then sustains a lower compressive stress at high compressive strain (as shown in Figure 2.9 (a)). Alsayednoor et al. (2013) obtained similar results: they found that when the strain is up to 80%, a more irregular honeycomb trends to be softer than a less regular one. The compressive stress and strain relation in the *y* direction of a perfectly regular honeycomb, obtained by Zhu and Mills (2000), which may be taken as the approximate upper bond for the compressive response of a random irregular honeycomb (Zhu et al., 2006). The Poisson's ratio of irregular honeycombs reduces with the increase in cell irregularity and the honeycomb compressive strain (as shown in Figure 2.9 (b)). Zhu et al (2006) obtained an approximate linear relationship

between the maximum cell wall bending strain and the overall honeycomb compressive strain, which can be used to predict the yielding of the cell walls when an irregular honeycomb undergoes in-plane compression.

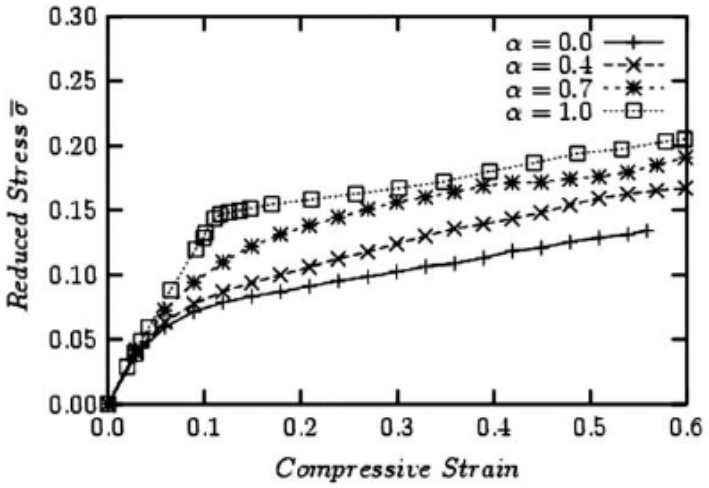

(a)

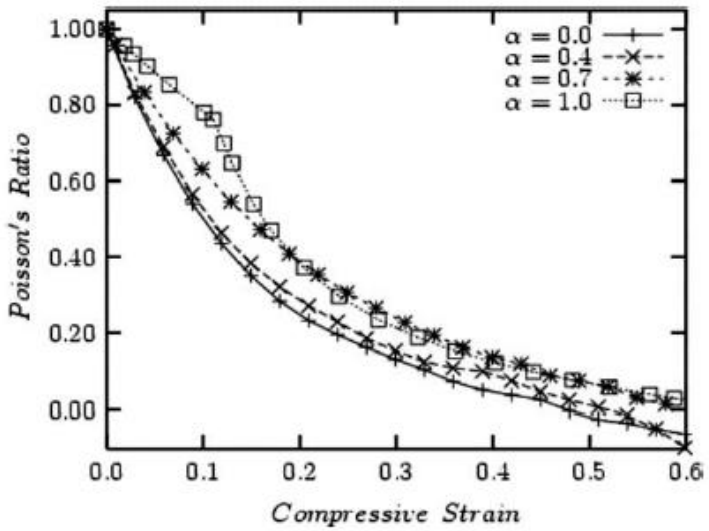

(b)

Figure 2.9. Effects of cell irregularity on the mean (a) reduced stress–strain relationships, and (b) Poisson's ratio results for Voronoi honeycombs (Zhu et al., 2006).

2.4.1.2 The elastic properties of macro-sized 3D foams

The elastic properties of macro-sized 3D foams depend on whether the cells of the foams are open or closed. The following sections will summarize the main results about the elastic properties of 3D foams.

2.4.1.2.1 Isotropic properties of regular and random Voronoi foams

Most of man-made and natural foams are anisotropic, but the structure of foams is usually represented by a regular unit, such as tetrakaidecahedron cells (Gibson and Ashby, 1997). Zhu et al. (1997a) analyzed a perfectly regular Kelvin model foam with uniform cell struts of different types of cross-section. They have obtained the analytic solutions for all the three independent elastic constants and found that a perfectly regular Kelvin foam is nearly isotropic. Warren and Kraynik (1997) also studied the elastic properties of the open-cell Kelvin foams, and found that the shear modulus in different directions are nearly equal and proved that the kelvin foam is nearly isotropic.

Zhu et al. (2000), and Zhu and Windle (2002) developed a software to construct periodic random irregular Voronoi tessellations and to study the mechanical properties of open-cell foams. As shown in Table 2.2, Zhu et al. (2000) found that the mean results of the non-dimensional Young's modulus of random irregular Voronoi open-cell foams in three directions are very similar, and that the Young's modulus, shear modulus and the Poisson's ratio satisfy the relation $G = \frac{E}{2(1+\nu)}$. So, a random Voronoi

open-cell foam is nearly isotropic.

Model no.	E_1^*	E_2^*	E_2^*	ν_{21}^*	ν_{23}^*	G_{12}^*
1	1.6915	1.5495	1.6543	0.45962	0.48298	0.5479
2	1.5049	1.5727	1.5281	0.48202	0.46820	0.5230
3	1.3569	1.3258	1.4092	0.49577	0.46004	0.4467
4	1.3367	1.3423	1.2997	0.46609	0.49355	0.4571
5	1.5681	1.3450	1.4675	0.44962	0.50414	0.4916
6	1.4122	1.3323	1.3941	0.46757	0.48779	0.4633
7	1.6535	1.5556	1.5606	0.44811	0.50265	0.5490
8	1.4562	1.4397	1.2987	0.41242	0.53923	0.5117
9	1.2560	1.3002	1.2759	0.48658	0.46991	0.4324
10	1.4516	1.4371	1.5480	0.50925	0.44617	0.4777
11	1.4584	1.4258	1.4798	0.48507	0.47004	0.4838
12	1.3868	1.4280	1.4082	0.48241	0.47064	0.4770
13	1.3631	1.2980	1.3410	0.47211	0.48902	0.4485
14	1.5293	1.5578	1.5715	0.48507	0.46171	0.5213
15	1.2940	1.3719	1.3864	0.51283	0.44210	0.4451
16	1.5350	1.4695	1.4624	0.45206	0.50093	0.5139
17	1.4151	1.4550	1.5529	0.52165	0.42870	0.4738
18	1.3788	1.3366	1.3562	0.47021	0.48826	0.4595
19	1.5137	1.4137	1.3193	0.40762	0.54547	0.5150
20	1.5255	1.3925	1.5349	0.48344	0.47317	0.4849
Mean	1.4544	1.4175	1.4424	0.47248	0.48124	0.4799
Standard deviation	0.11010	0.08641	0.10644	0.02859	0.02839	0.02984

Table 2.2. The non-dimensional Young's modulus, shear modulus and Poisson's ratio of 20 isotropic, periodic Voronoi honeycombs with relative density 0.01 and regularity parameter α =0.7, as determined by FEA (Zhu et al., 2000).

2.4.1.2.2 Boundary conditions

Choosing suitable boundary conditions is one of the most important steps to correctly obtain the elastic properties of regular foams or random irregular periodic Voronoi open-cell foams in the finite element analysis. According to the discussion in Section 2.4.1.1.2, among the three types of the typical boundary conditions, the most suitable choice is the periodic boundary condition. Zhu et al. (2000), and Zhu and Windle (2002) have demonstrated that the prescribed boundary conditions tend to overestimate the elastic properties, while the mixed boundary conditions tend to underestimate the elastic properties of open-cell foams. Therefore, the periodic

boundary conditions are used to obtained the mechanical properties in finite element simulations by most researchers, such as, Warren and Kraynik (1997), and Gong and Kyriakides (2005).

2.4.1.2.3 Linear elastic properties (under small deformation)

Open-cell and closed-cell foams have different deformation mechanisms. Gibson and Ashby (1997) have given a schematic, as shown in Figures 2.10 (a) and (b), that describes the main deformation mechanisms of open-cell and closed-cell foams under compression. Figure 2.10 (a) shows that for a low density open-cell foam, strut bending is the dominant deformation mechanism. With the increase of the foam relative density, stretching or compression and the transverse shear of the cell struts play an increasingly important role in the deformation (Gibson and Ashby, 1997, Warren and Kraynik, 1988, Zhu et al., 2000). The other possible mechanism is the fluid flow inside the cells, as shown in Figure 2.10 (b), which plays an important role in the deformation of closed-cell foams but which has a negligible effect on open-cell foams. In this PhD thesis, the fluid flow is not considered. The deformation mechanisms of closed-cell foams are quite different from those of open-cell foams. In addition to the bending, stretching or compression and transverse shear of the cell struts, the membranes of the cell faces are also stretched, which tends to increase the stiffness of closed-cell foams. Moreover, the compression of the cell fluid also leads to stiffness increasing until the membranes fracture. For open-cell foams, Gibson and

Ashby (1997) took cell strut bending as the sole deformation mechanism in the Gibson and Ashby model (as shown in Figure 2.4 (a)), and then used dimensional analysis to obtain the Young's modulus, shear modulus and Poisson's ratio as

$$E = E_S \rho^2 \tag{2.13}$$

$$G = \frac{3}{8} E_S \rho^2 \tag{2.14}$$

$$v = \frac{1}{3} \tag{2.15}$$

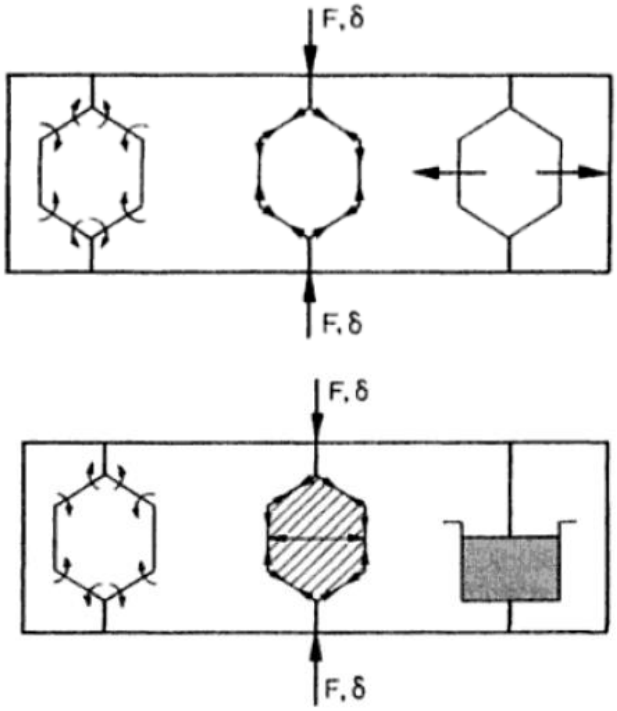

Figure 2.10. The schematic on mechanisms of deformation in foams: (a) open-cell foams with cell wall bending, cell wall axial deformation and fluid flow between cells, and (b) closed-cell foams with cell wall bending, edge compression and membrane stretching, and enclosed gas pressure (Gibson and Ashby, 1997).

where the coefficients are determined by fitting the formulas to the experimental data, E_S is the Young's modulus of the solid material, ρ is the relative density of the open-

cell foam. It can be seen from Equations (2.13 – 2.15) that the dimensionless Young's modulus, shear modulus and Poisson's ratio are 1, 3/8 and 1/3. All are independent of the foam relative density, and there is no micro- and nano-sized effects. Wicklein and Thoma (2005) also considered the elastic Poisson's ratio as a constant that is independent of the relative density. Zhu et al. (1997a) analysed the perfectly regular BCC structure model (Kelvin model), as shown in Figure 2.4 (c). This structure has cubic symmetry and hence has only three independent elastic constants. They considered the strut bending, torsion and stretching as the deformation mechanisms, and obtained the theoretical results of all three of the independent elastic constants/properties (i.e. the Young's modulus, shear modulus and Poisson's ratio) for regular Kelvin open-cell foams with struts of different types of cross-section. Moreover, Zhu et al. (1997a) found that the regular Kelvin foam is nearly isotropic. For the detailed derivation of the three independent elastic constants, readers can refer to Zhu et al. (1997a). The three independent elastic constants of regular open-cell Kelvin foams are obtained as (Zhu et al., 1997a)

$$E_{100} = \frac{6\sqrt{2}D_b D_C}{l^2(D_C l^2 + 12D_b)} = \frac{6\sqrt{2}E_S I}{l^4(1+\frac{12I}{Al^2})} \tag{2.16}$$

$$\frac{1}{G_{12}} = \frac{2\sqrt{2}l^2}{D_C} + \frac{\sqrt{2}l^4}{6D_b}\frac{8D_b + D_t}{5D_b + D_t} = \frac{2\sqrt{2}l^2}{E_S A} + \frac{\sqrt{2}l^4}{6E_S I}(\frac{8E_S I + G_S J}{5E_S I + G_S J}) \tag{2.17}$$

$$\nu_{12} = \frac{1}{2}\frac{D_C l^2 - 12D_b}{D_C l^2 + 12D_b} = \frac{1}{2}(\frac{Al^2 - 12I}{Al^2 + 12I}) \tag{2.18}$$

where E_{100}, G_{12} and ν_{12} are the Young's modulus of foam in the 100 lattice direction,

the shear modulus and Poisson's ratio of foam in lattice axes, respectively. D_b, D_t and D_C are the bending, torsion and axial stretching/compression rigidities of the cell struts, respectively. *l* is the cell wall length. E_S and G_S are the Young's modulus and shear modulus of the solid material. *A* and l are the cross-sectional area and the length of the cell struts. I is the second moment of the cell strut cross-sectional area. J is the polar second moment of the cell strut cross-sectional area. At the macro-meter scale, the obtained three independent elastic constants are independent of the cell size.

For open-cell Kelvin foam with uniform struts of a plateau border cross-section, the theoretical results (Zhu et al., 1997a) reduce to

$$E_{100} = \frac{1.009 E_S \rho^2}{1+1.514\rho} \tag{2.19}$$

$$G_{12} = \frac{0.32 E_S \rho^2}{1+0.96\rho} \tag{2.20}$$

$$\nu_{12} = 0.5\frac{1-1.514\rho}{1+1.514\rho} \tag{2.21}$$

where E_S is the Young's modulus of the solid material, and ρ is the foam relative density. The difference between Equations (2.16 – 2.18) and Equations (2.19 – 2.21) is caused by the shape of edge cross-section. According to Equation (2.7), it can be found that the area of edge cross-section (*A*) and the cell wall length (l) can influence the value of the relative density (ρ) of open-cell foams. Zhu et al. (1997a) found the relationship between the area of a plateau border cross-section (*A*) and the second moment (I), the polar second moment (J) of the cell edge cross-sectional area, then

the influence of the relative density on the independent elastic constants of open-cell Kelvin foam with uniform struts of a plateau border cross-section can be found in Equations (2.19 – 2.21). Equation (2.19) is almost the same as Equations (2.13). The numerical results of Zhu et al. (2000) clearly show that the foam relative density significantly influences the elastic properties of open-cell foams. Figures 2.11 and 2.12 show the dependences of Young's modulus and Poisson's ratio of open-cell foams on the relative density. As can be seen from the theoretical results of Equations (2.19) and (2.21), and the numerical results given in Figures 2.11 and 2.12, both the dimensionless Young's modulus and Poisson's ratio reduce with the increase of the foam relative density.

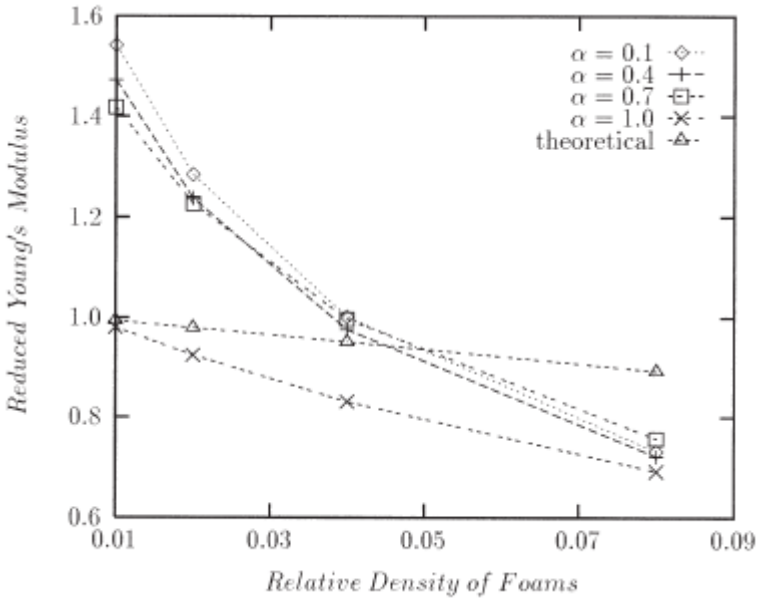

Figure 2.11. Effects of relative density on the reduced Young's modulus of random Voronoi foams with varying degrees of regularity (Zhu et al., 2000).

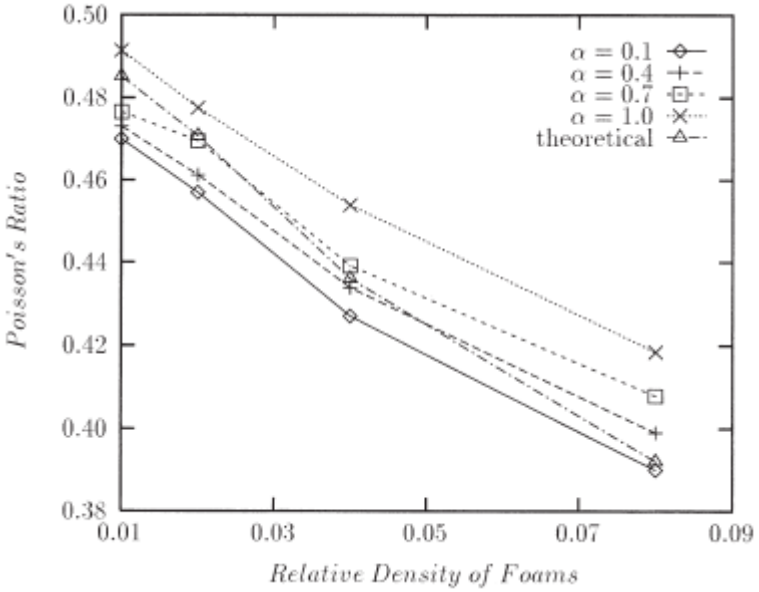

Figure 2.12. Effects of relative density on the Poisson's ratio of random Voronoi foams with varying degrees of regularity (Zhu et al., 2000).

Figure 2.11 shows that the theoretical result of the Young's modulus (Zhu et al., 1997a) of regular open-cell foam is larger than the numerical result (Zhu et al., 2000) of an irregular open-cell foam when the relative density is larger than 5%. This happens because the theoretical analysis (Zhu et al., 1997a) did not consider shear deformation mechanism, while the numerical results (Zhu et al., 2000) are obtained from the Timoshenko beam elements, which have taken the shear deformation mechanism into consideration. Christensen (2000) also studied the elastic behaviour of low density regular cellular solids using an analytical method. Almost all of the researchers (Kwon et al., 2003, Gibson and Ashby, 1997, Zhu et al., 2000, Zhu et al., 1997a, Zhu et al., 1997b, Zhu and Windle, 2002) treated the cell struts as beams and then used either analytical method or finite element method to obtain the mechanical properties of open-cell foams. Many researchers (Gong and Kyriakides, 2005, Gong et al., 2005a,

Gong et al., 2005b, Zhu et al., 2000, Zhu and Windle, 2002) analyzed the mechanical properties of perfectly regular Kelvin and irregular open-cell foams. Sullivan et al. (2008) did the theoretical analysis for an elongated Kelvin open-cell foam.

Finite element simulation results (Gan et al., 2005, Luxner et al., 2007, Van der Burg et al., 1997, Zhu et al., 2000) show that the degree of regularity has a great effect on the Young's modulus of open-cell foams. Zhu et al. (2000) and Van der Burg et al. (1997) found that a highly irregular open-cell foam has a larger Young's modulus than a more regular open-cell foam. Zhu et al. (2000) used periodic random irregular Voronoi foam models and periodic boundary conditions. Van der Burg et al. (1997) used non-periodic Voronoi foam models with prescribed boundary conditions. The geometrical models constructed by Luxner et al. (2007) and Gan et al. (2005) are slightly different from the definition of the Voronoi structure and hence their results are different from those obtained by Zhu et al. (2000) and Van der Burg et al. (1997). Although Li et al. (2006) studied the effects of cell irregularity on the elastic properties, their definition for the regularity is different from that given by Zhu et al (2000) and thus their results are incomparable to those obtained by Zhu et al (2000).

The mechanics analysis for closed-cell foams is more complicated than that for open-cell foams because closed-cell foams contain cell face membranes, as well as because of the effects of the gas or fluid pressure (as shown in Figure 2.10 (b)). Gibson and Ashby (1997), Mills et al. (2009), Mills and Zhu (1999), Roberts and Garboczi (2001), Konstantinidis et al. (2009) and Jebur et al. (2011, 2012) have done some

theoretical, numerical, and experimental analyses on closed-cell foams.

2.4.1.2.4 Non-linear elastic properties (under large deformation)

Linear elastic properties of 3D foams are related to the small deformations. However, polymer foams are elastomer, and are often stretched and compressed to large deformations. Therefore, the non-linear elastic properties of 3D foams are of important practical applications. Gibson and Ashby (1997) have given the schematic compressive and tensile stress-strain curve for elastomeric foams, as shown in Figures 2.13 and 2.14. The compressive stress and strain relationship of 3D foams contains linear elasticity, plateau, and densification regimes, while the tensile stress and strain relationship only contains linear elasticity and cell wall alignment regimes.

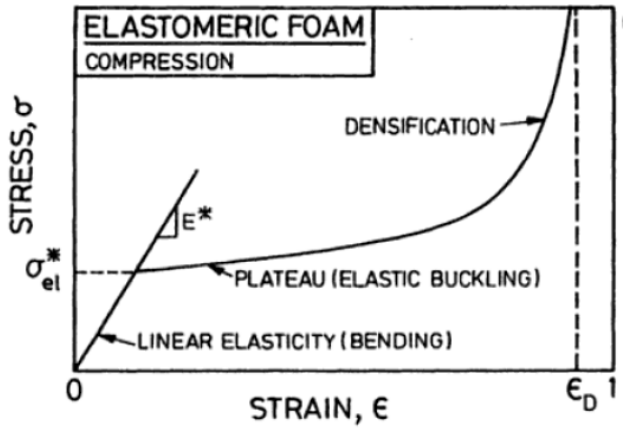

Figure 2.13. Schematic compressive stress-strain curve for elastomeric foams, showing the three regimes of linear elasticity, collapse and densifications (Gibson and Ashby, 1997).

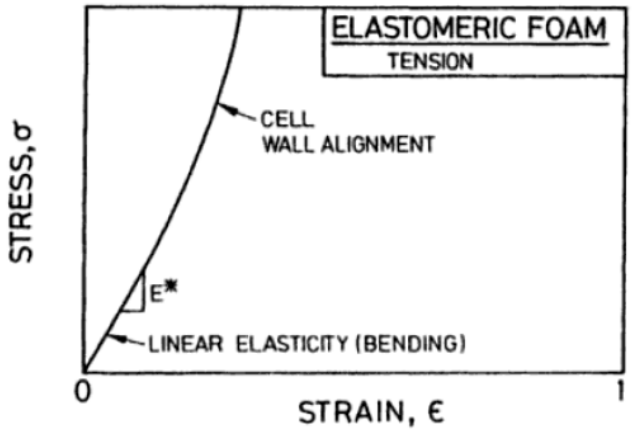

Figure 2.14. Schematic tensile stress-strain curve for elastomeric foams (Gibson and Ashby, 1997).

Many researchers (Laroussi et al., 2002, Mills, 2007a, Shulmeister et al., 1998, Wang and Cuitiño, 2000, Wicklein and Thoma, 2005, Zhang and Lu, 2007, Zhu et al., 1997b, Zhu and Windle, 2002, Luxner et al., 2007, Zhu and Mills, 1999) have done theoretical and numerical analyses on the non-linear elastic properties of 3D foams. Cell regularity has influenced the nonlinear elastic properties of 3D foams. Zhu and Windle (2002) have constructed random periodic Voronoi open-cell foams and then used periodic boundary conditions to perform finite element simulations for the high strain compression behaviour. They found that a more irregular open-cell foam has a larger tangential modulus at a small compressive strain, and a lower effective compressive stress when the compressive strain is large (as shown in Figure 2.15). Shulmeister et al. (1998) also obtained similar results, although their models were not periodic and they did not use periodic boundary conditions. Luxner et al. (2007) simulated the overall stress and strain response of Kelvin model with varying regularity, and showed the same trend as previous results (Shulmeister et al., 1998, Zhu and Windle, 2002).

However, Zhang and Lu (2007) found opposite results about the influence of cell regularity on compressive stress and strain response.

Zhu and Windle (2002) found that relative density has a significant influence on the relation of the stress and strain response. The larger the relative density, the smaller is the dimensionless compressive stress (as shown in Figure 2.16 (a)). Zhu and Windle (2002) also show that at low compression strains, the Poisson's ratio reduces with the increase of the relative density, and that at large compression strains the situation reverses; that is, increasing relative density leads to the increase of the Poisson's ratio (as shown in Figure 2.16 (b)). However, Zhang and Lu (2007) obtained opposite results. Wicklein and Thoma (2005) reported that relative density has no influence on the Poisson's ratio of irregular open-cell foams.

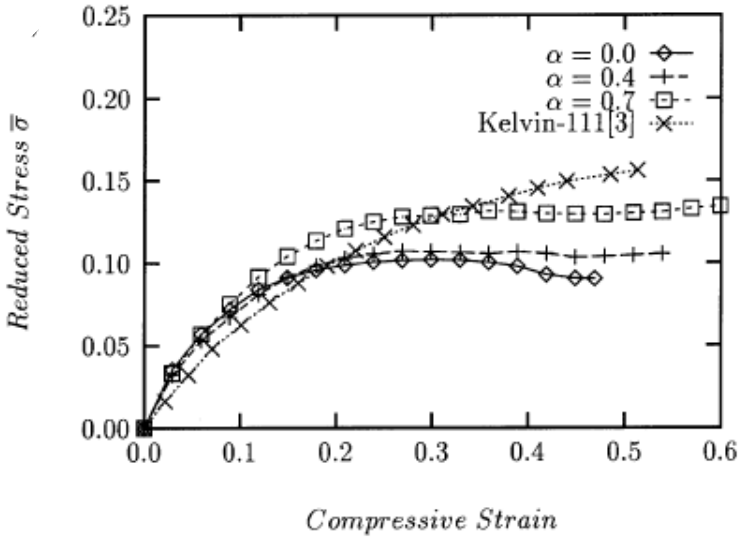

Figure 2.15. Effects of cell regularity on the mean dimensionless stress-strain relationships for random Voronoi foams, compared with the Kelvin foam ($\alpha = 1.0$) in the [111] direction (Zhu and Windle, 2002).

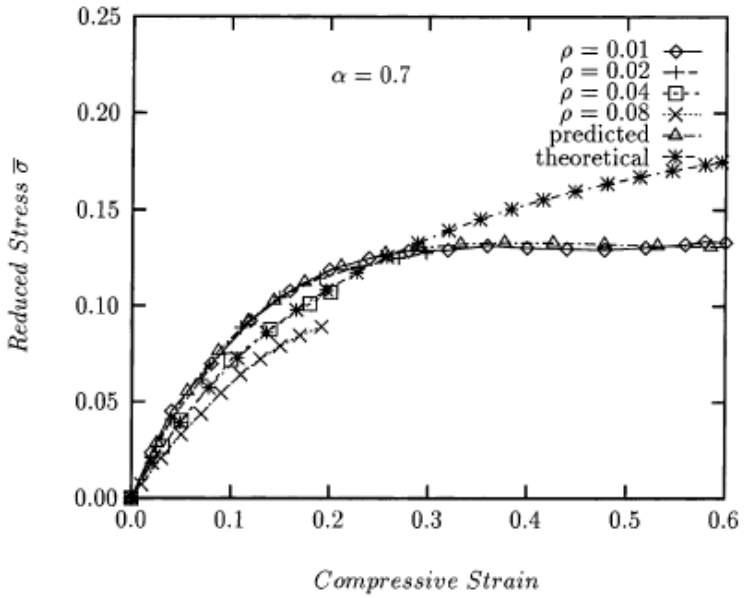

(a)

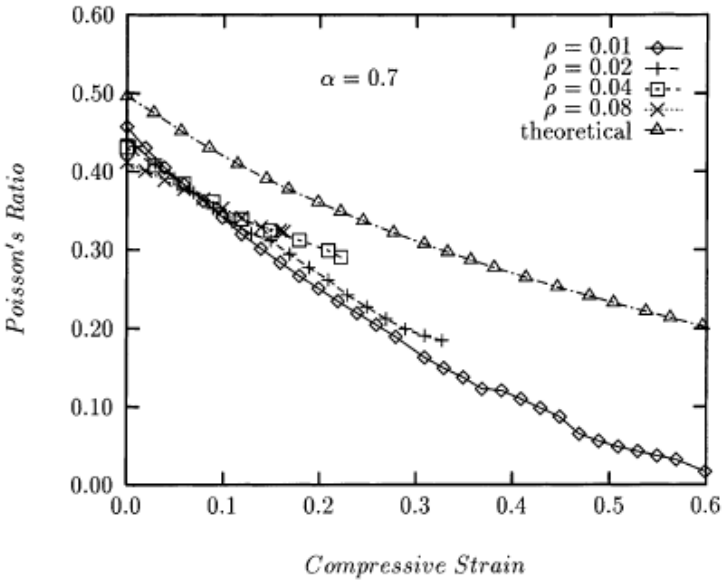

(b)

Figure 2.16. Effects of relative density on the (a) reduced compressive stress-strain relationships (b) Poisson's ratio of foams with $\alpha = 0.7$, compared with the theoretical results of a perfect regular foam in [111] direction and the predicted results of a random foam with $\alpha = 0.7$ (Zhu and Windle, 2002).

2.4.2 The elastic properties of micro- and nano-sized 2D honeycombs and 3D open-cell foams

With the advance of manufacturing techniques, micro- and nano-sized 2D honeycombs and 3D foams can be produced (Nishihara et al., 2005, Tamon et al., 2013, Wang et al., 2008) and they are widely used in many different areas, such as Micro-electromechanical Systems (MEMS), Nano-electromechanical Systems (NEMS), and nano-sensors (Biener et al., 2009, Duan, 2010, Kramer et al., 2004). The elastic properties of macro-sized 2D honeycombs and 3D foams (Gibson and Ashby, 1982, Gibson and Ashby, 1997, Gibson et al., 1982 , Laroussi et al., 2002, Mills, 2007b, Zhu et al., 2000, Zhu et al., 2001a, Zhu et al., 1997a, Zhu et al., 1997b, Zhu et al., 2006, Zhu and Windle, 2002) as described in the previous sections may not apply to their micro- and nano-sized counterparts. Therefore, understanding the mechanical properties of micro- and nano-sized 2D honeycombs and 3D foams becomes increasingly important. The following sections will briefly summarize the relevant mechanics theory and the main results on the elastic properties of micro- and nano-sized honeycombs and open-cell foams.

2.4.2.1 The size-dependent mechanical properties of the micro- and nano-sized structural elements

The basic building blocks of micro- and nano-sized 2D honeycombs and 3D open-cell

foams are the micro- or nano-sized struts and plates. Sufficient research evidence (Aifantis, 1999, Fleck and Hutchinson, 1993, Gao et al., 1999, Lam et al., 2003, Mindlin, 1963, Mindlin and Tiersten, 1962, Nix and Gao, 1998, Toupin, 1962, Tsagrakis et al., 2003, Yang et al., 2002, Zhu, 2008, Zhu, 2010b, Zhu and Wang, 2013, Zhu et al., 2012b) has shown that at the micro-meter scale, the strain gradient effect plays a very important role in the mechanical behaviour. At the nano-meter scale, surface elasticity (Duan et al., 2005, Miller and Shenoy, 2000, Gao et al., 2006, Zhu and Wang, 2013, Zhu et al., 2012b) and initial stress or strain (Zhu, 2008, Zhu, 2010b, Zhu et al., 2009, Zhu and Wang, 2013) dominate the effects on the mechanical properties of nano-sized structures.

The classical continuum mechanics theories do not contain any material length scale parameters and they may not be used for the size-dependent analysis of micro- and nano-sized structures. A couple-stress elasticity theory (Anthoine, 2000, Lubarda and Markenscoff, 2000, Mindlin, 1963, Mindlin and Tiersten, 1962, Toupin, 1962) was presented to analyze the size-dependent effects of micro and nano-sized structures. As there are two separate material length scale parameters (Anthoine, 2000, Lubarda and Markenscoff, 2000, Mindlin, 1963, Mindlin and Tiersten, 1962, Papargyri-Beskou et al., 2003, Toupin, 1962, Vardoulakis and Giannakopoulos, 2006), it is not convenient to experimentally determine them and to use the theory in application. A novel couple-stress elasticity theory has been developed by Yang et al. (2002), in which they define a symmetric curvature tensor as the only properly conjugated high

order strain measure. So, there is only one material length scale parameter involved in the theory and it consequently becomes easier to analyze the size-dependent effects for micro-sized structures.

Micropolar theory is also used to study the size-dependent effects on micro-sized honeycombs (Kumar and McDowell, 2004). Micropolar theory was developed by Cosserat brothers in 1909 (Nowacki, 1974). They assumed the body consists of the interconnected particles in the form of small rigid bodies. Each particle has six degree of freedom, and the deformation consists of the displacement and rotation which is independent of the deformation of the body. The total rotation of the junction in the body consists of the macroscopic rotation about the cell walls which is associated with the translation of the junction and the microscopic rotation of the particles which is independent the junction rotation. This theory is different from the couple stress theory in which the rotation is not independent and it is obtained from the anti-symmetric part of the displacement gradient tensor (Kumar and McDowell, 2004). Zhu and Mills (2000) also demonstrated that the small rotation is dependent of the translation of the strut junctions during the process of deformation.

The bending, transverse shear, torsion and axial stretching or compression rigidities of micro- and nano-sized structures have been obtained as follows. At the micro-meter scale, to obtain the bending rigidities, Zhu (2010b) applied a constant bending moment on a uniform cantilever at the free end, and made three assumptions. Firstly, the material of the uniform cantilever beam is linear elastic and the deformation is very

small. Secondly, the stress in the *z* direction is zero. Finally, during the bending process, the beam thickness is unchanged and the neutral surface of the bent beam is in the middle of the beam cross-section. Zhu (2010b) used Yang et al.'s (2002) couple-stress theory with only one material characteristic length scale parameter to consider the contribution of the couple-stresses on the stored deformation energy, and hence took the strain gradient effect into consideration. Then the bending rigidities of uniform plates and beams with circular cross section are obtained in Equations (2.22) and (2.25). These analytic results can fit Lam et al.'s (2003) experimental results. To find the transverse shear rigidity of micro-structural elements, Zhu (2010b) vertically applied a concentrated force at the free end of a uniform cantilever in the *y* direction, and assumed that the beam cross-sectional warping cannot affect the bending compression or extension in the longitudinal direction of the beam, then it cannot affect the normal stress from bending. According to the obtained stored stain energy, the vertical displacement at the free end of the cantilever can be found. Based on the Timoshenko beam theory, in this case, the total deflection of the free end of the cantilever is contributed by the bending and transverse shear. As the bending rigidity has already been obtained by Zhu (2010b), the transverse shear rigidity of uniform plates can be obtained as shown in Equation (2.23). When a uniform cell wall is uniaxial stretched or compressed, the strain gradient effect is absent. Therefore, the axial stretching or compression rigidities of uniform plates and beams with circular cross section are the same as the conventional ones and presented in Equations (2.24)

and (2.27). To obtain the torsion rigidity of micro-sized beams with circular cross section, Yang et al. (2002) applied a torque on a thin cylindrical bar and used Yang et al.'s (2002) couple-stress theory to obtained the stored strain energy. The torsional rigidity of the cylindrical bar with the strain gradient effect was obtained and given in Equation (2.26). For the detailed derivation of the bending, transverse shear and axial stretching or compression rigidities of micro-sized plates or beams, readers can refer to corresponding references as shown below.

For uniform plates with thickness at the micro-meter scale, the bending rigidity is given by (Zhu, 2010b, Yang et al., 2002)

$$D_b = \frac{E_S b h^3}{12(1-v_S^2)}[1+6(1-v_S)(\frac{l_m}{h})^2] \tag{2.22}$$

The transverse shear rigidity is obtained by (Zhu, 2010b)

$$D_S = \frac{G_S bh}{1.2} \cdot \frac{[1+6(1-v_S)(\frac{l_m}{h})^2]^2}{1+2.5(1+v_S)^2(\frac{l_m}{h})^2} \tag{2.23}$$[4]

The axial stretching or compression rigidity is shown by (Zhu, 2010b)

$$D_C = E_S bh \tag{2.24}$$[5]

For uniform beams with circular cross section, the bending rigidity is given by (Zhu, 2010b)

$$D_b = \frac{E_S \pi d^4}{64}[1+8(1+v_S)(\frac{l_m}{d})^2] \tag{2.25}$$

[4] 1.2 is the shear coefficient which can be introduced for the rectangular cross-section of the cell walls (Gere and Timoshenko, 1995)

[5] When a uniform cell wall is uniaxial stretched or compressed, the strain gradient effect is absent.

The torsion rigidity is obtained by (Yang et al., 2002)

$$D_t = \frac{G_S \pi d^4}{32}[1+24(\frac{l_m}{d})^2] \tag{2.26}$$

The axial stretching or compression rigidity is presented by (Zhu, 2010b)

$$D_C = \frac{E_S \pi d^2}{4} \tag{2.27}$$

In Equations (2.22), (2.23), (2.25) and (2.26), l_m is the material length parameter at the micro-meter scale (which can be experimentally measured and is usually in the range between submicron and microns, and different for different materials), *h* is the plate thickness, *b* is the plate width (which is assumed to be much larger than thickness *h*), and *d* is the diameter of the circular cross-section. E_S, G_S and v_S are the Young's modulus, shear modulus and the Poisson's ratio of the solid material. As can be seen from Equations (2.22), (2.23), (2.25) and (2.26), the bending, transverse shear and torsion rigidities of the micro-sized plates or beams are size-dependent. l_m / h or l_m / d can present the existence and level of the strain gradient effect. When the actual thickness (*h*) of the cell walls or diameter (*d*) of the cell struts is much larger than l_m, which means the size of plates or beams are very large and going to be at the macro-meter scale, then the bending rigidity D_b, transverse shear rigidity D_S and the torsion rigidity D_t reduce to those of their macro-sized counterparts. The thinner the micro-sized plates or the micro-sized beams, the larger the bending, transverse shear and torsion rigidities, which means the strain gradient effect becomes more significant.

Zhu et al. (2009) analyzed the pure bending of a nanoplate. They assumed that the

material on the surface and bulk is linear elastic and the deformation is very small, and the thickness of the nanoplate is unchanged during the bending process. They considered the contribution of the surface elasticity and initial stress at the nano-meter scale, and obtained the size-dependent bending rigidity of the nanoplate, as given in Equation (2.28). When the Poisson's ratio of the surface and the bulk material are the same and the initial stresses or strains in the surface and the bulk material are 0, this bending rigidity of the nanoplate becomes the same as Miller and Shenoy's result (Miller and Shenoy, 2000). In the similar manner, Zhu (2008) obtained the bending rigidity of the nanobeam with a circular cross section as shown in Equation (2.31). Zhu (2010b) obtained the transverse shear rigidity of the nanoplate in the same way used in obtaining transverse shear rigidity of the microplate (as shown in Equation (2.29)). Miller and Shenoy (2000) explained the size dependent elastic properties of nanosized structural element by the surface elastic modulus, bulk elastic modulus and thickness of the structure element. To find the torsion rigidity of uniform nanobeam, Shenoy (2002) considered the surface effect based on the conventional torsion rigidity and obtained the torsion rigidity of uniform nanobeam, as given in Equation (2.32). Miller and Shenoy (2000) considered the surface stress and bulk stress on the equilibrium of the force transmitted across the plate, and derived the axial stretching or compression rigidity, as shown in Equation (2.30). In the same manner, Zhu and Wang (2013) obtained the axial stretching or compression rigidity of nanobeam as shown in Equation (2.33). For the detailed derivation of the bending, transverse shear

and axial stretching or compression rigidities of nano-sized plates or beams, readers can refer to corresponding references as shown below.

For uniform plates with thickness at the nano-meter scale, the bending rigidity is given by (Zhu, 2010b, Zhu et al., 2009)

$$D_b = \frac{E_S b h^3}{12(1-v_S^2)}(1+6\frac{l_n}{h}+\nu_S\frac{1+v_S}{1-v_S}\varepsilon_0^L) \tag{2.28}$$

The transverse shear rigidity is obtained by (Zhu, 2010b)

$$D_S = \frac{G_S b h}{1.2}\cdot\frac{(1+6\frac{l_n}{h}+\nu_S\frac{1+v_S}{1-v_S}\varepsilon_0^L)^2}{1+10\frac{l_n}{h}+30(\frac{l_n}{h})^2} \tag{2.29}$$

The axial stretching or compression rigidity is shown by (Miller and Shenoy, 2000)

$$D_C = E_S b h(1+2\frac{l_n}{h}) \tag{2.30}$$

For uniform beams with circular cross section, the bending rigidity is given by (Zhu, 2008)

$$D_b = \frac{E_S \pi d^4}{64}[1+8\frac{l_n}{d}+\frac{\nu_S}{1-v_S}\varepsilon_0^L] \tag{2.31}$$

The torsion rigidity is obtained by (Zhu and Wang, 2013)

$$D_t = \frac{G_S \pi d^4}{32}(1+8\frac{l_n}{d}) \tag{2.32}$$

The axial stretching or compression rigidity is presented by (Zhu and Wang, 2013)

$$D_C = \frac{E_S \pi d^2}{4}(1+4\frac{l_n}{d}) \tag{2.33}$$

Where l_n is the material intrinsic length at the nano-meter scale, which can be

expressed by $l_n = S / E_S$, and may vary over a range from 10^{-11} to 10^{-9} m for different materials, *S* is the surface elasticity modulus. For uniform plates (*b* >> *h*), the initial strain in the cell wall length direction and width direction can be obtained as $\varepsilon_0^L = \varepsilon_0^W = \frac{\sigma_0^L}{E_S}(1-\nu_S) = -\frac{2\tau_0}{E_S h}(1-\nu_S)$, the initial strain in the thickness direction is $\varepsilon_0^h = -\frac{2\nu_S}{E_S}\sigma_0^L = \frac{4\nu_S\tau_0}{E_S h}$ (Zhu et al., 2012a, Zhu and Wang, 2013, Zhu et al., 2012b). τ_0 is the initial surface stress and σ_0^L is the initial stress of the solid material in the cell wall length direction. For uniform beams with a circular cross-section, the initial strain in the length direction is $\varepsilon_0^L = \frac{\sigma_0^L}{E_S}(1-\nu_S) = -\frac{4\tau_0}{E_S d}(1-\nu_S)$, and the initial strain in the radial direction of the beam cross-section is $\varepsilon_0^r = -\frac{2\tau_0}{E_S d}(1-3\nu_S) = \frac{1-3\nu_S}{2(1-\nu_S)}\varepsilon_0^L$ (Zhu et al., 2012a, Zhu and Wang, 2013, Zhu et al., 2012b). τ_0 is the initial surface stress and σ_0^L is the initial stress in the length direction of the cell struts (i.e. the beams), whose amplitude can be controlled to vary by an applied electric potential (Kramer et al., 2004, Weissmüller et al., 2003). The amplitude of the initial strain in the cell wall length direction also is controllable like the initial stress; however, it is limited to the range of the yield strain of the solid material. The yield strain of single crystal nano-materials or polymeric materials is 10% or larger (Zhu, 2010b). When the initial strain is zero, l_n / h or l_n / d can present the existence and level of the surface elasticity effect. When the actual thickness (*h*) of the cell walls or diameter (*d*) of the cell struts is much larger than l_n, the surface elasticity effect will disappear,

then the bending rigidity D_b, transverse shear rigidity D_S, the torsion rigidity D_t and axial stretching or compression rigidity D_C reduce to those of their macro-sized counterparts. When the initial strain effects are present, and the surface elasticity effects are absent (l_n / h or l_n / d is zero), then from Equations (2.28 – 2.33), the elastic rigidities will be influenced by the initial strain. The actual plate thickness *h* and the plate width *b* are given by $h = h_0(1+\varepsilon_0^h)$ and $b = b_0(1+\varepsilon_0^W)$, and the actual beam diameter of the circular cross-section is $d = d_0(1+\varepsilon_0^r)$, where h_0, b_0 and d_0 are the original thickness, width and diameter when the effects of the initial stresses/strains are absent. From Equations (2.28 – 2.33), the bending, transverse shear, torsion and axial stretching or compression rigidities are size-dependent. One thing that should be mentioned is that it is very difficult to obtain analytic results for the transverse shear rigidities of nano-sized beams with different types of cross-sections.

According to the elastic rigidities of micro- and nano-structure element which contains the effects of the strain gradient, the surface elasticity and the initial stress or strain, it can be found the elastic properties of solid material with these effects.

2.4.2.2 The elastic properties of micro- and nano-sized 2D regular honeycombs

As having discussed the in-plane deformation of macro-sized honeycombs, the bending, transverse shear and axial stretching or compression of the cell walls are the main deformation mechanisms. Zhu (2010b) and Zhu and Wang (2013) used the

classical structural mechanics analysis to obtain the five independent elastic constants of regular hexagonal honeycombs as functions of the elastic rigidities D_b, D_S, D_C and the length (l) of the cell walls or the cell struts as shown in Equations (2.8 – 2.12). As the elastic rigidities D_b, D_S and D_C are obtained and given in Equations (2.22 – 2.24) for micro-sized plates or beams and in Equations (2.28 – 2.30) for nano-sized plates or beams, substituting Equations (2.22 – 2.24) or (2.28 – 2.30) into Equations (2.8 – 2.12), the size-dependent elastic constants/properties of micro- or nano-sized regular hexagonal honeycombs can thus be easily obtained, as given in Equations (2.34 – 2.38) for micro-sized regular hexagonal honeycombs and in Equations (2.39 – 2.43) for nano-sized regular hexagonal honeycombs. For the detailed derivation of the five independent elastic constants of micro- and nano-sized regular hexagonal honeycombs, readers can refer to Zhu (2010b).

At the micro-meter scale, the non-dimensional in-plane Young's modulus is given as (Zhu, 2010b, Zhu, 2010a)[6]

$$\overline{E_1} = \frac{(1-\nu_S^2)E_1}{1.5E_S\rho^3}$$

$$= \frac{[1+6(1-\nu_S)(\frac{l_m}{h})^2]^2(1-\nu_S^2)}{[1+6(1-\nu_S)(\frac{l_m}{h})^2](1-\nu_S^2)+1.8\rho^2(1+\nu_S)[1+2.5(1+\nu_S)^2(\frac{l_m}{h})^2]+\frac{9}{4}\rho^2[1+6(1-\nu_S)(\frac{l_m}{h})^2]^2} \quad (2.34)$$

The in-plane Poisson's ratio of micro-sized honeycombs is obtained as (Zhu, 2010b)

[6] There is an error in the expression of the non-dimensional in-plane Young's modulus, which was corrected in Zhu (2010a).

$$\nu_{12}=\frac{[1+6(1-\nu_S)(\frac{l_m}{h})^2](1-\nu_S^2)+1.8\rho^2(1+\nu_S)[1+2.5(1+\nu_S)^2(\frac{l_m}{h})^2]-\frac{3}{4}\rho^2[1+6(1-\nu_S)(\frac{l_m}{h})^2]^2}{[1+6(1-\nu_S)(\frac{l_m}{h})^2](1-\nu_S^2)+1.8\rho^2(1+\nu_S)[1+2.5(1+\nu_S)^2(\frac{l_m}{h})^2]+\frac{9}{4}\rho^2[1+6(1-\nu_S)(\frac{l_m}{h})^2]^2} \tag{2.35}$$

Because there is no strain gradient effect when the honeycomb is uniformly compressed or stretched in the *z* direction, the non-dimensional out-of-plane Young's modulus of micro-sized honeycombs is given as (Zhu, 2010b)

$$\overline{E_3}=\frac{E_3}{E_S\rho}=1 \tag{2.36}$$

The non-dimensional out-of-plane shear modulus of micro-sized honeycombs is given as (Zhu, 2010b)

$$\overline{G_{31}}=\frac{G_{31}}{G_S\rho}=\frac{1}{2} \tag{2.37}$$

The out-of-plane Poisson's ratio of micro-sized honeycombs is the same as the solid material (Zhu, 2010b); that is,

$$\nu_{31}=\nu_S \tag{2.38}$$

At the nano-meter scale, the non-dimensional in-plane Young's modulus is given as (Zhu, 2010b, Zhu and Wang, 2013)

$$\overline{E_1}=\frac{(1+6\frac{l_n}{h}+\nu_S\frac{1+\nu_S}{1-\nu_S}\varepsilon_0^L)^2(1+2\frac{l_n}{h})(1-\nu_S^2)}{(1+6\frac{l_n}{h}+\nu_S\frac{1+\nu_S}{1-\nu_S}\varepsilon_0^L)(1+2\frac{l_n}{h})(1-\nu_S^2)+1.8\rho^2(1+2\frac{l_n}{h})(1+\nu_S)[1+10\frac{l_n}{h}+30(\frac{l_n}{h})^2]+\frac{9}{4}\rho^2(1+6\frac{l_n}{h}+\nu_S\frac{1+\nu_S}{1-\nu_S}\varepsilon_0^L)^2} \tag{2.39}$$

The in-plane Poisson's ratio of nano-sized honeycombs is obtained as (Zhu, 2010b, Zhu and Wang, 2013)

$$\nu_{12} = \frac{(1+6\frac{l_n}{h}+\nu_S\frac{1+\nu_S}{1-\nu_S}\varepsilon_0^L)(1+2\frac{l_n}{h})(1-\nu_S^2)+1.8\rho^2(1+2\frac{l_n}{h})(1+\nu_S)[1+10\frac{l_n}{h}+30(\frac{l_n}{h})^2]-\frac{3}{4}\rho^2(1+6\frac{l_n}{h}+\nu_S\frac{1+\nu_S}{1-\nu_S}\varepsilon_0^L)^2}{(1+6\frac{l_n}{h}+\nu_S\frac{1+\nu_S}{1-\nu_S}\varepsilon_0^L)(1+2\frac{l_n}{h})(1-\nu_S^2)+1.8\rho^2(1+2\frac{l_n}{h})(1+\nu_S)[1+10\frac{l_n}{h}+30(\frac{l_n}{h})^2]+\frac{9}{4}\rho^2(1+6\frac{l_n}{h}+\nu_S\frac{1+\nu_S}{1-\nu_S}\varepsilon_0^L)^2} \quad (2.40)$$

The non-dimensional out-of-plane Young's modulus of nano-sized honeycombs is given as (Zhu, 2010b, Zhu and Wang, 2013)

$$\overline{E_3} = \frac{E_3}{E_S\rho} = 1+2\frac{l_n}{h} \quad (2.41)$$

The non-dimensional out-of-plane shear modulus of nano-sized honeycombs is given as (Zhu, 2010b, Zhu and Wang, 2013)

$$\overline{G_{31}} = \frac{G_{31}}{G_S\rho} = \frac{1}{2}(1+2\frac{l_n}{h}) \quad (2.42)$$

The out-of-plane Poisson's ratio of nano-sized honeycombs is the same as the solid material (Zhu, 2010b, Zhu and Wang, 2013)

$$\nu_{31} = \nu_S \quad (2.43)$$

According to the previous research (Zhu, 2010b, Zhu and Wang, 2013), and the above equations, the elastic constants of micro- and nano-sized regular honeycombs are size-dependent: the thinner the cell walls, the larger the bending and transverse shear rigidities of the cell walls, and the larger the dimensionless Young modulus and shear modulus of the regular honeycombs (as shown in Figure 2.17 (a) and Figure 2.18 (a)), and the smaller the Poisson's ratio (as shown in Figure 2.17 (b) and Figure 2.18 (b)). If the surface modulus is negative (i.e. l_n / h or l_n / d is negative)[7], all of the effects

[7] If the surface modulus is negative, the surface stress is a compressive stress when the surface is

are inverted. It also can be found that the initial strain effect plays an important role in the elastic properties of nano-sized regular honeycombs. By varying the range of the initial strain in the cell wall directions between -0.1 and 0.1, the in-plane dimensionless Young's modulus can be controlled to reduce by about 45% or to increase by nearly 80% (as shown in Figure 2.19 (a)) (Zhu and Wang, 2013), and the in-plane Poisson's ratio is also tunable with the proportion of the range of the initial strain (as shown in Figure 2.19 (b)).

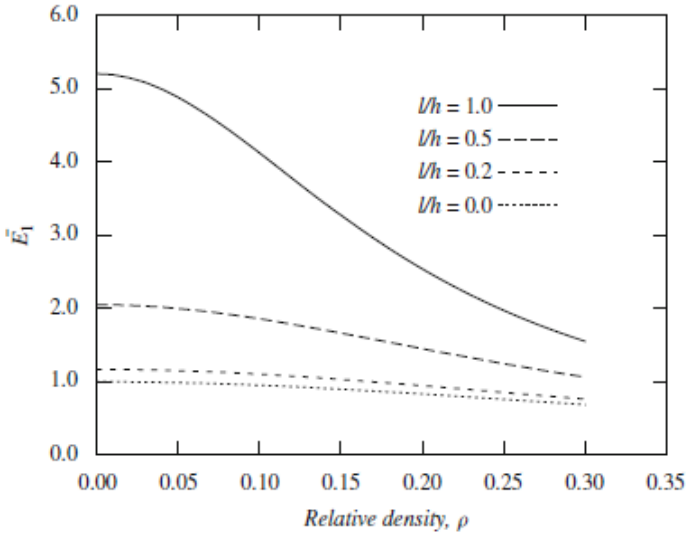

(a)

stretched. By atomistic simulations, Miller and Shenoy (2000) found that some materials have a negative surface elasticity modulus (i.e. $S < 0$), and their material intrinsic length is thus negative (i.e. $l_n = S / E_S < 0$). If the surface elasticity modulus is positive, an increment in surface stress results in the elongation of the surface; if the surface elasticity modulus is negative, the elongation of the surface results in a reduction in surface stress.

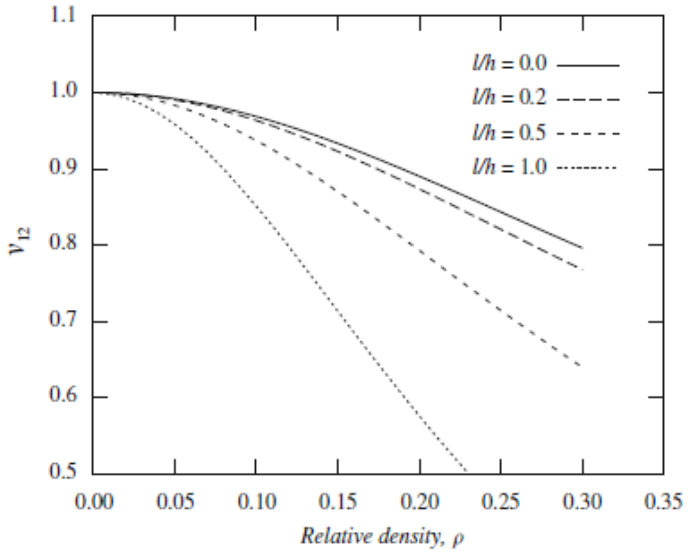

(b)

Figure 2.17. Size-dependent effect on the relationship between (a) the in-plane dimensionless Young's modulus, (b) the in-plane Poisson's ratio and the relative density of micro-sized regular honeycombs (Zhu, 2010b).

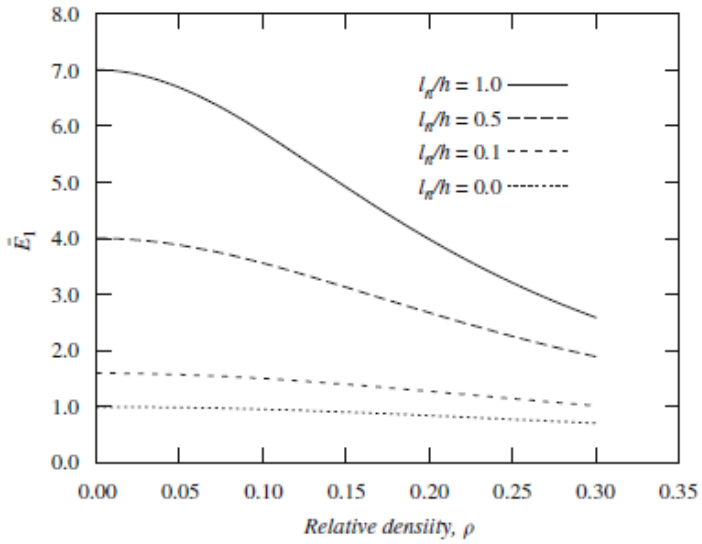

(a)

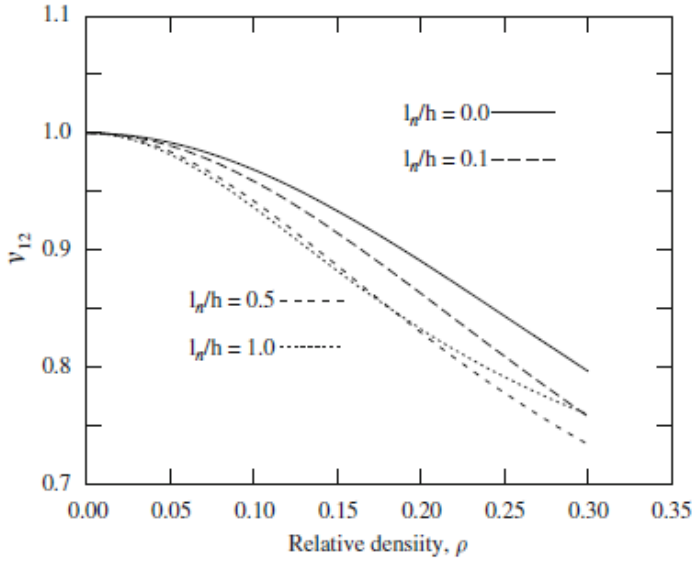

(b)

Figure 2.18. Size-dependent effect on the relationship between (a) the in-plane dimensionless Young's modulus, (b) the in-plane Poisson's ratio and the relative density of nano-sized regular honeycombs (Zhu, 2010b).

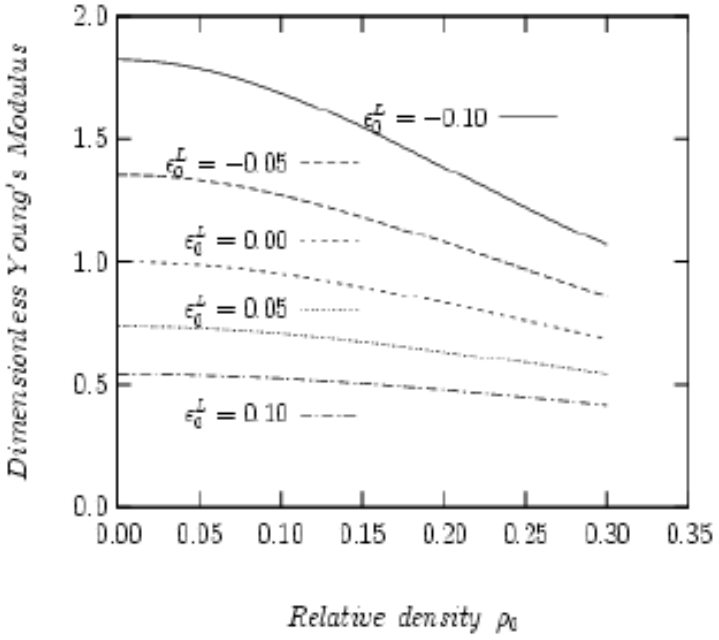

(a)

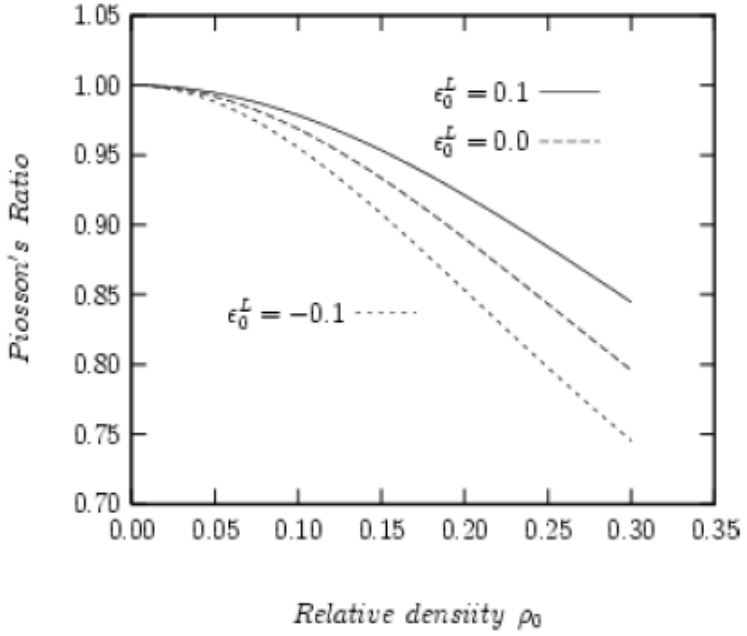

(b)

Figure 2.19. Relationship between tunable in-plane (a) dimensionless Young's modulus, (b) Poisson's ratio and the relative density of nano-sized regular honeycombs (Zhu and Wang, 2013).

2.4.2.3 The elastic properties of micro- and nano-sized 3D regular open-cell foams

Based on the analysis of classical structural mechanics and the conventional elastic rigidities of beams, Zhu et al. (1997a) have obtained all of the three independent elastic constants of macro-sized regular BCC open-cell foams as functions of the bending, torsion, and axial stretching or compression rigidities of the cell struts in Equations (2.16 – 2.18). When the bending, torsion, and axial stretching or compression rigidities in Equations (2.16 – 2.18) are replaced by the size-dependent rigidities (as shown in Equations (2.25 – 2.27) for micro-sized beams and Equations (2.31 – 2.33) for nano-sized beams), the three independent elastic constants of regular open-cell foams will

contain the strain gradient effect at the micro-meter scale and the effects of surface elasticity and initial stress/strain at the nano-meter scale. Zhu and Wang (2013) have obtained the size-dependent elastic properties for perfectly regular micro- and nano-sized Kelvin open-cell foams. They found that the smaller the cross-sectional area of the cell struts or the smaller the cell size if the relative density is fixed, the larger the dimensionless bending, torsion and stretching or compression rigidities of the cell struts, the larger the dimensionless Young's modulus and shear modulus (as shown in Figures 2.20 and 2.21), the structure will be more hard to bending, torsion and stretching or compression. However, the Poisson's ratio is almost independent of the cell size (as shown in Figure 2.22). By adjusting the amplitude of the initial strain in the cell strut length direction between -0.1 and 0.1, the dimensional Young's modulus can be controlled to increase or decrease over a range about 50% if the Poisson's ratio of the solid material is 0.1 (as shown in Figure 2.23). It implies that the effect of initial strain can greatly affect the elastic properties of regular open-cell foams. This tunable range depends on the amplitude of the initial strain, the relative density of open-cell foams, and the Poisson's ratio of the solid material. If the Poisson's ratio of the solid material is 0.4 instead of 0.1, the tunable range of the dimensional Young's modulus becomes 77% (Zhu and Wang, 2013).

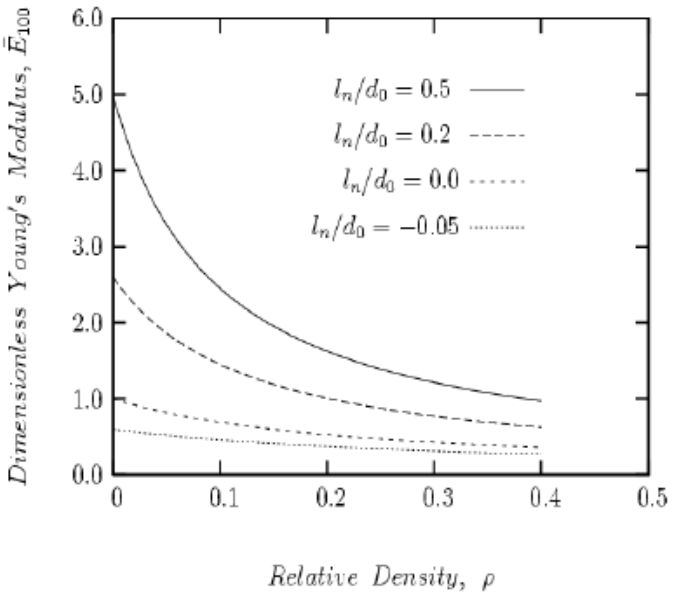

Figure 2.20. Size-dependent effect on the relationship between the in-plane dimensionless Young's modulus and the relative density of nano-sized regular open-cell foams (Zhu and Wang, 2013).

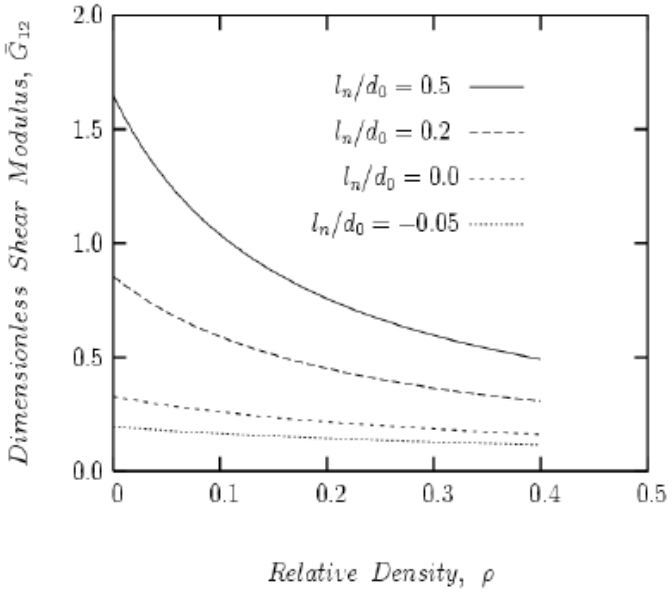

Figure 2.21. Size-dependent effect on the relationship between the in-plane dimensionless shear modulus and the relative density of nano-sized regular open-cell foams (Zhu and Wang, 2013).

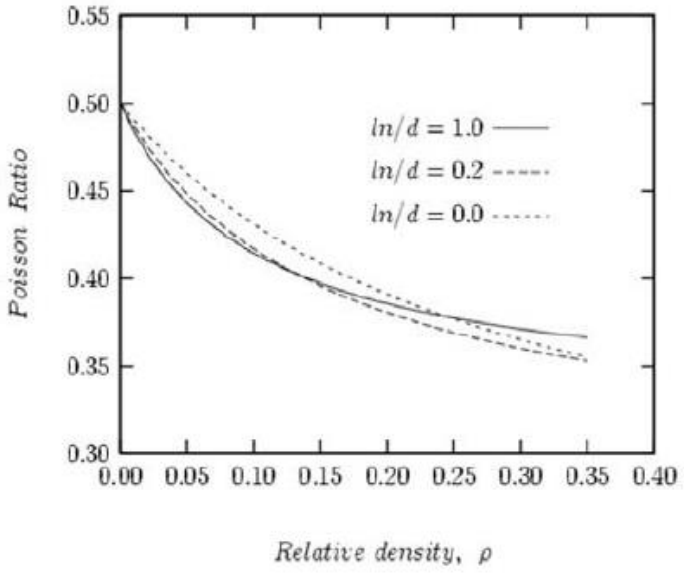

Figure 2.22. Size-dependent effect on the relationship between the in-plane Poisson's ratio and the relative density of nano-sized regular open-cell foams (Zhu and Wang, 2013).

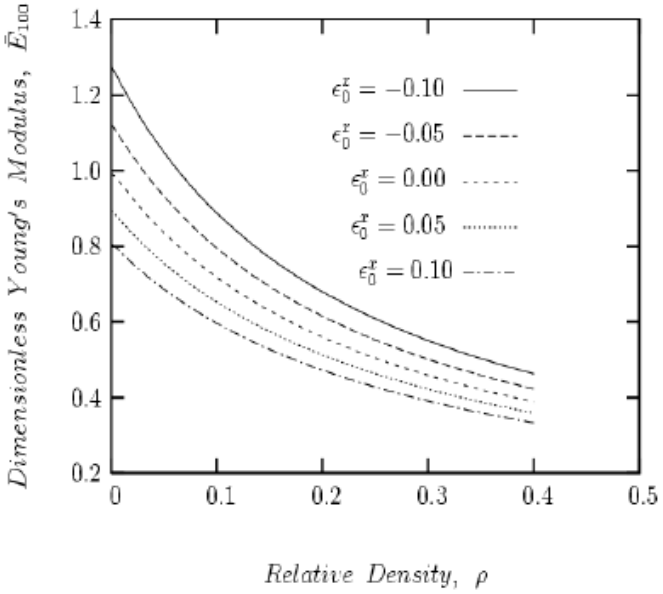

Figure 2.23. Relationship between tunable in-plane dimensionless Young's modulus and the relative density of nano-sized regular open-cell foams with the Poisson's ratio of the solid material $\nu_S = 0.1$ (Zhu and Wang, 2013).

Chapter 3 The elastic properties of micro- and nano-sized periodic random irregular honeycombs

3.1 Introduction

Cellular materials can be widely found in nature, including honeycombs, bones, and plant stems. With the advance of manufacturing techniques, micro- and nano-sized honeycombs can easily be produced (Nishihara et al., 2005). Many researchers (Gibson and Ashby, 1997, Silva et al., 1995, Masters and Evans, 1996, Chen et al., 1999, Zhu and Chen, 2011, Zhu et al., 2001a, Zhu and Mills, 2000, Zhu et al., 2006) have studied the mechanical properties of macro-sized regular and random irregular honeycombs. However, these results may not be applicable to micro- and nano-sized random irregular honeycombs because at the micro-meter scale the strain gradient effect greatly influences the mechanical properties of micro-sized honeycombs (Aifantis, 1999, Fleck and Hutchinson, 1993, Gao et al., 1999, Lam et al., 2003, Nix and Gao, 1998, Toupin, 1962, Yang et al., 2002, Zhu, 2008, Zhu, 2010b), and at the nano-meter scale the surface elasticity (Duan et al., 2005, Miller and Shenoy, 2000, Zhu et al., 2012b) and the initial stress or strain effects (Zhu, 2010b) play an important role (see Section 2.4.2.1) in the mechanical behaviours. According to the experimental results (Biener et al., 2009, Haiss et al., 1998, Kramer et al., 2004, Weissmüller et al., 2003), the range of the initial stresses could be controlled to vary over a large range

by adjusting the amplitude of an applied electric potential. Zhu (2010b) has done a theoretical analysis on the size-dependent and tunable elastic properties of micro- and nano-sized regular hexagonal honeycombs.

This chapter will explore the size-dependent and tunable elastic properties of micro- and nano-sized random irregular honeycombs using numerical simulations by the ANSYS finite element software.

3.2 Methodology

3.2.1 The main parameters of periodic random irregular honeycombs

Zhu et al. (2001a, 2006) developed a computer program to construct the representative unit periodic random irregular Voronoi honeycombs. The main parameters that are used to construct the unit periodic random irregular Voronoi honeycomb models are the degree of cell regularity, the honeycomb initial relative density, and the number of complete cells (see Section 2.3.1). The degree of cell regularity and the initial relative density are defined by Equations (2.2) and (2.4).

3.2.1.1 The degree of cell regularity

In this chapter, the degree of cell regularity is varied from 0.0 to 1.0. Figures 3.1 (a),

(b), and (c) show the unit periodic random irregular Voronoi honeycombs with different degrees of regularity α = 0.0, α = 0.4 and α =0.7. With the increase of the degree of cell regularity, the structure becomes more regular. When α = 0.0, it is a fully random irregular honeycomb, and if α = 1.0, it is a perfectly regular hexagonal honeycomb.

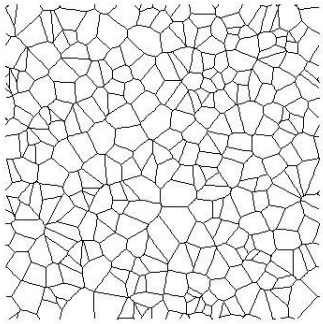

(a)

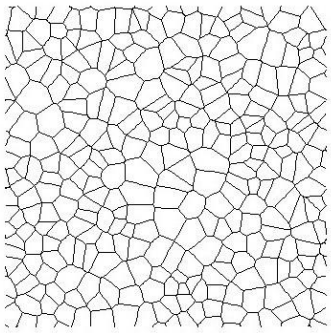

(b)

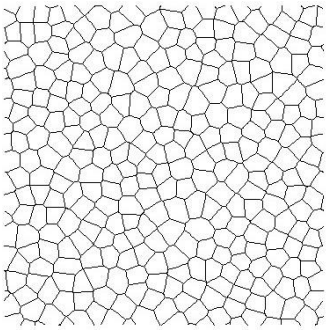

(c)

Figure 3.1. Voronoi honeycombs with 300 cells and different degrees of cell regularity: (a) α = 0.0, (b) α = 0.4, (c) α =0.7.

3.2.1.2 The relative density

All of the cell walls in a micro- or nano-sized honeycomb are assumed to have the same uniform thickness. The cell wall width is assumed to be a unit and to be much larger than the thickness. The dependences of the elastic properties of micro- or nano-sized honeycombs on the relative density, over the range from 0.01 to 0.3,[8] will be investigated. For a given relative density, the initial cell wall thickness can be determined from Equation (2.4).

3.2.1.3 The number of complete cells

The mean elastic properties are obtained from 20 similar random irregular Voronoi honeycomb models with the same combination of parameters, such as the degree of cell regularity, cell number, and the initial relative density. According to previous research (Zhu et al., 2001a), the number of complete cells in a random irregular Voronoi honeycomb model has a limited influence on the mean results of the non-dimensional Young's modulus and Poisson's ratio, and it only affects their standard deviation. A smaller number of complete cells will lead to a larger standard deviation of the non-dimensional Young's modulus and Poisson's ratio. So, in this part the number of complete cells in each of the random irregular Voronoi honeycomb models is set as 300 (as shown in Figures 3.1 (a), (b), and (c)).

[8] According to Gibson and Ashby (1997), the relative density of cellular solids is generally less than 0.3.

3.2.2 Finite element simulations

Micro- and nano-sized random irregular honeycombs are simulated using the ANSYS finite element software. The following sections show more details about how to obtain the simulation results for the elastic properties.

3.2.2.1 Element type and cross section

In finite element simulations, each of the cell walls is partitioned into 3-9 BEAM3 elements, depending on the cell wall relative length. The material is linear elastic, and it has no influence how to mesh the element, the mesh is just the same as the case in Chapter 4 (under the large deformation). According to the previous studies (Silva et al., 1995, Zhu, 2010b), the main in-plane deformation mechanisms of honeycombs are the cell wall bending, transverse shear, and axial stretching or compression. Therefore, the chosen type of elements should be able to incorporate these main deformation mechanisms in the simulations. The BEAM3 element[9] indeed meets this requirement. The Timoshenko beam theory is different, the transverse shear strain is constant through the cross section, the cross section of the Timoshenko beam (such as 3D BEAM189 in ANSYS) remains plane and it has a rotation after deformation due to the shear deformation. However, the Beam3 element is based on the Euler-Bernoulli beam theory. In the Euler-Bernoulli beam theory, the cross section of the beam remains

[9] BEAM3 element is a 2D elastic uniaxial beam element with bending, stretching and compression capabilities (ANSYS).

plane and it is perpendicular to the neutral axis after deformation. In ANSYS, the shear deflection constant has been used to consider the transverse shear strain energy in the BEAM3 (Euler-Bernoulli beam) element. This type of element has only two nodes and the shear deflection constant depends on the cross section of the beam element. The shear deflection constant is equal to the ratio of the actual beam cross-sectional area to the effective area resisting shear deformation. Since all of the cell walls of the random irregular honeycombs are assumed to have the same thickness and width, the cross section of the beam element is chosen as a rectangle and the shear deflection constant is 6/5 (ANSYS). When using this type of element in the simulations, three key parameters or constants have to be input, which are: the beam thickness, the material Young's modulus and Poisson's ratio.

3.2.2.2 Material properties

One of the main aims of this chapter is to obtain the size-dependent linear elastic properties of micro- and nano-sized random irregular honeycombs. In finite element simulations, the solid material is assumed to be linear elastic, and thus only the Young's modulus and Poisson's ratio of the solid material need to be input. For any commercial finite element software, such as ANSYS or ABAQUS, there are no types of element that could directly incorporate the size-dependent effect into the simulations. There are two possible ways to deal with this issue. One is to program a user subroutine to directly take into consideration the size-dependent effect, the other

is to input the equivalent values for the beam thickness, the material Young's modulus and Poisson's ratio. In this chapter, the three equivalent parameters for the beam element are obtained from the size-dependent bending, transverse shear and axial stretching or compression rigidities.[10]

3.2.2.3 The equivalent deformation rigidities of micro- and nano-sized cell walls

For a micro- and nano-sized 2D random irregular Voronoi honeycomb with a given initial relative density ρ_0, the initial cell wall thickness h_0 can be obtained from Equation (2.4). The size-dependent bending rigidity D_b, transverse shear rigidity D_S, and axial stretching or compression rigidity D_C of the cell walls with a unit width (which is assumed to be much larger than the thickness) can be obtained from Equations (2.22 - 2.24) for micro-sized honeycombs and from Equations (2.28 - 2.30) for nano-sized honeycombs. Therefore, the size-dependent effects on the deformation mechanisms at the micro- and nano-meter scales can be incorporated into the finite element simulations by imposing the following relations[11]:

$$\frac{E_e h_e^3}{12} = D_b \tag{3.1}$$

$$\frac{G_e h_e}{1.2} = \frac{E_e h_e}{2.4(1+v_e)} = D_S \tag{3.2}$$

[10] This happens mainly because the main in-plane deformation mechanisms of honeycombs are the cell wall bending, transverse shear, and axial stretching or compression (Silva et al., 1995, Zhu, 2010b).

[11] Because the cell wall width is assumed to be a unit, it is expressed by "1" in Equations (3.1 - 3.3).

$$E_e h_e = D_C \,. \tag{3.3}$$

The equivalent three parameters for the BEAM3 element (i.e. the equivalent solid Young's modulus E_e, Poisson's ratio v_e and beam thickness h_e) can be determined from Equations (3.1 - 3.3), and are given as

$$E_e = \sqrt{\frac{D_C^3}{12 D_b}} \tag{3.4}$$

$$v_e = \frac{D_C}{2.4 D_S} - 1 \tag{3.5}$$

$$h_e = \sqrt{\frac{12 D_b}{D_C}} \tag{3.6}$$

When the size-dependent effects are absent at the micro- and nano-meter scales (i.e. $l_m / h = 0$ in Equations (2.22 - 2.24), $l_n / h = 0$ in Equations (2.28 - 2.30)), the bending, transverse shear, and axial stretching or compression rigidities reduce to those of their conventional counterparts. For macro-sized random Voronoi honeycomb with a given degree of regularity and Poisson's ratio of the solid material, the non-dimensional Young's modulus is dependent only on the initial relative density and is independent of the actual cell wall thickness.[12] In all of the simulations in this chapter, the Young's modulus of the solid material, E_S, is fixed at $2 \times 10^5 \, MPa$ and the Poisson's ratio of the solid material, v_s, is fixed at 0.4.[13] The strain gradient effect at the micro-meter scale and the surface elasticity effect at the nano-meter are incorporated into the simulations by choosing different values of l_m / h and l_n / h in

[12] Silva et al. (1995) and Zhu et al. (2001a) gave an expression of the effective Young's modulus which is dependent on the initial relative density and Poisson's ratio of the solid material.

[13] Because the obtained elastic properties (i.e. the Young's modulus) will be dimensionless, the settings of the Young's modulus and Poisson's ratio of the solid materials are not very important.

Equations (2.22 - 2.24) and (2.28 - 2.30). Their values are set to 0.0, 0.2, 0.5, and 1.0, respectively. For the given values of l_m / h and l_n / h, the equivalent Young's modulus E_e, Poisson's ratio v_e and cell wall thickness h_e are obtained from Equations (3.4 - 3.6). It should be mentioned that the cell wall thickness is different for each of the similar models, which have the same degree of cell regularity and the same relative density, because their total cell wall lengths are different. Therefore, the equivalent Young's modulus E_e, Poisson's ratio v_e and cell wall thickness h_e which were obtained from Equations (3.4 - 3.6) are different for each of the similar models.

The initial stress or strain affects the bending, transverse shear, and axial stretching or compression rigidities of nano-sized cell walls. The amplitudes of the initial stresses in the length and width directions of the cell walls are the same (Zhu et al., 2012a) and are given as $\sigma_0^L = \sigma_0^W = -2\tau_0 / h$, where τ_0 is the initial surface stress, *h* is the actual thickness of the cell walls. They can be controlled to either increase or reduce about 10% at the nano-meter scale (Zhu et al., 2012a). When the initial stress or strain effect is present, the actual width *b*, length *l* and thickness *h* of the cell walls can be obtained as:

$$b = b_0(1+\varepsilon_0^L) \tag{3.7}$$

$$l = l_0(1+\varepsilon_0^L) \tag{3.8}$$

and

$$h = h_0(1+\varepsilon_0^h) \tag{3.9}$$

where $\varepsilon_0^L = -\frac{2\tau_0}{hE_S}(1-\nu_S)$ and $\varepsilon_0^h = -\frac{2\nu_S}{E_S}\sigma_0^L$ (Zhu, 2010b). From Equations (2.28 - 2.30), it can be seen that the bending rigidity D_b, transverse shear rigidity D_S and axial stretching or compression rigidity D_C can be controlled by adjusting the amplitude of the initial stress σ_0^L or the initial strains ε_0^L (in the length direction) and ε_0^h (in the thickness direction). By using Equations (3.1 - 3.6), the equivalent Young's modulus E_e, Poisson's ratio ν_e and cell wall thickness h_e can be obtained for the beam element in finite element simulations.

At the nano-meter scale, the materials are usually a single crystal and they have amuch larger yield strength. The amplitude of the recoverable initial elastic strain in the cell wall length direction can thus be controlled to vary over a range from -0.1 to 0.1 by application of an electric potential (Biener et al., 2009, Haiss et al., 1998, Kramer et al., 2004, Zhu et al., 2012a, Zhu et al., 2012b, Zhu and Wang, 2013). In this chapter, the amplitude of the initial strain ε_0^L is set to -0.06, -0.03, 0, 0.03 and 0.06, respectively.

To validate the correction of the equivalent values of the Young's modulus E_e, Poisson's ratio ν_e and cell wall thickness h_e for the beam element in simulations, a single horizontal micro sized beam cantilever structure is tested. The left hand side of the cantilever is fixed and a concentrated transverse load (a small load is assumed as 1×10^{-6} N) is applied to the free end. The Young's modulus and Poisson's ratio of the solid material are assumed as $2\times10^5\ N/\mu m^2$ and 0.3, respectively. l_m/h is assumed as 0.2. The thickness, width and length of the cantilever are assumed as 0.03

μm, 1 μm, and 100 μm, respectively. According to Equations (3.4 – 3.6), the equivalent Young's modulus, Poisson's ratio and the thickness of the cantilever are 1.71378×10^5 $N/\mu m^2$, 0.2794 and 0.035 μm. Then, the obtained deflection of the free end from the finite element simulation is nearly 0.54 μm which is close to the theoretical result of small deflection (a small deflection is about 0.56 μm). Although the value of the equivalent Poisson's ratio v_e could be negative or larger than 0.5, which is physically meaningless for the conventional solid materials, the obtained deflection of the cantilever from the finite element simulation is exactly the same as the theoretical prediction. This suggests that the adoption of the equivalent values of the Young's modulus E_e, Poisson's ratio v_e and cell wall thickness h_e can properly incorporate the size-dependent effect in finite element simulations and, hence, correctly predict the mechanical behaviours of micro- and nano-sized random irregular honeycombs.

3.2.2.4 The model treatment for the initial strain effect

The geometric model of a periodic random irregular Voronoi honeycomb is constructed by the computer program from Zhu et al. (2001a, 2006). Each of the cell walls has the same uniform thickness. Given the honeycomb relative density, the cell wall thickness can be obtained from Equation (2.4). Each of the cell walls is partitioned into a number of BEAM3 elements. To consider the size-dependent effect, the equivalent Young's modulus E_e, Poisson's ratio v_e and cell wall thickness h_e

can be used instead of the original values.

When the initial strain effect ε_0^L is absent, the geometry of the unit periodic random Voronoi honeycomb model is as shown in Figure 3.2. The side length of the unit model is L=60 *mm*. The origin of the *xy* coordinate system is at the bottom left of the model (as shown in Figure 3.3) and the nodal coordinates of the nodes in the beam element are denoted as (x, y). When the effect of the initial strain ε_0^L is present, the corresponding nodal coordinates are noted as (x', y') and are related to the original coordinates by

$$x' = x(1+\varepsilon_0^L) \tag{3.10}$$

$$y' = y(1+\varepsilon_0^L) \tag{3.11}$$

Thus, the side length of the unit model becomes $L' = L(1+\varepsilon_0^L)$ when the effect of the initial strain is present.

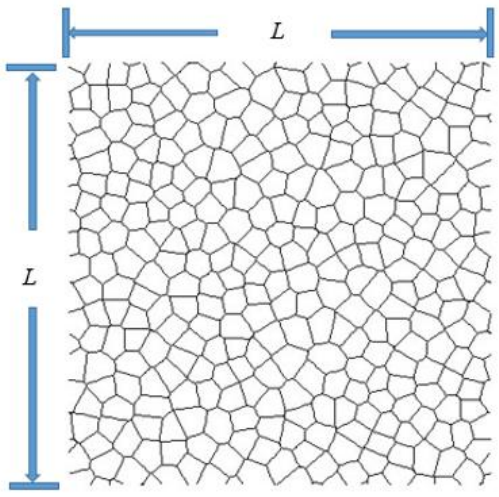

Figure 3.2. The representative unit periodic random irregular honeycombs with the degree of cell regularity α = 0.7.

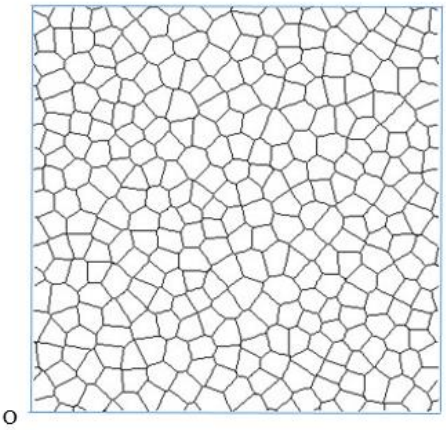

Figure 3.3. The left bottom point shows on the representative unit periodic random irregular honeycombs with the degree of cell regularity α = 0.7.

3.2.2.5 Boundary conditions

Since the irregular random Voronoi honeycomb models are periodic, periodic boundary conditions are the most suitable boundary conditions for the simulations. According to the definition of periodic boundary conditions, the constraint equations that are used in the simulations are given as follows:[14]

$$u_i^{left} - u_j^{left} = u_{i'}^{right} - u_{j'}^{right} \tag{3.12}$$

$$v_i^{left} - v_j^{left} = v_{i'}^{right} - v_{j'}^{right} \tag{3.13}$$

$$\theta_i^{left} = \theta_{i'}^{right} \tag{3.14}$$

$$u_i^{top} - u_j^{top} = u_{i'}^{bottom} - u_{j'}^{bottom} \tag{3.15}$$

$$v_i^{top} - v_j^{top} = v_{i'}^{bottom} - v_{j'}^{bottom} \tag{3.16}$$

$$\theta_i^{top} = \theta_{i'}^{bottom} \tag{3.17}$$

Where *i* and *j* are nodes on the left or top edge of the periodic random irregular Voronoi

[14] Equations (3.12 – 3.14) are the constraint equations on the left and right edges of the structure. Equations (3.15 – 3.17) are the constraint equations on the top and bottom edges of the structure.

honeycomb, while i' and j' are the corresponding nodes on the right or bottom edge.

3.2.2.6 Loading

To restrain possible rigid displacements for the structural model, one node on the bottom edge is fixed in the *y* direction and another node on the left edge is fixed in the *x* direction. To obtain the effective Young's modulus and Poisson's ratio, a compressive strain (i.e. -0.1%) is applied on a node which locates on the top edge and corresponds to the fixed bottom node in the *y* direction (as shown in Figure 3.4 (a)). After the deformation, the corresponding compressive force (reaction force) on the fixed bottom node in the *y* direction and the expansion on the right node which corresponds to the fixed left node in the *x* direction can be obtained. Thus the effective Young's modulus and Poisson's ratio can be determined. To obtain the effective in-plane bulk modulus, a compressive strain (i.e. -0.1%) is applied in both the *x* and *y* directions (as shown in Figure 3.4 (b)). To obtain the effective shear modulus, a compressive strain (i.e. -0.1%) is applied in the *y* direction and a tensile strain (i.e. 0.1%) is simultaneously applied in the *x* direction (as shown in Figure 3.4 (c)). The shear effect can be generated by these compressive and tensile strains.

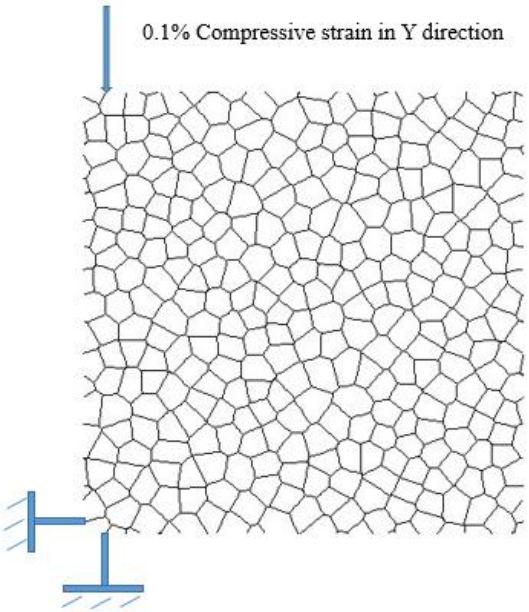
0.1% Compressive strain in Y direction

(a)

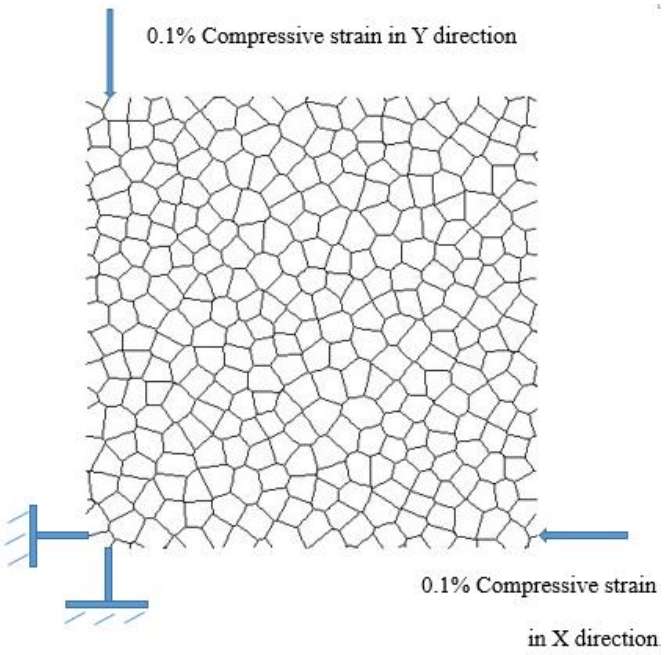
0.1% Compressive strain in Y direction
0.1% Compressive strain
in X direction

(b)

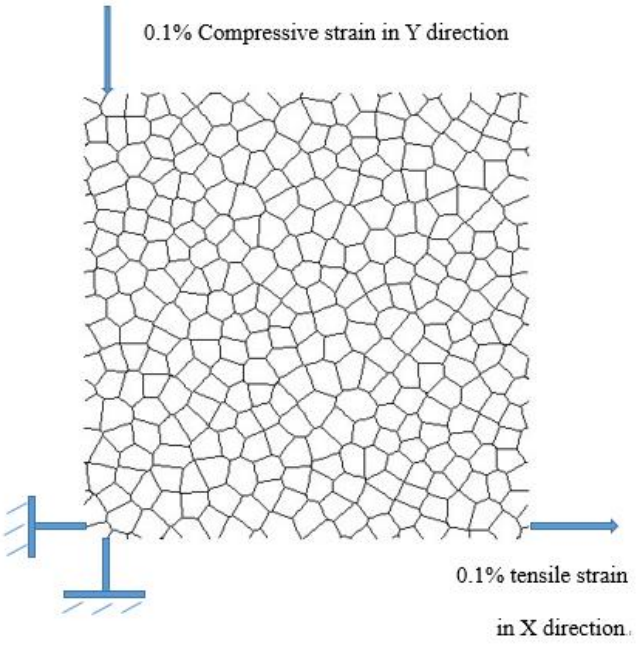

(c)

Figure 3.4. The loading schematic diagram of the representative unit periodic random irregular honeycombs with the degree of the cell regularity α = 0.7: (a) to find the effective Young's modulus and Poisson's ratio, (b) to find the effective bulk modulus, and (c) to find the effective shear modulus.

3.3 Results and Discussion

The micro- and nano-sized random irregular honeycombs are made by a solid material with Young's modulus E_S and Poisson's ratio v_S. In this chapter, each point in the figures is the mean value obtained from 20 different random irregular honeycomb models with the same combination of the parameters, such as the degree of cell regularity, the relative density, and the cell wall thickness (i.e. the ratio of l_m / h or l_n / h), and the error bar shows the standard deviation. The in-plane effective stresses[15]

[15] When the displacement is applied on the edge node of the structure, the reaction force can be found on the corresponding node (as shown in Figure 3.4). The in-plane effective stress is the obtained reaction force per unit area on the edge of the honeycomb in the *x* and *y* direction.

and strains can be obtained as

$$\sigma_x = \frac{F_x}{A_{yz}} = \frac{F_x}{L_y L_z} \tag{3.18}$$

$$\sigma_y = \frac{F_y}{A_{xz}} = \frac{F_y}{L_x L_z} \tag{3.19}$$

$$\varepsilon_x = \frac{\Delta u_x}{L_x} \tag{3.20}$$

$$\varepsilon_y = \frac{\Delta u_y}{L_y} \tag{3.21}$$

The in-plane effective Young's modulus can be given as

$$E_1 = E_2 = \frac{\sigma_y}{\varepsilon_y} \tag{3.22}$$

The in-plane Poisson's ratio can be found by

$$\nu_{12} = -\frac{\varepsilon_x}{\varepsilon_y} \tag{3.23}$$

And the in-plane effective bulk modulus can be obtained as

$$K = \frac{|\sigma_x| + |\sigma_y|}{2(|\varepsilon_x| + |\varepsilon_y|)} \tag{3.24}$$

Where F_x and F_y are the total nodal forces in the *x* and *y* directions, A_{xz} and A_{yz} are the areas of the top and right surfaces, L_x, L_y and L_z are the side lengths in *x*, *y* and *z* directions, $L_x = L_y = 60$ *mm* and L_z is assumed to be a unity, Δu_x and Δu_y are the elongations in the *x* and *y* directions. When the initial strain effect is present, the side lengths L_x and L_y should be multiplied by $(1+\varepsilon_0^L)$. The in-plane effective Young's modulus, Poisson's ratio and bulk modulus obtained from the periodic RVEs represent the elastic properties of micro- and nano-sized irregular

honeycombs.

For both micro- and nano-sized random irregular honeycombs, the in-plane non-dimensional Young's modulus is normalized by $1.5E_S\rho_0^3/(1-v_S^2)$ (Gibson and Ashby, 1997, Zhu, 2010b) [16] and given as

$$\overline{E_1}=\frac{E_1(1-v_S^2)}{1.5E_S\rho_0^3} \tag{3.25}$$

Similarly, the out-of-plane Young's modulus is normalized by $E_S\rho_0$ and given as

$$\overline{E_3}=\frac{E_3}{E_S\rho_0} \tag{3.26}$$

the out-of-plane shear modulus is normalised by $G_S\rho_0$ and given as

$$\overline{G_{31}}=\frac{G_{31}}{G_S\rho_0} \tag{3.27}$$

and the in-plane bulk modulus is normalised by $E_S\rho_0$ and given as

$$\overline{K}=\frac{K}{E_S\rho_0} \tag{3.28}$$

where E_S, v_S and G_S are the Young's modulus, Poisson's ratio and shear modulus of the solid material, ρ_0 is the initial relative density of the representative unit periodic random irregular honeycomb. The non-dimensional elastic properties are to diminish the effects of the initial relative density and the elastic properties of solid materials, then these results would be more useful.

[16] This happens mainly because the plane strain bending of the cell walls is the dominant deformation mechanism. And if the size-dependent and initial stress or strain affects are absent, then the non-dimensional Young's modulus can be approached to 1 when the initial relative density is close to 0. Another reason is that it can be easily to show the tunable range of the non-dimensional Young's modulus with the initial stress or strain effect.

3.3.1 Size-dependent elastic properties of micro-sized random irregular honeycombs

For random irregular micro-sized honeycombs with degrees of regularity α =0.0 and 0.7, the size-dependent effect on the relationship between the non-dimensional in-plane Young's modulus and the honeycomb relative density is obtained and the results are shown in Figures 3.5 (a) and (b). As can be seen, the thinner the cell walls, the larger the non-dimensional Young's modulus. Equations (2.22 – 2.23) show the size-dependent bending and transverse shear rigidities of the micro-sized plates as functions of the value of l_m / h, where l_m is the material intrinsic length parameter at the micro-meter scale (i.e. a material property which can be experimentally measured) and the value of l_m / h present the existence and level of the strain gradient effect. When the cell wall is thinner *h*, the dimensionless bending and transverse shear rigidities of the micro-sized plates (i.e. cell walls) would be larger, it implies that the micro-sized plates would be stiffer and hard to bending, and the whole of the micro-sized honeycomb is harder to compress, that is why the non-dimensional Young's modulus of micro-sized honeycombs becomes larger. The non-dimensional Young's modulus reduces with the increase of the honeycomb relative density. This is because when the cell size and structure of a honeycomb remain unchanged, the relative density of the honeycomb is proportional to the thickness of cell wall (as shown in Equation 2.4). When the relative density is increased, the cell wall becomes thicker, and the smaller the dimensionless bending and transverse shearing rigidities of the cell

walls, and consequently the smaller the dimensionless Young's modulus of the honeycomb. According to Equation (2.4), for honeycombs with a fixed relative density, the smaller the cell size, the thinner the cell wall thickness, and thus the larger the non-dimensional Young's modulus of the honeycombs. If the cell wall thickness is much larger than the material length parameter l_m of the strain gradient effect (i.e. $l_m / h = 0$), the bending and transverse shear rigidities of the micro elements will become the conventional rigidities without the strain gradient effect. Then the Young's modulus of the micro-sized random irregular honeycomb reduces to that of its macro-sized counterpart.

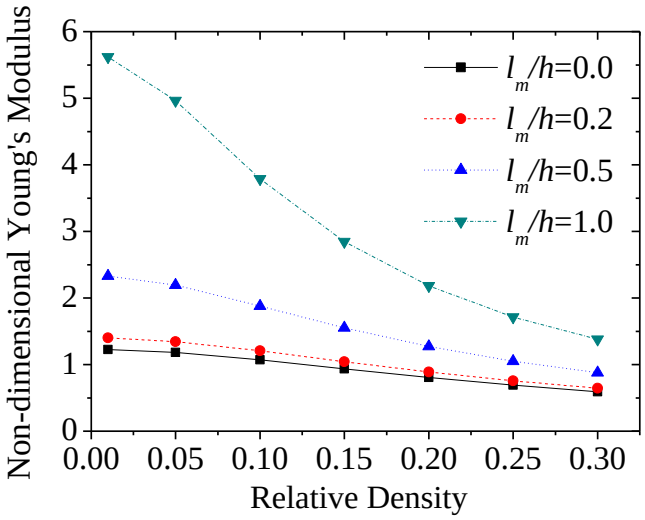

(a)

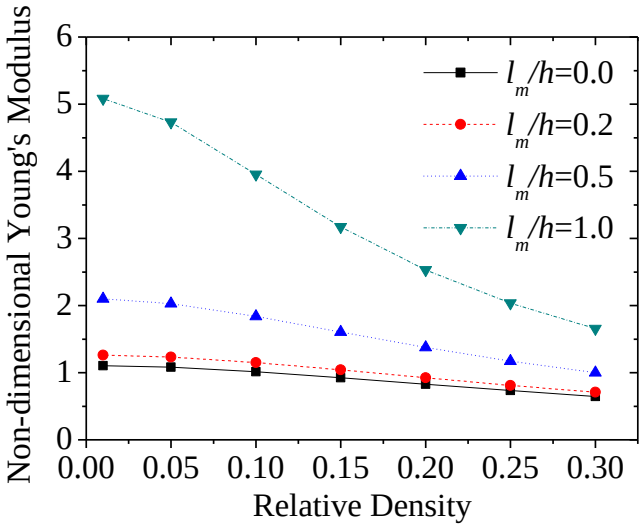

(b)

Figure 3.5. Size-dependent effect on the relationship between the non-dimensional Young's modulus and the relative density of micro-sized random irregular honeycombs with degrees of the cell regularity (a) α =0.0, (b) α =0.7.

Figure 3.6 shows the effects of cell regularity on the non-dimensional Young's modulus of random irregular honeycombs with $l_m / h_0 = 0.5$ and constant initial relative densities $\rho_0 = 0.01$ and $\rho_0 = 0.2$. As can be seen, when the honeycomb relative density is small (e.g. $\rho_0 = 0.01$), the non-dimensional Young's modulus reduces with the increase of the regularity. This trend is similar to the macro-sized honeycombs (Zhu et al., 2001a). However, when the honeycomb relative density is large (e.g. $\rho_0 = 0.2$), the larger the regularity, the larger would be non-dimensional Young's modulus. This trend is reversed when the relative density is nearly 0.15 for random irregular honeycombs with $l_m / h_0 = 0.5$. This phenomenon is also similar to the results from the macro-sized irregular honeycombs (Zhu et al., 2001a). From the results of the macro-sized irregular honeycombs, the opposite trend occurs when the relative density is nearly 0.22. Based on the results obtained from the macro- and

micro-sized honeycombs, it is suggested that the increase of l_m / h_0 leads to the trend change taking place at a smaller relative density.

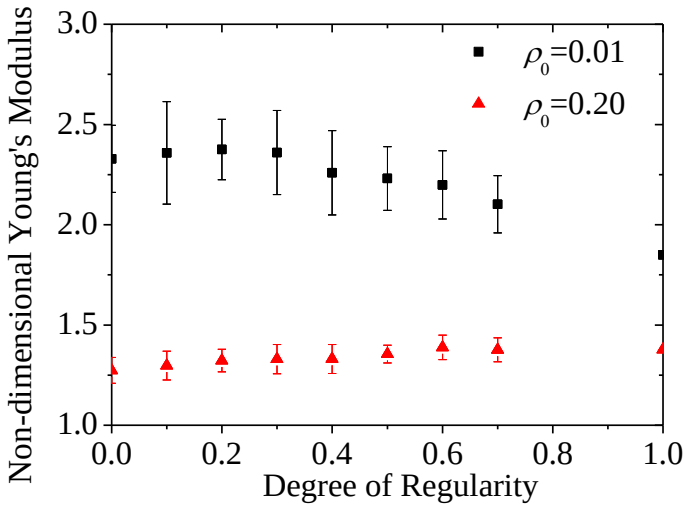

Figure 3.6. Effect of the cell regularity on the non-dimensional Young's modulus of micro-sized random irregular honeycombs with $l_m / h_0 = 0.5$.

Figures 3.7 (a) and (b) show the size-dependent effect on the relationship between the non-dimensional bulk modulus and the relative density of micro-sized random irregular honeycombs. Generally, the thinner the cell walls, the larger the non-dimensional bulk modulus because thinner cell walls have a larger non-dimensional bending stiffness. As can be seen from Figures 3.7 (a) and (b), the non-dimensional bulk modulus slightly increases with the increment of the relative density and the reduction of the cell wall thickness. Since the increase of the non-dimensional bulk modulus is so small, it can be ignored.

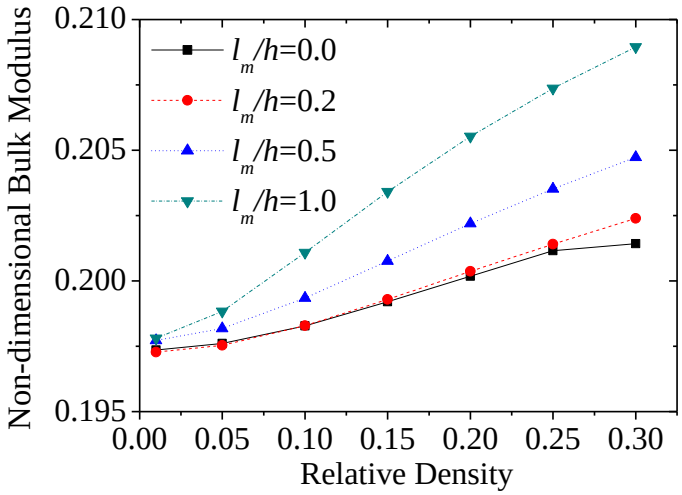

(a)

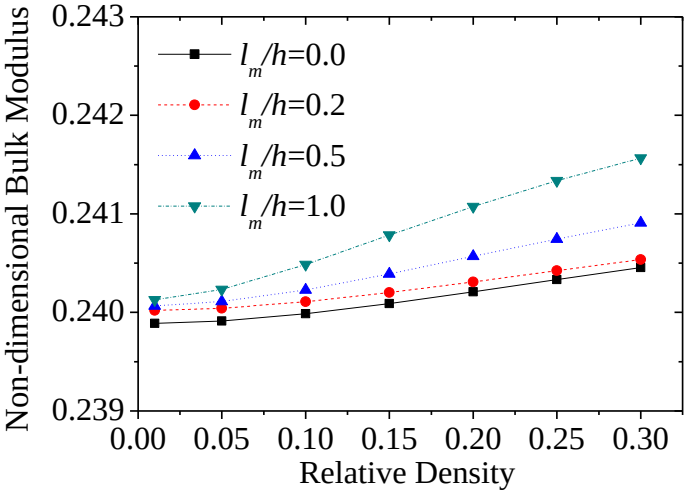

(b)

Figure 3.7. Size-dependent effect on the relationship between the non-dimensional bulk modulus and the relative density of micro-sized random irregular honeycombs with degrees of the cell regularity (a) α =0.0, (b) α =0.7.

Figure 3.8 shows the effect of cell regularity on the non-dimensional bulk modulus of random irregular honeycombs with $l_m / h_0 = 0.5$, and constant initial relative densities $\rho_0 = 0.01$ and $\rho_0 = 0.2$. As can be seen, the cell regularity has a significant effect on the non-dimensional bulk modulus. As the degree of regularity increases, the non-dimensional bulk modulus increases significantly. In contrast, the effect of the relative

density on the non-dimensional bulk modulus is very limited. One thing should be mentioned, when the degree of regularity is 1.0 (i.e. a perfect regular honeycomb) the non-dimensional bulk modulus is very close to 0.25, which is the same as that of macro-sized irregular honeycombs (Zhu et al., 2001a). This happens because the strain gradient effect is completely absent in this case.[17]

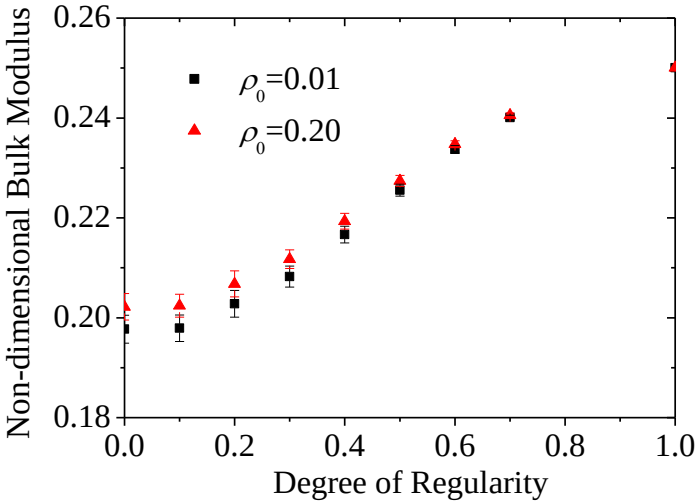

Figure 3.8. Effect of cell regularity on the non-dimensional bulk modulus of micro-sized random irregular honeycombs with $l_m / h_0 = 0.5$.

Figures 3.9 (a) and (b) present the size-dependent effect on the relationship between the Poisson's ratio and the relative density of micro-sized random irregular honeycombs with degrees of the cell regularity α =0.0 and 0.7. In general, the thinner the cell walls or the larger the honeycomb relative density, the smaller the Poisson's ratio. When the relative density tends to 0, the Poisson's ratio approaches a unity.

[17] For a regular honeycomb, the deformation mechanism is the axial stretching or compression when the displacements are applied like Figure 3.4 (b).

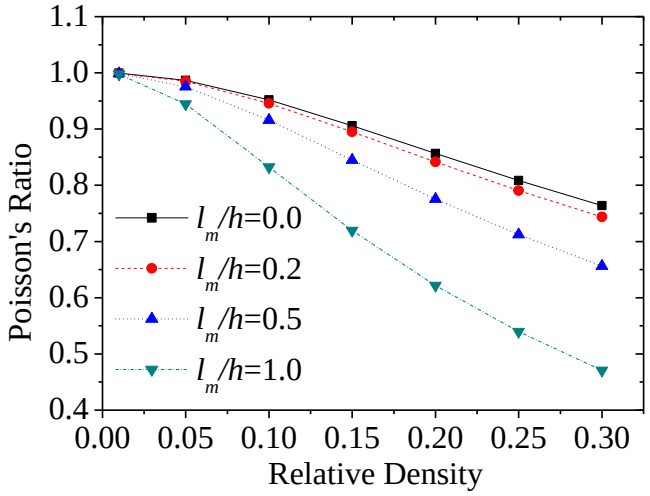

(a)

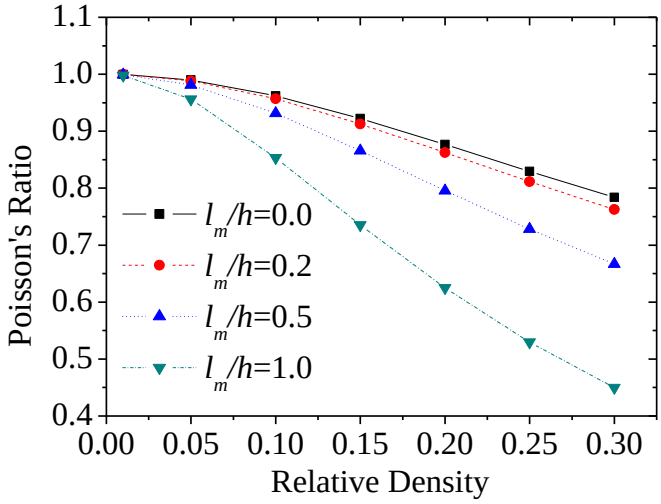

(b)

Figure 3.9. Size-dependent effect on the relationship between the Poisson's ratio and the relative density of micro-sized random irregular honeycombs with degrees of cell regularity (a) α =0.0, (b) α =0.7.

Figure 3.10 displays the effect of the cell regularity on the Poisson's ratio of micro-sized random irregular honeycombs with $l_m / h_0 = 0.5$, and constant initial relative densities $\rho_0 = 0.01$ and $\rho_0 = 0.2$. As can be seen, the cell regularity has a very limited effect on the Poisson's ratio.

Zhu et al. (2001a) have already demonstrated the in-plane isotropic properties of

random irregular honeycombs. The size-dependent non-dimensional in-plane shear modulus of micro-sized honeycombs can thus be obtained from the in-plane non-dimensional Young's modulus and Poisson's ratio. Therefore, the results for the in-plane shear modulus are not presented separately.

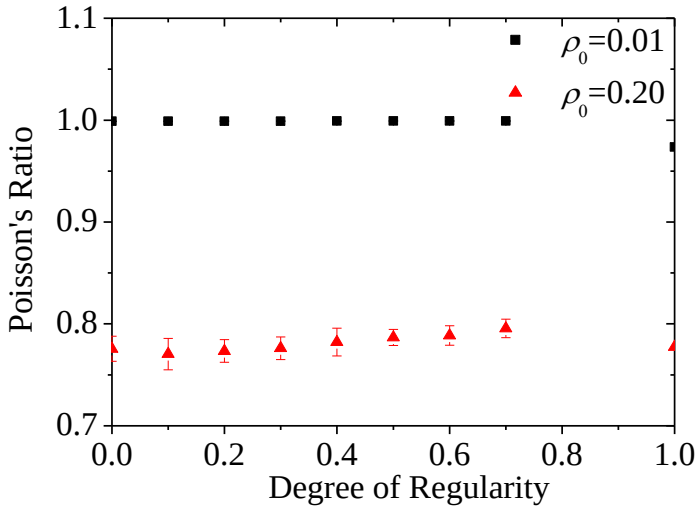

Figure 3.10. Effect of cell regularity on the Poisson's ratio of micro-sized random irregular honeycombs with $l_m / h_0 = 0.5$.

Since there is no strain gradient effect in the out-of-plane deformation, the out-of plane dimensionless Young's modulus of micro-sized random irregular honeycombs is simply a unity, the out-of-plane dimensionless shear modulus is approximately 0.5, and the out-of-plane Poisson's ratio is the same as that of the solid material. So, all of the out-of-plane elastic properties of the micro-sized random irregular honeycombs are the same as those of their macro-sized counterparts.

3.3.2 Size-dependent elastic properties of nano-sized random irregular honeycombs

At the nano-meter scale, the surface elasticity and the initial stress or strain have the effects on elastic properties of nano-sized random irregular honeycombs. When the initial stress or strain effect is absent, the size-dependent effect on the relationship between the non-dimensional Young's modulus and the relative density of nano-sized random irregular honeycombs with degrees of cell regularity α =0.0 and 0.7 are shown in Figures 3.11 (a) and (b), where the value of l_n / h presents the existence and level of the surface elasticity effect. As can be seen, the thinner the cell walls (*h*), the larger the value of l_n / h, the larger the dimensionless Young's modulus of the nano-sized honeycombs. This is because the bending, transverse shear and axial stretching or compression rigidities of the nano-sized cell walls are larger (as shown in Equations (2.28 – 2.30)), and the whole of nano-sized honeycomb becomes stiffer and hard to compress. When the cell walls become smaller, the surface area to volume ratio becomes larger, thus the surface elasticity will have a larger influence on the cell walls and the whole structure. In addition, the larger the relative density, the smaller the dimensionless Young's modulus. For nano-sized random irregular honeycombs with a fixed relative density, the smaller the cell size, the larger the dimensionless Young's modulus. These results are consistent with the nano-sized regular hexagonal honeycombs (Zhu, 2010b). If the cell wall thickness is much larger than the material intrinsic length at the nano-meter scale (i.e. $l_n / h \approx 0$), the surface elasticity effect

disappears, then all of the results of the nano-sized honeycombs reduce to those of their macro-sized counterparts (Zhu et al., 2001a). It can be found that the surface elasticity plays an important role in the elastic properties of the nano-sized irregular honeycombs.

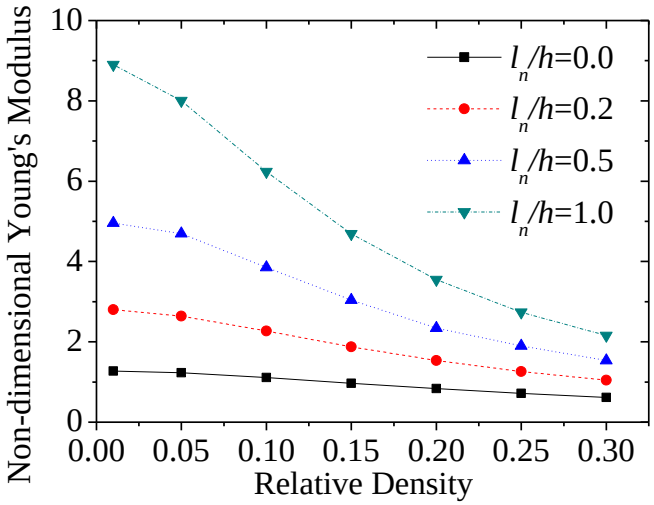

(a)

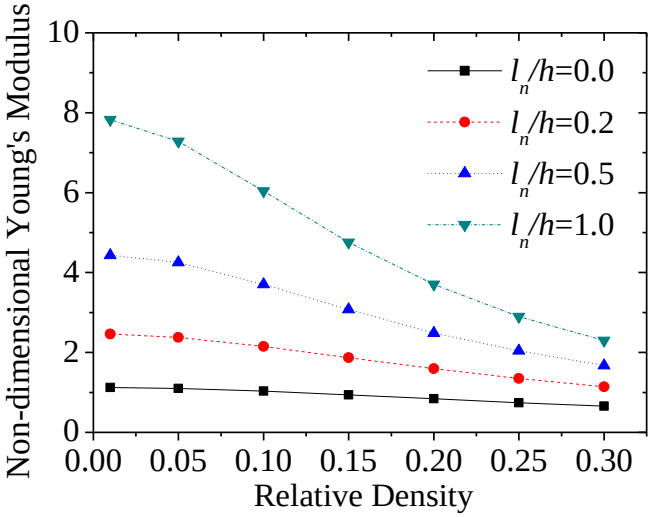

(b)

Figure 3.11. Size-dependent effect on the relationship between the non-dimensional Young's modulus and the relative density of nano-sized random irregular honeycombs with degrees of the cell regularity (a) α =0.0, (b) α =0.7.

Where the surface modulus effect is absent (i.e. $l_n/h=0$), the effect of the cell wall

initial strain on the relationship between the non-dimensional Young's modulus and the relative density of nano-sized random irregular honeycombs with degrees of the cell regularity α =0.0 and 0.7 are presented in Figures 3.12 (a) and (b). At the nano-meter scale, the amplitude of the recoverable initial elastic strain in the cell wall length direction can be controlled to vary over a range from -0.1 to 0.1 by adjusting the amplitude of an applied electric potential (Zhu, 2010b, Zhu et al., 2012a). As can be seen in Figures 3.12 (a) and (b), the larger the honeycomb relative density, the smaller the non-dimensional Young's modulus. In addition, the dimensionless Young's modulus can be controlled either to increase about 60% or to reduce nearly 35% when the initial strain ε_0^L in the cell wall length direction is controlled to vary the range from -0.06 to 0.06. When the honeycomb is at the nano-meter scale, the surface area to volume ratio becomes larger, then the initial surface stress effect will play an important role. According to the expression of the initial strain in the cell wall length direction or width direction ($\varepsilon_0^L = \varepsilon_0^W = \frac{\sigma_0^L}{E_S}(1-\nu_S) = -\frac{2\tau_0}{E_S h}(1-\nu_S)$), and thickness direction ($\varepsilon_0^h = -\frac{2\nu_S}{E_S}\sigma_0^L = \frac{4\nu_S\tau_0}{E_S h}$) (Zhu et al., 2012a, Zhu and Wang, 2013, Zhu et al., 2012b), it can be found that when the initial strain in the cell wall length direction is positive, the initial strain in the thickness direction of the cell walls is negative. This means the length of cell walls extends and the thickness of cell walls shrinks before the honeycomb is subjected to external force or stress (as shown in Equations (3.7 – 3.9)), it leads to the larger slenderness ratio, then the beam element will become more

easily to bend, that is why the non-dimensional Young's modulus of the nano-sized irregular honeycomb is smaller. Whether the surface modulus effect is present or absent, the tunable percentage of the non-dimensional Young's modulus depends on the tunable range of the initial strain ε_0^L (Zhu, 2010b, Zhu et al., 2012a). If the value of the initial strain in the cell wall direction ε_0^L is different from those given in Figures 3.12 (a) and (b), the non-dimensional Young's modulus of the nano-sized random irregular honeycombs can still be obtained by scaling up or scaling down the results. According to the above descriptions, it can be found that the effect of the initial strain plays important role in the elastic properties of man-sized irregular honeycombs.

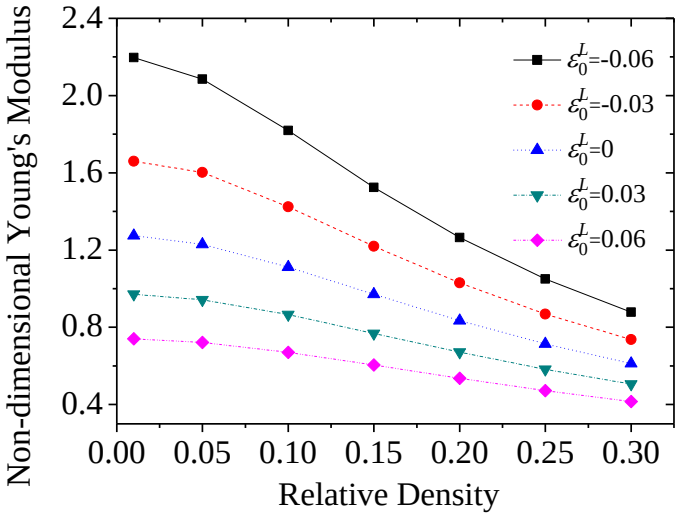

(a)

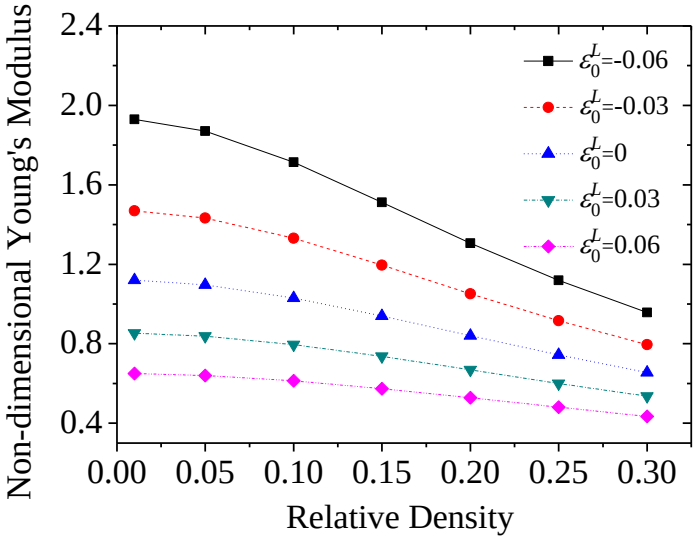

(b)

Figure 3.12. Effect of the cell wall initial stress or strain on the relationship between the non-dimensional Young's modulus and the relative density of nano-sized random irregular honeycombs with degrees of the cell regularity (a) α =0.0, (b) α =0.7.

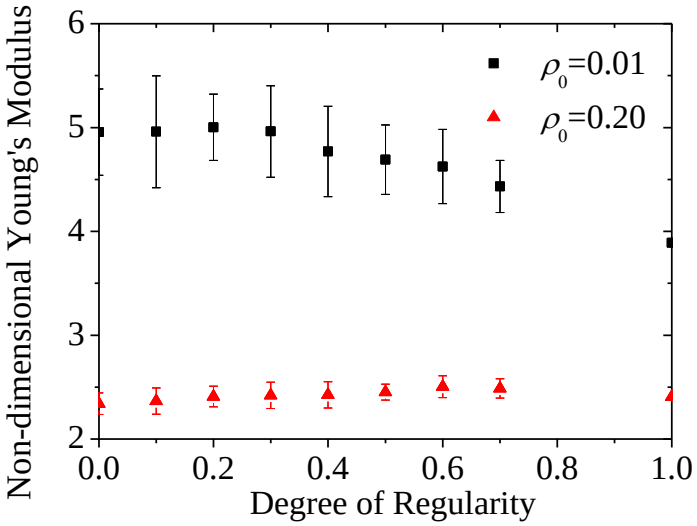

Figure 3.13. Effect of the cell regularity on the non-dimensional Young's modulus of nano-sized random irregular honeycombs with $l_n / h = 0.5$.

The effect of cell regularity on the non-dimensional Young's modulus of nano-sized random irregular honeycombs with $l_n / h = 0.5$ and constant initial relative densities $\rho_0 = 0.01$ and $\rho_0 = 0.2$ are shown in Figure 3.13, where the initial strain effect is

absent. If the initial relative density is very small (i.e. $\rho_0 = 0.01$), increasing the degree of cell regularity leads to a decrease of the non-dimensional Young's modulus. However, the trend is reversed when the initial relative density is large (i.e. $\rho_0 = 0.2$), this situation occurs when the initial relative density is close to 0.15. It also can be seen that the thinner the cell wall thickness, the smaller the relative density when this changed trend occurs. These results are the similar to the micro-sized random irregular honeycombs. One thing should be mentioned for Figure 3.13, the largest standard deviation of the non-dimensional Young's modulus is about 10%, which indicates that the 20 similar models have quite different dimensionless Young's modulus.

Where the initial stress or strain effect is absent, the size-dependent effect on the relationship between the non-dimensional bulk modulus and the relative density of nano-sized random irregular honeycombs with degrees of the cell regularity α =0.0 and α =0.7 are shown in Figures 3.14 (a) and (b). As can be seen, at the nano-meter scale, the cell wall thickness significantly affects the non-dimensional bulk modulus of a nano-sized random irregular honeycomb, while the effect of the relative density on the non-dimensional bulk modulus is so small that it can be ignored. This happens because the cell wall axial stretching or compression is the dominant deformation mechanism and the surface modulus thus significantly affects the axial stretching or compression stiffness at the nano-meter scale.

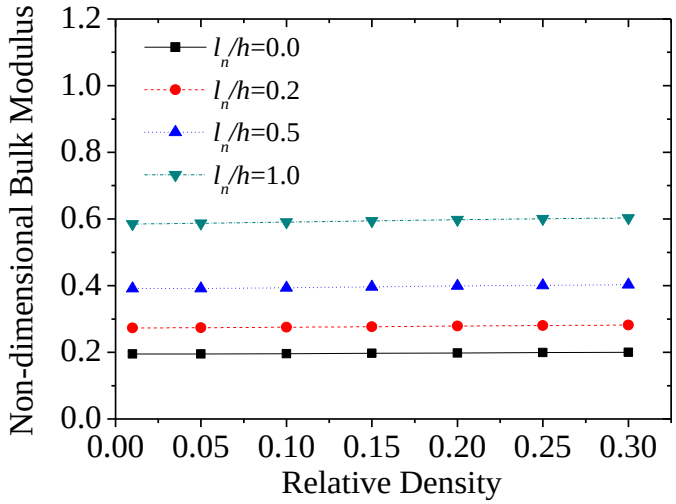

(a)

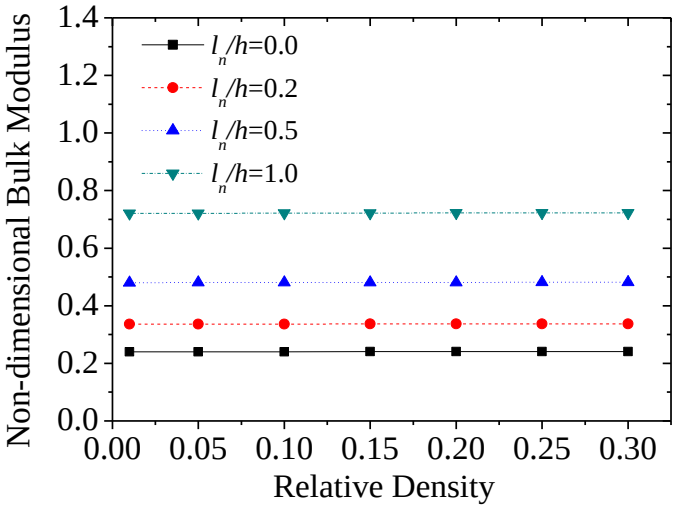

(b)

Figure 3.14. Size-dependent effect on the relationship between the non-dimensional bulk modulus and the relative density of nano-sized random irregular honeycombs with degrees of the cell regularity (a) α =0.0, (b) α =0.7.

Figures 3.15 (a) and (b) show the effect of the cell wall initial stress or strain on the relationship between the non-dimensional bulk modulus and the relative density of nano-sized random irregular honeycombs with $l_n / h = 0.5$ and degrees of the cell regularity α =0.0 and 0.7. The amplitude of the initial strain in the cell wall direction is controlled to vary from -0.06 to 0.06, and the controllable range of the non-

dimensional bulk modulus of nano-sized random irregular honeycombs with α =0.0 is smaller than that of honeycombs with α =0.7. The results of the dimensionless bulk modulus presented in Figures 3.14 (a) and (b), and Figures 3.15 (a) and (b) can be approximated by $0.195(1+\frac{2l_n}{h})(1-\frac{2v_S}{1-v_S}\varepsilon_0^L)/(1+\varepsilon_0^L)$ for nano-sized random irregular honeycombs with α =0.0, and by $0.24(1+\frac{2l_n}{h})(1-\frac{2v_S}{1-v_S}\varepsilon_0^L)/(1+\varepsilon_0^L)$ for those with α =0.7.[18]

Figure 3.16 indicates that the honeycomb regularity has a significant effect on the dimensionless bulk modulus, the larger the degree of regularity, the larger the dimensionless bulk modulus. This happens mainly because as the regularity increases, the deformation mechanism of the cell wall stretching or compression plays an increasingly important role when a honeycomb is under in-plane compressive stress in *x* and *y* direction. The honeycomb initial relative density has a limited effect on the dimensionless bulk modulus of nano-sized random irregular honeycombs, which is consistent with the results of their macro- and micro-sized counterparts. The error bars indicate that the standard deviation is small.

[18] The non-dimensional bulk modulus of nano-sized random irregular honeycombs can be described by the expression $(1+\frac{2l_n}{h})(1-\frac{2v_S}{1-v_S}\varepsilon_0^L)/(1+\varepsilon_0^L)$, the derivation of this expression is shown from Equations (3.29 – 3.36)

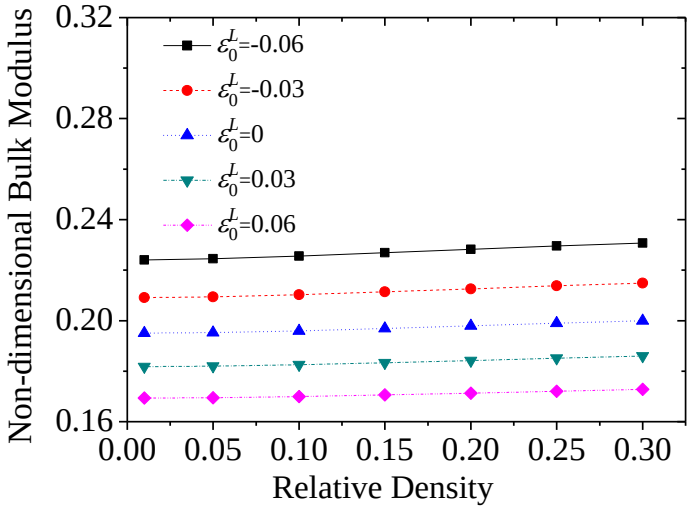

(a)

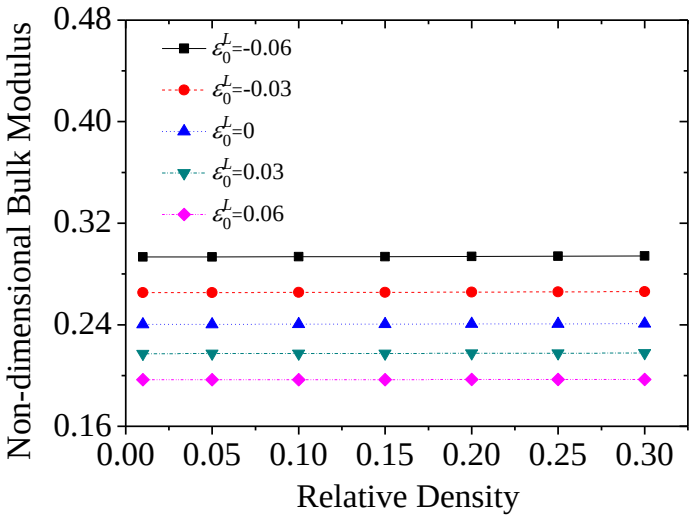

(b)

Figure 3.15. Effect of the cell wall initial stress or strain on the relationship between the non-dimensional bulk modulus and the relative density of nano-sized random irregular honeycombs with degrees of cell regularity (a) α =0.0, (b) α =0.7.

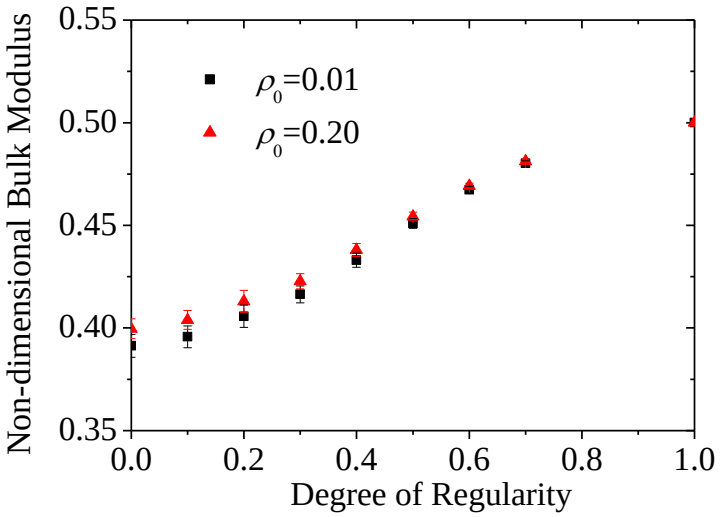

Figure 3.16. Effect of the cell regularity on the non-dimensional bulk modulus of nano-sized random irregular honeycombs with $l_n / h = 0.5$.

Figures 3.17 (a) and (b) show the size-dependent effect on the relationship between the Poisson's ratio and the relative density of nano-sized random irregular honeycombs with degrees of cell regularity α =0.0 and 0.7, where the initial stress or strain effect is absent. When the relative density tends to 0, the Poisson's ratio approaches a unity. When the relative density is fixed at 0.25, and the cell wall thickness is much larger than the material intrinsic length, the values of Poisson's ratio are nearly 0.81 for α =0.0 and 0.84 for α =0.7, these results are consistent with the results from Zhu et al. (2001a). The relative density significantly affects the in-plane Poisson's ratio of nano-sized random irregular honeycombs. Generally, the larger the relative density, the smaller the in-plane Poisson's ratio. In addition, the thinner cell walls, the smaller the in-plane Poisson's ratio. However, the influence of the cell wall thickness on the in-plane Poisson's ratio of nano-sized random irregular honeycombs is very small.

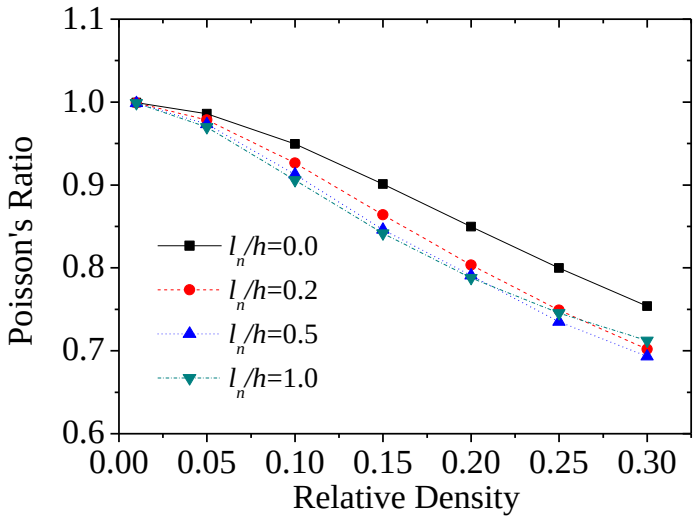

(a)

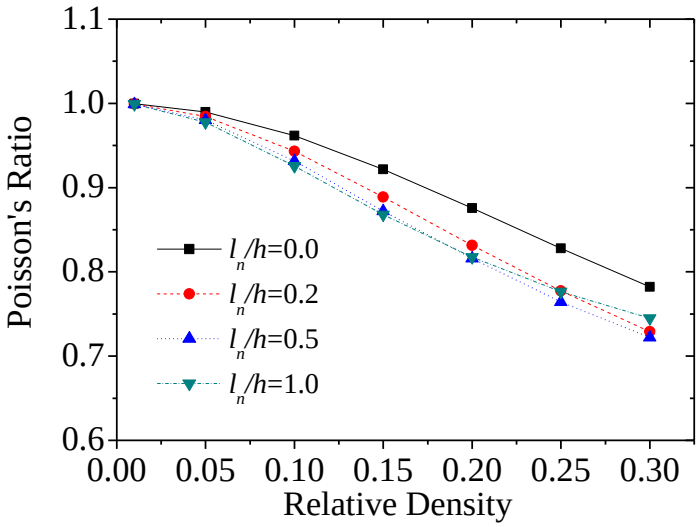

(b)

Figure 3.17. Size-dependent effect on the relationship between the Poisson's ratio modulus and the relative density of nano-sized random irregular honeycombs with degrees of the cell regularity (a) α =0.0, (b) α =0.7.

Where the effect of the surface elasticity is absent, the effect of the cell wall initial stress or strain on the relationship between the Poisson's ratio and the relative density of nano-sized random irregular honeycombs with degrees of cell regularity α =0.0 and 0.7 are shown in Figures 3.18 (a) and (b). As can be seen, the Poisson's ratio can be controlled to vary over a considerable range by the application of an initial strain.

The range of the tunable Poisson's ratio is nearly proportional to the range of the tunable initial strain and strongly depends on the honeycomb relative density.

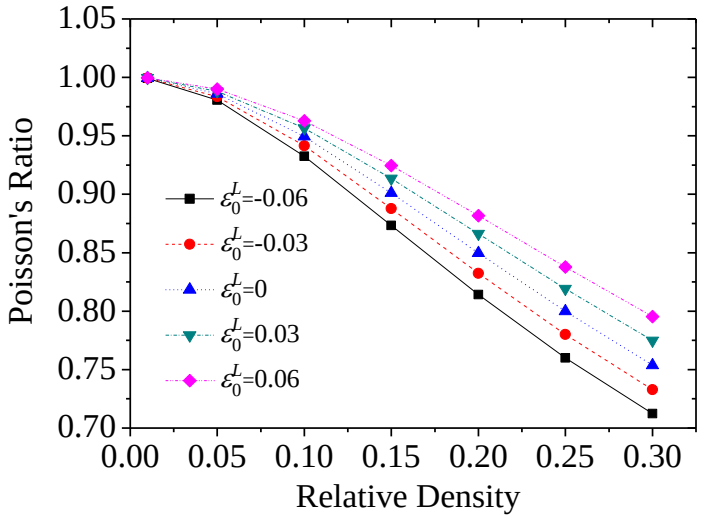

(a)

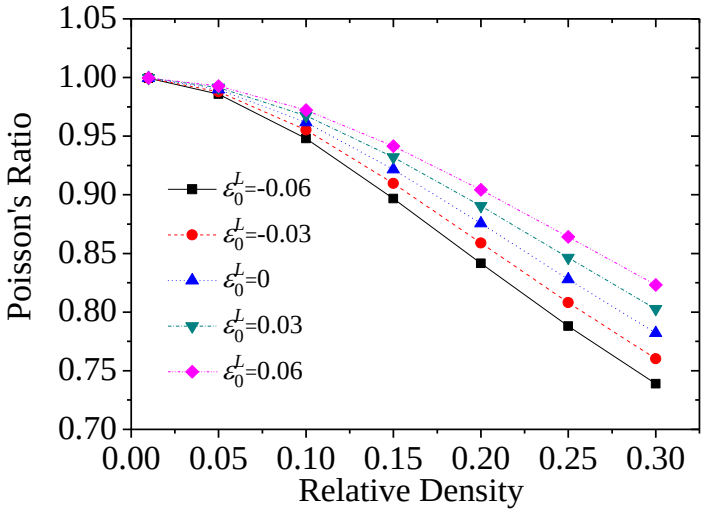

(b)

Figure 3.18. Effect of the cell wall initial stress/strain on the relationship between the Poisson's ratio and the relative density of nano-sized random irregular honeycombs with degrees of cell regularity (a) α =0.0, (b) α =0.7.

Figure 3.19 shows the relations between the cell regularity and the Poisson's ratio of nano-sized random irregular honeycombs with $l_n / h = 0.5$. As can be seen, the effect

of cell regularity on the Poisson's ratio of nano-sized honeycombs is negligible.

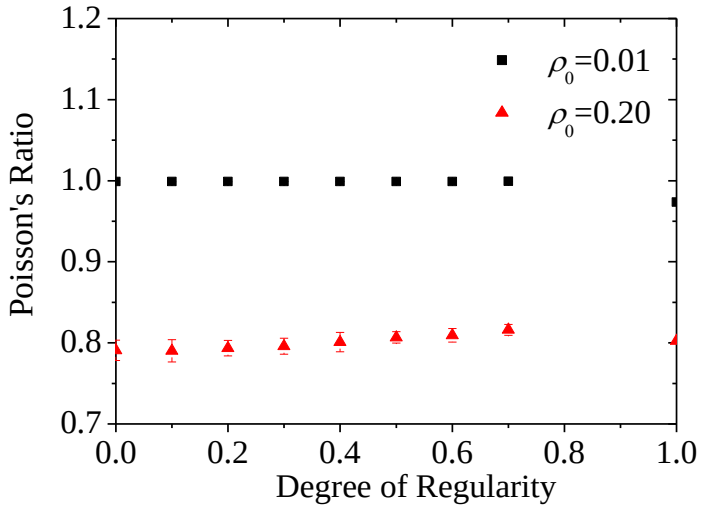

Figure 3.19. Effect of cell regularity on the Poisson's ratio of nano-sized random irregular honeycombs with $l_n / h = 0.5$.

For nano-sized honeycombs, the out-of-plane Young's modulus and shear modulus can be obtained as (Zhu, 2010b):

$$E_3 = (1+2\frac{l_n}{h})E_S\rho \tag{3.29}$$

$$G_{31} = \frac{1}{2}(1+\frac{2l_n}{h})G_S\rho \tag{3.30}$$

where ρ is the relative density of nano-sized honeycombs when the initial strain effect is present. ρ is a function of the initial strain and is given as

$$\rho = \frac{h\sum_{k=1}^{M} l_k}{L'^2} = \frac{h_0(1+\varepsilon_0^h)\sum_{k=1}^{M} l_{0k}(1+\varepsilon_0^L)}{L^2(1+\varepsilon_0^L)^2} = \frac{h_0(1+\varepsilon_0^h)\sum_{k=1}^{M} l_{0k}}{L^2(1+\varepsilon_0^L)} \tag{3.31}$$

where $\varepsilon_0^h = -\frac{2\nu_S}{E_S}\sigma_0^L$ is the initial strain in thickness direction of the cell walls

(Zhu et al., 2012a), $\sigma_0^L = -2\tau_0 / h$ is the initial stress in length direction of the cell walls (Zhu et al., 2012a), $\varepsilon_0^L = -\frac{2\tau_0}{hE_S}(1-\nu_S)$ is the initial strain in length direction of the cell walls (Zhu, 2010b), and the relationship between ε_0^h and ε_0^L is given by

$$\varepsilon_0^h = -\frac{2\nu_S}{1-\nu_S}\varepsilon_0^L \tag{3.32}$$

By substituting Equation (3.32) into Equation (3.31), the relative density can be obtained as

$$\rho = \frac{h_0(1-\frac{2\nu_S}{1-\nu_S}\varepsilon_0^L)\sum_{k=1}^{M} l_{0k}}{L^2(1+\varepsilon_0^L)} \tag{3.33}$$

By substituting Equations (3.29), (3.30) and (3.33) into Equations (3.26) and (3.27), the normalized out-of-plane Young's modulus can be obtained as

$$\overline{E_3} = \frac{E_3}{E_S\rho_0} = (1+\frac{2l_n}{h})\cdot(1-\frac{2\nu_S}{1-\nu_S}\varepsilon_0^L)/(1+\varepsilon_0^L) \tag{3.34}$$

The dimensionless out-of-plane shear modulus can be given as

$$\overline{G_{31}} = \frac{G_{31}}{G_S\rho_0} = \frac{1}{2}(1+\frac{2l_n}{h})(1-\frac{2\nu_S}{1-\nu_S}\varepsilon_0^L)/(1+\varepsilon_0^L) \tag{3.35}$$

Based on the results given in Figures 3.14 and 3.15, the dimensionless bulk modulus can be approximated by

$$\overline{K} = \frac{K}{E_S\rho_0} = K(\alpha)(1+\frac{2l_n}{h})(1-\frac{2\nu_S}{1-\nu_S}\varepsilon_0^L)/(1+\varepsilon_0^L) \tag{3.36}$$

while the out-of-plane Poisson's ratio is the same as that of the solid material,

$$\nu_{31} = \nu_S \tag{3.37}$$

The factor $K(\alpha)$ is the dimensionless bulk modulus of the macro-sized random

irregular honeycombs, whose value depends on the degree of cell regularity and is almost independent of the initial relative density (as shown in Figures 3.14 and 3.15). According to the previous research (Zhu, 2010b, Zhu et al., 2012b), nano-sized honeycombs with regular hexagonal cells, regular equilateral triangular cells, or square cells have the same dimensionless out-of-plane Young's modulus, shear modulus and Poisson's ratio, this suggests that the cell shape of nano-sized honeycombs does not affect the out-of-plane elastic properties.

3.4 Summary

All of the five independent elastic constants (i.e. E_1, ν_{12}, E_3, G_{31}, and ν_{31}) are obtained for micro- and nano-sized random irregular honeycombs. At the micro-meter scale, the linear elastic properties of random irregular honeycombs are size-dependent due to the strain gradient effect. At the nano-meter scale, the linear elastic properties of random irregular honeycombs are not only size-dependent due to the surface elasticity effect, but they are also tunable and controllable with the effect of the initial stress or strain.

Chapter 4 The high strain compression of micro- and nano-sized periodic random irregular honeycombs

4.1 Introduction

With the advance of manufacturing techniques, micro- and nano-sized regular honeycombs can now be easily produced (Nishihara et al., 2005, Tamon et al., 2013) and they have already been widely used in different engineering applications, such as the actuator material of nano-sensors (Kramer et al., 2004). Understanding the linear and nonlinear deformation behaviours of micro- and nano-sized random irregular honeycombs is essential, not only for the precise design of such materials but also for their correct applications in different areas.

This chapter will focus on the numerical simulation of the high strain compression behaviours of low-density micro- and nano-sized random irregular honeycombs. As discussed in Chapter 3, the strain gradient effects (Aifantis, 1999, Fleck and Hutchinson, 1993, Gao et al., 1999, Lam et al., 2003, Toupin, 1962, Yang et al., 2002, Zhu, 2008, Zhu, 2010b, Zhu and Wang, 2013, Zhu et al., 2012b) may dominate the deformation behaviours at the micro-meter scale, and the surface elasticity and the initial stress or strain effects become the main deformation mechanisms at the nano-meter scale (Duan et al., 2005, Miller and Shenoy, 2000, Zhu and Wang, 2013, Zhu et al., 2012b). As in Chapter 3, a commercial finite element software (ANSYS) is used

to perform the large deformation simulations in this chapter, and the effects of the size-dependent, initial stress or strain, and cell regularity on the high strain compression behaviours of micro- and nano-sized random irregular honeycombs will be explored.

4.2 Methodology

4.2.1 Parameters setting on random irregular honeycomb models

As in Chapter 3, all of the geometrical models of random irregular Voronoi honeycombs are periodic and they are constructed by Zhu et al.'s (2001a, 2006) program. In order to construct a correct geometrical model for a random irregular honeycomb, three parameters must be input to the computer, which are: the degree of regularity, the relative density, and the number of complete cells in a model.[19] As discussed previously, if the degree of regularity is 0, the constructed model is a fully irregular periodic honeycomb. Meanwhile, if the degree of regularity is 1.0, then the constructed model is a perfectly regular hexagonal honeycomb. In this chapter the degrees of cell regularity are set to 0.0, 0.2, 0.4, and 0.7.

The simulations are focused on low-density honeycombs, and the relative density of periodic random irregular honeycombs is thus set to 0.01 in this chapter.[20] All of the cell walls in the model are assumed to be uniform and to have the same thickness, and the width of the cell walls is assumed to be a unit and to be much larger than the

[19] Their definitions and equations are presented in Section 2.3.1 of Chapter 2.
[20] Generally, the relative density of cellular solid materials is less than 0.3 (Gibson and Ashby, 1997).

wall thickness. The cell wall thickness can be determined from the definition of the relative density (as shown in Equation (2.4)).

Similarly to Chapter 3, each data for the high strain compression behaviour of random irregular honeycombs will be obtained from 10 to 20 similar models. Zhu et al. (2006) have demonstrated that the larger the number of complete cells, the smaller the standard deviation of the results of the similar models. Since large compression simulations of honeycombs involve geometrical nonlinearity, the larger the number of complete cells in a model, the longer computer time needed for a simulation. Moreover, the simulation may become more likely to be unstable. This is a geometrically non-linear problem and the solution is achieved by iteration in each loading step. It is problem to find the global minimum for a function of multi-variables. The larger the irregular model, the larger the number of variables, and the longer time it would take and the more difficult to obtain a convergent solution, i.e. more difficult to achieve stable solution. Therefore, the number of complete cells in each model is set to 100 for the simulations in this chapter.

4.2.2 Finite element simulations

As discussed in Chapter 3, the commercial finite element software ANSYS is used to perform all the computer simulations. Each of the cell walls in the random irregular honeycomb models is partitioned into a number of BEAM3 elements with a rectangular cross-section. Although the honeycombs are in-plane compressed to a

strain of 60%, the strain in the solid material is quite small because the relative density of the honeycombs is assumed to be 0.01. The solid material of the honeycombs is assumed to linear elastic, and to have a Young's modulus $E_S = 2\times10^5\,MPa$ and a Poisson's ratio v_S =0.4. It has previously been demonstrated (Zhu et al., 2001a, Zhu et al., 2006) that the Poisson's ratio of the solid material has very limited effects on simulation results.

At the micro- and nano-meter scales, the bending, transverse shear and axial stretching or compression rigidities are size-dependent, and are given by Equations (2.22 – 2.24) for micro-sized honeycombs and Equations (2.28 – 2.30) for nano-sized honeycombs. The equivalent solid Young's modulus E_e, Poisson's ratio v_e and beam thickness h_e can be determined from Equations (3.4 – 3.6). Similarly to Chapter 3, the values of l_m/h and l_n/h are set to 0.0, 0.2, 0.5, and 1.0. The amplitude of the initial strain ε_0^L is set to -0.06, 0, and 0.06 because the amplitude of the recoverable initial elastic strain in the cell wall length direction can be controlled to vary over a range from -0.1 to 0.1 by application of an electric potential (Biener et al., 2009, Haiss et al., 1998, Kramer et al., 2004, Zhu et al., 2012a, Zhu et al., 2012b, Zhu and Wang, 2013). The model treatment for the initial strain effect is the same as in Chapter 3, which can be expressed by Equations (3.10 – 3.11).

Since all of the random irregular honeycombs are periodic, the periodic boundary conditions that have already been described in Chapter 3 are used for the high strain compression simulations of random irregular honeycombs. The models are

compressed to a strain of about 60%.[21] In contrast to linear elastic analysis, in the "Analysis Options" section of the ANSYS software, the "Large Displacement Static" needs to be selected and the "Nonlinear Options" needs to be "ON". For the loading step, there are three important settings for the process, which are: "load step", "substep" and "equilibrium iteration". Figure 4.1 gives a schematic diagram of this. In order to achieve the convergence of the loading, the "load step" is set to two steps. In the first "load step", the models are compressed up to a strain of about 30%. In the second 'load step', the models are further compressed 30% (i.e., in total 60%).

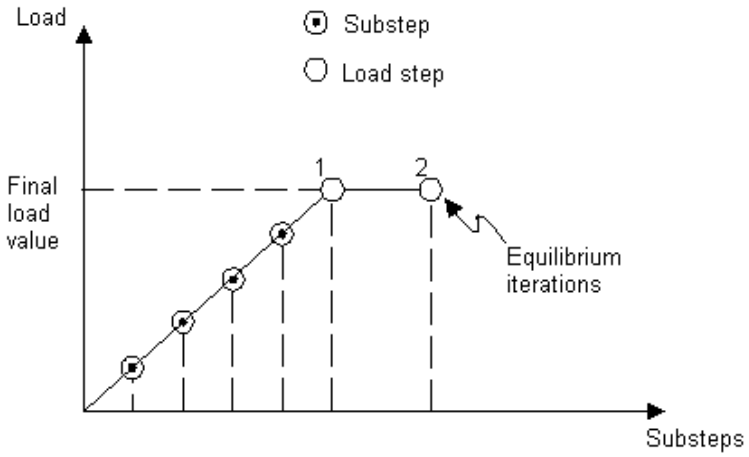

Figure 4.1. Schematic diagram of load Step, substep and equilibrium iteration (ANSYS).

In each "load step", it may needs to set the "substep", which divides the whole of "load step" into several steps.[22] The "substep" is also known as "time step", so the high strain compression simulations can be controlled by time. In this chapter, the "time

[21] Similarly to Chapter 3, in order to avoid the possible rigid displacement on the structure, one node on the bottom edge is fixed in *y* direction, and another node on the left edge is fixed in *x* direction. The compressive strain is applied in the *y* direction on a top node which corresponding the fixed bottom node (similarly to Figure 3.4 (a)).

[22] An accurate solution can be obtained.

step" is set to automatic time stepping because the automatic time stepping can automatically determine the time step size. According to the ANSYS tutorial document (ANSYS), there are two loading types for the "substep": one is ramped load, and the other is stepped load. As can be seen from Figures 4.2 (a) and (b), if the load is ramped, then it increases gradually at each "substep" until the end of the "load step". If the load is stepped, then the full load is added into the first "substep" and stays constant during the rest of the "load step". Generally, ramped load is suitable for static analysis, and stepped load is used in transient analysis (ANSYS). Based on the above description, ramped load is selected in the simulations of this chapter.

Since high strain compression involves geometrical nonlinearity, the solutions are achieved by iteration, and convergence is, therefore, a very important issue. For convenience, the convergence tolerance on all the solutions of force and displacement is set to 5%, and the equilibrium iteration is accordingly set to 300 for iteration corrections on the solutions of each "substep" and "load step". The loading goes into the next step if the correction solution meets the convergence tolerance.

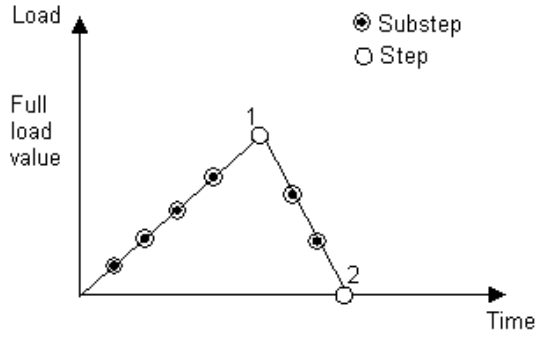

(a)

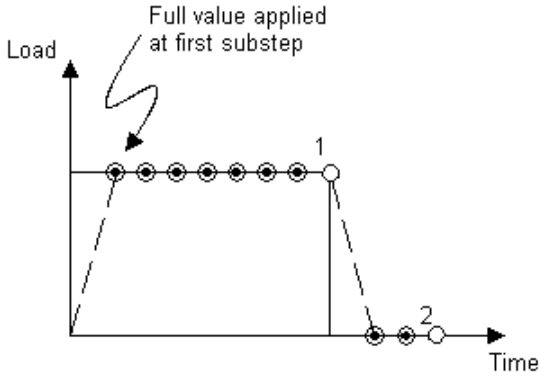

(b)

Figure 4.2. Schematic diagram: (a) Ramped loads (b) Stepped loads (ANSYS).

4.3 Results and Discussion

In this chapter, each data is obtained from 10 to 20 similar models, which have the same combination of the parameters (such as the degree of regularity, the relative density and the number of complete cells). Since it is quite difficult to compress the models to a strain of 60% due to the convergence issue, sometimes it needs to run more than 50 similar models for each combination of the parameters in order to obtain sufficient useful results.

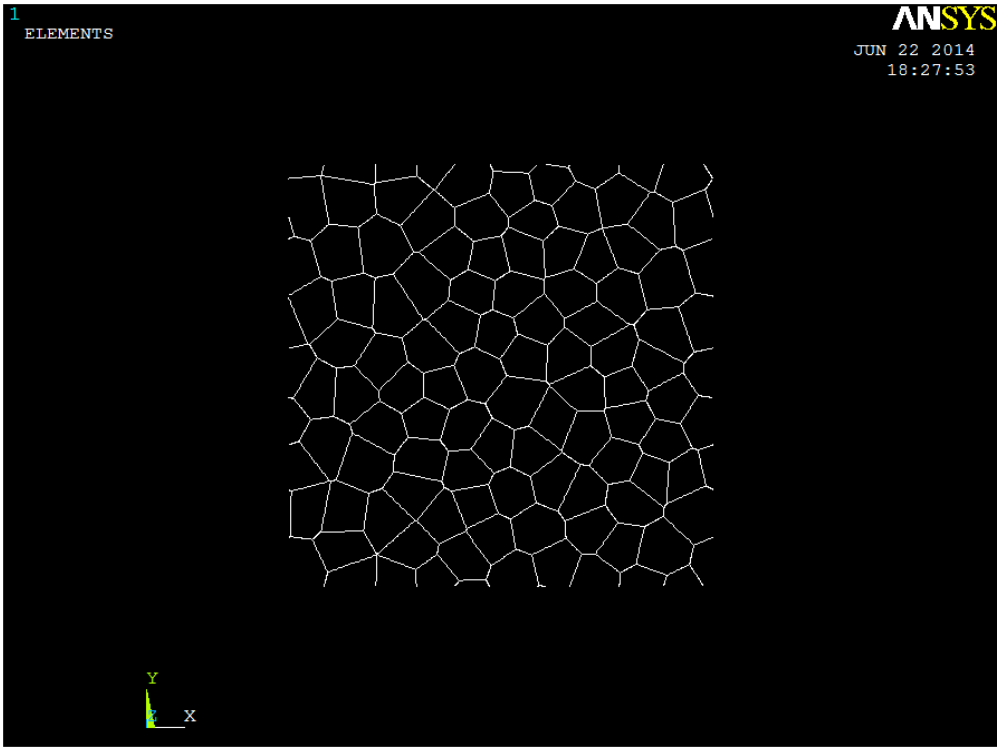
1
ELEMENTS
ANSYS
JUN 22 2014
18:27:53
Y
X

(a)

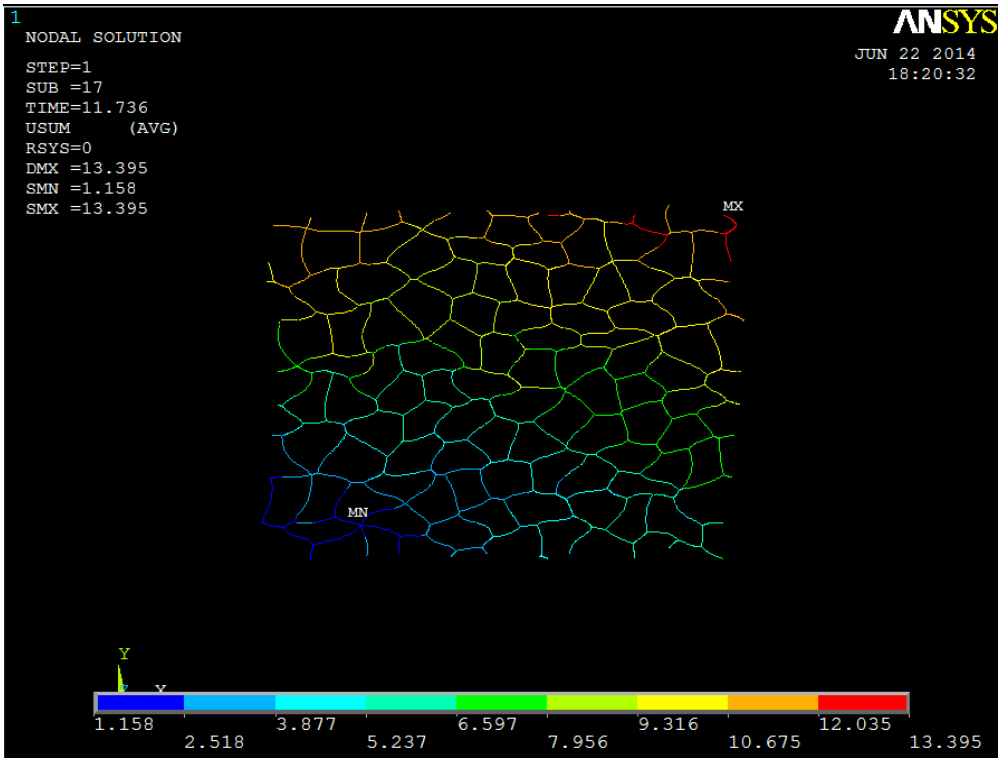
1
NODAL SOLUTION
STEP=1
SUB =17
TIME=11.736
USUM (AVG)
RSYS=0
DMX =13.395
SMN =1.158
SMX =13.395
ANSYS
JUN 22 2014
18:20:32
MX
MN
Y
1.158
2.518
3.877
5.237
6.597
7.956
9.316
10.675
12.035
13.395

(b)

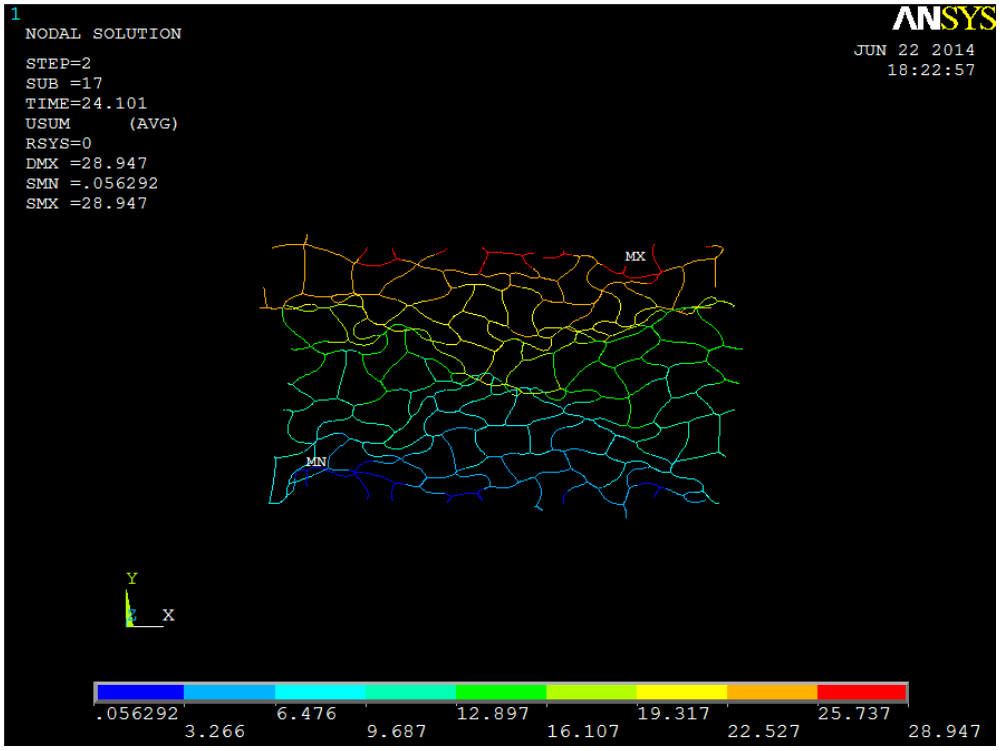

(c)

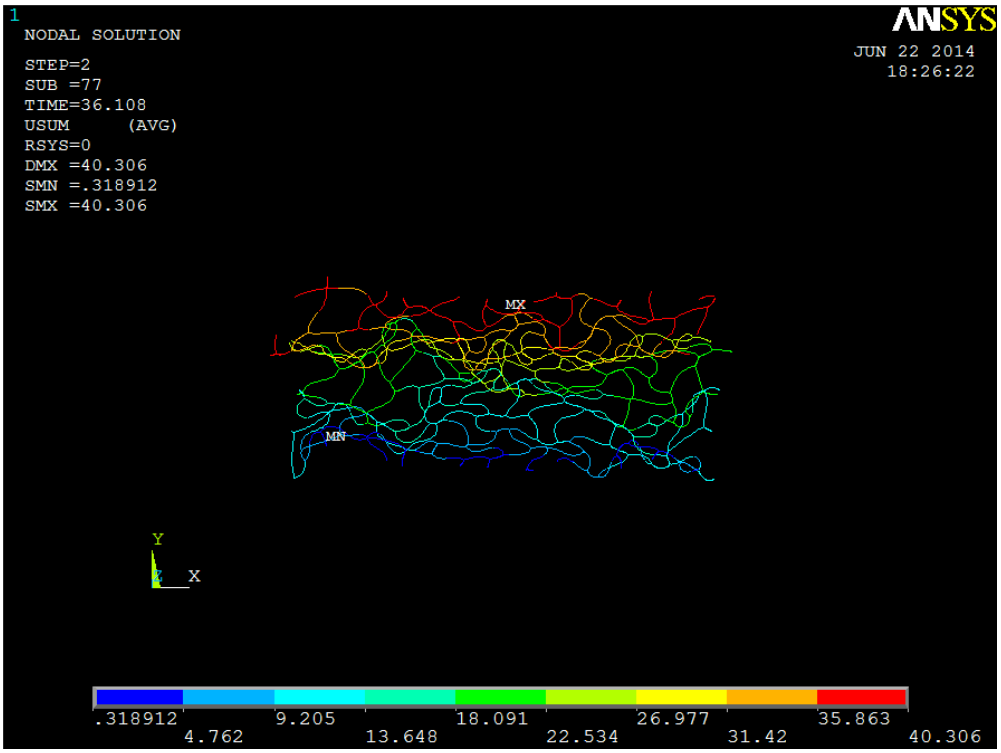

(d)

Figure 4.3. The deformation of periodic random irregular honeycombs with degree of regularity α = 0.7 (a) ε_y = 0.0, (b) ε_y = 0.196, (c) ε_y = 0.402, and (d) ε_y = 0.602.

The contact problem of the beam elements is not considered in this chapter. As can be seen in Figures 4.3 (a), (b), (c), and (d),[23] there is an overlap between the cell walls in some places of the deformed honeycomb when the compressive strain is 40% or larger. The compressive stress, strain, and Poisson's ratio can be obtained as described in Chapter 3.

The compressive stress is normalized by the Young's modulus of solid material and by the cube of the initial honeycomb relative density, and is given as (Zhu et al., 2006)

$$\overline{\sigma} = \frac{\sigma}{E_S \rho_0^3} \tag{4.1}$$

where σ is the compressive stress, E_S is the Young's modulus of the solid material, and ρ_0 is the relative density of the random irregular honeycomb when the effects of the initial stress or strain are absent.

4.3.1 Size-dependent high strain compression behaviour of micro-sized periodic random irregular honeycombs

At the micro-meter scale, the strain gradient effect plays an important role in the mechanical behaviour (Aifantis, 1999, Toupin, 1962, Zhu, 2010b). This section will show how the cell wall thickness and cell regularity affect the relation between compressive stress and strain, as well as the relation between the Poisson's ratio and the compressive strain of micro-sized periodic random irregular honeycombs.

[23] In these figures, they also show the maximum and minimum deflection solution (SMN and SMX).

4.3.1.1 Size-dependent relations between the compressive stress and strain

The size-dependent effect on the mean dimensionless relation between the compressive stress and strain of low density micro-sized periodic random irregular honeycombs are presented in Figures 4.4 (a), (b), (c), and (d). The honeycomb relative density is fixed at 0.01, and the range of degree of cell regularity is varied from 0.0 to 0.7. As can be seen from these figures, with the increase of the applied compressive strain from 0% to 60%, the dimensionless compressive stress increases monotonously, no matter what the degree of cell regularity. For micro-sized random irregular honeycombs with the same degree of regularity, to compress them to the same compressive strain, the thinner the cell walls, the larger the dimensionless compressive stress is required. When the thickness of the cell walls is much larger than the material intrinsic length l_m, the strain gradient effects are absent, that is, $l_m / h = 0$, and the results reduce to those of the conventional macro-sized counterparts.

Figure 4.4 (a) shows that for irregular honeycomb with $l_m / h = 0$ and $\alpha = 0.0$, when it is compressed up to 60%, the mean dimensionless stress[24] is about 0.15,

[24] The mean dimensional stress is the mean results obtained from 10 to 20 models with the same combination of the parameters, as mentioned in Section 4.3, each data is obtained from 10 to 20 similar models. This dimensional stress has been normalized by the Young's modulus of solid materials and by the cube of the relative density of the honeycomb, and thus the results will more be useful. The mean dimensional stress represents the compressive stress under the different applied compressive strain on the honeycomb in *y* direction. The relationship between the mean dimensional

which is almost the same as the value 0.14 of Zhu et al. (2006). This suggests that the results obtained in this chapter are reasonable. The errors shown in Figures 4.4 (a), (b), (c), and (d) represent the standard deviations of the data. It can be found that the thinner the cell wall thickness, the larger the standard deviations. For honeycombs with the same cell wall thickness, the larger the compressive strain or stress, the larger the standard deviation. This may happen because compressing irregular honeycombs to large strains leads to a large fluctuation in the convergent solutions. Figures 4.4 (a), (b), (c), and (d) indicate that the strain gradient effects have a significant influence on the relationships between the compressive stress and strain of micro-sized periodic random irregular honeycombs.

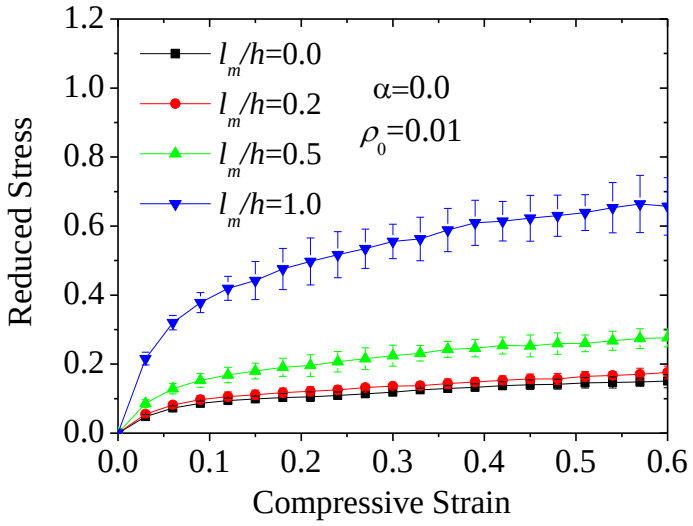

(a)

stress and the compressive strain represents the compressive behavior of honeycombs with a different low relative density or made of a different solid material.

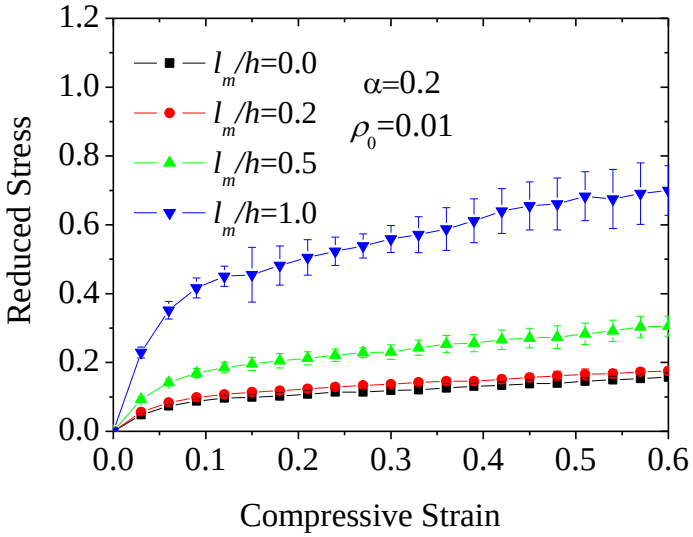
Reduced Stress
Compressive Strain
l_m/h=0.0
l_m/h=0.2
l_m/h=0.5
l_m/h=1.0
α=0.2
ρ_0=0.01

(b)

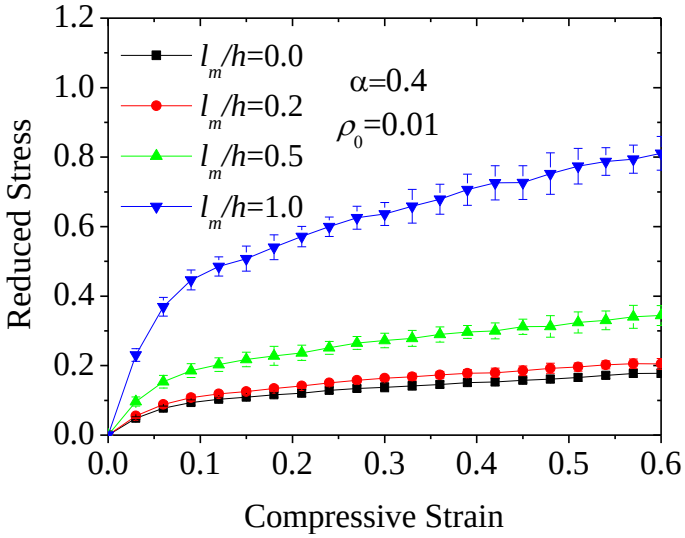
Reduced Stress
Compressive Strain
l_m/h=0.0
l_m/h=0.2
l_m/h=0.5
l_m/h=1.0
α=0.4
ρ_0=0.01

(c)

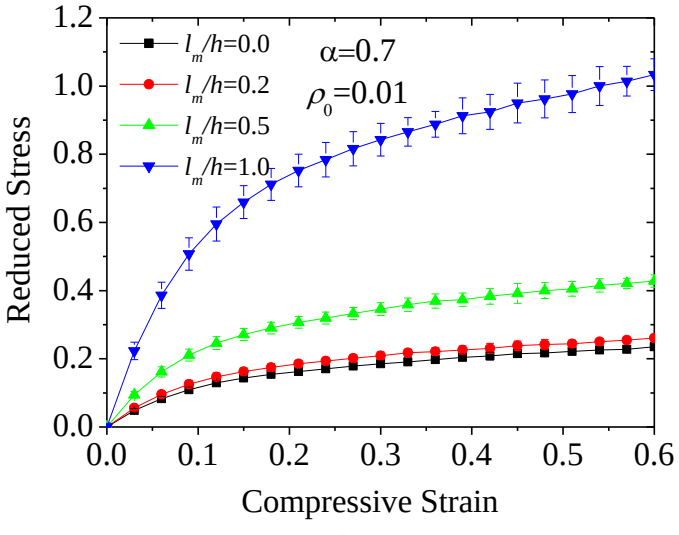
Reduced Stress
Compressive Strain
l_m/h=0.0
l_m/h=0.2
l_m/h=0.5
l_m/h=1.0
α=0.7
ρ_0=0.01

(d)

Figure 4.4. The size-dependent effect on the mean dimensionless stress and strain relationship of low density micro-sized periodic random irregular honeycombs with relative density $\rho_0 = 0.01$. (a) $\alpha = 0.0$, (b) $\alpha = 0.2$, (c) $\alpha = 0.4$, and (d) $\alpha = 0.7$.

4.3.1.2 Effect of cell regularity on the high strain compression stress and strain relations

In addition to the size-dependent effect, cell regularity may also affect the compressive stress and strain response of low density micro-sized irregular honeycombs. Figure 4.5 presents the effect of cell regularity on the mean dimensionless compressive stress and strain relation of low density micro-sized periodic random irregular honeycombs with fixed values $\rho_0 = 0.01$ and $l_m / h = 0.5$. As can be seen from the compressive stress and strain relations of micro-sized random irregular honeycombs in Figure 4.5, when the compressive strain is smaller, the larger the degree of the cell regularity, the smaller the tangent modulus. In contrast, when the compressive strain is larger than 10%, the larger the degree of the cell regularity of a micro-sized random irregular honeycomb, the larger mean dimensionless compressive stress, and the smaller the standard deviation. This indicates that if the strain gradient effect is present, the effect of cell regularity exists at the micro-meter scale. When the strain gradient effect is absent (i.e. $l_m / h = 0$), the obtained dimensionless compressive stress and strain relations reduce to those of their macro-sized counterparts (Chen et al., 1999, Silva and Gibson, 1997, Zhu et al., 2006).

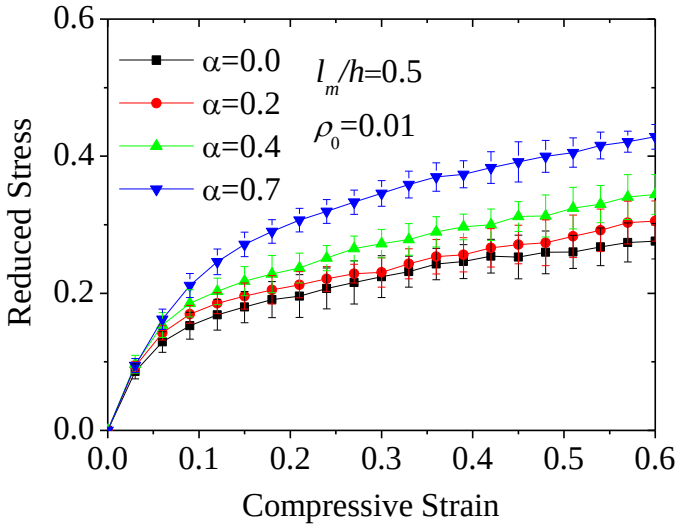

Figure 4.5. Effect of cell regularity on the dimensionless compressive stress and strain relation for micro-sized periodic random irregular honeycombs with ρ_0 = 0.01 and $l_m / h = 0.5$.

4.3.1.3 Size-dependent relations between the in-plane Poisson's ratio and compressive strain

This section explores the size-dependent relations between the in-plane Poisson's ratio and the compressive strain of low density micro-sized irregular honeycombs (with ρ_0 = 0.01). As can be seen from Figures 4.6 (a), (b), (c), and (d), for micro-sized irregular honeycombs with different degrees of regularity, the in-plane Poisson's ratio reduces sharply with the increase of the compressive strain, whether the size-dependent effect is present or absent. This finding is consistent with the previous research result (Zhu et al., 2006) for macro-sized irregular honeycombs. Figures 4.6 (a), (b), (c), and (d) also indicate that the effect of the cell wall thickness (i.e. the value of l_m / h) on the relations between the in-plane Poisson's ratio and the compressive strain of micro-

sized irregular honeycombs are negligible. It can also be observed that when the compressive strain of the micro-sized irregular honeycombs approached 60%, the value of the in-plane Poisson's ratio becomes negative, which is the same as the finding for macro-sized irregular honeycombs (Zhu et al., 2006). This happens because the mean cell wall junction rotation is approximately proportional to the amplitude of the honeycomb compressive strain (Zhu et al., 2006), which is confirmed by the simulations for micro-sized irregular honeycombs with different degrees of regularity, whether the strain gradient effect is present or absent.

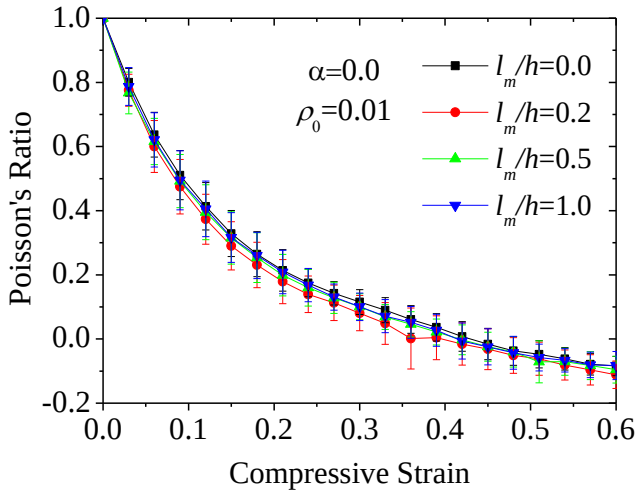

(a)

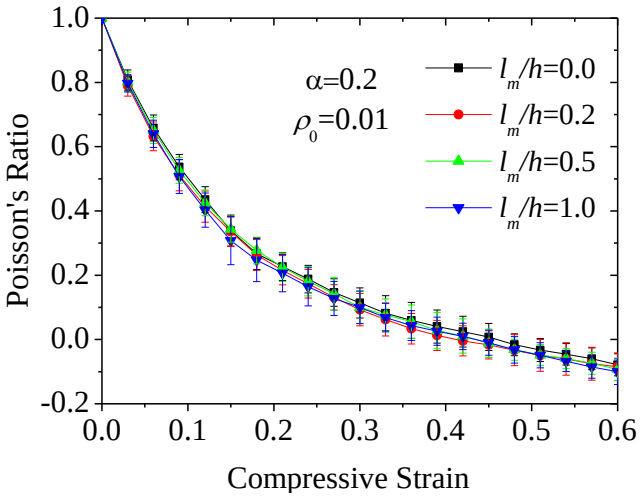

(b)

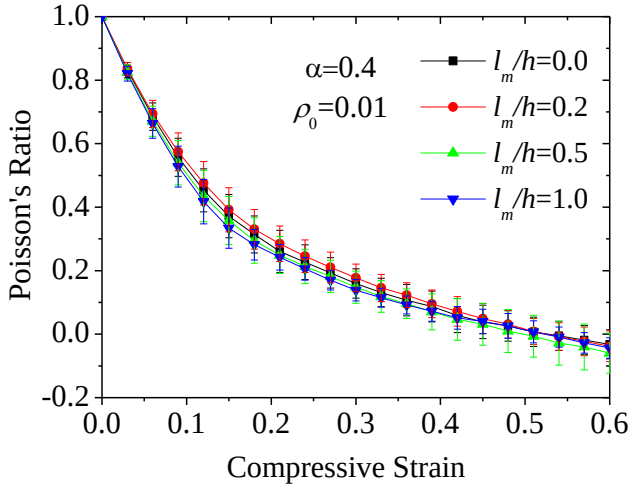

(c)

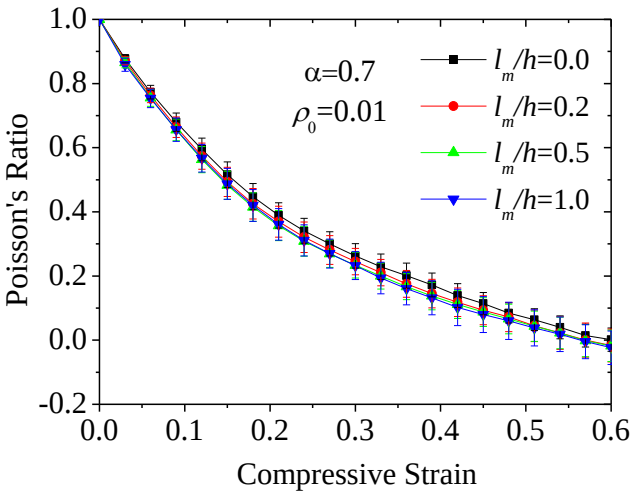

(d)

Figure 4.6. Size-dependent relations between the in-plane Poisson's ratio and compressive strain of low density micro-sized irregular honeycombs with the relative density $\rho_0 = 0.01$. (a) $\alpha = 0.0$, (b) $\alpha = 0.2$, (c) $\alpha = 0.4$, and (d) $\alpha = 0.7$.

4.3.1.4 Effect of cell regularity on the relation between the in-plane Poisson's ratio and the compressive strain

When the strain gradient effect is present, the effect of cell regularity on the in-plane Poisson's ratio and the compressive strain of micro-sized periodic random irregular honeycombs with $\rho_0 = 0.01$ are shown in Figure 4.7. As can be seen, the greater the degree of cell regularity, the larger the in-plane Poisson's ratio, which is consistent

with the finding for the macro-sized irregular honeycombs (Zhu et al., 2006). With the increase of the compressive strain, the in-plane Poisson's ratio of micro-sized irregular honeycombs reduces and becomes negative when the compressive strain approached 60%, and the strain gradient effect does not influence this trend.

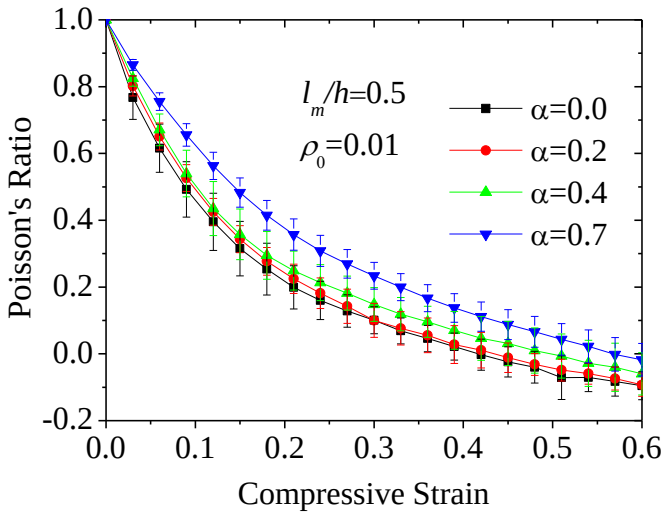

Figure 4.7. Effect of cell regularity on the relation between the in-plane Poisson's ratio and compressive strain of micro-sized irregular honeycombs with ρ_0 = 0.01 and $l_m / h = 0.5$.

4.3.2 Effects of the size-dependent and initial stress or strain on high strain compression behaviour of nano-sized periodic random irregular honeycombs

The surface elasticity and initial stress or strain can affect the mechanical behaviour of nano-sized materials (Duan et al., 2005, Miller and Shenoy, 2000, Zhu, 2010b, Zhu et al., 2012b). This section will present the effects of cell wall thickness, initial stress

or strain, and cell regularity on the relations between the compressive stress and strain, and the relation between the in-plane Poisson's ratio and the compressive strain of nano-sized periodic random irregular honeycombs.

4.3.2.1 The in-plane compressive stress and strain response with the size-dependent and initial stress or strain effects

Figures 4.8 (a), (b), (c), and (d) show the effect of surface elasticity on the relations between the dimensionless compressive stress and strain of low density nano-sized periodic random irregular honeycombs with fixed relative density ρ_0 = 0.01 and different degrees of cell regularity from 0.0 to 0.7. As can be seen, the dimensionless stress increases monotonously with the increase of the honeycomb compressive strain from 0% to 60%. When the surface modulus is positive, the thinner the cell wall thickness, the larger are the dimensionless compressive stress and the tangent modulus. If the surface modulus is negative, the effect of the cell wall thickness on the dimensionless compressive stress and the tangent modulus are inverted. When the cell thickness is much larger than the material intrinsic length l_n, i.e. $l_n / h = 0$, the size-dependent effect vanishes, and the relations between the dimensionless stress and the compressive strain of nano-sized irregular honeycombs reduce to those of their macro-sized counterparts. This point has been demonstrated from the results at the micro-meter scale (as shown in Section 4.3.1.1).

According to Figures 4.8 (a), (b), (c), and (d), when the surface modulus is positive,

the thinner cell walls (i.e. larger value of l_n / h) and larger compressive strain result in the larger standard deviation of the dimensionless compressive stress. This may happen because a large compressive strain leads to large fluctuation on the solutions. In general, the size-dependent behaviours of nano-sized irregular honeycombs are very similar to their micro-sized counterparts.

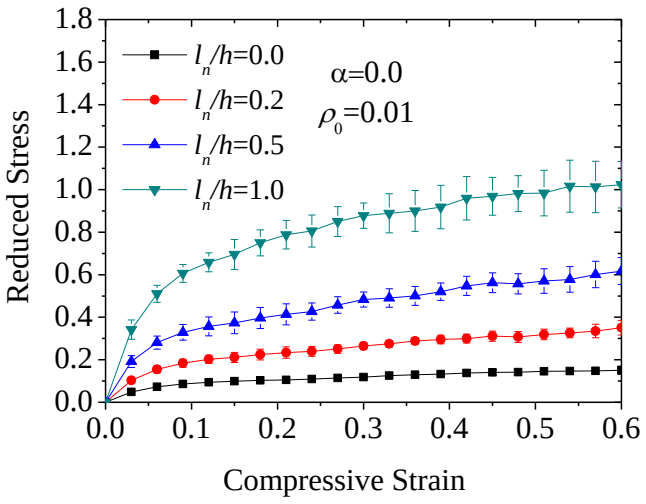

(a)

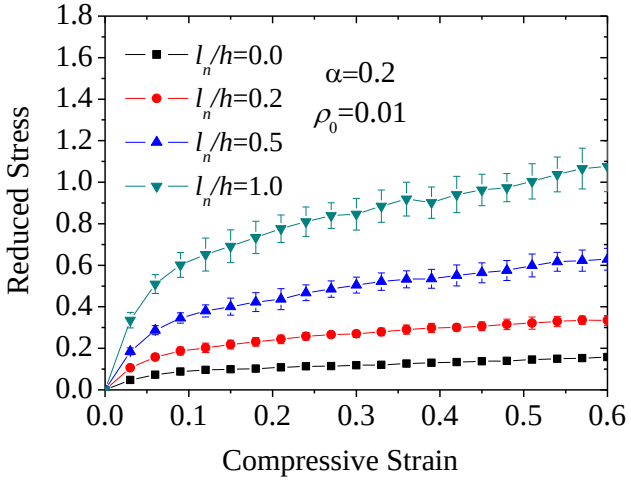

(b)

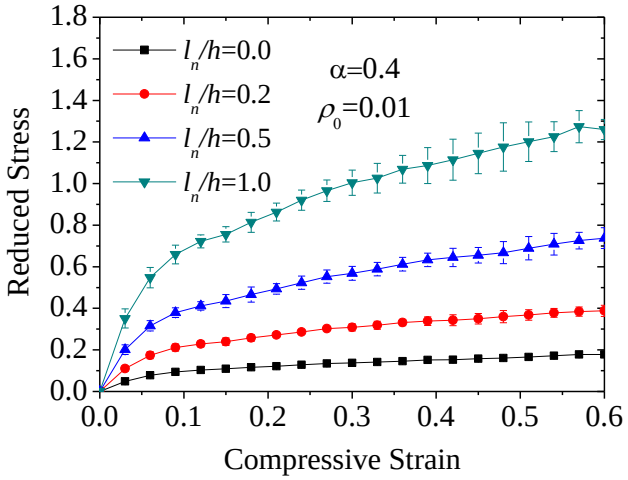

(c)

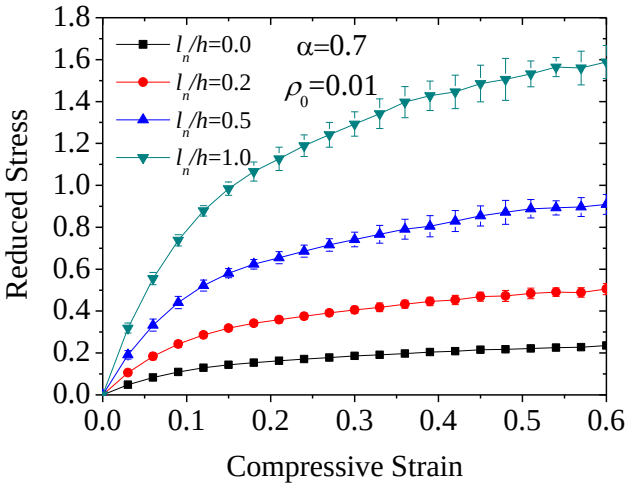

(d)

Figure 4.8. The size-dependent effect on the mean dimensionless stress and strain response for low density nano-sized periodic random irregular honeycombs with relative density ρ_0 = 0.01. (a) α = 0.0, (b) α = 0.2, (c) α = 0.4, and (d) α =0.7.

Figure 4.9 illustrates the effect of initial stress or strain on the dimensionless stress and the compressive strain of low density nano-sized irregular honeycomb with relative density ρ_0 = 0.01 and cell regularity α = 0.2. For the same amplitude of compressive strain, when the initial strain in the length direction of the cell walls is adjusted to vary between -6% and 6%, the dimensionless compressive stress of nano-sized irregular honeycombs can be controlled to either reduce about 45% or increase

about 70%. Therefore, the initial stress or strain can significantly affect the compressive stress and strain relations of nano-sized honeycombs.

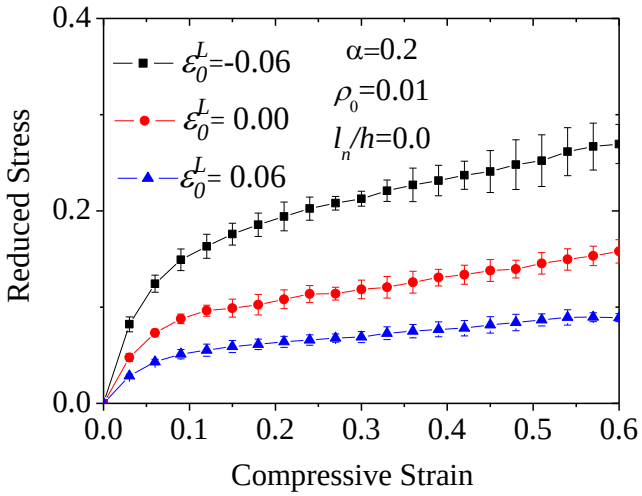

Figure 4.9. Effect of initial stress or strain on the dimensionless stress and the compressive strain of low density nano-sized irregular honeycombs with $\rho_0 = 0.01$ and $\alpha = 0.2$.

4.3.2.2 Effect of cell regularity on the in-plane compressive stress and strain relations of nano-sized honeycombs

In addition to the size-dependent and initial stress or strain effects, cell regularity may also affect the compressive stress and strain response of nano-sized periodic random irregular honeycombs. When the surface elasticity effect is present, the effect of cell regularity on the relation between the dimensionless compressive stress and strain of nano-sized irregular honeycombs with $l_n / h = 0.5$ and different degrees of regularity are shown in Figure 4.10. As can be seen, the greater the degree of cell regularity, the smaller is the tangent modulus when the compressive strain is small, and the larger is

the dimensionless compressive stress when the compressive strain is larger than 10%. This trend is consistent with the results for macro-sized honeycombs (Chen et al., 1999, Silva and Gibson, 1997, Zhu et al., 2006) and micro-sized counterparts (as shown in Section 4.3.1.2).

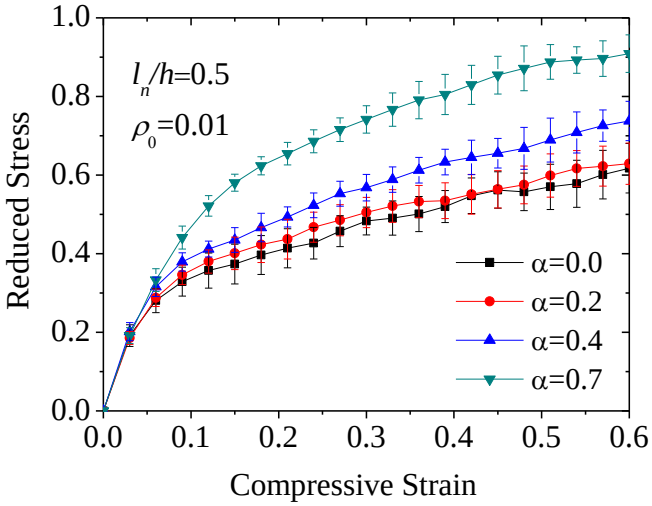

Figure 4.10. Effect of cell regularity on the relation between the dimensionless stress and the compressive strain of nano-sized periodic random irregular honeycombs with the $\rho_0 = 0.01$ and $l_n / h = 0.5$.

4.3.2.3 Effect of the size-dependent and initial stress or strain on the relations of the in-plane Poisson's ratio and the compressive strain

This section presents the size-dependent effect on the relations between the in-plane Poisson's ratio and the compressive strain of low density nano-sized random irregular honeycombs. As can be seen from Figures 4.11 (a), (b), (c), and (d), whether the size-dependent effect is present or absent, the in-plane Poisson's ratio decreases

monotonously with the increase of the compressive strain and becomes negative when the compressive strain approaches 60%. This trend is consistent with the findings for macro- (Zhu et al., 2006) and micro-sized (as shown in Section 4.3.1.3) irregular honeycombs. This indicates that the effect of cell wall thickness (i.e. the value of l_n/h) on the relations between the in-plane Poisson's ratio and the compressive strain is negligible.

Based on this result, the size-dependent effect cannot affect the existent large scale junction rotation when the compressive strain is applied to a large value at the nano-meter scale. It also has a limited effect on the Poisson's ratio of strain response for low density nano-sized periodic random irregular honeycombs. Figures 4.11 (a), (b), (c), and (d) also show the standard deviation of the mean Poisson's ratio that is obtained from 10 – 20 models with the same set parameters.

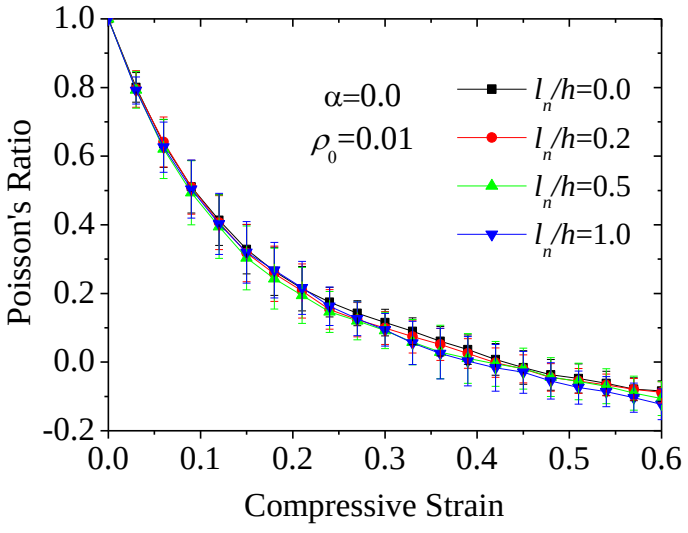

(a)

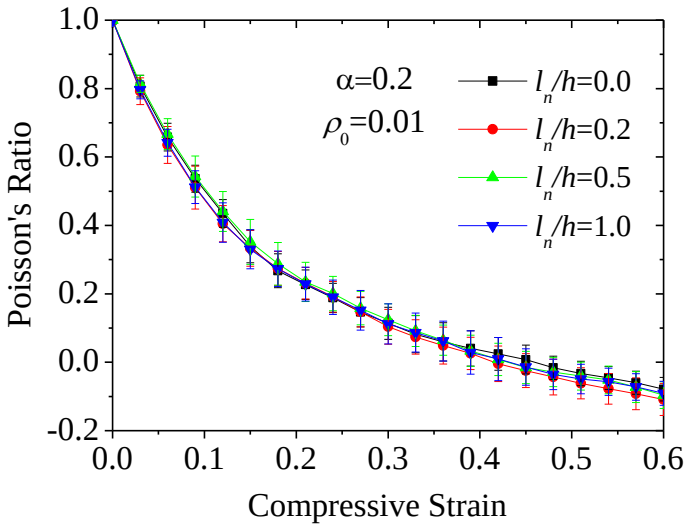
α=0.2
ρ_0=0.01
l_n/h=0.0
l_n/h=0.2
l_n/h=0.5
l_n/h=1.0
Poisson's Ratio
Compressive Strain
1.0
0.8
0.6
0.4
0.2
0.0
-0.2
0.0
0.1
0.2
0.3
0.4
0.5
0.6

(b)

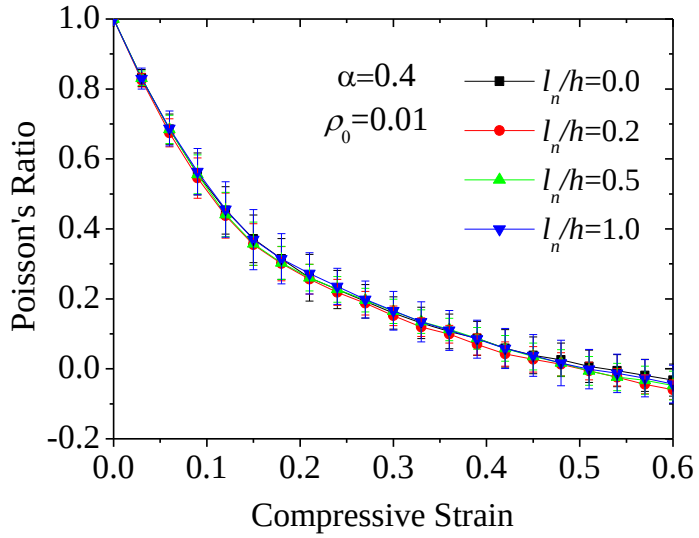
α=0.4
ρ_0=0.01
l_n/h=0.0
l_n/h=0.2
l_n/h=0.5
l_n/h=1.0
Poisson's Ratio
Compressive Strain
1.0
0.8
0.6
0.4
0.2
0.0
-0.2
0.0
0.1
0.2
0.3
0.4
0.5
0.6

(c)

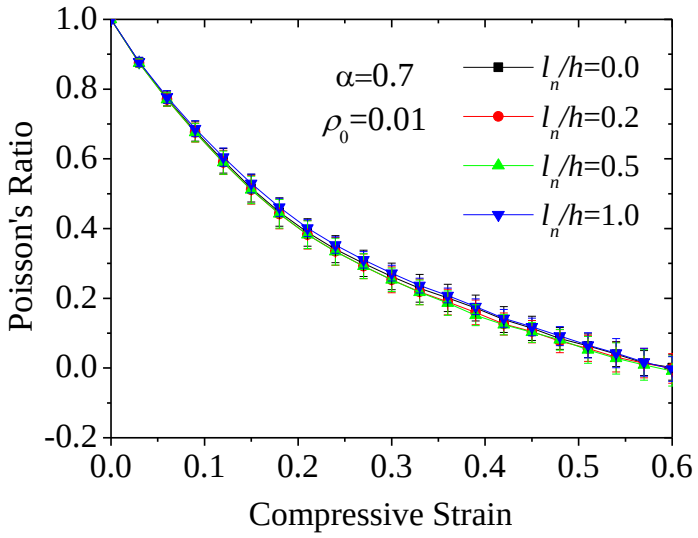
α=0.7
ρ_0=0.01
l_n/h=0.0
l_n/h=0.2
l_n/h=0.5
l_n/h=1.0
Poisson's Ratio
Compressive Strain
1.0
0.8
0.6
0.4
0.2
0.0
-0.2
0.0
0.1
0.2
0.3
0.4
0.5
0.6

(d)

Figure 4.11. Effect of the size-dependent on the in-plane Poisson's ratio and the compressive strain response for low density nano-sized random irregular honeycombs with $\rho_0 = 0.01$. (a) α = 0.0, (b) α = 0.2, (c) α = 0.4, and (d) α =0.7.

When the size-dependent effect is absent ($l_n / h = 0$), the initial stress or strain effects on the relationship between the in-plane Poisson's ratio and honeycomb compressive strain for low density nano-sized periodic random irregular honeycombs with the relative density $\rho_0 = 0.01$ and degree of cell regularity α = 0.2 is shown in Figure 4.12. When the initial strain in the axial direction of the cell walls is controlled from -0.06 to 0.06, the value of Poisson's ratio remains almost unchanged. The Poisson's ratio becomes negative when the honeycomb compressive strain is large. This suggests that junction rotation is an important deformation mechanism.

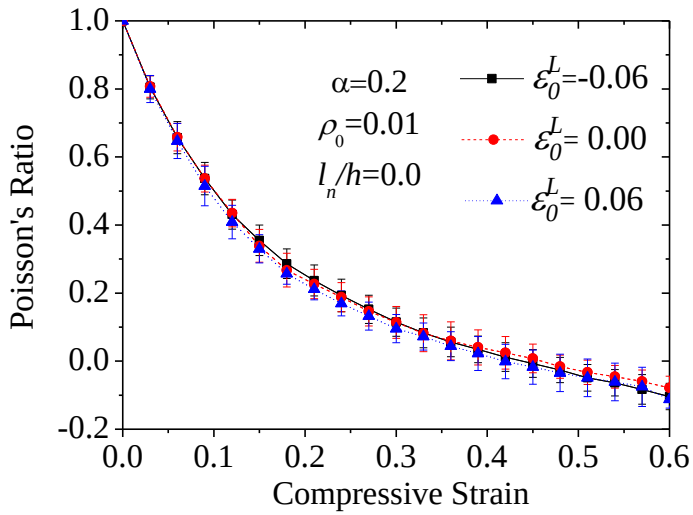

Figure 4.12. The initial stress or strain effects on the relationship between the Poisson's ratio and honeycomb compressive strain for low density nano-sized periodic random irregular honeycombs with $\rho_0 = 0.01$ and α = 0.2.

4.3.2.4 Effect of cell regularity in the relationship between the in-plane Poisson's ratio and compressive strain

The above section shows that the effects of the size-dependent and initial stress or strain on the in-plane Poisson's ratio are negligible. This section presents the effect of cell regularity on the in-plane Poisson's ratio, as shown in Figure 4.13. For the same level of honeycomb compressive strain, the larger the degree of cell regularity, the larger the value of the Poisson's ratio. Meanwhile, when the Poisson's ratio becomes negative, the smaller the degree of cell regularity, the larger the absolute value of the Poisson's ratio. This effect is believed to be attributed to the junction rotation mechanism. The structure consists of many beams, and the connections of beams can be defined as junction. When a deformation is applied to the structure, the junctions will translate and rotate. This finding is consistent with the results for macro- (Zhu et al., 2006) and micro-meter scales (as shown in Section 4.3.1.4).

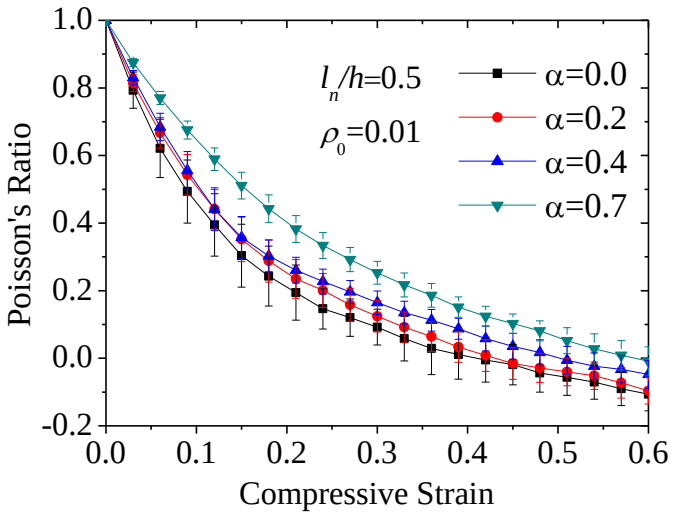

Figure 4.13. Effect of cell regularity on the relationship between the in-plane Poisson's ratio and compressive strain of nano-sized periodic random irregular honeycombs with

$\rho_0 = 0.01$ and $l_n / h = 0.5$.

4.4 Summary

This chapter shows the size-dependent, initial stress or strain, and cell regularity effects on the in-plane high strain compression behaviour of low density micro- and nano-sized periodic random irregular honeycombs. It is found that the size-dependent (cell wall thickness) significantly affects the in-plane compressive stress. When the surface modulus is positive, the thinner the cell walls, the larger the dimensionless compressive stress and the tangent modulus. If the surface modulus is negative, then the effects are inverted. The initial stress or strain in the cell wall direction can also greatly affect the compressive stress and strain relationship of low density micro- and nano-sized periodic random irregular honeycombs. By adjusting the amplitude of the initial strain of the micro- and nano-sized cell walls from -0.06 to 0.06, the dimensionless compressive stress and the tangent modulus can be controlled to vary over a range of about 115%. However, the size-dependent (cell wall thickness) and initial stress or strain have limited effects on the relationship between the in-plane Poisson's ratio and the compressive strain of low density micro- and nano-sized periodic random irregular honeycombs. In addition, the degree of cell regularity can affect the compressive stress and strain relationship, as well as the relation between the in-plane Poisson's ratio and the compressive strain of low density micro- and nano-sized periodic random irregular honeycombs. The greater the degree of cell regularity,

the larger the dimensionless compressive stress and the in-plane Poisson's ratio. At a high compressive strain, more irregular micro- and nano-sized honeycombs have a smaller tangent modulus.

Chapter 5 The elastic properties of micro- and nano-sized periodic random irregular open-cell foams

5.1 Introduction

Cellular materials include honeycombs and open-cell foams. The linear and geometrically nonlinear elastic properties of low density micro- and nano-sized random irregular honeycombs are investigated in Chapters 3 and 4. This chapter will present the simulation results on the linear elastic properties of low density micro- and nano-sized periodic random irregular open-cell foams. The elastic properties of macro-sized regular and random irregular open-cell foams have been studied by many researchers (Gibson and Ashby, 1997, Konstantinidis et al., 2009, Li et al., 2006, Roberts and Garboczi, 2002, Warren and Kraynik, 1997, Zhu et al., 2000, Zhu et al., 1997a, Zhu and Wang, 2013). Although Zhu and Wang (2013) have done a theoretical analysis of the elastic properties of micro- and nano-sized regular open-cell foams, they did not investigate the elastic properties of micro- and nano-sized periodic random irregular open-cell foams.

In this chapter, the strain gradient effect at the micro-meter scale, and the surface elasticity and initial strain effects at the nano-meter scale are incorporated into the finite element simulations by using a commercial finite element software ANSYS. The effects of the cell strut diameter, initial stress or strain, and cell regularity on the

elastic properties of micro- and nano-sized open-cell foams will be investigated.

5.2 Methodology

5.2.1 The main parameters of periodic random irregular open-cell foams

Zhu et al. (2000), and Zhu and Windle (2002) developed a computer program to construct geometric models of the representative unit periodic random irregular open-cell foams. The main parameters of constructing the representative unit periodic random irregular open-cell foams are the degree of cell regularity, the initial relative density of open-cell foams and the number of complete cells. The definitions for the degree of cell regularity and the initial relative density of open-cell foams are given by Equations (2.5) and (2.7).

5.2.1.1 The degree of cell regularity

In this chapter, irregular open-cell foams are simulated with different degrees of cell regularity, from 0.0 to 0.7. Figures 5.1 (a), (b), and (c) present unit periodic random irregular open-cell foams with 125 complete cells and different degrees of cell regularity: α = 0.0, α = 0.4 and α =0.7. As can be seen, with the increase of the degree of cell regularity, the structure becomes more regular. If the degree of cell

regularity is 0.0, then the structure of open-cell foam is fully irregular (as shown in Figure 5.1 (a)), and when the degree of regularity is 1.0, the structure of the open-cell foam is a perfectly regular BCC foam (or Kelvin foam).

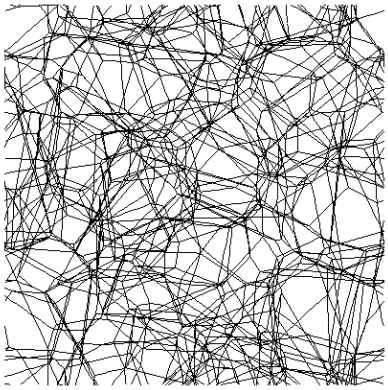

(a)

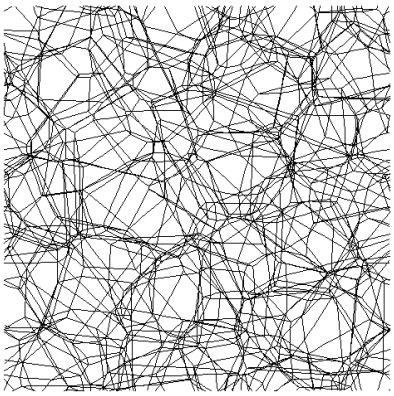

(b)

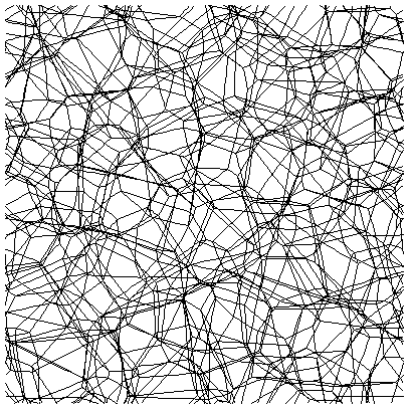

(c)

Figure 5.1. Voronoi open-cell foams with 125 complete cells and different degrees of cell regularity: (a) α = 0.0, (b) α = 0.4, and (c) α =0.7.

5.2.1.2 The relative density

In this chapter, for the convenience in simulations, all the cell struts in the same open-cell foam model are assumed to have the same uniform and circular cross-sectional area. The elastic properties of low-density micro- and nano-sized periodic random irregular open-cell foams are analyzed with different relative densities, from 0.01 to 0.3. The cross-sectional area can be obtained from Equation (2.7).

5.2.1.3 The number of complete cells

According to the previous research (Zhu et al., 2000, Zhu and Windle, 2002), the number of complete cells has a limited effect on the elastic properties of periodic random irregular open-cell foams, and it only affects the standard deviation of the elastic properties. For the convenience of comparison with the results of macro-sized irregular open-cell foams (Zhu et al., 2000), the number of complete cells is fixed at 125 (as shown in Figures 5.1 (a), (b), and (c)). In this chapter, the mean elastic properties are obtained from 20 similar periodic random irregular open-cell foam models with the same combination of parameters, including the degree of cell regularity, the foam relative density, and the number of complete cells.

5.2.2 Finite element simulations

All the finite element simulations are performed by using ANSYS (which is commercial software). The following sections will show the details of how to obtain the simulation results for the elastic properties of low density micro- and nano-sized periodic random irregular open-cell foams.

5.2.2.1 Element type and cross section

In the finite element simulations, each of the cell struts is divided into 3-9 BEAM189 elements depending on their length compared to the mean strut length of the irregular open-cell foam model. Since the cell strut bending, torsion and axial stretching or compression are the main deformation mechanisms of open-cell foams (Zhu et al., 2000, Zhu et al., 1997a, Zhu and Wang, 2013), the beam elements should be able to incorporate these main deformation mechanisms into the simulations. The BEAM189 element is a three node Timoshenko beam element, which indeed meets this requirement and is also able to deal with the transverse shear deformation. The cross-section of all the cell struts is assumed to be circular and to have the same uniform area. Three key parameters should be input for the BEAM189 elements, these are the material Young's modulus, Poisson's ratio, and the radius of the cross-section of the beam element.

5.2.2.2 Material properties

To obtain the elastic properties of low density micro- and nano-sized periodic random irregular open-cell foams, the solid material is assumed to be linear elastic. Since there are no elements in the ANSYS software that can directly consider the size-dependent effect, the equivalent values for the radius of the cell strut cross-section, the Young's modulus, and Poisson's ratio of the BEAM189 elements are obtained from the size-dependent bending rigidity, torsion rigidity, and axial stretching or compression rigidity of the micro- or nano-sized cell struts.

5.2.2.3 The equivalent deformation rigidities of micro- and nano-sized cell struts

In this chapter, the Young's modulus of the solid material E_S is fixed at $2\times10^5 MPa$ and the Poisson's ratio of the solid material v_S is always fixed at 0.1. Since the simulated results are normalized, the value of E_S does not affect the results. For a given initial relative density ρ_0, the initial cell strut cross-sectional area A of a micro- and nano-sized periodic random irregular open-cell foam can be obtained from Equation (2.7). Then, the radius R_0 or diameter d_0 of the cross-section of beam element can be easily found from A. Equations (2.25 – 2.27) give the size-dependent bending rigidity D_b, torsion rigidity D_t, and axial stretching or compression rigidity D_C of the cell struts for micro-sized open-cell foams, and Equations (2.31 – 2.33)

present those for nano-sized open-cell foams. Thus, at the micro- and nano-meter scales, the size-dependent effect on the deformation mechanisms can be taken into account in the finite element simulations by using the following relations:

$$E_e \frac{\pi R_e^4}{4} = D_b \tag{5.1}$$

$$G_e \frac{\pi R_e^4}{2} = E_e \frac{\pi R_e^4}{4(1+v_e)} = D_t \tag{5.2}$$

$$E_e \pi R_e^2 = D_C \tag{5.3}$$

where E_e is the equivalent material Young's modulus, v_e is the Poisson's ratio and R_e is the radius of the cross-section of the BEAM189 elements. They can be obtained as:

$$E_e = \frac{D_c^2}{4\pi D_b} \tag{5.4}$$

$$v_e = \frac{D_b}{D_t} - 1 \tag{5.5}$$

$$R_e = 2\sqrt{\frac{D_b}{D_C}} \tag{5.6}$$

At the micro- or nano-meter scale, if the size-dependent effect is absent, it means $l_m / d = 0$ in Equations (2.25 – 2.27) or $l_n / d = 0$ in Equations (2.31 – 2.33). Thus, the size-dependent bending rigidity D_b, torsion rigidity D_t and axial stretching or compression rigidity D_C of the cell struts reduce to those their conventional macro-sized counterparts. For macro-sized random irregular open-cell foams with a given degree of cell regularity, their dimensionless Young's modulus is dependent only on the initial relative density and is independent of the actual cross-sectional area of cell

struts (Zhu et al., 2000). The strain gradient effect at the micro-meter scale or the surface elasticity effect at the nano-meter scale can be incorporated into the finite element simulations by varying the value of l_m / d or l_n / d in Equations (2.25 – 2.27) or Equations (2.31 – 2.33). In this chapter, their values are set to 0.0, 0.5, and 1.0, respectively. For different values of l_m / d and l_n / d, the equivalent material Young's modulus E_e, Poisson's ratio v_e and the radius of the cross-section of beam element R_e can be obtained from Equations (5.4 – 5.6). For similar random irregular models with the same degree of cell regularity and the same relative density, their total cell strut lengths are different. Thus, the equivalent material Young's modulus E_e, Poisson's ratio v_e, and the radius of the cross-section of beam element R_e are different for each of the similar models. In Equations (2.25 – 2.27) and Equations (2.31 – 2.33), *d* is the diameter of cross-section of cell struts.

At the nano-meter scale, the initial stress or strain effect also plays an important role in that it affects the bending, torsion and axial stretching or compression rigidities of the cell struts. For a beam element with a uniform circular cross-section, the initial residual stress in axial direction of the cell struts is $\sigma_0^L = -4\tau_0 / d$ and in the radial direction is $\sigma_0^r = -2\tau_0 / d$ (Zhu et al., 2012a), where τ_0 is the initial surface stress and it is assumed to be the same in both axial and radial directions. The initial residual elastic strain in the axial direction is $\varepsilon_0^L = -\frac{4\tau_0}{E_S d}(1-v_S)$ and in the radial direction is $\varepsilon_0^r = -\frac{2\tau_0}{E_S d}(1-3v_S) = \frac{1-3v_S}{2(1-v_S)}\varepsilon_0^L$ (Zhu et al., 2012a). Nano-sized materials are

usually a single crystal and have a much larger yield strength. According to the previous research (Biener et al., 2009, Haiss et al., 1998, Kramer et al., 2004, Zhu et al., 2012a, Zhu et al., 2012b, Zhu et al., 2013), the amplitude of the recoverable initial elastic strain in the axial direction of the cell struts can be controlled to vary a range from -0.1 to 0.1 by application of the electric potential. In this chapter, the amplitude of the initial elastic strain ε_0^L is thus set to -0.10, 0, and 0.10, respectively. When the initial stress or strain effect is present ($\varepsilon_0^L \neq 0$), the actual length and cross-sectional diameter of the cell struts can be obtained as:

$$l = l_0(1+\varepsilon_0^L) \tag{5.7}$$

$$d = d_0(1+\varepsilon_0^r) \tag{5.8}$$

where l_0 and d_0 are the initial length and cross-sectional diameter of the cell struts. As can be seen from Equations (2.31 – 2.33), the bending rigidity D_b, torsion rigidity D_t, and axial stretching or compression rigidity D_C of the cell struts can be controlled to vary by adjusting the amplitude of the initial stress or strain. For different amplitudes of the initial stress or strain, the equivalent material Young's modulus E_e, Poisson's ratio v_e, and the cross-sectional radius R_e of the beam elements can be obtained from Equations (5.4 – 5.6).

To demonstrate the correct use of the equivalent values of Young's modulus E_e, Poisson's ratio v_e, and the cross-sectional radius R_e of the cross-section of the beam elements in finite element simulations, the deflection of a single horizontal micro- or nano-sized cantilever beam was analyzed with its left end fixed and a concentrated

force applied at its right end. Although the equivalent value of Poisson's ratio v_e could be negative or larger than 0.5, which is meaningless for the conventional isotropic solid materials, the deflection obtained from finite element simulation by using the equivalent properties is almost identical to theoretical result. Therefore, it is believed that by using the equivalent properties for the beam elements, the size-dependent and the initial stress or strain effects can be correctly incorporated into the finite element simulations of micro- or nano-sized open-cell foams.

5.2.2.4 The model treatment for the initial strain effect

The geometric model of the unit periodic random irregular open-cell foams is a cube with a side length L=30 *mm* in the *x*, *y* and *z* directions (as shown in Figure 5.2). The origin of the *xyz* coordinate system is at the front bottom left of the cubic model (as shown in Figure 5.3) and the nodal coordinates in each of the beam elements are registered as (*x*, *y*, *z*). When the effect of the initial strain in the strut length direction ε_0^L is absent, the geometric model is the original one. When the effect of the initial strain is present, the geometric structure shrinks or extends depending on the value of ε_0^L, and the corresponding nodal coordinates of the cell struts are registered as (*x'*, *y'*, *z'*) and given by:

$$x' = x(1+\varepsilon_0^L) \tag{5.9}$$

$$y' = y(1+\varepsilon_0^L) \tag{5.10}$$

$$z' = z(1+\varepsilon_0^L) \tag{5.11}$$

The side length of the geometric model can be presented by

$$L_x^{'} = L_y^{'} = L_z^{'} = L(1+\varepsilon_0^L) \tag{5.12}$$

And the volume of the structure is given by

$$V^{'} = V_0(1+\varepsilon_0^L)^3 \tag{5.13}$$

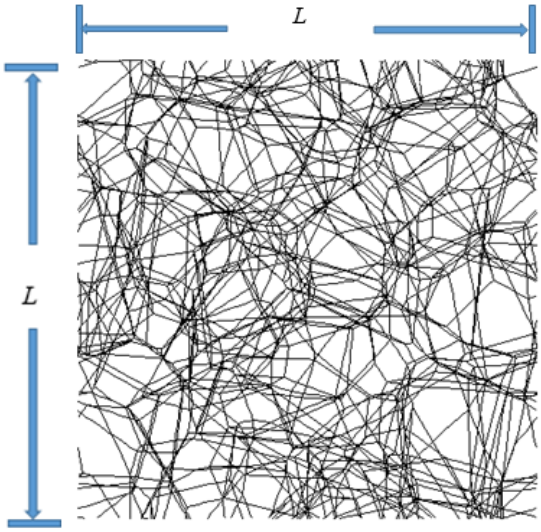

Figure 5.2. A representative unit periodic random irregular open-cell foam with the degree of cell regularity α = 0.0.

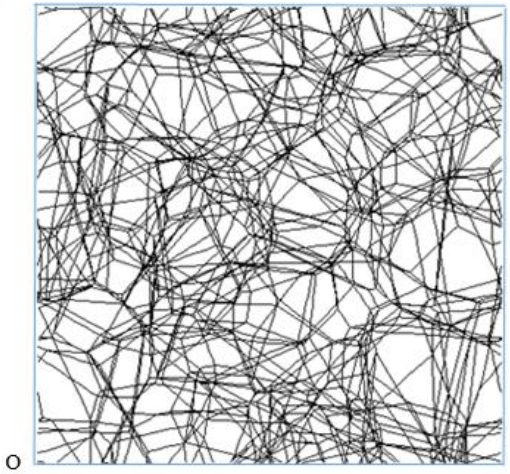

Figure 5.3. The left bottom point shows on the representative unit periodic random irregular open-cell foams with the degree of cell regularity α = 0.0.

5.2.2.5 Boundary conditions

Since all of the geometric models of the unit random irregular open-cell foams are periodic, the periodic boundary conditions are the most suitable boundary conditions (as described in Section 2.4.1.2.2) to be used in the simulations. The periodic boundary conditions for the displacements and rotations of the corresponding nodes on the left and right,[25] top and bottom,[26] front and back surfaces[27] of the periodic random irregular unit open-cell foam model can be described as

$$u_i^{left} - u_j^{left} = u_{i'}^{right} - u_{j'}^{right} \tag{5.14}$$

$$v_i^{left} - v_j^{left} = v_{i'}^{right} - v_{j'}^{right} \tag{5.15}$$

$$w_i^{left} - w_j^{left} = w_{i'}^{right} - w_{j'}^{right} \tag{5.16}$$

$$\theta_i^{left} = \theta_{i'}^{right} \tag{5.17}$$

$$u_i^{top} - u_j^{top} = u_{i'}^{bottom} - u_{j'}^{bottom} \tag{5.18}$$

$$v_i^{top} - v_j^{top} = v_{i'}^{bottom} - v_{j'}^{bottom} \tag{5.19}$$

$$w_i^{top} - w_j^{top} = w_{i'}^{bottom} - w_{j'}^{bottom} \tag{5.20}$$

$$\theta_i^{top} = \theta_{i'}^{bottom} \tag{5.21}$$

$$u_i^{front} - u_j^{front} = u_{i'}^{back} - u_{j'}^{back} \tag{5.22}$$

$$v_i^{front} - v_j^{front} = v_{i'}^{back} - v_{j'}^{back} \tag{5.23}$$

$$w_i^{front} - w_j^{front} = w_{i'}^{back} - w_{j'}^{back} \tag{5.24}$$

[25] Equations (5.14 - 5.17) are the constraint equations on the left and right surfaces of the periodic random irregular unit open-cell foam model.

[26] Equations (5.18 - 5.21) are the constraint equations on the top and bottom surfaces of the periodic random irregular unit open-cell foam model.

[27] Equations (5.22 - 5.25) are the constraint equations on the front and back surfaces of the periodic random irregular unit open-cell foam model.

$$\theta_i^{front} = \theta_{i'}^{back} \tag{5.25}$$

Where i and j are nodes on the left, top, or front surface of the periodic random irregular unit open-cell foam model, and i' and j' are the corresponding nodes on the right, bottom, or back surface of the periodic random irregular unit open-cell foam model.

5.2.2.6 Loading

To restrain possible rigid displacements for the structure, one node on the bottom surface is fixed in the *y* direction, one node on the left surface is fixed in the *x* direction, and another node on the front surface is fixed in the *z* direction. To obtain the effective Young's modulus and Poisson's ratio, a displacement (-0.1%*L*) in the *y* direction is applied to a node on top surface of the model and the corresponding node on the bottom surface is fixed in *y* direction (as shown in Figure 5.4 (a)). The corresponding compressive force in the *y* direction and the expansion in the *x* direction can be obtained for deformed foam model, and the effective Young's modulus and Poisson's ratio can thus be obtained from the stress and strains. To obtain the effective shear modulus, a compressive strain (-0.1%) is applied in the *y* direction and a tensile strain (0.1%) is simultaneously applied in the *x* direction (as shown in Figure 5.4 (b)). The corresponding compressive stress in *y* direction and tensile stress in the *x* direction can be obtained, and the effective shear modulus can thus be determined.

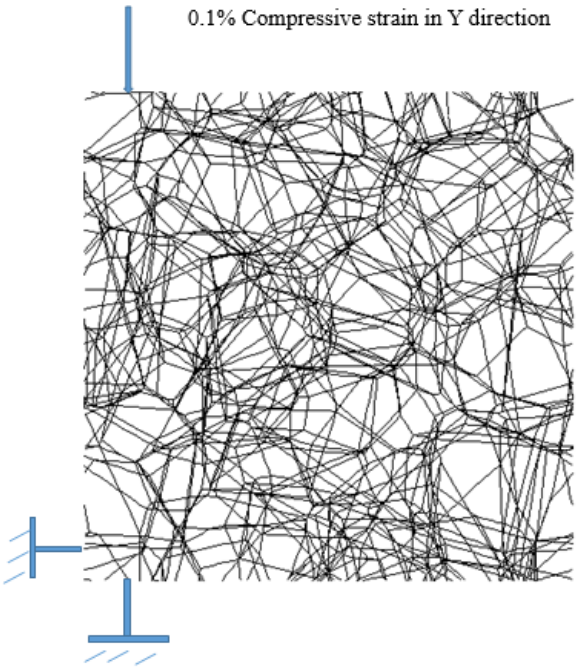

(a)

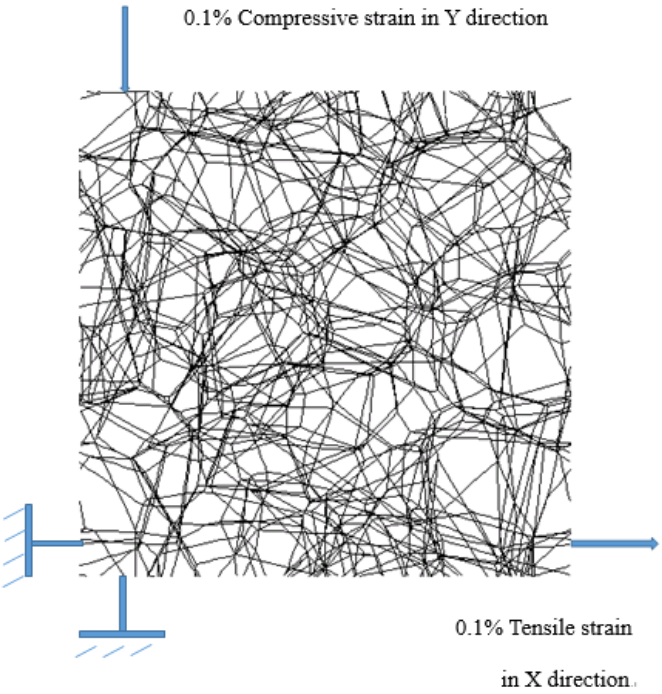

(b)

Figure 5.4. Loading schematic diagram on the representative unit periodic random irregular open-cell foams with the degree of cell regularity α = 0.0 (a) for finding the effective Young's modulus and Poisson's ratio, and (b) for finding the effective shear modulus.

5.3 Results and Discussion

In this chapter, each data in the figures is the mean value obtained from 20 different random irregular open-cell foams with the same combination of the parameters, such as the degree of cell regularity, the initial relative density, the size-dependent effect ratios (l_m / d or l_n / d), and the initial strain (ε_0^L). In the figures, the error bar shows the standard deviation.

According to Zhu et al. (1997a), there are only there independent elastic constants for a perfect regular BCC open-cell foams, including the effective Young's modulus, shear modulus, and Poisson's ratio. The effective stresses and strains can be given by

$$\sigma_x = \frac{F_x}{A_{yz}} = \frac{F_x}{L_y L_z} \tag{5.26}$$

$$\sigma_y = \frac{F_y}{A_{xz}} = \frac{F_y}{L_x L_z} \tag{5.27}$$

$$\varepsilon_x = \frac{\Delta u_x}{L_x} \tag{5.28}$$

$$\varepsilon_y = \frac{\Delta u_y}{L_y} \tag{5.29}$$

The effective Young's modulus can be obtained by

$$E_1 = \frac{\sigma_y}{\varepsilon_y} \tag{5.30}$$

The effective shear modulus is given by (Zhu et al., 2000)[28]

$$G_{12} = \frac{|\sigma_x| + |\sigma_y|}{2(|\varepsilon_x| + |\varepsilon_y|)} \tag{5.31}$$

[28] This reference does not directly give the equation of the effective shear modulus, but their obtained the effective shear modulus is nearly the same as the results when l_m / d =0.0 in Figure 5.7.

The effective Poisson's ratio can be presented by

$$\nu_{12} = -\frac{\varepsilon_x}{\varepsilon_y} \tag{5.32}$$

Where F_x and F_y are the forces in the *x* and *y* directions; A_{yz} and A_{xz} are the areas of the top and right surfaces; L_x, L_y and L_z are the side lengths in *x*, *y* and *z* directions $L_x = L_y = L_z = 30$ *mm*; and, Δu_x and Δu_y are the elongations in the *x* and *y* directions. When the initial strain effect is present, the side lengths L_x, L_y and L_z should be multiplied by $(1+\varepsilon_0^L)$ (as shown in Equation (5.12)).

The elastic anisotropy of the BCC open-cell foams can be measured by the Zener's anisotropy factor (Zhu et al., 1997a)

$$A^* = \frac{2(S_{11}-S_{12})}{S_{44}} = \frac{2(1+\nu_{12})\ G_{12}}{E_1} \tag{5.33}$$

If $A^* = 1$, the material is isotropic, then there are only two independent elastic constants, and the shear modulus can be obtained from the Young's modulus and Poisson's ratio $G_{12} = \frac{E_1}{2(1+\nu_{12})}$. The isotropic properties of macro-sized periodic random irregular open-cell foams were already demonstrated by Zhu et al. (2000).

For low density micro- and nano-sized periodic random irregular open-cell foams, the bending, torsion and axial stretching or compression of the cell struts are the main deformation mechanisms. The dimensionless Young's modulus can be expressed by

$$\overline{E_1} = \frac{E_1}{E_S \rho_0^2} \tag{5.34}$$

The dimensionless shear modulus is given by

$$\overline{G_{12}} = \frac{G_{12}}{E_S \rho_0^2} \tag{5.35}$$

Where E_S is the Young's modulus of the solid material, ρ_0 is the initial relative density of the representative unit periodic random irregular open-cell foam.

5.3.1 Size-dependent elastic properties of micro-sized periodic random irregular open-cell foams

This section will present the elastic properties of micro-sized periodic random irregular open-cell foams with the strain gradient effect. Figures 5.5 (a) and (b) show the size-dependent effect on the relationship between the non-dimensional Young's modulus and the relative density of open-cell foams with degrees of cell regularity 0.0 and 0.7. The smaller the cross-sectional diameter of the cell struts, the larger the value of l_m / d_0 and the larger the non-dimensional Young's modulus. This characteristic of micro-sized open-cell foams is consistent with the feature of micro-sized honeycombs (as shown in Chapter 3). This illustrates that the strain gradient has a significant effect on the elastic properties of micro-sized honeycombs and open-cell foams. This finding strongly supports the previous research (Aifantis, 1999, Lam et al., 2003, Toupin, 1962, Zhu, 2010b).

Apart from the size-dependent effect, the non-dimensional Young's modulus of micro-sized random irregular open-cell foams reduces with the increase of the relative density because of the effect of the transverse shear deformation. If the cross-sectional

diameter of the cell struts is much larger than the material intrinsic length parameter l_m, then the value of l_m / d_0 is close to 0 and the non-dimensional Young's modulus of micro-sized periodic random irregular open-cell foams reduces to those of their macro-sized counterparts. When the relative density is close to 0 and the value of l_m / d_0 is 0, the non-dimensional Young's modulus of a highly irregular honeycomb is nearly 1.0. Zhu et al. (1997a) found that the dimensionless Young's modulus of a very low density perfect regular macro-sized BCC open-cell foam with uniform cell struts of a plateau border cross-section is 1.0. Meanwhile, for highly random irregular macro-sized open-cell foams with cell struts of a plateau border cross-section, Zhu et al. (2000) found that their dimensionless Young's modulus is about 50% larger than 1.0. The findings in this chapter are consistent with the results of Zhu et al (1997a, 2000) because all of the cell struts have a uniform circular cross-section in this case and their bending stiffness is smaller than that of their counterparts with a plateau border cross-section (Zhu et al., 1997a, Zhu et al., 2000) if the cross-sectional areas of the cell struts are the same in both cases.[29]

[29] At the micro-meter scale, the bending stiffness of a beam with plateau border cross-section is $D_b = E_S \frac{20\sqrt{3}-11\pi}{24} d^4[1+23.18(1+\nu_S)(\frac{l_m}{d})^2]$ (Zhu, 2010b).

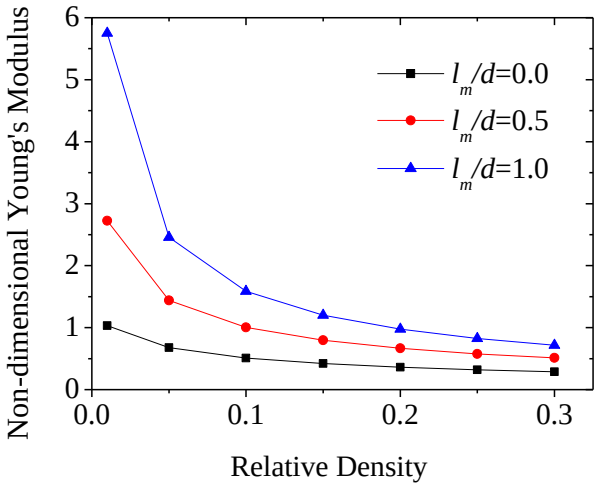

(a)

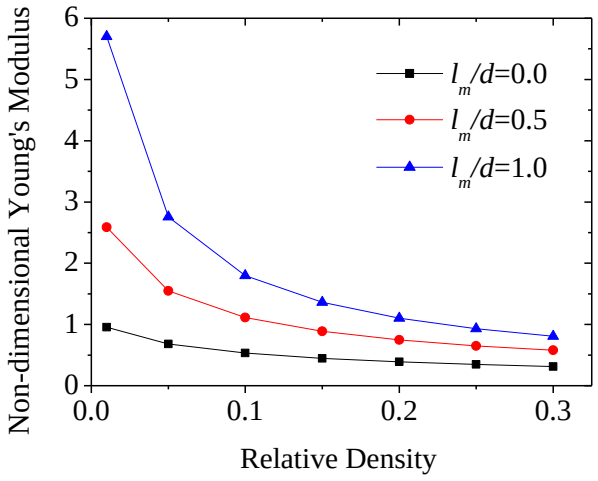

(b)

Figure 5.5. Size-dependent effect on the relationship between the non-dimensional Young's modulus and the relative density of micro-sized random irregular open-cell foams with degrees of cell regularity (a) α =0.0, and (b) α =0.7.

According to the previous research (Zhu et al., 2000, Sotomayor and Tippur, 2014b), in general, cell regularity has an influence on the Young's modulus of macro-sized irregular open-cell foams. Figure 5.6 shows the effect of cell regularity on the non-dimensional Young's modulus of micro-sized periodic random irregular open-cell foams with $l_m / d_0 = 0.5$ and different initial relative densities, 0.01 and 0.20, respectively. As can be seen, when the initial relative density is very small ($\rho_0 = 0.01$),

the non-dimensional Young's modulus reduces with the increase of the degree of cell regularity. This finding is consistent with the macro-sized random irregular open-cell foams (Zhu et al., 2000). If the initial relative density is large (e.g. $\rho_0 = 0.2$), then the trend is totally reversed and the more regular open-cell foams have a larger non-dimensional Young's modulus than their less regular counterparts. From Figures 5.5 (a) and (b), it can be found that this change occurs when the relative density is about 0.03 for micro-sized random irregular open-cell foams and $l_m / d_0 = 0.5$. This is very similar to the results from the macro-sized periodic random irregular open-cell foams. For example, Zhu et al.'s (2000) results show that the opposite trend occurs when the relative density is about 0.04. It is conjectured that increasing the value of l_m / d_0 leads to the occurrence of the opposite trend at a smaller relative density. Sotomayor and Tippur (2014b) modeled random irregular open-cell foams with the relative density from 0.03 to 0.09 and found that more regular open-cell foams are stiffer than their less regular counterparts.

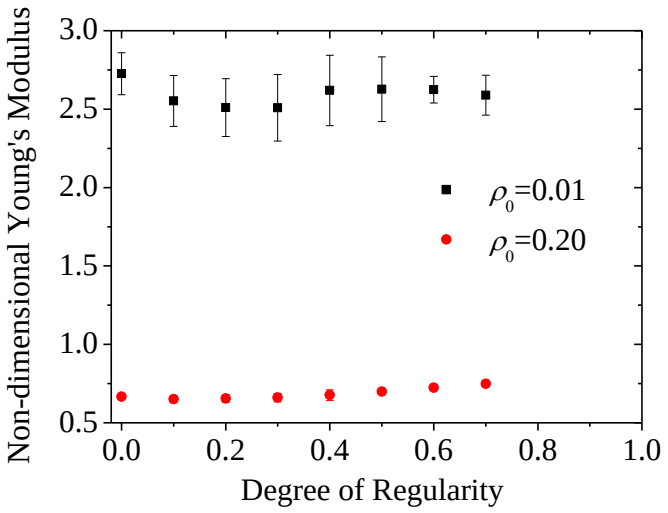

Figure 5.6. Effect of cell regularity on the non-dimensional Young's modulus of micro-

sized random irregular open-cell foams with $l_m / d_0 = 0.5$.

Figures 5.7 (a) and (b) present the size-dependent effect on the relationship between the non-dimensional shear modulus and the relative density of micro-sized periodic random irregular open-cell foams with degrees of cell regularity 0.0 and 0.7. As can be seen, for micro-sized open-cell foams with the same relative density: the smaller cross-sectional diameter of the cell struts (i.e. the larger the value of l_m / d_0), the larger the non-dimensional shear modulus. The non-dimensional shear modulus decreases with the increase of the foam relative density. When the cross-sectional diameter of the cell struts is much larger than the material intrinsic length parameter, the strain gradient effect becomes absent and the non-dimensional shear modulus of micro-sized periodic random irregular open-cell foams reduces to those of their macro-sized counterparts. The simulated results are consistent with the theoretical results of regular open-cell foams (Zhu et al., 1997a, Zhu and Wang, 2013).

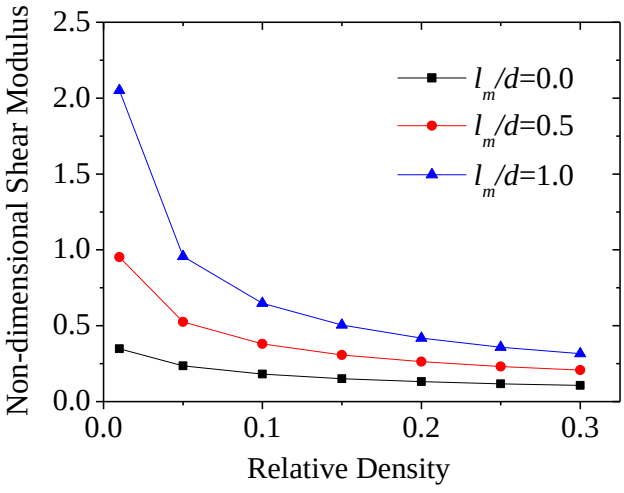

(a)

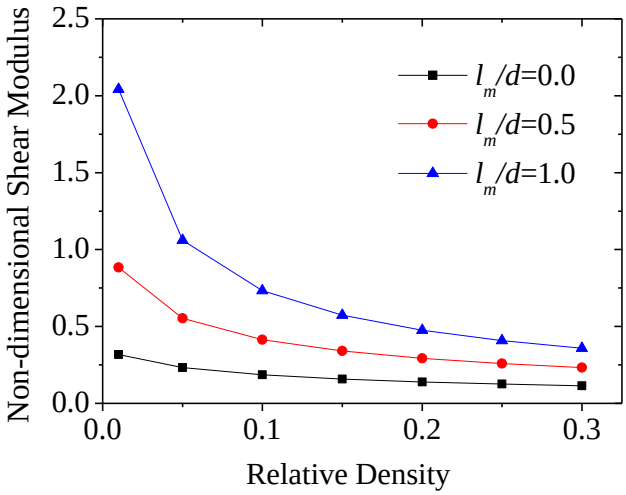

(b)

Figure 5.7. Size-dependent effect on the relationships between the non-dimensional shear modulus and the relative density of micro-sized random irregular open-cell foams with degrees of cell regularity (a) α =0.0, and (b) α =0.7.

Cell regularity also influences the shear modulus of micro-sized periodic random irregular open-cell foams. As can be seen in Figure 5.8, for low density micro-sized open-cell foams with $l_m / d_0 = 0.5$ and $\rho_0 = 0.01$: the greater the degree of cell regularity, the smaller the non-dimensional shear modulus. If the initial relative density is 0.20 (i.e. $\rho_0 = 0.2$), then the trend is reversed and this change occurs when the initial relative density is about 0.025 (see Figures 5.7 (a) and (b)). This is consistent with the relationship between the non-dimensional Young's modulus and cell regularity of micro-sized periodic random irregular open-cell foams.

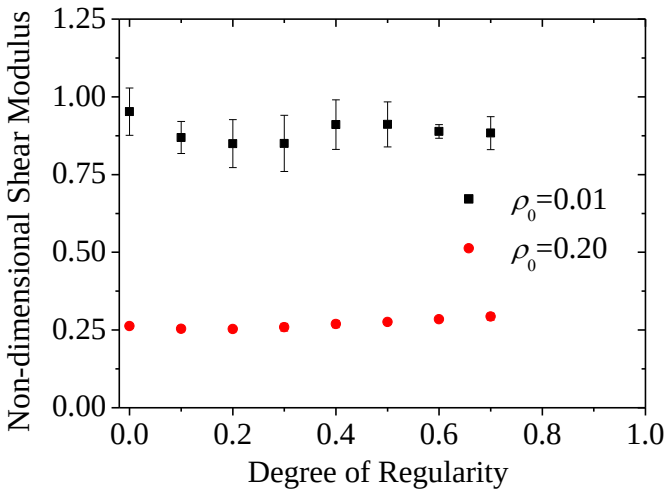

Figure 5.8. Effect of cell regularity on the non-dimensional shear modulus of micro-sized random irregular open-cell foams with $l_m / d_0 = 0.5$.

Besides the Young's modulus and shear modulus, the Poisson's ratio is another independent elastic constant for open-cell foams. Figures 5.9 (a) and (b) show the size-dependent effect on the relationship between the Poisson's ratio and the relative density of micro-sized random irregular open-cell foams with degrees of cell regularity 0.0 and 0.7. As can be seen, in general, the Poisson's ratio reduces with the increase of the relative density and with the decrease of the cross-sectional diameter of the cell struts. It can also be found that if the relative density is very close to 0, then the Poisson's ratio is nearly 0.5. This finding is consistent with both the theoretical results of macro- or nano-sized regular open-cell foams (Zhu et al., 1997a, Zhu and Wang, 2013) and with the simulation results of macro-sized irregular open-cell foams (Zhu et al., 2000).

In contrast from the effect on the Young's modulus and shear modulus of micro-sized open-cell foams, cell regularity has a limited effect on the Poisson's ratio,

whether or not the strain gradient effect is present or absent (as shown in Figure 5.10). This result supports the finding from macro-sized periodic random irregular open-cell foams (Zhu et al., 2000).

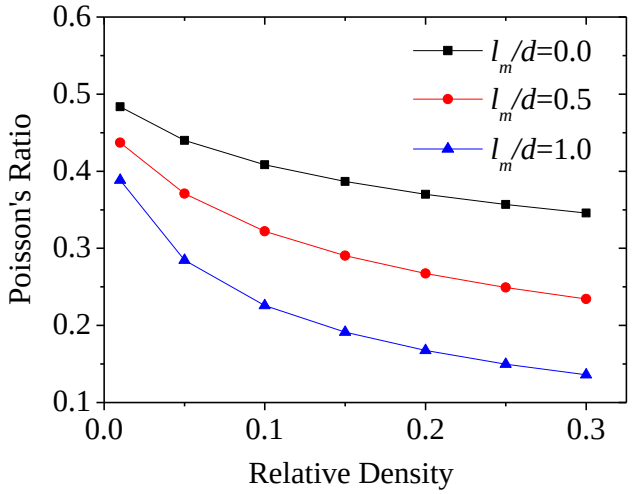

(a)

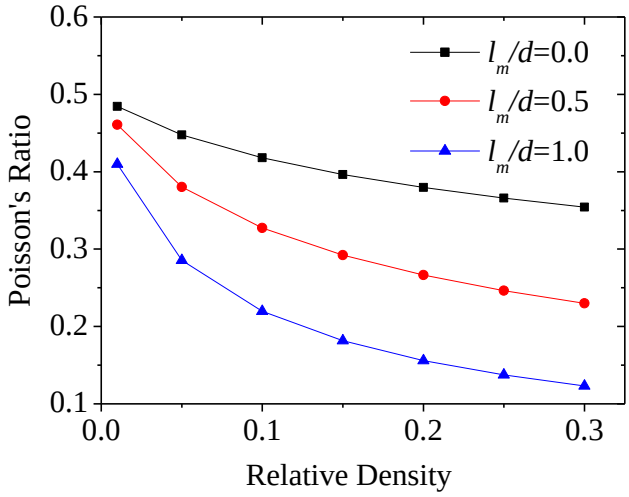

(b)

Figure 5.9. Size-dependent effect on the relationship between the Poisson's ratio and the relative density of micro-sized random irregular open-cell foams with degrees of cell regularity (a) α =0.0, and (b) α =0.7.

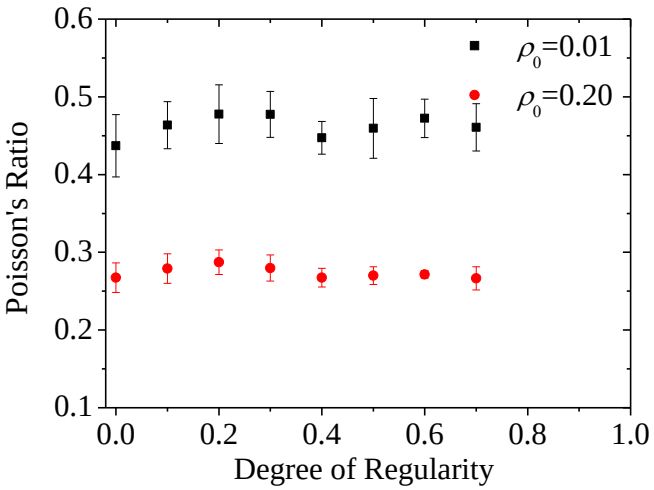

Figure 5.10. Effect of cell regularity on the Poisson's ratio of micro-sized random irregular open-cell foams with $l_m / d_0 = 0.5$.

According to the previous research (Zhu and Wang, 2013), the Zener's anisotropy factor can be used as a measure for the elastic anisotropy of the regular BCC open-cell foams. Based on the simulation results of the non-dimensional Young's modulus, shear modulus, and Poisson's ratio, the Zener's anisotropy factor can be obtained from Equation (5.33). As can be seen in Figures 5.11 (a) and (b), in all the cases, the Zener's anisotropy factor is always very close to 1.0, which indicates that micro-sized periodic random irregular micro-sized open-cell foams are always nearly isotropic. There is a little bit difference on the results with different size effects, it does not mean that micro- or nano-sized honeycombs or open-cell foams are more anisotropic. The number of the models is sufficiently large, the obtained mean results would be isotropic. This finding strongly supports the previous study about the isotropic properties of macro-sized regular open-cell foams (Zhu et al., 1997a) and periodic random irregular open-cell foams (Zhu et al., 2000). It can also explain why the trends

on the non-dimensional shear modulus are very similar to the trends on the non-dimensional Young's modulus (as shown in Figures 5.5 – 5.8).

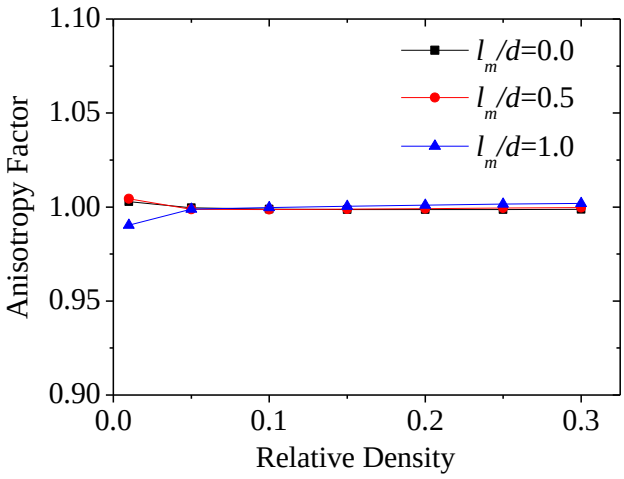

(a)

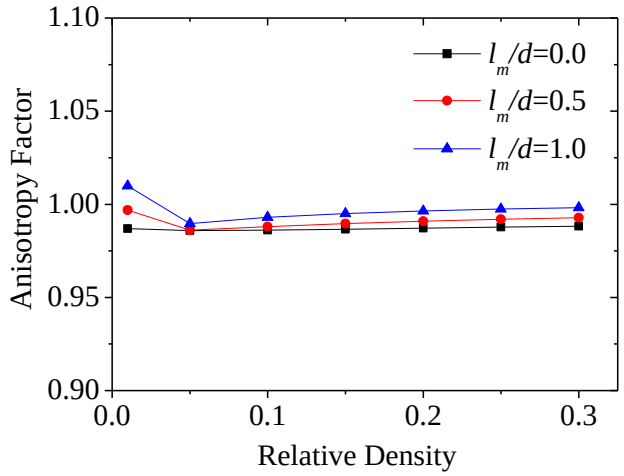

(b)

Figure 5.11. Size-dependent effect on the relationship between the Zener's anisotropy factor and the relative density of micro-sized random irregular open-cell foams with degrees of cell regularity (a) α =0.0, and (b) α =0.7.

5.3.2 Size-dependent elastic properties of nano-sized periodic random irregular open-cell foams

The effects of the surface elasticity and the initial stress or strain on the elastic properties of random irregular nano-sized open-cell foams are investigated in this

section. Figures 5.12 (a) and (b) show the relationships between the non-dimensional Young's modulus and the relative density of nano-sized periodic random irregular open-cell foams with degrees of regularity 0.0 and 0.7 when the effect of the initial stress or strain ($\varepsilon_0^L = 0.0$) is absent. If the relative density is fixed, then the smaller the cross-sectional diameter of the cell struts, the larger the non-dimensional Young's modulus will be. This feature is similar to the properties of micro-sized open-cell foams (as shown in Section 5.3.1) and is consistent with the feature of nano-sized honeycombs (as shown in Chapter 3). This finding supports the previous studies (Duan et al., 2005, Miller and Shenoy, 2000, Zhu and Wang, 2013, Zhu et al., 2012b, Zhu et al., 2014a). According to the previous work (Zhu and Wang, 2013), for nano-sized regular BCC open-cell foams with uniform cell struts of a square cross-section and $l_n / d = 0.5$, the non-dimensional Young's modulus is about 4.8 when the relative density is close to 0. In this chapter, the non-dimensional Young's modulus of nano-sized irregular open-cell foams with a circular cross-section and $l_n / d = 0.5$ is about 4.8 if the degree of cell regularity is α = 0.0 and 4.5 if the degree of cell regularity is α = 0.7. These findings are consistent with those of Zhu and Wang (2013) and are thus acceptable.

Figures 5.12 (a) and (b) also show that the larger the relative density, the smaller the non-dimensional Young's modulus. This trend is the same with the previous results (Zhu et al., 2000, Zhu et al., 1997a, Zhu and Wang, 2013). When the cross-sectional diameter of the cell struts is much larger than the material intrinsic length parameter

l_n, the value of l_n / d tends to 0 and the non-dimensional Young's modulus of nano-sized periodic random irregular open-cell foams reduces to the results of their macro-sized counterparts (Zhu et al., 2000).

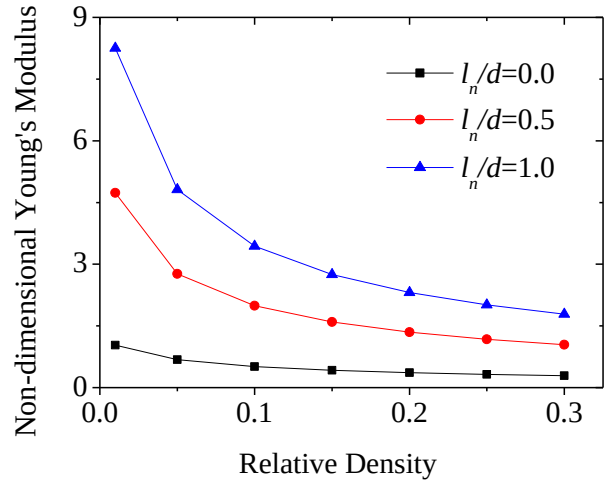

(a)

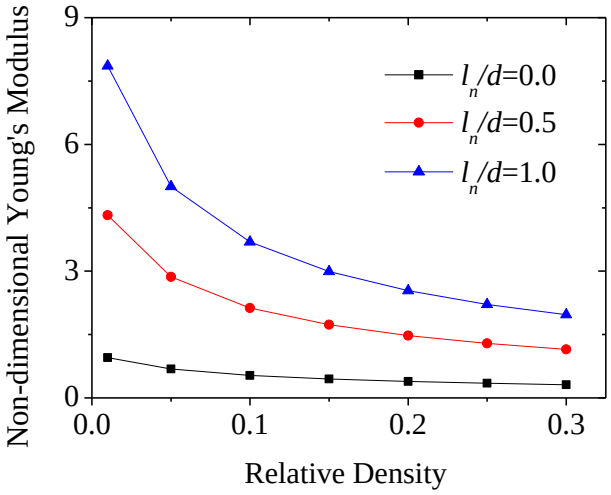

(b)

Figure 5.12. Size-dependent effect on the relationship between the non-dimensional Young's modulus and the relative density of nano-sized random irregular open-cell foams with degrees of cell regularity (a) α =0.0, and (b) α =0.7.

When the surface elasticity effect (size-dependent effect) is absent ($l_n / d = 0.0$), the initial stress or strain effect on the relationships between the non-dimensional Young's modulus and the relative density of nano-sized periodic random irregular open-cell foams with different degrees of cell regularity is shown in Figures 5.13 (a) and (b).

According to the previous research (Biener et al., 2009, Haiss et al., 1998, Kramer et al., 2004, Zhu et al., 2012a, Zhu et al., 2012b, Zhu et al., 2013), the amplitude of the recoverable initial elastic strain in the axial direction of the cell struts can be controlled from -0.1 to 0.1 by adjusting the amplitude of an applied electric potential at the nano-meter scale. As can be seen in Figures 5.13 (a) and (b), the non-dimensional Young's modulus reduces with the increase of the relative density. By adjusting the initial strain in the axial direction of the cell struts over the range between -0.1 and 0.1, the non-dimensional Young's modulus of nano-sized irregular open-cell foams can be controlled to increase by about 25% or to reduce by nearly 20%. These results are consistent with the results of Zhu and Wang (2013).[30] If the amplitude of the applied initial strain is different from -0.1 or 0.1, then the dimensionless Young's modulus of a nano-sized periodic random irregular open-cell foam can still be obtained by scaling up or scaling down the relevant results.

[30] According to Zhu and Wang (2013), the non-dimensional Young's modulus increases about 28% and decreases about 19% for nano-sized regular open-cell foams when the Poisson's ratio of solid materials is 0.1.

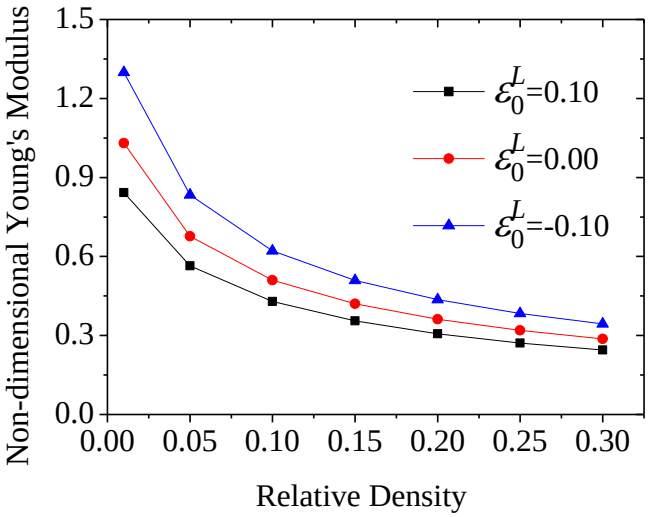

(a)

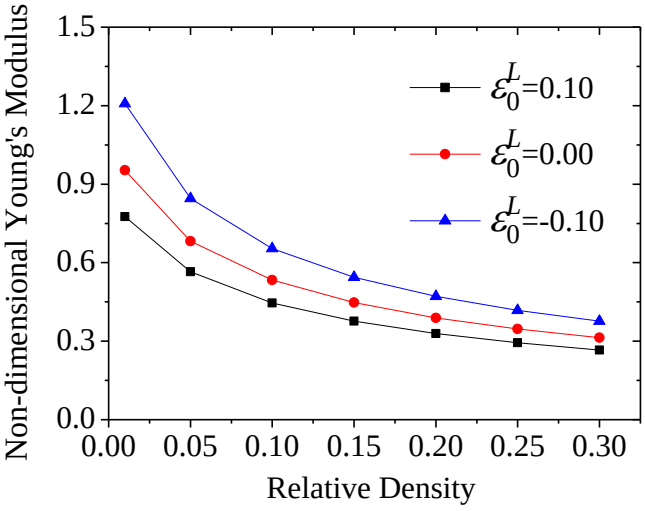

(b)

Figure 5.13. Effect of the initial strain on the relationships between the non-dimensional Young's modulus and the relative density of nano-sized random irregular open-cell foams with degrees of cell regularity (a) α =0.0, and (b) α =0.7.

Besides the surface elasticity and initial stress or strain effects, the cell regularity effect on the non-dimensional Young's modulus of nano-sized periodic random irregular open-cell foams is considered and presented in Figure 5.14. When the initial strain effect is absent ($\varepsilon_0^L = 0.0$), if the initial relative density is very small ($\rho_0 = 0.01$), then a more irregular nano-sized open-cell foam has a larger non-dimensional Young's

modulus than a less irregular one. This trend is inverted when the initial relative density is large. The trend change occurs when the initial relative density is about 0.028 (as shown in Figures 5.12 (a) and (b)) and $l_n / d = 0.5$. This finding is consistent with the micro-sized periodic random irregular open-cell foams (as shown in Section 5.3.1) and is similar to the macro-sized periodic random irregular open-cell foams in which the trend change occurs when the relative density is about 0.04 (Zhu et al., 2000).

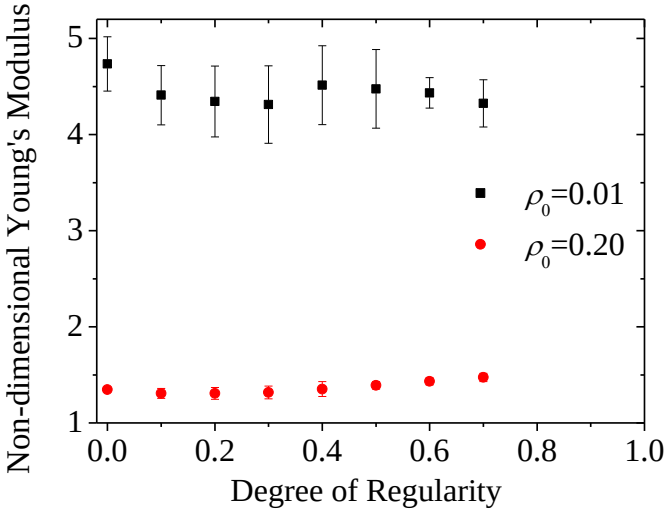

Figure 5.14. Effect of cell regularity on the non-dimensional Young's modulus of nano-sized random irregular open-cell foams with $l_n / d = 0.5$.

As the value of l_n / d increases, the trend change occurs at a smaller relative density. For nano-sized irregular open-cell foams with $l_n / d \le 0.5$ and whose relative density is larger than 0.028: the larger the degree of cell regularity, the larger the non-dimensional Young's modulus. As can be seen in Figure 5.14, the largest standard deviation of the non-dimensional Young's modulus is about 10%.[31]

[31] This means that these 20 similar random models have very different non-dimensional Young's modulus.

When the initial strain effect is absent ($\varepsilon_0^L = 0.0$), the size-dependent effect on the relationship between the non-dimensional shear modulus and the relative density of nano-sized periodic random irregular open-cell foams with different degrees of cell regularity 0.0 and 0.7 is shown in Figures 5.15 (a) and (b). As can be seen, the smaller the cross-sectional diameter of the cell struts, the larger the non-dimensional shear modulus. Meanwhile, the smaller the relative density, the larger the non-dimensional shear modulus. If the cross-sectional diameter of the cell struts is much larger than the material intrinsic length parameter, the size-dependent effect would be absent and the non-dimensional shear modulus of nano-sized periodic random irregular open-cell foams reduces to those of their macro-sized counterparts. These features are consistent with the micro-sized irregular open-cell foams (as shown in Section 5.3.1).

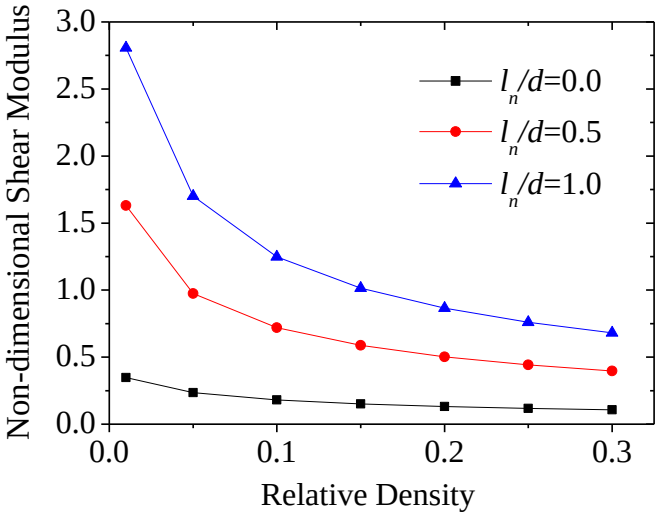

(a)

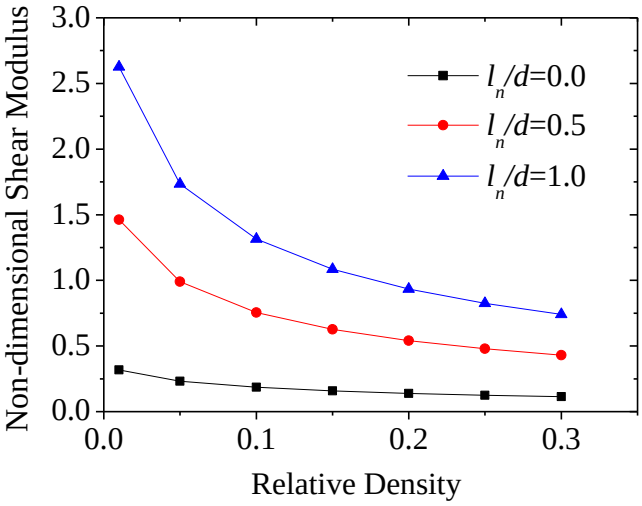

(b)

Figure 5.15. The size-dependent effect on the relationship between the non-dimensional shear modulus and the relative density of nano-sized random irregular open-cell foams with degrees of cell regularity (a) α =0.0, and (b) α =0.7.

When the size-dependent effect is absent, the initial strain effect on the dimensionless shear modulus of nano-sized irregular open-cell foams with degrees of regularity 0.0 and 0.7 is shown in Figures 5.16 (a) and (b). By adjusting the amplitude of the initial strain in the cell strut length direction between -0.1 and 0.1, the dimensionless shear modulus can be controlled to vary over a range about 50%. This is very similar to the range of the non-dimensional Young's modulus of nano-sized regular (Zhu and Wang, 2013) and irregular open-cell foams (as shown in Section 5.3.2 in the description of Figure 5.13).

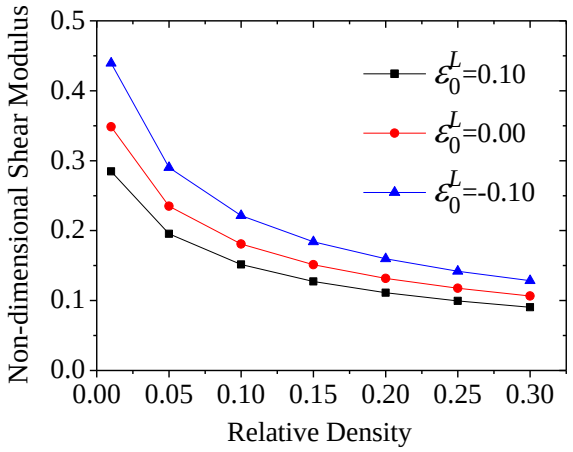

(a)

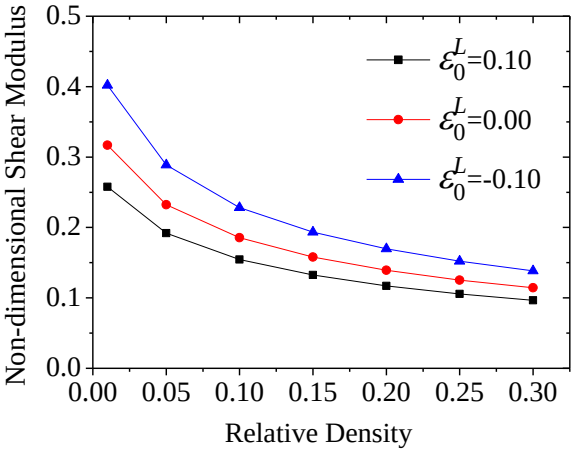

(b)

Figure 5.16. Effect of the cell strut initial strain on the relationship between the non-dimensional shear modulus and the relative density of nano-sized random irregular open-cell foams with degrees of cell regularity (a) α =0.0, and (b) α =0.7.

When the initial strain effect is absent, cell regularity effect on the dimensionless shear modulus of nano-sized periodic random irregular open-cell foams with $l_n / d = 0.5$ is presented in Figure 5.17. When the initial relative density is very small (nearly 0.01): the larger the degree of cell regularity, the smaller the non-dimensional shear modulus. This trend is reversed with the increase of the initial relative density. According to Figures 5.15 (a) and (b), the trend change occurs when the initial relative density is 0.028, which is consistent with the relationship between the non-dimensional Young's

modulus and cell regularity of nano-sized periodic random irregular open-cell foams.

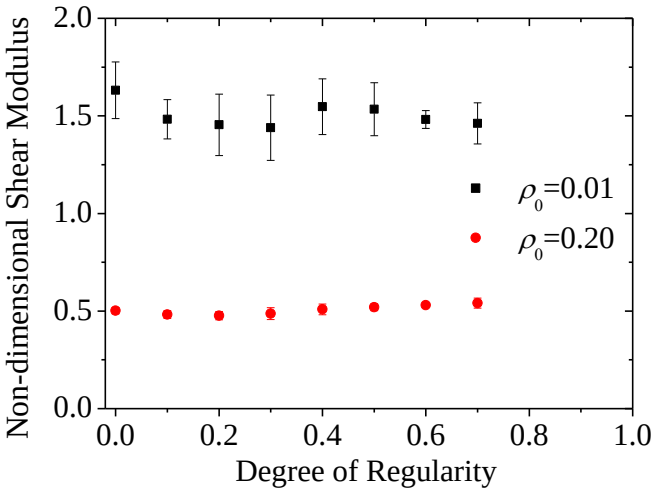

Figure 5.17. The effect of cell regularity on the non-dimensional shear modulus of nano-sized random irregular open-cell foams with $l_n / d = 0.5$.

When the initial strain effect is absent, the size-dependent effect on the relationship between the Poisson's ratio and the relative density of nano-sized periodic random irregular open-cell foams is shown in Figures 5.18 (a) and (b). Generally, the Poisson's ratio reduces with the increase of the relative density. When the relative density approaches 0, the Poisson's ratio is very close to 0.5. This supports the theoretical and simulation results of the macro-sized regular and irregular open-cell foams (Zhu et al., 2000, Zhu et al., 1997a), and is consistent with the results of the nano-sized regular open-cell foams (Zhu and Wang, 2013) and micro-sized irregular open-cell foams (as shown in Section 5.3.1). As can be seen, the smaller the cross-sectional diameter of the cell struts, the smaller the Poisson's ratio. Similar to macro- (Zhu et al., 2000) and micro-sized periodic random irregular open-cell foams (as shown in Section 5.3.1), the degree of cell regularity has a very limited effect on the Poisson's ratio (as shown

in Figure 5.19).

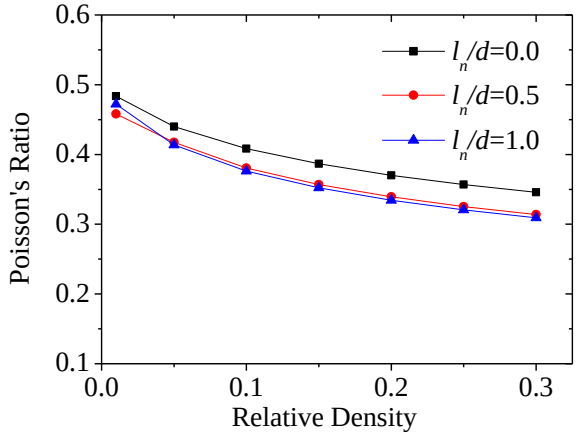

(a)

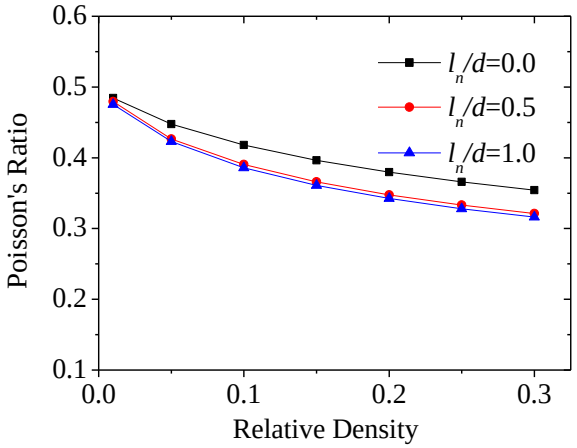

(b)

Figure 5.18. Size-dependent effect on the relationship between the Poisson's ratio and the relative density of nano-sized random irregular open-cell foams with degrees of cell regularity (a) α =0.0, and (b) α =0.7.

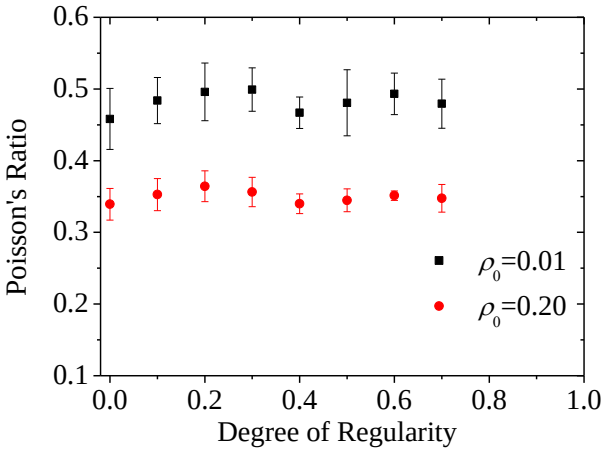

Figure 5.19. Effect of cell regularity on the Poisson's ratio of nano-sized random irregular open-cell foams with $l_n / d = 0.5$.

When the size-dependent effect is absent, the initial strain effect on the relationship between the Poisson's ratio and the relative density of nano-sized periodic random irregular open-cell foams is shown in Figures 5.20 (a) and (b). As can be seen, the Poisson's ratio can be controlled to increase or decrease by adjusting the amplitude of the initial strain in the axial direction of the cell struts over the range between -0.1 and 0.1, and the tunable range of the Poisson's ratio is approximately proportional to the amplitude of the applied initial strain. This finding is consistent with the results of nano-sized periodic random irregular honeycombs (as shown in Chapter 3).

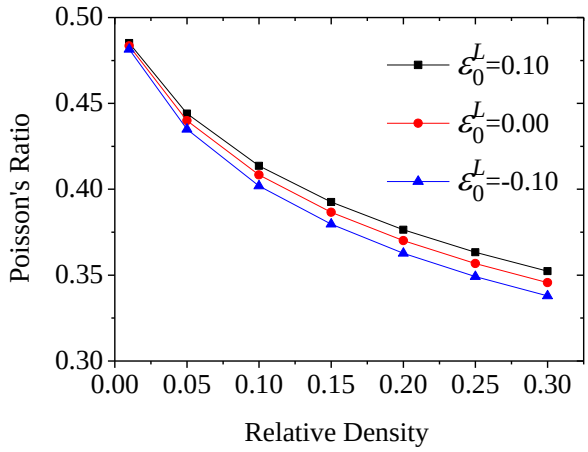

(a)

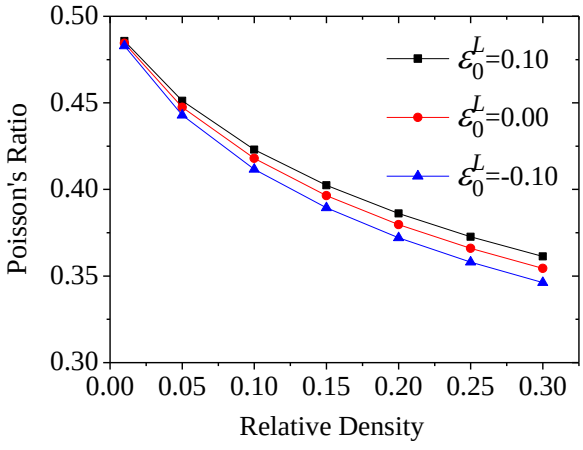

(b)

Figure 5.20. The effect of the cell strut initial strain on the relationship between the Poisson's ratio and the relative density of nano-sized random irregular open-cell foams with degrees of cell regularity (a) α =0.0, and (b) α =0.7.

According to the definition of the Zener's anisotropy factor (as shown in Equation (5.33)), the isotropic properties of nano-sized periodic random irregular open-cell foams are shown in Figures 5.21 (a), (b) and 5.22 (a), (b). As can be seen, the Zener's anisotropy factor is always very close to 1.0 in all the cases, which indicates that nano-sized periodic random irregular open-cell foams are isotropic. The cell strut size, initial strain, relative density, and cell regularity do not affect the isotropic property of nano-sized random irregular open-cell foams. This finding strongly supports the previous research about the isotropic properties of macro- (Zhu et al., 2000) and micro-sized periodic random irregular open-cell foams (as shown in Section 5.3.1).

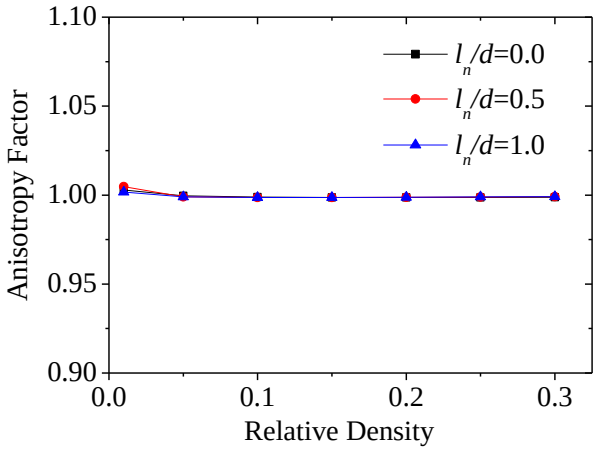

(a)

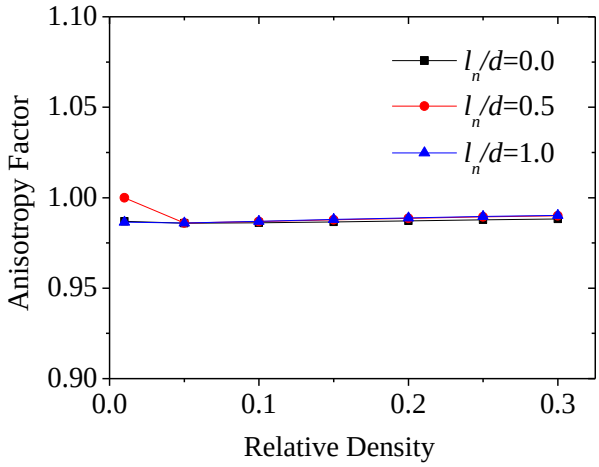

(b)

Figure 5.21. The size-dependent effect on the relationship between the Zener's anisotropy factor and the relative density of nano-sized random irregular open-cell foams with degrees of cell regularity (a) α =0.0, and (b) α =0.7.

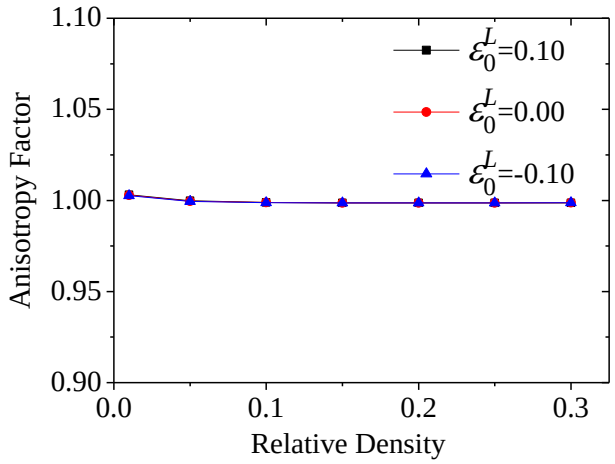

(a)

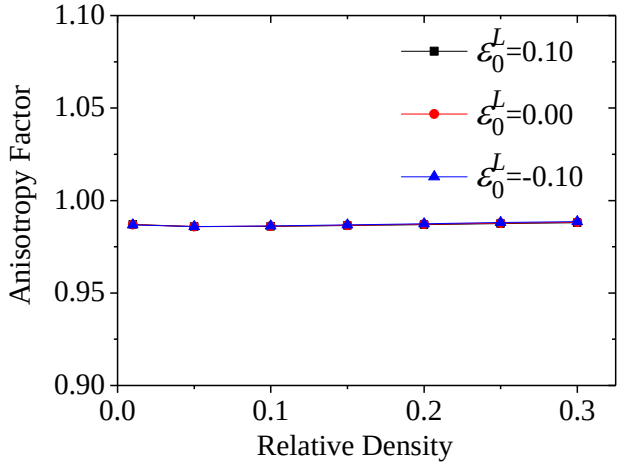

(b)

Figure 5.22. The effect of the cell strut initial strain on the relationship between the Zener's anisotropy factor and the relative density of nano-sized random irregular open-cell foams with degrees of cell regularity (a) α =0.0, and (b) α =0.7.

5.4 Summary

In this chapter, the Young's modulus, shear modulus and Poisson's ratio of micro- and nano-sized periodic random irregular open-cell foams are obtained from computer

simulations. At the micro-meter scale, the strain gradient effect plays an important role in the elastic properties of irregular open-cell foams. At the nano-meter scale, the surface elasticity and initial stress or strain have significant effects on the elastic properties of irregular open-cell foams. The smaller the cross-sectional diameter of the cell struts, the larger the non-dimensional Young's modulus and shear modulus of micro- and nano-sized periodic random irregular open-cell foams, and the smaller their Poisson's ratios. The non-dimensional Young's modulus and shear modulus of micro- and nano-sized periodic random irregular open-cell foams reduce with the increase of the relative density. When the initial strain effect is absent, if the relative density is very small (nearly 0.01), then more regular micro- and nano-sized open-cell foams have smaller non-dimensional Young's modulus and shear modulus than less regular ones. When the relative density is about 0.03, this trend is reversed for micro-sized irregular foam with $l_m / d_0 = 0.5$ or nano-sized irregular foams with $l_n / d = 0.5$. It has also been found that cell regularity has a limited effect on the Poisson's ratio. The non-dimensional Young's modulus and shear modulus of nano-sized irregular open-cell foams can be controlled to increase or reduce over a range of about 50% by adjusting the applied initial strain in the axial direction of the cell struts between -0.1 and 0.1. It is found that the Zener's anisotropy factors of micro- and nano-sized periodic random irregular open-cell foams with different relative densities are always very close to 1.0, whether the size-dependent effect or the initial strain effect is present or absent.

Chapter 6 The high strain compression of micro- and nano-sized periodic random irregular open-cell foams

6.1 Introduction

The linear elastic properties of micro- and nano-sized random irregular open-cell foams were presented in Chapter 5. This chapter will show the geometrically nonlinear elastic properties of low-density micro- and nano-sized random irregular open-cell foams by computational simulations. The strain gradient effect plays an important role in the deformation of open-cell foams at the micro-meter scale, and the surface elasticity and initial stress or strain effects become the dominant deformation mechanisms at the nano-meter scale. Since there are no types of element in the commercial finite element software (ANSYS) that could directly deal with such effects, the equivalent material Young's modulus, Poisson's ratio, and beam element cross-sectional area are again used to incorporate these effects into the computer simulations (by using ANSYS software in this case). This chapter will mainly consider the size-dependent, initial stress or strain, and cell regularity effects on the relationships between the compressive stress and the Poisson's ratio against the compressive strain response of micro- and nano-sized random irregular open-cell foams.

6.2 Methodology

6.2.1 Parameters setting on random irregular open-cell foams

As in Chapter 5, the geometric models of the representative unit periodic random irregular open-cell foams are constructed by the computer program that was developed by Zhu et al. (2000), and Zhu and Windle (2002). The main parameters that are used to construct the representative unit periodic random irregular open-cell foams include the degree of cell regularity, the initial relative density, and the number of complete cells of open-cell foams. The greater the degree of cell regularity, the more regular the open-cell foams will be. When α = 0.0, it is a fully random irregular open-cell foam; and when α = 1.0, it is a perfectly regular open-cell foam. In this chapter, the degrees of regularity are set to 0.0, 0.2, 0.4, and 0.7.

To model the high strain compression of micro- and nano-sized low-density periodic random irregular open-cell foams, the relative density is constantly fixed at 0.01. All of the cell struts of the open-cell foams are assumed to have the same uniform and circular cross-sectional area, which can thus be determined from Equation (2.7).

Similarly to Chapter 5, the mean dimensionless compressive stress and the mean Poisson's ratio are obtained from 10-20 similar random irregular open-cell foams models. According to the results of Zhu and Windle (2002), the larger the number of complete cells, the longer time it takes to compress an open-cell foam to a certain compressive strain and the less likely it is to have a convergent result. Zhu and Windle (2002) also found that the number of complete cells does not affect the mean

compressive stress and strain response of open-cell foams. They also found that the smaller the number of complete cells, the larger the standard deviation of the dimensionless compressive stress. In order to enhance the possibility to have convergent results for the high strain compression of open-cell foams, the number of complete cells is fixed at 27 in this chapter.

6.2.2 Finite element simulations

As described in the previous chapters, ANSYS (which is commercial software) is used to perform the finite element simulations on the high strain compression behaviour of micro- and nano-sized periodic random irregular open-cell foams. Each of the cell struts is partitioned into 3-9 BEAM189 elements, depending upon the cell strut length compared to the mean strut length. Similarly to Chapter 4, since the relative density of the open-cell foams is very low (i.e. 0.01), the solid material is assumed to be linear elastic in the finite element simulations for the high strain compression of open-cell foams. The Young's modulus (E_S) and Poisson's ratio (v_S) of solid materials are set as $2\times10^5\ MPa$ and 0.1, respectively.

The bending, torsion and axial stretching or compression rigidities of uniform beams are size-dependent at the micro- and nano-meter scales, and they are obtained by Equations (2.25 – 2.27) for micro-sized open-cell foams and Equations (2.31 – 2.33) for nano-sized open-cell foams. The equivalent material Young's modulus E_e, Poisson's ratio v_e, and radius of the cross-section of beam R_e can be given from

Equations (5.4 – 5.6). The values of l_m / d and l_n / d are set to 0.0, 0.2, 0.5, and 1.0, respectively. The amplitude of the initial strain in the strut length direction ε_0^L is set to -0.1, 0, and 0.1. The model treatment for the initial strain effect is the same as in Chapter 5, and it can be given by Equations (5.9 – 5.11).

Given that the unit random irregular open-cell foams are periodic, the periodic boundary conditions are the most suitable boundary conditions for the high strain compression simulations of random irregular open-cell foams. The constraint equations are given in Chapter 5 by Equations (5.14 – 5.25). The models are compressed in *y* direction to a strain up to 60% (as shown in Figure 6.1).[32] The setting of the large displacement in ANSYS is very similar to that in Chapter 4. "Large Displacement Static" is selected in the "Analysis Options" section of the ANSYS software, and the "Nonlinear Options" also needs to be "ON" for the large strain simulations. As in Chapter 4, "load step", "substep" (or "time step") and "equilibrium iteration" are the three main important settings for the loading step process. In order to enhance the possibility to achieve convergent results for the high strain compression of random irregular open-cell foams, the "load step" is set to two steps. The foams are compressed 30% in the first "load step" and further compressed another 30% in the second "load step". In each of the "load step", the "time step" is set to automatic time stepping, which can automatically determine the time step size and hence improve the

[32] To avoid possible rigid displacement of the whole model, one node on the bottom edge is fixed in the *y* direction, one node on the left edge is fixed in the *x* direction and another node on the front edge is fixed in the *z* direction. The compressive strain is applied in the *y* direction on a top node, which corresponds to the fixed bottom node (as shown in Figure 6.1).

convergence efficiency of the simulations. In this chapter, the simulations are static, so the ramped load is selected as the loading type of the "substep" (as shown in Figure 4.2 (a)).

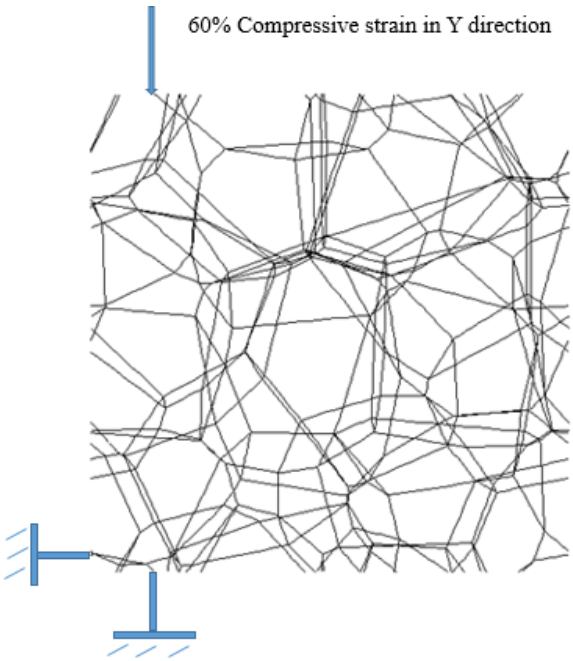

Figure 6.1. Loading schematic diagram on a representative unit periodic random irregular open-cell foam with the degree of cell regularity α = 0.7.

The high strain compression of open-cell foams involves geometrical nonlinearity, and the convergent solutions are achieved by equilibrium iterations. Since the structural models are three dimensional and irregular, it is difficult to achieve convergence for large strain compressions. The convergence tolerance on all the solutions of force is thus set to 2%, and the number of the equilibrium iterations is set to 500. All of the solutions are iteratively corrected in each "substep" and "load step" until the corrected solution meets the convergence tolerance, the simulation then goes into the next step.

6.3 Results and Discussion

In this chapter, each data is obtained from 10 to 20 similar models with the same parameter settings, such as the degree of cell regularity, relative density and number of complete cells of open-cell foams. Due to the convergence issue, it is very difficult to compress the irregular models to a strain of 60%. If a model is compressed to a strain about 40% or larger, then the results will be recorded as useful. More than 50 similar models usually need to be run in order to have a sufficient number of models to be compressed up to 60%.

The cell strut contact problem is not considered in this chapter. As can be seen from Figures 6.2 (a), (b), (c), and (d), cell strut overlap takes place when the open-cell foam model is compressed to 40%.

The compressive stress, strain and Poisson's ratio can be obtained as described in Chapter 5. The compressive stress is normalized by the Young's modulus of the solid material and by the square of the open-cell foam initial relative density, and is given as (Zhu and Windle, 2002)

$$\bar{\sigma} = \frac{\sigma}{E_S \rho_0^2} \tag{6.1}$$

where σ is the compressive stress, E_S is the Young's modulus of the solid material, and ρ_0 is the relative density of the random irregular open-cell foams when the effect of the initial stress or strain is absent.

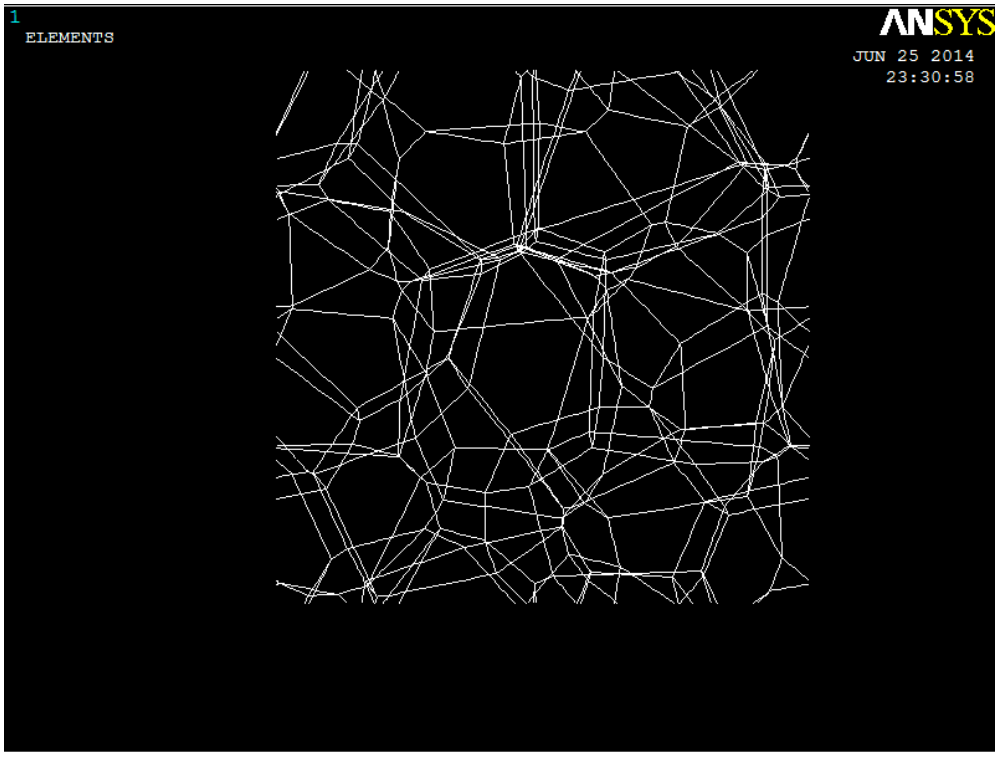
1
ELEMENTS
ANSYS
JUN 25 2014
23:30:58

(a)

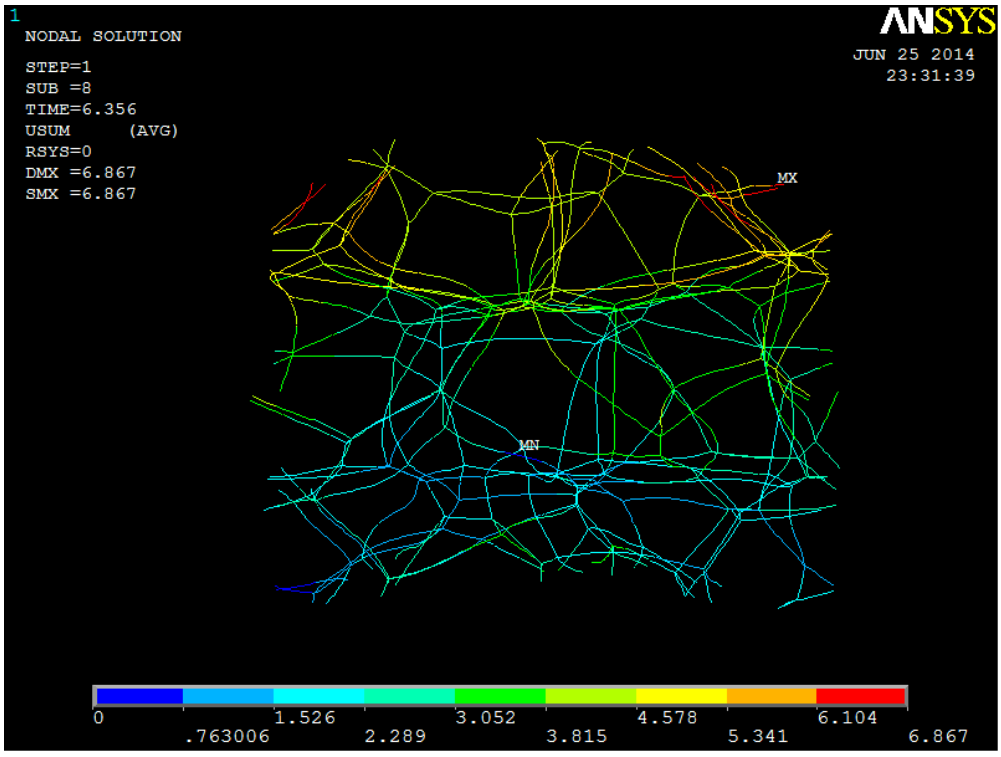
1
NODAL SOLUTION
STEP=1
SUB =8
TIME=6.356
USUM (AVG)
RSYS=0
DMX =6.867
SMX =6.867
ANSYS
JUN 25 2014
23:31:39
MX
MN
0
.763006
1.526
2.289
3.052
3.815
4.578
5.341
6.104
6.867

(b)

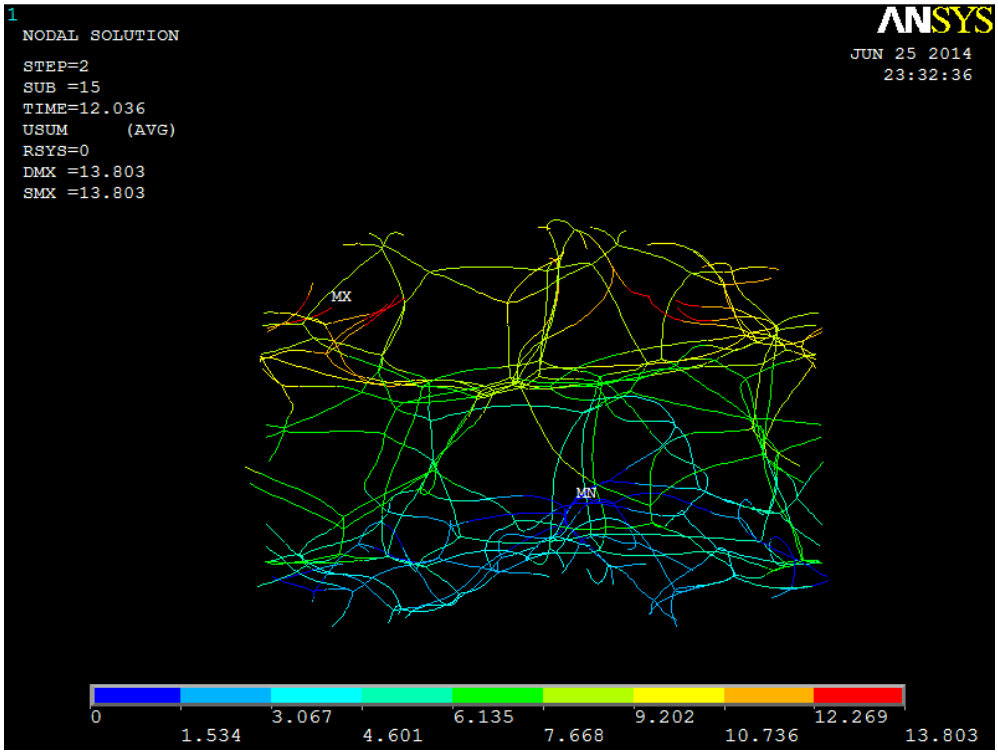

(c)

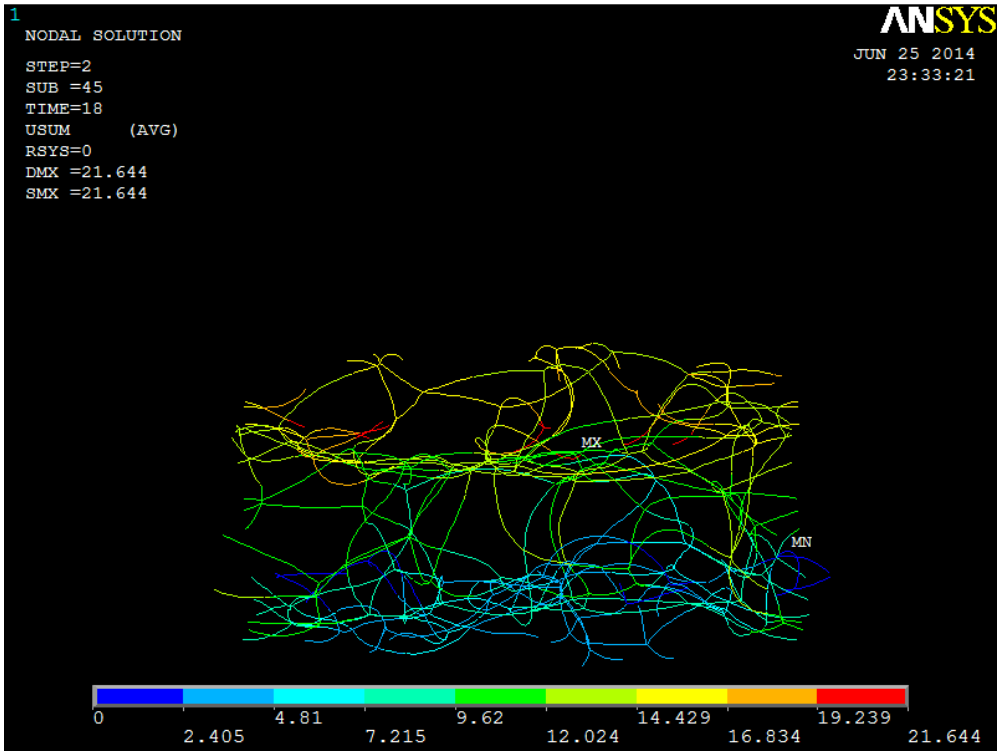

(d)

Figure 6.2. Compressive deformation of periodic random irregular open-cell foams with degree of regularity $\alpha = 0.7$. (a) $\varepsilon_y = 0.0$, (b) $\varepsilon_y = 0.212$, (c) $\varepsilon_y = 0.401$, and (d) $\varepsilon_y = 0.6$.

6.3.1 Size-dependent effect on the high strain compression of micro-sized random irregular open-cell foams

The strain gradient effect plays an important role in the mechanical behaviour of materials and structures at the micro-meter scale (Aifantis, 1999, Toupin, 1962). This section will present how the diameter of the cell struts and the degree of cell regularity affect the relationships of the compressive stress and the compressive strain, and of the Poisson's ratio versus the compressive strain of micro-sized periodic random irregular open-cell foams.

6.3.1.1 Size-dependent effect on the relationship between the compressive stress and strain

The size-dependent effect on the relations between the mean dimensionless stress and strain response for low density micro-sized periodic random irregular open-cell foams are presented in Figures 6.3 (a), (b), (c), and (d). The relative density of the open-cell foams is fixed at 0.01. The range of the degree of the cell regularity is from 0.0 to 0.7. As can be seen from Figures 6.3 (a), (b), (c), and (d), for micro-sized open-cell foams with different degrees of cell regularity, the dimensionless compressive stress increases gradually with the increase of the applied compressive strain from 0% to 60% in the *y* direction. For micro-sized random irregular open-cell foams with the same degree of cell regularity, when the surface modulus is positive ($l_m / d > 0$), the smaller

the cell strut diameter (i.e. the larger the value of l_m / d), the larger the dimensionless compressive stress and the larger the tangent modulus. If the surface modulus is negative ($l_m / d < 0$), then the effect is inverted. For any values of compressive strain between 0% and 40% (or larger), when the value of l_m / d is increased from 0.0 to 1.0, the dimensionless compressive stresses of micro-sized open-cell foams with different degrees of cell regularity increase more than six times. According to the findings of Zhu and Windle (2002), the compressive stress and strain relationship of macro-sized open-cell foams depends only on the relative density and the cell regularity. For low density open-cell foams, cell strut bending and torsion are the dominant deformation mechanisms. At the micro-meter scale, both the bending and the torsion rigidities of the cell struts are larger than those of their macro-sized counterparts. This is why at the micro-meter scale, the larger the value of l_m / d, the larger the dimensionless compressive stress of the open-cell foams.

When the diameter of the cell wall is much larger than the material intrinsic length l_m (i.e. $l_m / d \approx 0$), the strain gradient effect is absent and the relationships between the dimensionless compressive stress and the foam compressive strain reduce to those of the conventional macro-sized counterparts. It can be seen from Figure 6.3 (d) that, for micro-sized random irregular open-cell foams with $l_m / d = 0$ and $\alpha = 0.7$, the dimensionless plateau stress is about 0.1 when the compressive strain is up to 60%, which is about 23% smaller than Zhu and Windle's (2002) result (about 0.13). The reason for this difference is the shape of the cross-section of cell struts. Zhu and

Windle (2002) used a plateau border cross-section for the cell struts, while in this chapter the cross-section of cell struts is assumed to be a circle. For the same cross-section area, a beam/strut with a plateau border cross-section has a larger bending stiffness than a beam/strut with a circular cross-section.[33] This is why Zhu and Windle (2002) obtained dimensionless compressive stresses larger than the results for macro-sized open-cell foams (i.e. $l_m / d = 0$) in this chapter.

For micro-sized random irregular open-cell foams, when the surface modulus is positive ($l_m / d > 0$), the smaller the cell strut diameter, the larger the standard deviations. If the cell strut diameter is the same, then the larger the foam compressive strain, the larger the standard deviations. This happens because there is large fluctuation on the convergent solution when an irregular open-cell foam is compressed to a large strain. The results shown in Figures 6.3 (a), (b), (c), and (d) indicate that the strain gradient effect (i.e. the value of l_m / d) has a significant influence on the relationships between the compressive stress and strain of low density micro-sized periodic random irregular open-cell foams.

[33] At the micro-meter scale, the bending stiffness of a beam with plateau border cross-section is $D_b = E_S \frac{20\sqrt{3} - 11\pi}{24} d^4 [1 + 23.18(1 + \nu_S)(\frac{l_m}{d})^2]$ (Zhu, 2010b).

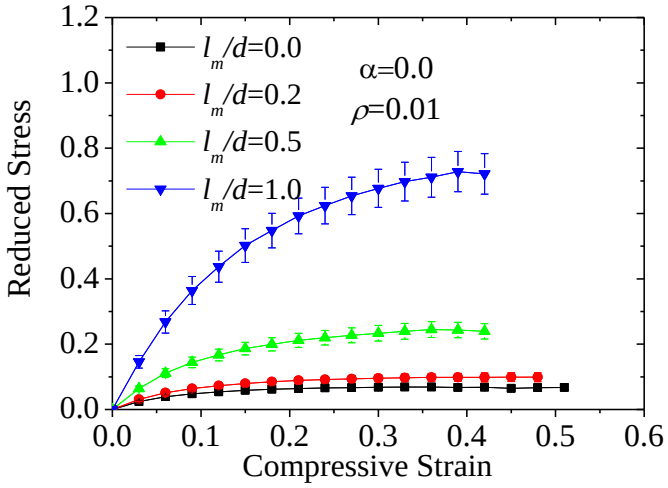
Reduced Stress
Compressive Strain
l_m/d=0.0
l_m/d=0.2
l_m/d=0.5
l_m/d=1.0
α=0.0
ρ=0.01

(a)

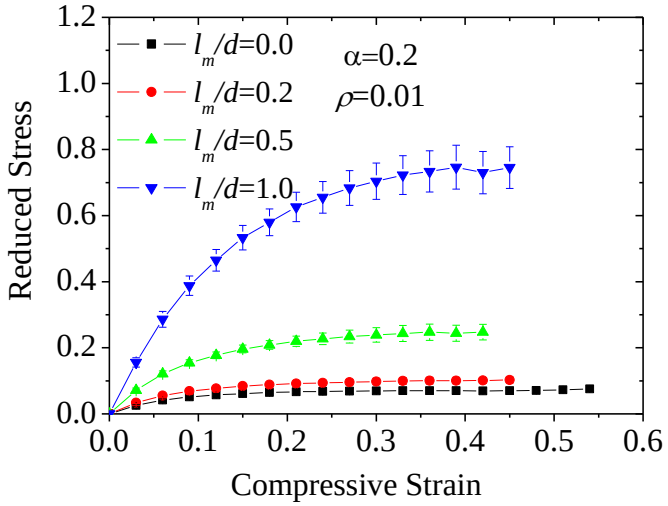
Reduced Stress
Compressive Strain
l_m/d=0.0
l_m/d=0.2
l_m/d=0.5
l_m/d=1.0
α=0.2
ρ=0.01

(b)

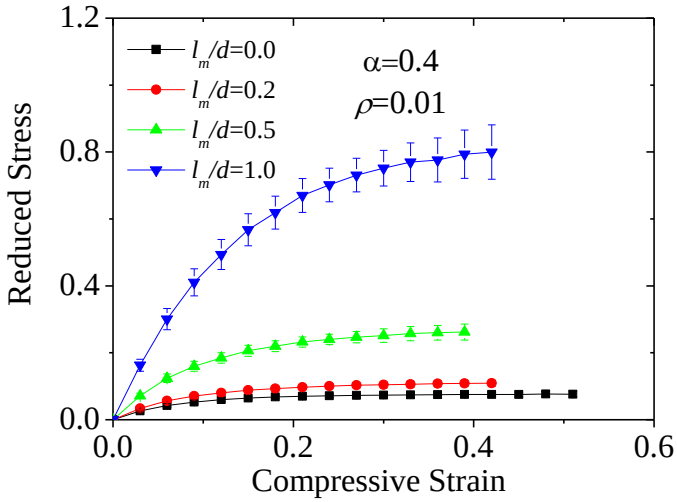
Reduced Stress
Compressive Strain
l_m/d=0.0
l_m/d=0.2
l_m/d=0.5
l_m/d=1.0
α=0.4
ρ=0.01

(c)

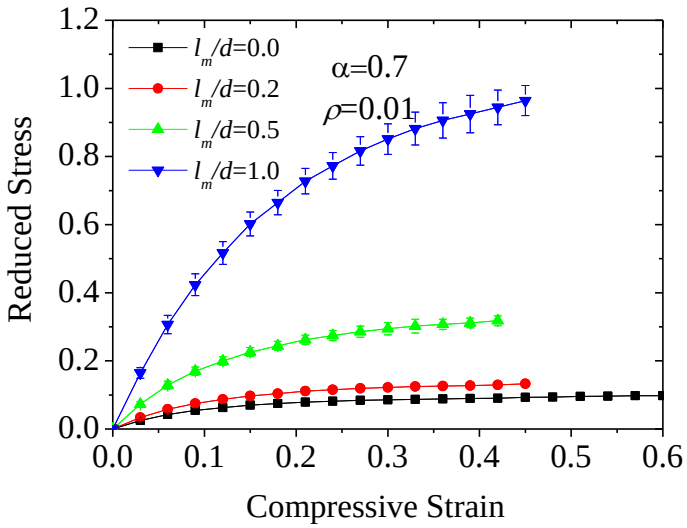

Figure 6.3. The size-dependent effect on the mean dimensionless stress and strain response for low density micro-sized periodic random irregular open-cell foams with the relative density ρ_0 = 0.01. (a) α = 0.0, (b) α = 0.2, (c) α = 0.4, and (d) α =0.7.

6.3.1.2 Effect of cell regularity on the relationship between the compressive stress and strain

Apart from the strain gradient effect, the cell regularity may also affect the relationship between the compressive stress and strain of low density micro-sized random irregular open-cell foams. Figure 6.4 presents the effects of cell regularity on the relationship between the mean dimensionless compressive stress and compressive strain for low density micro-sized random irregular open-cell foams with fixed relative density ρ_0 = 0.01 and $l_m / d = 0.5$. When the compressive strain is small, the larger the degree of cell regularity, the smaller the tangent modulus. Figure 6.4 also clearly shows that when the compressive strain is larger than 10%, the larger the degree of cell regularity of micro-sized random irregular open-cell foams, the larger the mean dimensionless

compressive stress and the smaller the standard deviations. When the strain gradient effect is absent (i.e. $l_m / d = 0$), the results of the relations on the mean dimensionless compressive stress and strain reduce to those of the macro-sized random irregular open-cell foams, which is consistent with those of Zhu and Windle (2002). The results shown in Figures 6.3 and 6.4 demonstrate that the degree of cell regularity can significantly affect the relationship between the compressive stress and strain, whether or not the strain gradient effect is present or absent.

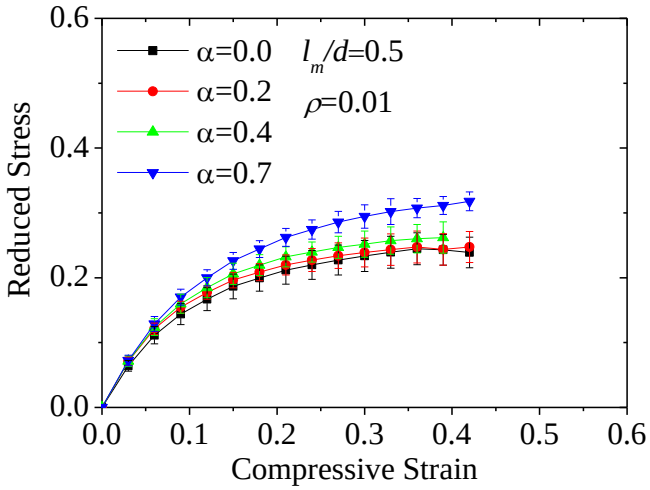

Figure 6.4. Effect of cell regularity on the dimensionless compressive stress and strain relation for micro-sized periodic random irregular open-cell foams with $\rho_0 = 0.01$ and $l_m / d = 0.5$.

6.3.1.3 Size-dependent effect on the relationship between Poisson's ratio and the compressive strain

This section will explore the size-dependent effect on the relationship between the Poisson's ratio and the compressive strain of low density micro-sized periodic random

irregular open-cell foams with a fixed relative density 0.01. Figures 6.5 (a), (b), (c), and (d) show that for micro-sized periodic random irregular open-cell foams with different degrees of cell regularity, whether the size-dependent effect is present or absent, the Poisson's ratio reduces deeply with the increase of the applied compressive strain in the *y* direction. The Poisson's ratio of low density open-cell foams is very close to 0.5 when the foam compressive strain is very small. When the cell strut diameter is large (i.e. $l_m / d \approx 0$), the relationships between the Poisson's ratio and the compressive strain of micro-sized open-cell foams reduce to those of their macro-sized counterparts. These findings are consistent with the theoretical and simulation results of macro-sized regular and random irregular open-cell foams (Zhu et al., 1997b, Zhu and Windle, 2002). As can be seen from Figures 6.5 (a), (b), (c), and (d), when the foam compressive strain is smaller than 10%, the larger the cell strut diameter (i.e. the smaller the value of l_m / d), the larger the Poisson's ratio. On the contrary, when the compressive strain is larger than 10%, the larger cell strut diameter, the smaller the Poisson's ratio.

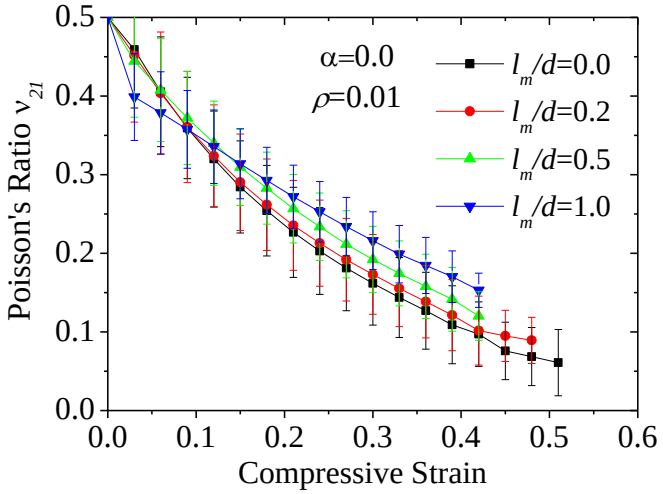

(a)

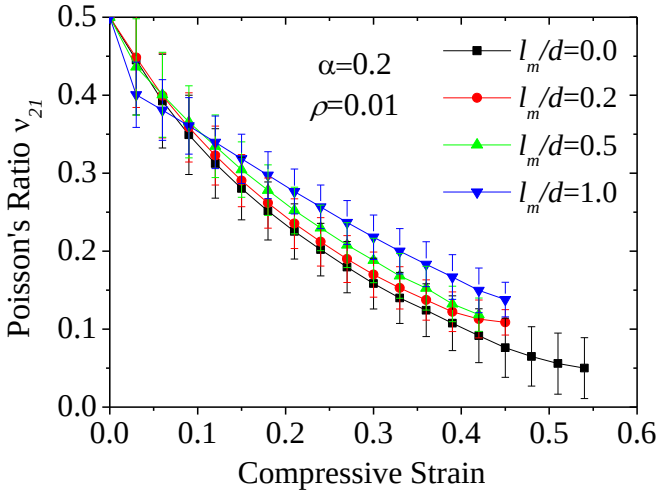

(b)

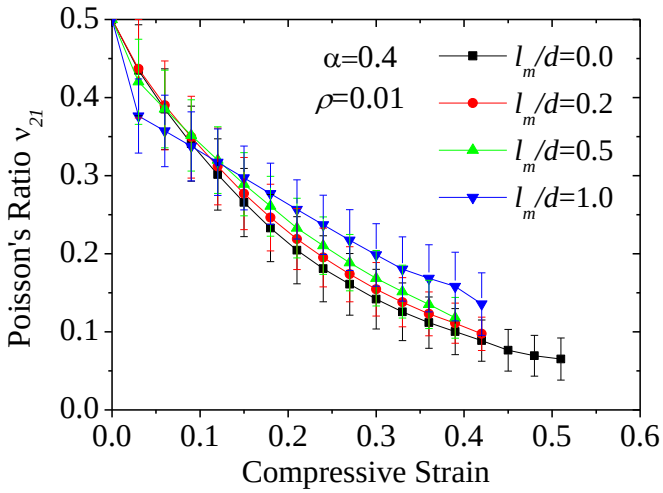

(c)

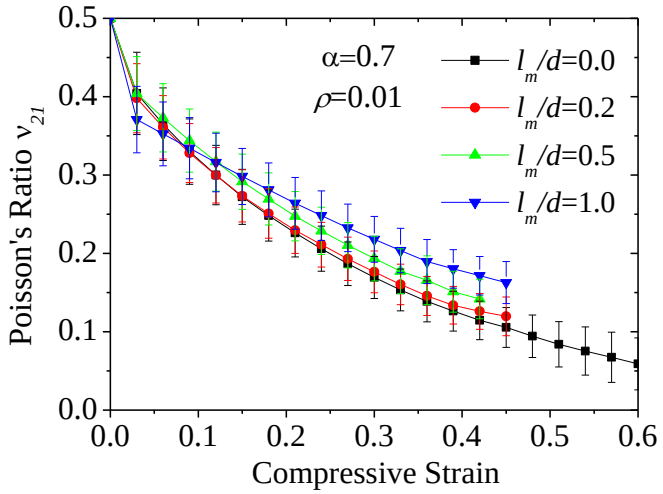

(d)

Figure 6.5. Size-dependent relations between the Poisson's ratio and compressive strain of low density micro-sized irregular open-cell foams with the relative density $\rho_0 = 0.01$. (a) $\alpha = 0.0$, (b) $\alpha = 0.2$, (c) $\alpha = 0.4$, and (d) $\alpha = 0.7$.

6.3.1.4 Effect of cell regularity on the relationship between Poisson's ratio and compressive strain

When the strain gradient effect is present, the effect of cell regularity on the relationship between the Poisson's ratio and the compressive strain of low density micro-sized periodic random irregular open-cell foams with relative density 0.01 are shown in Figure 6.6. As can be seen, the Poisson's ratio reduces with the increase of the compressive strain from 0% to about 40%, and the effect of cell regularity on the relationship between the Poisson's ratio and the compressive strain of micro-sized random irregular open-cell foams are very small.

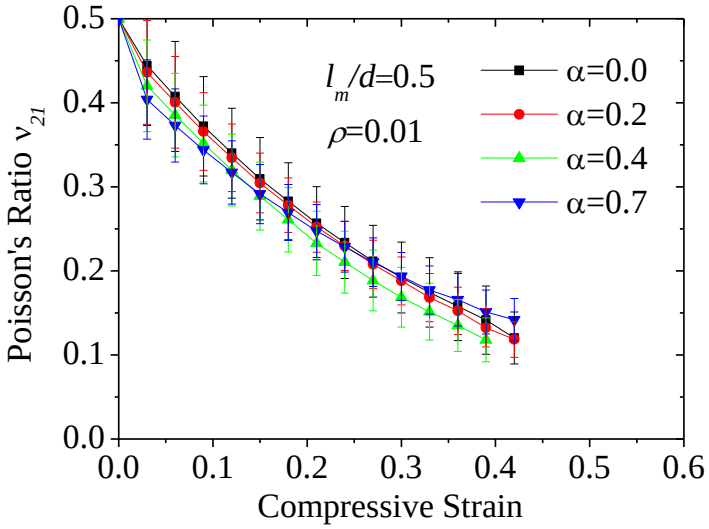

Figure 6.6. Effect of cell regularity on the relation between the in-plane Poisson's ratio and compressive strain of micro-sized irregular open-cell foams with ρ_0 = 0.01 and $l_m / d = 0.5$.

6.3.2 Size-dependent and tunable effects on the high strain compression of nano-sized random irregular open-cell foams

At the nano-meter scale, the surface elasticity and the initial stress or strain can affect the mechanical behaviour of nano-sized materials or structures (Duan et al., 2005, Miller and Shenoy, 2000, Zhu and Karihaloo, 2008). This section will investigate the effects of the cell strut diameter, the initial stress or strain, and the degree of cell regularity on the relationships of the compressive stress versus strain, and the Poisson's ratio versus the compressive strain of nano-sized random irregular open-cell foams.

6.3.2.1 Size-dependent and tunable effects on the relationship between the compressive stress and strain

Figures 6.7 (a), (b), (c), and (d) present the effect of surface elasticity on the relationship between the mean dimensionless compressive stress and strain of low density nano-sized random irregular open-cell foams with the fixed relative density ρ_0 = 0.01 and different degrees of cell regularity, from 0.0 to 0.7. As can be seen, the dimensionless compressive stress increases gradually with the increase of the compressive strain from 0% to 60% in the *y* direction. For nano-sized random irregular open-cell foams with the same degree of cell regularity, when the surface modulus is positive ($l_n / d > 0$), to compress the structure to the same compressive strain, the

smaller the cell strut diameter, the larger the dimensionless compressive stress and the tangent modulus. If the surface modulus is negative ($l_n / d < 0$), the effect is inverted.

When the cell strut diameter is much larger than the material intrinsic length l_n (i.e. $l_n / d \approx 0$), the size-dependent effect vanishes and the relations between the dimensionless compressive stress and strain of nano-sized periodic random irregular open-cell foams reduce to those of the conventional macro-sized counterparts, which has already been demonstrated from the results of micro-sized open-cell foams (as shown in Section 6.3.1.1). For nano-sized periodic random irregular open-cell foams, when the surface modulus is positive ($l_n / d > 0$), the smaller the cell strut diameter, the larger the standard deviations. If the cell strut diameter is the same, the larger the compressive strain, the larger the standard deviations. This mainly happens because there is large fluctuation on the convergent solution when the applied compressive strain is large. These findings are consistent with the results of the micro-sized open-cell foams (as shown in Section 6.3.1.1). In general, the size-dependent behaviours of nano-sized periodic random irregular open-cell foams are very similar to those of micro-sized periodic random irregular open-cell foams. Surface elasticity can significantly affect the relationship between the compressive stress and strain of low density nano-sized periodic random irregular open-cell foams.

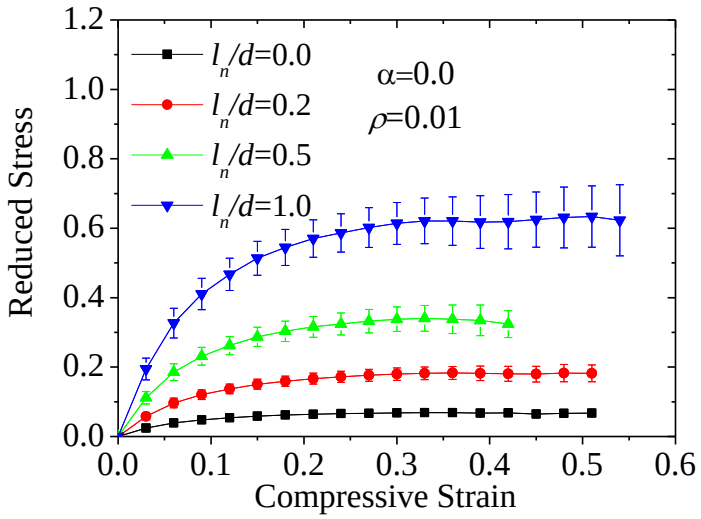
Reduced Stress
Compressive Strain
l_n/d=0.0
l_n/d=0.2
l_n/d=0.5
l_n/d=1.0
α=0.0
ρ=0.01

(a)

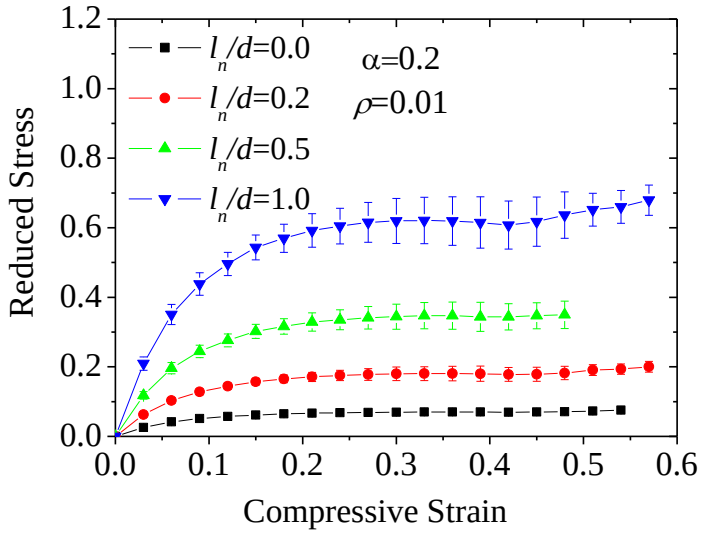
Reduced Stress
Compressive Strain
l_n/d=0.0
l_n/d=0.2
l_n/d=0.5
l_n/d=1.0
α=0.2
ρ=0.01

(b)

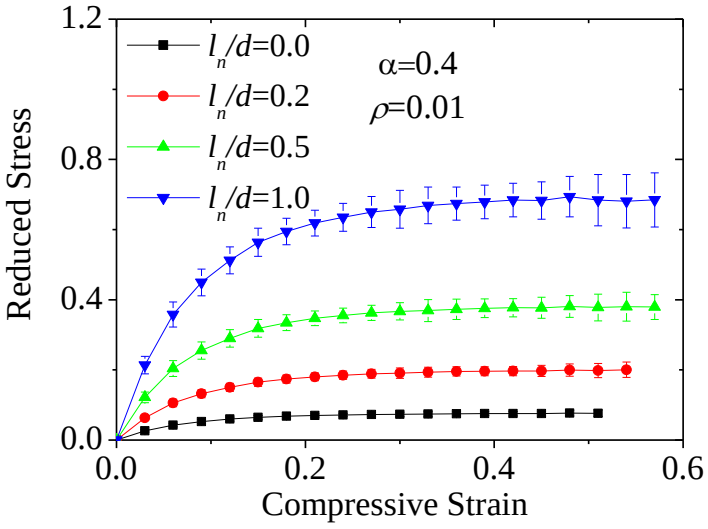
Reduced Stress
Compressive Strain
l_n/d=0.0
l_n/d=0.2
l_n/d=0.5
l_n/d=1.0
α=0.4
ρ=0.01

(c)

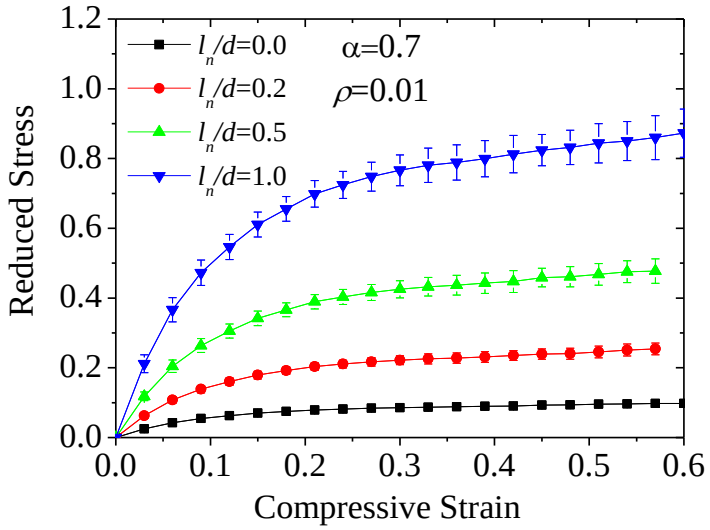

(d)

Figure 6.7. Size-dependent effect on the mean dimensionless compressive stress and strain response of low density nano-sized periodic random irregular open-cell foams with relative density ρ_0 = 0.01 (a) α = 0.0, (b) α = 0.2, (c) α = 0.4, and (d) α =0.7.

The initial stress or strain effect on the relationship between the mean dimensionless compressive stress and strain of low density nano-sized periodic random irregular open-cell foams is presented in Figures 6.8 (a) and (b). For free nano-sized open-cell foams, when adjusting the initial strain in the length direction of the cell struts from -10% to 10%, the cell struts become fatter and shorter or thinner and longer, and the initial size of the unit cell model of the nano-sized open-cell foams will shrink or expand, the dimensionless compressive stress can be controlled to either increase by approximately 30% or reduce by about 20%, consequently the nano-sized open-cell foams become stiffer (i.e. have a larger tangent modulus) or softer (i.e. have a smaller tangent modulus). Therefore, the initial stress or strain can significantly affect the relationships between the dimensionless compressive stress and strain of nano-sized

open-cell foams. When the applied initial strain is the same, the larger the foam compressive strain, the larger the standard deviation of the dimensionless compressive stress, which suggests that standard deviation depends mainly on the amplitude of the foam compressive strain.

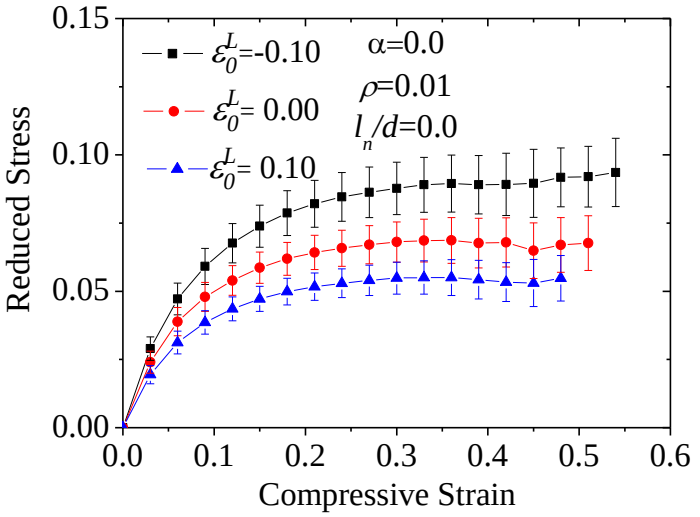

(a)

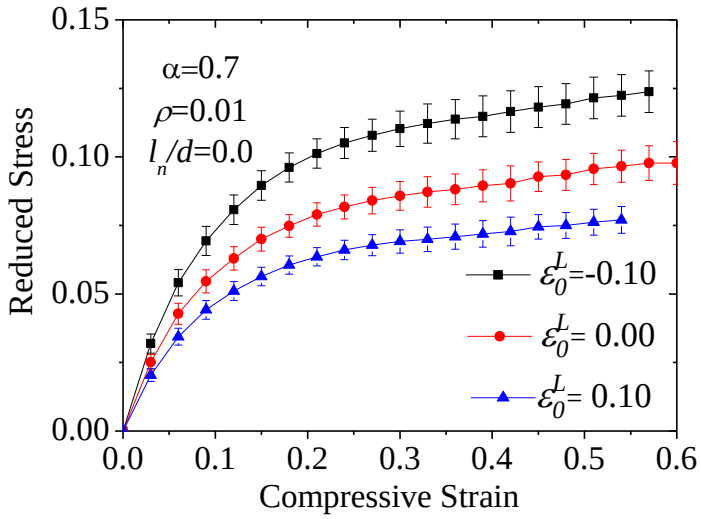

(b)

Figure 6.8. Effect of initial stress or strain on the dimensionless compressive stress and strain of low density nano-sized irregular open-cell foams with ρ_0 = 0.01. (a) α = 0.0, and (b) α = 0.7.

6.3.2.2 Effect of cell regularity on the relationship between the compressive stress and strain

In addition to the surface elasticity and initial stress or strain effects, cell regularity may also affect the compressive stress and strain response of low density nano-sized periodic random irregular open-cell foams. When the surface elasticity effect is present and the initial stress or strain effect is absent, the effect of cell regularity on the mean dimensionless compressive stress and strain of the nano-sized periodic random irregular open-cell foams with relative density 0.01 and $l_n / d = 0.5$ is presented in Figure 6.9. As can be seen, the greater the degree of cell regularity, the

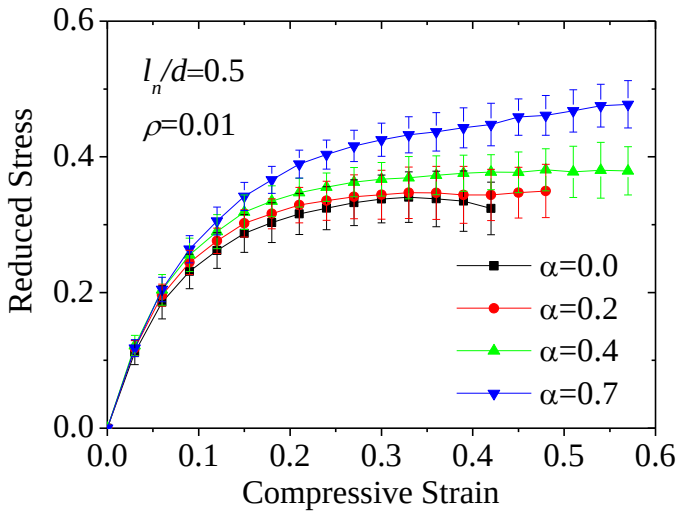

Figure 6.9. Effect of cell regularity on the dimensionless compressive stress and strain relation for nano-sized periodic random irregular open-cell foams with $\rho_0 = 0.01$ and $l_n / d = 0.5$.

smaller the tangent modulus when the compressive strain is small. When the foam compressive strain is larger than 10%, the greater the degree of cell regularity, the

larger the compressive stress. These findings are consistent with the results of the macro-sized (Zhu and Windle, 2002) and micro-sized irregular open-cell foams (as shown in Section 6.3.1.2).

6.3.2.3 Size-dependent and tunable effects on the relationship between the Poisson's ratio and compressive strain

This section presents the size-dependent effect on the relationship between the Poisson's ratio and compressive strain of low density nano-sized periodic random irregular open-cell foams. As can be seen from Figures 6.10 (a), (b), (c), and (d), for nano-sized open-cell foams with different values of l_n / d , the Poisson's ratio decreases monotonously with the increase of the compressive strain in the *y* direction. This trend is consistent with those of the macro-sized (Zhu and Windle, 2002) and micro-sized irregular open-cell foams (as shown in Section 6.3.1.3). The cell strut diameter (i.e. the value of l_n / d) has a very limited effect on the relationship between the Poisson's ratio and the compressive strain of low density nano-sized periodic random irregular open-cell foams. When the compressive strain is very small, the Poisson's ratio is close to 0.5, which is consistent with the results of macro-sized open-cell foams (Zhu et al., 1997b, Zhu and Windle, 2002) and micro-sized irregular open-cell foams (as shown in Section 6.3.1.3). The standard deviations, which are obtained from 10-20 models with the same set parameters, of the mean Poisson's ratio are also shown in Figures 6.10 (a), (b), (c), and (d).

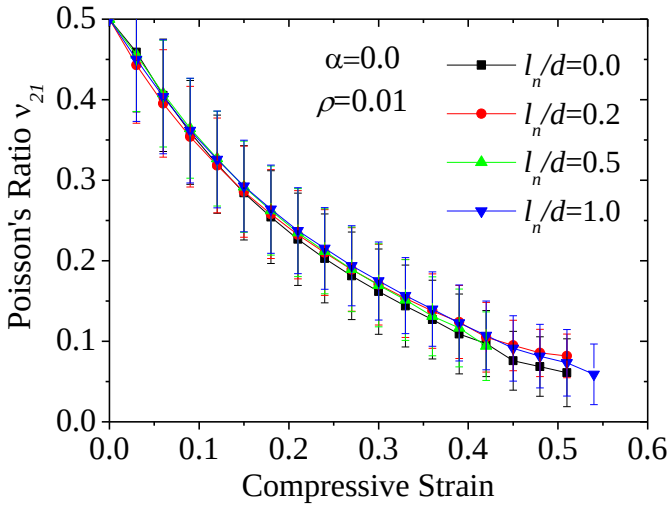
α=0.0
ρ=0.01
l_n/d=0.0
l_n/d=0.2
l_n/d=0.5
l_n/d=1.0
Poisson's Ratio ν_21
Compressive Strain
0.0
0.1
0.2
0.3
0.4
0.5
0.6

(a)

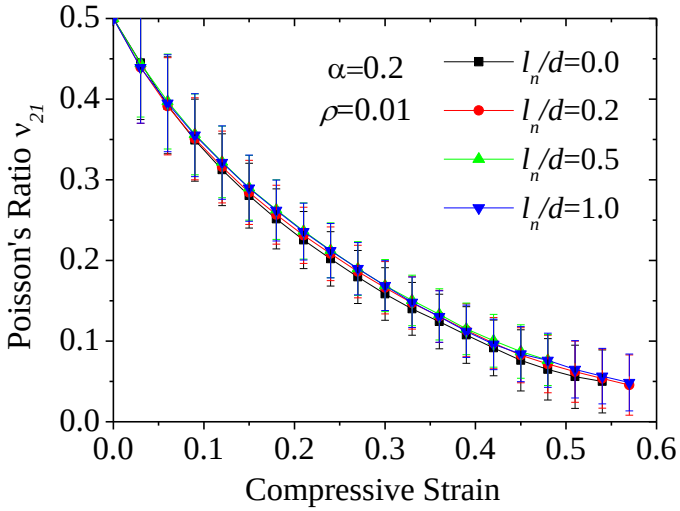
α=0.2
ρ=0.01
l_n/d=0.0
l_n/d=0.2
l_n/d=0.5
l_n/d=1.0
Poisson's Ratio ν_21
Compressive Strain
0.0
0.1
0.2
0.3
0.4
0.5
0.6

(b)

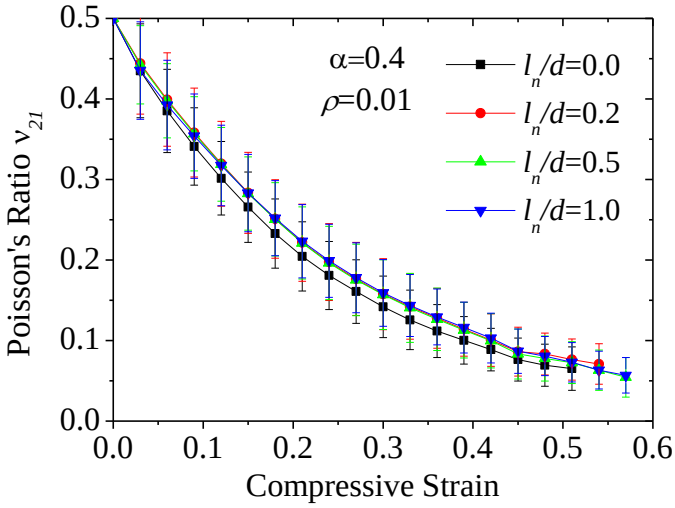
α=0.4
ρ=0.01
l_n/d=0.0
l_n/d=0.2
l_n/d=0.5
l_n/d=1.0
Poisson's Ratio ν_21
Compressive Strain
0.0
0.1
0.2
0.3
0.4
0.5
0.6

(c)

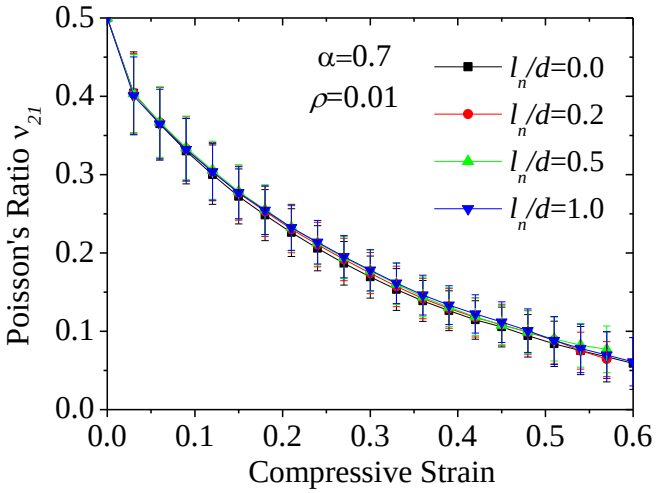

(d)

Figure 6.10. Size-dependent relations between the Poisson's ratio and the compressive strain response of low density nano-sized random irregular open-cell foams with ρ_0 = 0.01. (a) α = 0.0, (b) α = 0.2, (c) α = 0.4, and (d) α =0.7.

When the size-dependent effect is absent ($l_n / d = 0$), the initial stress or strain effect on the relationship between the Poisson's ratio and compressive strain of low density nano-sized periodic random irregular open-cell foams is presented in Figures 6.11 (a) and (b). As can be seen, when the initial strain in the length direction of the cell struts is controlled to vary from -10% to 10%, the influence of the initial strain effect on the Poisson's ratio is limited.

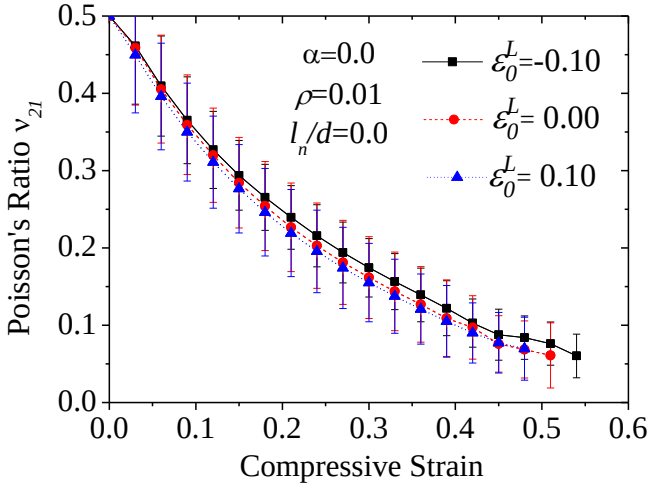

(a)

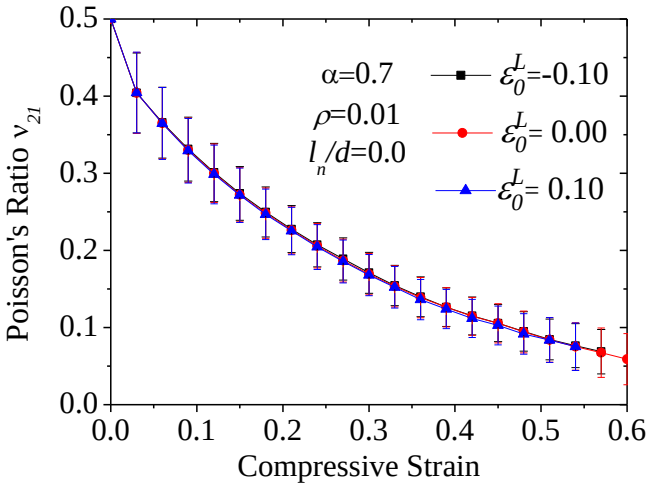

(b)

Figure 6.11. Effect of the initial stress or strain on the relationship between the Poisson's ratio and compressive strain of low density nano-sized periodic random irregular open-cell foams with relative density $\rho_0 = 0.01$. (a) $\alpha = 0.0$, and (b) $\alpha = 0.7$.

6.3.2.4 Effect of cell regularity on the relationship between the Poisson's ratio and compressive strain

When the surface elasticity effect is present ($l_n / d \neq 0$) and the initial stress or strain effect is absent ($\varepsilon_0^L = 0$), the effect of cell regularity on the relationship between the Poisson's ratio and compressive strain of low density nano-sized periodic random irregular open-cell foams is shown in Figure 6.12. As can be seen, the larger the compressive strain, the smaller Poisson's ratio. And the effect of the degree of cell regularity on the Poisson's ratio is negligible. This finding is consistent with the results of the micro-sized irregular open-cell foams (as shown in Section 6.3.1.4).

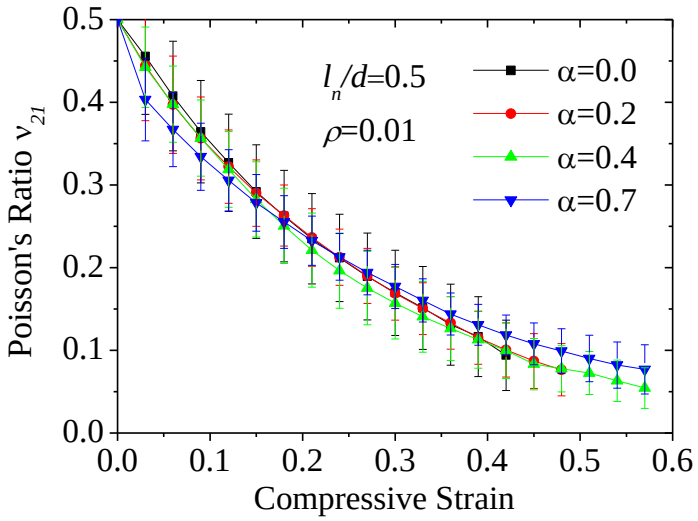

Figure 6.12. Effect of cell regularity on the relation between the Poisson's ratio and compressive strain of nano-sized irregular open-cell foams with relative density ρ_0 = 0.01 and $l_n / d = 0.5$.

6.4 Summary

In this chapter, the effects of the size-dependent (the cell strut diameter), the initial stress or strain, and the cell regularity on the high strain compression behaviour of low density micro- and nano-sized periodic random irregular open-cell foams are investigated and presented. It is found that the cell strut diameter (i.e. the value of l_m / d and l_n / d) can significantly affect the dimensionless compressive stress of micro- and nano-sized irregular open-cell foams. When l_m / d > 0 and the surface modulus is positive (i.e. l_n / d > 0), the smaller the cell strut diameter, the larger the dimensionless compressive stress and the tangent modulus. If the surface modulus is negative (i.e. l_n / d < 0), the effect is inverted. The initial stress or strain in the cell

strut length direction can also affect the compressive stress of low density nano-sized periodic random irregular open-cell foams. The dimensionless compressive stress of nano-sized open-cell foams can be controlled to vary over a range of about 50% by adjusting the amplitude of the initial strain of the cell struts in the length direction from -10% to 10%. In addition, the cell regularity can affect the compressive stress and strain response for micro- and nano-sized periodic random irregular open-cell foams. The greater the degree of cell regularity, the larger the dimensionless compressive stress. When the compressive strain is large, more regular micro- and nano-sized open-cell foams have a larger tangent modulus than the less regular foams.

At the micro-meter scale, the strain gradient can affect the Poisson's ratio of irregular open-cell foams. For micro-sized open-cell foams, when the compressive strain is less than 10%, the larger cell strut diameter, the larger Poisson's ratio. Meanwhile, if the compressive strain is larger than 10%, the trend is inverted. However, the surface elasticity and the initial stress or strain have very limited effects on the Poisson's ratio of nano-sized periodic random irregular open-cell foams. It is also found that cell regularity has a negligible effect on the Poisson's ratio of low density micro- and nano-sized irregular open-cell foams.

Chapter 7 Conclusion and future work

7.1 Conclusion

This thesis has reviewed the mechanical properties of macro-sized regular and irregular honeycombs and open-cell foams. However, these results may not apply to their micro- and nano-sized counterparts. It has generally been recognized that the strain gradient effect plays an important role in the deformation at the micro-meter scale, while the surface elasticity and initial stress or strain effects are the main deformation mechanisms at the nano-meter scale. This research work aimed to investigate the elastic properties and the high strain compressive responses of micro- and nano-sized periodic random irregular honeycombs and open-cell foams by numerical simulation analysis using the commercial finite element software ANSYS. Since there are no types of elements that could directly incorporate the size-dependent effects into the simulations in commercial finite element software, the equivalent material properties (Young's modulus and Poisson's ratio) and the equivalent thickness of 2D beams or the equivalent radius of 3D beams are used to incorporate the size effects into the simulations. According to the equivalence of the bending, transverse shear, torsion and axial stretching or compression rigidities, the equivalent Young's modulus, Poisson's ratio, and cross-sectional size can be obtained.

The elastic properties of micro- and nano-sized periodic random irregular Voronoi honeycombs are studied in Chapter 3. The five independent elastic constants: E_1, ν_{12},

E_3, G_{31}, and v_{31} are obtained. The results show that the elastic properties of micro- and nano-sized irregular honeycombs are size-dependent. The thinner the cell wall thickness, the larger the non-dimensional Young's modulus and bulk modulus, and the smaller the Poisson's ratio. For nano-sized irregular honeycombs, the elastic properties also depend on the initial stress or strain. For example, the non-dimensional Young's modulus of nano-sized irregular honeycombs can be controlled to vary over a range of nearly 100% by adjusting the initial strain in the cell wall direction between -0.06 and 0.06. The cell regularity also can affect the elastic properties of micro- and nano-sized irregular honeycombs. For irregular honeycombs with $l_m / d_0 = 0.5$ or $l_n / d = 0.5$, if the initial relative density is less than 0.15, the non-dimensional Young's modulus reduces with the increase of the cell regularity. Meanwhile, if the initial relative density is larger than 0.15, this effect is inverted. However, with the increase of the cell regularity, the dimensionless bulk modulus always increases, and the Poisson's ratio remains nearly unchanged.

The high strain compressive responses of micro- and nano-sized periodic random irregular honeycombs were simulated in Chapter 4. It was found that the thinner the cell wall thickness, the larger the tangent modulus and the dimensionless in-plane compressive stress of micro- or nano-sized irregular honeycombs will be. The dimensionless compressive stress of nano-sized irregular honeycombs can be controlled to vary over a range of nearly 115% by adjusting the amplitude of the initial strain in the cell wall direction between -0.06 and 0.06. The greater the degree of cell

regularity, the larger the dimensionless compressive stress and in-plane Poisson's ratio will be.

The linear elastic properties of micro- and nano-sized periodic random irregular open-cell foams are investigated in Chapter 5. It was found that the smaller cross-sectional diameter of the cell struts, the larger the non-dimensional Young's modulus and shear modulus, and the smaller the Poisson's ratio. When the initial strain effect is present and the Poisson's ratio of solid material is 0.1, the non-dimensional Young's modulus and shear modulus of nano-sized irregular open-cell foams can be controlled to vary over a range of nearly 50% by adjusting the initial strain in the axial direction of the cell struts between -0.1 and 0.1. For micro- and nano-sized irregular open-cell foams with $l_m / d_0 = 0.5$ or $l_n / d = 0.5$, if the initial relative density is less than 0.03, the greater the degree of cell regularity, the smaller the non-dimensional Young's modulus and shear modulus will be. This trend is very similar to that of micro- and nano-sized irregular honeycombs. According to the Zener's anisotropy factor, micro- and nano-sized periodic random irregular open-cell foams are almost isotropic, whether or not the strain gradient, the surface elasticity, or the initial strain effect is present or absent. The isotropic properties are independent of the relative density.

The high strain compressive responses of micro- and nano-sized periodic random irregular open-cell foams are presented in Chapter 6. It was found that the smaller the cross-sectional diameter of the cell struts, the larger the tangent modulus and the dimensionless compressive stress will be. The dimensionless compressive stress of

nano-sized irregular open-cell foams can be controlled to vary over a range of about 50% by adjusting the amplitude of the initial strain in the cell struts direction between -0.1 and 0.1. The cell regularity has an effect on the compressive stress and strain response for micro- and nano-sized periodic random irregular open-cell foams. The greater the cell regularity, the larger the tangent modulus and the dimensionless compressive stress if the compressive strain is large.

All of the results obtained for micro- and nano-sized random irregular honeycombs and open-cell foams are consistent with those of their macro-sized regular or irregular counterparts. This research work is the extension work in the elastic properties of honeycombs and open-cell foams. It is focused on the micro- and nano-sized irregular honeycombs and open-cell foams, in the previous work, they were focused on the macro-sized regular and irregular honeycombs and open-cell foams and the micro-and nano-sized regular honeycombs and open-cell foams. Because the micro- and nano-sized regular and irregular honeycombs and open-cell foams already can be produced, so this research work about the irregular structure is very useful. The obtained results in this research can be used as a guide in the design of more reliable micro- or nano-sized/structured materials and can help to enhance the applications of such materials in many different areas. Such as nano-sensor or membrane, according to the obtained results, it can be found that when the initial relative density of honeycombs or open-cell foams is very small, more irregular structure would be stiffer, if the initial relative density is larger, this effect is inverted. Due to requirement about the material strength

of nano-sensor or membrane in the engineering, the strength of micro- and nano-sized honeycombs and open-cell foams can be influenced and controlled by the regularity and the initial relative density.

There is another novelty that is the methodology, in the analysis of the micro- and nano-sized regular honeycomb, due to the regular structure, Zhu (2010b) can easily to find the stiffness matrix of the regular honeycombs, and directly obtained the theoretical elastic properties with micro- and nano-sized effects. However, this method is difficult to apply in irregular structure, because the stiffness matrix is different and needs more time to find in each irregular structure. The novel point in the method is about finding the equivalent material properties by the elastic rigidities of the element with micro- and nano-sized effects. According to these equivalent values, applying the displacement on the structure in ANSYS can obtain the relevant stress and strain, then the elastic properties of the micro- and nano-sized irregular honeycombs and open-cell foams can be found. It can save a lot of time.

7.2 Research limitations and recommendations for future work

No matter how rigorous it may be, no research project can cover all aspects of the subject area it purports to investigate. This study is no exception to this rule. There are a number of limitations in the simulations of this thesis. Firstly, all of the simulations are based on the idealized geometric models of periodic random irregular Voronoi

honeycombs or open-cell foams. Secondly, all of the cell walls/struts are assumed to be straight and uniform in thickness or diameter, and they are modeled by uniform beam elements. Thirdly, the solid materials are assumed to be linear elastic, the material nonlinearity is not taken into account.

In reality, the cell walls or the cell struts may be curved or not uniform in thickness or diameter. In the future, CT images of real materials could be used to construct the geometric models for finite element simulations. Instead of beam elements, shell or solid elements could be used to represent the cell walls or the cell struts. Once honeycombs or open-cell foams undergo large strain compression, the solid material may become nonlinear elastic, or elastic-plastic, or viscoelastic. In addition, cellular materials, such as bones, are usually hierarchical and self-similar. In this research work, the simulations have taken a long time to produce, so optimizing the simulation process is another improvement. All of these factors could be taken into consideration in future simulations.

References

ADIGA, S. P., JIN, C., CURTISS, L. A., MONTEIRO-RIVIERE, N. A. & NARAYAN, R. J. 2009. Nanoporous membranes for medical and biological applications. *Wiley Interdisciplinary Reviews: Nanomedicine and Nanobiotechnology,* 1**,** 568-581.

AIFANTIS, E. C. 1999. Strain gradient interpretation of size effects. *International Journal of Fracture,* 95**,** 299-314.

ALSAYEDNOOR, J., HARRISON, P. & GUO, Z. 2013. Large strain compressive response of 2-D periodic representative volume element for random foam microstructures. *Mechanics of Materials,* 66**,** 7-20.

ANSYS ANSYS finite element software.

ANTHOINE, A. 2000. Effect of couple-stresses on the elastic bending of beams. *International Journal of Solids and Structures,* 37**,** 1003-1018.

ATKINSON, M. 1995. Further analysis of the size effect in indentation hardness tests of some metals. *Journal of Materials Research,* 10**,** 2908-2915.

BIENER, J., WITTSTOCK, A., ZEPEDA-RUIZ, L. A., BIENER, M. M., ZIELASEK, V., KRAMER, D., VISWANATH, R. N., WEISSMULLER, J., BAUMER, M. & HAMZA, A. V. 2009. Surface-chemistry-driven actuation in nanoporous gold. *Nature Materials,* 8**,** 47-51.

BILOUSOV, O. V., CARVAJAL, J. J., MATEOS, X., SOL , R., MASSONS, J., D AZ, F. & AGUIL , M. 2013. *Nanoporous GaN epitaxial layers grown by Chemical Vapor Deposition* [Online]. Available: http://science24.com/paper/28924 [Accessed 6th December 2014].

BOOTS, B. N. 1982. The arrangement of cells in "random" networks. *Metallography,* 15**,** 53-62.

BOUAKBA, M., BEZAZI, A. & SCARPA, F. 2012. FE analysis of the in-plane mechanical properties of a novel Voronoi-type lattice with positive and negative Poisson's ratio configurations. *International Journal of Solids and Structures,* 49**,** 2450-2459.

CAMMARATA, R. C. 1994. Surface and interface stress effects in thin films. *Progress in Surface Science,* 46**,** 1-38.

CHEN, C., LU, T. J. & FLECK, N. A. 1999. Effect of imperfections on the yielding of two-dimensional foams. *Journal of the Mechanics and Physics of Solids,* 47**,** 2235-2272.

CHEN, D. H. 2011. Bending deformation of honeycomb consisting of regular hexagonal cells. *Composite Structures,* 93**,** 736-746.

CHRISTENSEN, R. M. 2000. Mechanics of cellular and other low-density materials. *International Journal of Solids and Structures,* 37**,** 93-104.

DEQIANG, S., WEIHONG, Z. & YANBIN, W. 2010. Mean out-of-plane dynamic plateau stresses of hexagonal honeycomb cores under impact loadings.

Composite Structures, 92**,** 2609-2621.
DOYOYO, M. & MOHR, D. 2003. Microstructural response of aluminum honeycomb to combined out-of-plane loading. *Mechanics of Materials,* 35**,** 865-876.
DRENCKHAN, W. & LANGEVIN, D. 2010. Monodisperse foams in one to three dimensions. *Current Opinion in Colloid & Interface Science,* 15**,** 341-358.
DUAN, H. 2010. Surface-enhanced cantilever sensors with nano-porous films. *Acta Mechanica Solida Sinica,* 23**,** 1-12.
DUAN, H. L., WANG, J., HUANG, Z. P. & KARIHALOO, B. L. 2005. Size-dependent effective elastic constants of solids containing nano-inhomogeneities with interface stress. *Journal of the Mechanics and Physics of Solids,* 53**,** 1574-1596.
ERG. *Duocel® Foam Energy Absorbers* [Online]. ERG Aerospace Corporation. Available: http://www.ergaerospace.com/products/energy-absorbers.htm [Accessed 5th December 2014].
FLECK, N., MULLER, G., ASHBY, M. & HUTCHINSON, J. 1994. Strain gradient plasticity: theory and experiment. *Acta Metallurgica et Materialia,* 42**,** 475-487.
FLECK, N. A. & HUTCHINSON, J. W. 1993. A phenomenological theory for strain gradient effects in plasticity. *Journal of the Mechanics and Physics of Solids,* 41**,** 1825-1857.
GAN, Y. X., CHEN, C. & SHEN, Y. P. 2005. Three-dimensional modeling of the mechanical property of linearly elastic open cell foams. *International Journal of Solids and Structures,* 42**,** 6628-6642.
GAO, H., HUANG, Y., NIX, W. D. & HUTCHINSON, J. W. 1999. Mechanism-based strain gradient plasticity— I. Theory. *Journal of the Mechanics and Physics of Solids,* 47**,** 1239-1263.
GAO, W., YU, S. & HUANG, G. 2006. Finite element characterization of the size-dependent mechanical behaviour in nanosystems. *Nanotechnology,* 17**,** 1118.
GERE, J. M. & TIMOSHENKO, S. P. 1995. *Mechanics of Materials*, London: Chapman & Hall.
GIBSON, L. J. & ASHBY, M. F. 1982. The Mechanics of Three-Dimensional Cellular Materials. *Proc. R. Soc. Lond. A,* vol. 382, no. 1782**,** 43-59.
GIBSON, L. J. & ASHBY, M. F. 1997. *Cellular solids structure and properties*, Cambridge University Press.
GIBSON, L. J., ASHBY, M. F., SCHAJER, G. S. & ROBERTSON, C. I. 1982 The Mechanics of Two-Dimensional Cellular Materials. *Proc. R. Soc. Lond. A,* vol. 382, no. 1782**,** 25-42.
GONG, L. & KYRIAKIDES, S. 2005. Compressive response of open cell foams Part II: Initiation and evolution of crushing. *International Journal of Solids and Structures,* 42**,** 1381-1399.
GONG, L., KYRIAKIDES, S. & JANG, W. Y. 2005a. Compressive response of open-cell foams. Part I: Morphology and elastic properties. *International Journal of Solids and Structures,* 42**,** 1355-1379.

GONG, L., KYRIAKIDES, S. & TRIANTAFYLLIDIS, N. 2005b. On the stability of Kelvin cell foams under compressive loads. *Journal of the Mechanics and Physics of Solids,* 53**,** 771-794.

HAISS, W., NICHOLS, R. J., SASS, J. K. & CHARLE, K. P. 1998. Linear correlation between surface stress and surface charge in anion adsorption on Au(111). *Journal of Electroanalytical Chemistry,* 452**,** 199-202.

HAQUE, M. A. & SAIF, M. T. A. 2003. Strain gradient effect in nanoscale thin films. *Acta Materialia,* 51**,** 3053-3061.

HUTCHINSON, J. W. 2000. Plasticity at the micron scale. *International Journal of Solids and Structures,* 37**,** 225-238.

JAMES REN, X. & SILBERSCHMIDT, V. V. 2008. Numerical modelling of low-density cellular materials. *Computational Materials Science,* 43**,** 65-74.

JEBUR, Q. F., HARRISON, P., GUO, Z., SCHUBERT, G. & NAVEZ, V. 2011. Characterisation and Modelling of a Melt-Extruded LDPE Closed Cell Foam. *Applied Mechanics and Materials,* 70**,** 105-110.

JEBUR, Q. H., HARRISON, P., GUO, Z., SCHUBERT, G., JU, X. & NAVEZ, V. 2012. Characterisation and modelling of a transversely isotropic melt-extruded low-density polyethylene closed cell foam under uniaxial compression. *Proceedings of the Institution of Mechanical Engineers, Part C: Journal of Mechanical Engineering Science,* 226**,** 2168-2177.

JETZER, M. 2010. *S-II Insulation* [Online]. The Apollo Flight Journal. Available: http://history.nasa.gov/afj/s-ii/s-ii-insulation.html [Accessed 5th December 2014].

KHAN, M. K., BAIG, T. & MIRZA, S. 2012. Experimental investigation of in-plane and out-of-plane crushing of aluminum honeycomb. *Materials Science and Engineering: A,* 539**,** 135-142.

KIM, B. & CHRISTENSEN, R. M. 2000. Basic two-dimensional core types for sandwich structures. *International Journal of Mechanical Sciences,* 42**,** 657-676.

KONSTANTINIDIS, I. C., PARADISIADIS, G. & TSIPAS, D. N. 2009. Analytical models for the mechanical behavior of closed and open-cell Al foams. *Theoretical and Applied Fracture Mechanics,* 51**,** 48-56.

KRAMER, D., VISWANATH, R. N. & WEISSMULLER, J. 2004. Surface-Stress Induced Macroscopic Bending of Nanoporous Gold Cantilevers. *Nano letter,* 4**,** 793-796.

KRAYNIK, A. M., REINELT, D. A. & VAN SWOL, F. 2003. Structure of random monodisperse foam. *PHYSICAL REVIEW,* E 67.

KUMAR, R. S. & MCDOWELL, D. L. 2004. Generalized continuum modeling of 2-D periodic cellular solids. *International Journal of Solids and Structures,* 41**,** 7399-7422.

KWON, Y. W., COOKE, R. E. & PARK, C. 2003. Representative unit-cell models for open-cell metal foams with or without elastic filler. *Materials Science and Engineering: A,* 343**,** 63-70.

LAM, D. C. C., YANG, F., CHONG, A. C. M., WANG, J. & TONG, P. 2003. Experiments and theory in strain gradient elasticity. *Journal of the Mechanics and Physics of Solids,* 51**,** 1477-1508.

LAROUSSI, M., SAB, K. & ALAOUI, A. 2002. Foam mechanics: nonlinear response of an elastic 3D-periodic microstructure. *International Journal of Solids and Structures,* 39**,** 3599-3623.

LI, K., GAO, X. L. & SUBHASH, G. 2006. Effects of cell shape and strut cross-sectional area variations on the elastic properties of three-dimensional open-cell foams. *Journal of the Mechanics and Physics of Solids,* 54**,** 783-806.

LIN, T. C., YANG, M. Y. & HUANG, J. S. 2013. Effects of solid distribution on the out-of-plane elastic properties of hexagonal honeycombs. *Composite Structures,* 100**,** 436-442.

LUBARDA, V. A. & MARKENSCOFF, X. 2000. Conservation integrals in couple stress elasticity. *Journal of the Mechanics and Physics of Solids,* 48**,** 553-564.

LUXNER, M. H., STAMPFL, J. & PETTERMANN, H. E. 2007. Numerical simulations of 3D open cell structures – influence of structural irregularities on elasto-plasticity and deformation localization. *International Journal of Solids and Structures,* 44**,** 2990-3003.

M LLER, P. & SA L, A. 2004. Elastic effects on surface physics. *Surface Science Reports,* 54**,** 157-258.

MA, Q. & CLARKE, D. R. 1995. Size dependent hardness of silver single crystals. *Journal of Materials Research,* 10**,** 853-863.

MASTERS, I. G. & EVANS, K. E. 1996. Models for the elastic deformation of honeycombs. *Composite Structures,* 35**,** 403-422.

MCELHANEY, K., VLASSAK, J. & NIX, W. 1998. Determination of indenter tip geometry and indentation contact area for depth-sensing indentation experiments. *Journal of Materials Research,* 13**,** 1300-1306.

MERAGHNI, F., DESRUMAUX, F. & BENZEGGAGH, M. L. 1999. Mechanical behaviour of cellular core for structural sandwich panels. *Composites Part A: Applied Science and Manufacturing,* 30**,** 767-779.

MILLER, R. E. & SHENOY, V. B. 2000. Size-dependent elastic properties of nanosized structural elements. *Nanotechnology,* 11**,** 139.

MILLS, N. J. 2007a. The high strain mechanical response of the wet Kelvin model for open-cell foams. *International Journal of Solids and Structures,* 44**,** 51-65.

MILLS, N. J. 2007b. *Polymer Foams Handbook: Engineering and Biomechanics Applications and Design Guide*, Butterworth-Heinemann, UK.

MILLS, N. J., ST MPFLI, R., MARONE, F. & BR HWILER, P. A. 2009. Finite element micromechanics model of impact compression of closed-cell polymer foams. *International Journal of Solids and Structures,* 46**,** 677-697.

MILLS, N. J. & ZHU, H. X. 1999. The high strain compression of closed-cell polymer foams. *Journal of the Mechanics and Physics of Solids,* 47**,** 669-695.

MINDLIN, R. D. 1963. Influence of couple-stresses on stress concentrations. *Experimental Mechanics,* 3**,** 1-7.

MINDLIN, R. D. & TIERSTEN, H. F. 1962. Effects of couple-stresses in linear elasticity. *Archive for Rational Mechanics and Analysis,* 11**,** 415-448.

NISHIHARA, H., MUKAI, S. R., YAMASHITA, D. & TAMON, H. 2005. Ordered Macroporous Silica by Ice Templating. *Chem. Mater,* 17**,** 683-689.

NIX, W. D. 1989. Mechanical properties of thin films. *Metallurgical transactions A,* 20**,** 2217-2245.

NIX, W. D. & GAO, H. 1998. Indentation size effects in crystalline materials: A law for strain gradient plasticity. *Journal of the Mechanics and Physics of Solids,* 46**,** 411-425.

NOWACKI, W. 1974. The Linear Theory of Micropolar Elasticity. *In:* NOWACKI, W. & OLSZAK, W. (eds.) *Micropolar Elasticity.* Springer Vienna.

PAN, S. D., WU, L. Z., SUN, Y. G., ZHOU, Z. G. & QU, J. L. 2006. Longitudinal shear strength and failure process of honeycomb cores. *Composite Structures,* 72**,** 42-46.

PAPARGYRI-BESKOU, S., TSEPOURA, K. G., POLYZOS, D. & BESKOS, D. E. 2003. Bending and stability analysis of gradient elastic beams. *International Journal of Solids and Structures,* 40**,** 385-400.

PAPKA, S. D. & KYRIAKIDES, S. 1994. In-plane compressive response and crushing of honeycomb. *Journal of the Mechanics and Physics of Solids,* 42**,** 1499-1532.

ROBERTS, A. P. & GARBOCZI, E. J. 2001. Elastic moduli of model random three-dimensional closed-cell cellular solids. *Acta Materialia,* 49**,** 189-197.

ROBERTS, A. P. & GARBOCZI, E. J. 2002. Elastic properties of model random three-dimensional open-cell solids. *Journal of the Mechanics and Physics of Solids,* 50**,** 33-55.

RUBIO-BOLLINGER, G., BAHN, S. R., AGRA T, N., JACOBSEN, K. W. & VIEIRA, S. 2001. Mechanical Properties and Formation Mechanisms of a Wire of Single Gold Atoms. *Physical Review Letters,* 87**,** 026101.

SHENOY, V. B. 2002. Size-dependent rigidities of nanosized torsional elements. *International Journal of Solids and Structures,* 39**,** 4039-4052.

SHULMEISTER, V., VAN DER BURG, M. W. D., VAN DER GIESSEN, E. & MARISSEN, R. 1998. A numerical study of large deformations of low-density elastomeric open-cell foams. *Mechanics of Materials,* 30**,** 125-140.

SILVA, M. J. & GIBSON, L. J. 1997. The effects of non-periodic microstructure and defects on the compressive strength of two-dimensional cellular solids. *International Journal of Mechanical Sciences,* 39**,** 549-563.

SILVA, M. J., HAYES, W. C. & GIBSON, L. J. 1995. The effects of non-periodic microstructure on the elastic properties of two-dimensional cellular solids. *International Journal of Mechanical Sciences,* 37**,** 1161-1177.

SOTOMAYOR, O. E. & TIPPUR, H. V. 2014a. Role of cell regularity and relative density on elasto-plastic compression response of random honeycombs generated using Voronoi diagrams. *International Journal of Solids and Structures,* 51**,** 3776-3786.

SOTOMAYOR, O. E. & TIPPUR, H. V. 2014b. Role of cell regularity and relative density on elastoplastic compression response of 3-D open-cell foam core sandwich structure generated using Voronoi diagrams. *Acta Materialia,* 78**,** 301-313.

ST LKEN, J. S. & EVANS, A. G. 1998. A microbend test method for measuring the plasticity length scale. *Acta Materialia,* 46**,** 5109-5115.

SULLIVAN, R. M., GHOSN, L. J. & LERCH, B. A. 2008. A general tetrakaidecahedron model for open-celled foams. *International Journal of Solids and Structures,* 45**,** 1754-1765.

SUN, Y. & PUGNO, N. M. 2013. In plane stiffness of multifunctional hierarchical honeycombs with negative Poisson's ratio sub-structures. *Composite Structures,* 106**,** 681-689.

SUN, Z. H., WANG, X. X., SOH, A. K., WU, H. A. & WANG, Y. 2007. Bending of nanoscale structures: Inconsistency between atomistic simulation and strain gradient elasticity solution. *Computational Materials Science,* 40**,** 108-113.

TAMON, H., AKATSUA, T., MORI, H. & SANO, N. 2013. Synthesis of Zeolite Monolith with Hierarchical Micro/Macropores by Ice-Templating and Steam-Assisted Crystallization. *Chemical Engineering Transactions,* 32.

TOUPIN, R. A. 1962. Elastic materials with couple stresses. *Arch.Ration.Mech.Anal.,* 11**,** 385-414.

TRIANTAFYLLIDIS, N. & SCHRAAD, M. W. 1998. Onset of failure in aluminum honeycombs under general in-plane loading. *Journal of the Mechanics and Physics of Solids,* 46**,** 1089-1124.

TSAGRAKIS, I., KONSTANTINIDIS, A. & AIFANTIS, E. C. 2003. Strain gradient and wavelet interpretation of size effects in yield and strength. *Mechanics of Materials,* 35**,** 733-745.

VAN DER BURG, M. W. D., SHULMEISTER, V., VAN DER GEISSEN, E. & MARISSEN, R. 1997. On the Linear Elastic Properties of Regular and Random Open-Cell Foam Models. *Journal of Cellular Plastics,* 33**,** 31-54.

VARDOULAKIS, I. & GIANNAKOPOULOS, A. E. 2006. An example of double forces taken from structural analysis. *International Journal of Solids and Structures,* 43**,** 4047-4062.

WADLEY. 2014. *Ultralight Cellular Materials* [Online]. Wadley Research Group. Available: http://www.virginia.edu/ms/research/wadley/celluar-materials.html [Accessed 5th December 2014].

WAGNER, T., HAFFER, S., WEINBERGER, C., KLAUS, D. & TIEMANN, M. 2013. Mesoporous materials as gas sensors. *Chemical Society Reviews,* 42**,** 4036-4053.

WANG, Y. & CUITI O, A. M. 2000. Three-dimensional nonlinear open-cell foams with large deformations. *Journal of the Mechanics and Physics of Solids,* 48**,** 961-988.

WANG, Z., LI, F., ERGANG, N. S. & STEIN, A. 2008. Synthesis of monolithic 3D ordered macroporous carbon/nano-silicon composites by diiodosilane

decomposition. *Carbon,* 46**,** 1702-1710.
WARREN, W. E. & KRAYNIK, A. M. 1987. Foam mechanics: the linear elastic response of two-dimensional spatially periodic cellular materials. *Mechanics of Materials,* 6**,** 27-37.
WARREN, W. E. & KRAYNIK, A. M. 1988. The Linear Elastic Properties of Open-Cell Foams. *Journal of Applied Mechanics,* 55**,** 341-346.
WARREN, W. E. & KRAYNIK, A. M. 1997. Linear Elastic Behavior of a Low-Density Kelvin Foam With Open Cells. *Journal of Applied Mechanics,* 64**,** 787-794.
WARREN, W. E., KRAYNIK, A. M. & STONE, C. M. 1989. A constitutive model for two-dimensional nonlinear elastic foams. *Journal of the Mechanics and Physics of Solids,* 37**,** 717-733.
WEISSM LLER, J., VISWANATH, R. N., KRAMER, D., ZIMMER, P., W RSCHUM, R. & GLEITER, H. 2003. Charge-induced reversible strain in a metal. *Science* 312-315.
WICKLEIN, M. & THOMA, K. 2005. Numerical investigations of the elastic and plastic behaviour of an open-cell aluminium foam. *Materials Science and Engineering: A,* 397**,** 391-399.
XU, S., BEYNON, J. H., RUAN, D. & LU, G. 2012. Experimental study of the out-of-plane dynamic compression of hexagonal honeycombs. *Composite Structures,* 94**,** 2326-2336.
YANG, F., CHONG, A. C. M., LAM, D. C. C. & TONG, P. 2002. Couple stress based strain gradient theory for elasticity. *International Journal of Solids and Structures,* 39**,** 2731-2743.
ZHANG, J.-L. & LU, Z.-X. 2007. Numerical Modeling of the Compression Process of Elastic Open-cell Foams. *Chinese Journal of Aeronautics,* 20**,** 215-222.
ZHAO, Q., YIN, M., ZHANG, A. P., PRESCHER, S., ANTONIETTI, M. & YUAN, J. 2013. Hierarchically Structured Nanoporous Poly(Ionic Liquid) Membranes: Facile Preparation and Application in Fiber-Optic pH Sensing. *Journal of the American Chemical Society,* 135**,** 5549-5552.
ZHU, H. X. 2008. The effects of surface and initial stresses on the bending stiffness of nanowires. *Nanotechnology,* 19**,** 405703.
ZHU, H. X. 2010a. Corrigendum to "Size-dependent elastic properties of micro- and nano-honeycombs" [J. Mech. Phys. Solids 58 (2010) 696–709]. *Journal of the Mechanics and Physics of Solids,* 58**,** 843.
ZHU, H. X. 2010b. Size-dependent elastic properties of micro- and nano-honeycombs. *Journal of the Mechanics and Physics of Solids,* 58**,** 696-709.
ZHU, H. X. & CHEN, C. Y. 2011. Combined effects of relative density and material distribution on the mechanical properties of metallic honeycombs. *Mechanics of Materials,* 43**,** 276-286.
ZHU, H. X., HOBDELL, J. R. & WINDLE, A. H. 2000. Effects of cell irregularity on the elastic properties of open-cell foams. *Acta Materialia,* 48**,** 4893-4900.
ZHU, H. X., HOBDELL, J. R. & WINDLE, A. H. 2001a. Effects of cell irregularity

on the elastic properties of 2D Voronoi honeycombs. *Journal of the Mechanics and Physics of Solids,* 49**,** 857-870.

ZHU, H. X. & KARIHALOO, B. L. 2008. Size-dependent bending of thin metallic films. *International Journal of Plasticity,* 24**,** 991-1007.

ZHU, H. X., KNOTT, J. F. & MILLS, N. J. 1997a. Analysis of the elastic properties of open-cell foams with tetrakaidecahedral cells. *Journal of the Mechanics and Physics of Solids,* 45**,** 319-343.

ZHU, H. X. & MELROSE, J. R. 2003. A Mechanics Model for the Compression of Plant and Vegetative Tissues. *Journal of Theoretical Biology,* 221**,** 89-101.

ZHU, H. X. & MILLS, N. J. 1999. Modelling the creep of open-cell polymer foams. *Journal of the Mechanics and Physics of Solids,* 47**,** 1437-1457.

ZHU, H. X. & MILLS, N. J. 2000. The in-plane non-linear compression of regular honeycombs. *International Journal of Solids and Structures,* 37**,** 1931-1949.

ZHU, H. X., MILLS, N. J. & KNOTT, J. F. 1997b. Analysis of the high strain compression of open-cell foams. *Journal of the Mechanics and Physics of Solids,* 45**,** 1875-1904.

ZHU, H. X., THORPE, S. M. & WINDLE, A. H. 2001b. The geometrical properties of irregular two-dimensional Voronoi tessellations. *Philosophical Magazine A,* 81**,** 2765-2783.

ZHU, H. X., THORPE, S. M. & WINDLE, A. H. 2006. The effect of cell irregularity on the high strain compression of 2D Voronoi honeycombs. *International Journal of Solids and Structures,* 43**,** 1061-1078.

ZHU, H. X., WANG, J. X. & KARIHALOO, B. L. 2009. Effects of surface and initial stresses on the bending stiffness of trilayer plates and nanofilms. *Journal of mechanics of materials and structures* 4**,** 589-604.

ZHU, H. X., WANG, Z., FAN, T. & ZHANG, D. 2012a. Tunable Bending Stiffness, Buckling Force, and Natural Frequency of Nanowires and Nanoplates. *World Journal of Nano Science and Engineering,* 2**,** 161-169.

ZHU, H. X. & WANG, Z. B. 2013. Size-dependent and tunable elastic and geometric properties of hierarchical nano-porous materials. *Science of Advanced Materials,* 5**,** 677-686.

ZHU, H. X. & WINDLE, A. H. 2002. Effects of cell irregularity on the high strain compression of open-cell foams. *Acta Materialia,* 50**,** 1041-1052.

ZHU, H. X., YAN, L. B., ZHANG, R. & QIU, X. M. 2012b. Size-dependent and tunable elastic properties of hierarchical honeycombs with regular square and equilateral triangular cells. *Acta Materialia,* 60**,** 4927-4939.

ZHU, H. X., ZHANG, H. C., YOU, J. F., KENNEDY, D., WANG, Z. B., FAN, T. X. & ZHANG, D. 2014a. The elastic and geometrical properties of micro- and nano-structured hierarchical random irregular honeycombs. *Journal of Materials Science,* 49**,** 5690-5702.

ZHU, H. X., ZHANG, H. C., YOU, J. F. & WANG, Z. B. 2013. Mechanical and geometrical properties of hierarchically nano-structured random irregular honeycombs. *3rd International Conference on Manipulation, Manufacturing*

and Measurement on the Nanoscale (3M-NANO 2013). Suzhou, China: IEEE Computer Society.

ZHU, H. X., ZHANG, P., BALINT, D., THORPE, S. M., ELLIOTT, J. A., WINDLE, A. H. & LIN, J. 2014b. The effects of regularity on the geometrical properties of Voronoi tessellations. *Physica A: Statistical Mechanics and its Applications,* 406**,** 42-58.

Appendix: Publications

Journal papers

ZHU, H. X., ZHANG, H. C., YOU, J. F., KENNEDY, D., WANG, Z. B., FAN, T. X. & ZHANG, D. 2014. The elastic and geometrical properties of micro- and nano-structured hierarchical random irregular honeycombs. *Journal of Materials Science*, 49**,** 5690-5702.

YOU, J. F., ZHANG, H. C., ZHU, H. X. & KENNEDY, D. The high strain compression behaviour of micro- and nano-structured random irregular honeycombs, in preparation.

ZHANG, H. C., ZHU, H. X., YOU, J. F. & KENNEDY, D. The elastic properties of micro- and nano-structured random irregular open-cell foams, in preparation.

ZHANG, H. C., ZHU, H. X., YOU, J. F. & KENNEDY, D. The high strain compression behaviour of micro- and nano-structured random irregular open-cell foams, in preparation.

Conference papers/proceedings

ZHANG, H. C., ZHU, H. X., YOU, J. F. & KENNEDY, D. 2013. Effects of cell irregularity on the elastic properties of nano-sized honeycombs. *In:* 13th International Conference on Computational Mechanics CM13, 25-27 March 2013, Durham, UK.

ZHANG, H. C., ZHU, H. X., YOU, J. F. & KENNEDY, D. 2014. Modeling the high strain compression of nano-sized random irregular Voronoi honeycombs. *In:* 8th International Conference on Advanced Computational Engineering and Experimenting (ACE-X2014), 30 June - 03 July 2014, Paris, France.

ZHU, H. X., YOU, J. F. & ZHANG, H. C. 2014. High strain compression behaviour of nano-structured hierarchical irregular honeycombs *In:* 11th World Congress on Computational Mechanics (WCCM XI), 5th European Conference on Computational Mechanics (ECCM V), 6th European Conference on Computational Fluid Dynamics (ECFD VI), 20-25 July 2014, Barcelona, Spain.

ZHU, H. X., ZHANG, H. C., YOU, J. F. & WANG, Z. B. 2013. Mechanical and

geometrical properties of hierarchically nano-structured random irregular honeycombs. *3rd International Conference on Manipulation, Manufacturing and Measurement on the Nanoscale (3M-NANO 2013).* Suzhou, China: IEEE Computer Society.